Conformational Isomerization of Small Carboxylic Acids Isolated in Low-Temperature Rare-Gas Matrices

Ermelinda M. S. Maçôas

Conformational Isomerization of Small Carboxylic Acids Isolated in Low-Temperature Rare-Gas Matrices

Ermelinda M. S. Maçôas

Academic Dissertation to be presented for public criticism, with the permission of the Faculty of Science and Technology of the University of Coimbra, in order to obtain the PhD in Chemistry.

Coimbra 2005

Acknowledgments

The supervisor of the PhD project, Professor Rui Fausto, is acknowledged for the fruitfully discussions determinant to the direction of the investigation work, for his patience, while facing divergent opinions, and for his wise advice, while giving me all the freedom needed to grow up as a scientist.

Professor Markku Räsänen is acknowledged for open the doors of the Laboratory of Physical-Chemistry to this work, for the many interesting discussions held in front of the spectrometer and for his guidance, which was important from both the scientific and the personal points of view.

I would like to express my gratitude also to Leonid Khriachtchev, who shared with me his knowledge during the long hours spent in the laboratory, stimulating my criticism and holding me back from jumping into conclusions many times.

To my dear office mates in the Laboratory of Physical-Chemistry in Helsinki, Jan Lundell and Mika Pettersson, I owe special thanks for their cheerful way of hosting me, for opening the door of their homes to me and, because we all have our blue moments, for being there when I needed their support. Their contribution to this work is equally acknowledged.

To my Finnish girl friends, Meppu and Leea, and to my unforgettable flatmate, Agus, I want to express my deepest gratitude for all the sweet moments we shared together; they sure made my life colourful while in Finland. I want also to express my gratitude to my closest flatmates and friends in Helsinki, Arno with his books and films, Édgar with his music, Frederic with his cooking, Lidja with her incredible good mood and Piotr with his peculiar ideas. Living abroad is always hard but it would be much harder without you.

The Portuguese Foundation for Science and Technology is thanked for the grant that directly supported my work (SFRH/BD/4863/2001). And the CSC-Center for Scientific Computing in Finland is thanked for providing the resources for the computations.

To the Department of Chemistry of the University of Coimbra, in particular the Group of Photochemistry and Molecular Spectroscopy, and the Department of Chemistry of the University of Helsinki, in particular the Laboratory of Physical Chemistry, I express my gratitude for making available the technical resources used in this work

Finally, I dedicate this thesis to my parents and to Manuel that have always supported my decisions.

Abstract

The conformational isomerization of a series of carboxylic acids (formic, acetic and propionic acid) isolated in solid rare gases is studied in this work. The infrared induced conformational isomerization is investigated by narrowband excitation of the isolated molecules. The effects of nature of the excited mode, excitation energy, solid environment and deuteration on the isomerization quantum yields are addressed. This work makes also important contributions to the study of dissipative tunnelling in condensed media, by analysing the dark conformational isomerization within the carboxylic group for the matrix isolated molecules. In this context, the effects of temperature, solid environment and deuteration in the dark isomerization are investigated. The conformational selectivity of the photochemistry of formic and acetic acids is also tested, by analysing the dependence of the ultraviolet induced decomposition on the structure of the initially excited conformer. Theoretical calculations are used to aid the interpretation of the experimental results.

Resumo

Neste trabalho são estudados os processos de isomerização conformacional numa série de ácidos carboxílicos (ácidos fórmico, acético e propiónico) isolados em matrizes de gases raros (Ar, Kr e Xe). A isomerização conformacional induzida por excitação vibracional é investigada através do uso de uma fonte de radiação infravermelha com uma largura de banda de aproximadamente 0.1 cm^{-1}. São analisados os efeitos da natureza do modo vibracional excitado, energia de excitação, ambiente e deuteração no rendimento quântico de isomerização. Este trabalho pretende também contribuir para o estudo do efeito túnel em fase condensada, ao analisar a isomerização conformacional do grupo carboxílico na ausência de radiação. Neste contexto, são investigados os efeitos da temperatura, ambiente e deuteração. A selectividade conformacional exibida pela fotoquímica dos ácido fórmico e acético é testada através do estudo da influência da conformação na determinação dos caminhos de fotodecomposição dos monómeros destes compostos isolados em matrizes. São usados cálculos teóricos para auxiliar a interpretação dos resultados experimentais.

List of original publications

This thesis is based on the following publications, which shall be referred to by the Roman numeral I-IX in the text:

I. *Vibrational spectroscopy of cis- and trans-formic acid in solid argon.*
Ermelinda M. S. Maçôas, Jan Lundell, Mika Pettersson, Leonid Khriachtchev, Rui Fausto and Markku Räsänen *J. Mol. Spectrosc.* **2003**, *219*, 70-80.

II. *Reactive vibrational excitation spectroscopy of formic acid in solid argon: Quantum yield for infrared induced trans→cis isomerization and solid state effects on the vibrational spectrum.*
Ermelinda M. S. Maçôas, Leonid Khriachtchev, Mika Pettersson, Jonas Juselius, Rui Fausto and Markku Räsänen *J. Chem. Phys.* **2003**, *119*, 11765-11772.

III. *Cis→trans conversion of formic acid by dissipative tunneling in solid rare gases: Influence of environment on the tunneling rate.*
Mika Pettersson, Ermelinda M. S. Maçôas, Leonid Khriachtchev, Jan Lundell, Rui Fausto and Markku Räsänen *J. Chem. Phys.* **2002**, *117*, 9095-9098.

IV. *Infrared-induced conformational interconversion in carboxylic acids isolated in low-temperature rare-gas matrices.*
Ermelinda M. S. Maçôas, Leonid Khriachtchev, Mika Pettersson, Jan Lundell, Rui Fausto and Markku Räsänen *Vib. Spectrosc.* **2004**, *34*, 73-84.

V. *Rotational isomerism in acetic acid: The first experimental observation of the high-energy conformer.*

Ermelinda M. S. Maçôas, Leonid Khriachtchev, Mika Pettersson, Rui Fausto and Markku Räsänen *J. Am. Chem. Soc.* **2003**, *125*, 16188-16189.

VI. *Photochemistry and vibrational spectroscopy of the trans and cis conformers of acetic acid in solid Ar.*
Ermelinda M. S. Maçôas, Leonid Khriachtchev, Rui Fausto and Markku Räsänen *J. Phys. Chem. A* **2004**, *108*, 3380-3389.

VII. *Rotational isomerism of acetic acid isolated in rare-gas matrices: Effect of medium and isotopic substitution on IR-induced isomerization quantum yield and cis→trans tunneling rate.*
Ermelinda M. S. Maçôas, Leonid Khriachtchev, Mika Pettersson, Rui Fausto and Markku Räsänen *J. Chem. Phys.* **2004**, *121*, 1331-1338.

VIII. *Internal rotation in propionic acid: Near-infrared induced isomerization in solid argon.*
Ermelinda M. S. Maçôas, Leonid Khriachtchev, Mika Pettersson, Rui Fausto and Markku Räsänen, *J. Phys. Chem. A*, **2005**, *109*, 3617-3624.

IX. *Rotational isomerization of small carboxylic acids isolated in argon matrices: Tunneling and quantum yields for the photoinduced processes.*
Ermelinda M. S. Maçôas, Leonid Khriachtchev, Mika Pettersson, Rui Fausto and Markku Räsänen *Phys. Chem. Chem. Phys.* **2005**, *7*, 743-749.

Contents

Preface

This publication covers the work done by the author in collaboration with the group of Photochemistry and Molecular Spectroscopy of the University of Coimbra, Portugal, and the group of Physical-Chemistry of the University of Helsinki, Finland, to be presented for discussion at the University of Coimbra in order to obtain the PhD in Chemistry.

Primarily, the aim of the study here presented was to investigate photochemically induced conformational isomerization processes in a series of carboxylic acids isolated in low-temperature rare-gas matrices (4-60 K). The targeted molecules were formic (HCOOH, FA), acetic (CH_3COOH, AA) and propionic (CH_3CH_2COOH, PA) acids. The molecules isolated in solid rare gases were excited with near (NIR) and mid-infrared (MIR) light and the conformational changes induced were monitored by infrared (IR) absorption spectroscopy. One of the main motivations of this work was to investigate the influence of the nature of the excited mode over the course of the particular type of unimolecular reactions considered. This issue has attracted much attention over the years, but only very specific clear-cut examples of mode-selective photochemistry have been reported so far. The possibilities of using laser sources to drive selective chemical reactions were realized quite early after their emergence. Ideally, excitation of a particular vibrational mode would cause the bond or functional group where the energy is deposited to undergo a chemical reaction, giving the desired product. However, in practice, energy relaxation processes can quickly deactivate the initially excited mode. The properties of the narrowband radiation source used in the experiments here reported, with a range of tuneability extending from the ultraviolet (UV) to the MIR, allowed us to study the effect of the nature of the excited vibrational mode on the rotamerization quantum yields, as well as the effect of local environment, excitation energy and isotopic substitution.

Additionally, whenever relevant, the effect of thermal excitation on the rotamerization process was also investigated.

The conformational equilibria were also characterized by theoretical methods, giving a valuable contribution to the analysis of the experimental data. An investigation of the structural, energetic and vibrational properties of the targeted molecules was performed by ab inito calculations at different levels of theory.

Preliminary indications on the importance of the tunneling effect for rotamerization of formic acid have open the way for extensive studies of dark isomerization processes. A lot of effort was put into understanding the mechanism behind the observed rotamerization at energies below the reaction barrier. In this quest, the effects of medium, local environment, isotopic substitution and temperature on the tunneling rate were addressed for the two studied molecules exhibiting a biconformational framework (formic and acetic acids).

The electronic excitation of formic and acetic acids with ultraviolet (UV) radiation was also undertaken in order to investigate the possibility of conformationally selective photolysis. If different conformers can be photolysed to give different products, the control of conformational population through vibrational excitation can be used to control the outcome of photodecomposition. This possibility can be presented as an attractive and much simpler approach to the control of reactivity, when compared with the very sophisticated laser methods that have been reported as successful for certain carefully selected molecular systems.

The present publication consists of four chapters. In the first chapter a brief description of the current status of knowledge of conformational isomerization is given, with specific emphasis over isomerization of carboxylic acids and related compounds. The technique of matrix isolation IR spectroscopy is introduced and some relevant aspects of conformational isomerization studies in rare-gas matrices are presented that might be useful for readers less familiarized with the subject. The experimental and computational methods are described in the second chapter. The third chapter contains the main results obtained for each of the molecules studied,

according to the nature of the studied phenomena: characterization of the conformational equilibrium, tunneling, isomerization quantum yield and selectivity of UV induced photolysis. An exhaustive analysis of the results can be found in the papers published earlier in international scientific publications reproduced as appendixes (papers I-IX). The present work is dedicated to summarize the results obtained and extract general conclusions from the systematic studies undertaken within the scope of the PhD project of the author. Final conclusions and achievements of this systematic investigation are presented in the fourth chapter, where the author leaves also some ideas about possible future developments to the present understanding of the issues here addressed.

1. Introduction

The present study of conformational isomerization in rare-gas matrices is concentrated in a series of simple carboxylic acids: formic (FA), acetic (AA) and propionic (PA) acid. The conformational studies on the chosen set of molecules can aid to understand the reactivity of biologically relevant molecular systems, where the conformational properties of the carboxylic group play an important role.[1-4] Small carboxylic acids are frequently used as model compounds to study a variety of chemical phenomena. To have an idea on how exhaustively studied this molecules have been we can consider a simple search in the *ISI Web of Knowledge* (http://isi15.isiknowledge.com/) for scientific papers containing the name of one of the studied molecules in the title. This search will give a rhythm of 50, 90 and 290 papers a year containing the words *propionic acid*, *formic acid* and *acetic acid* in the title, respectively. Simple organic molecules like carboxylic acids are also compounds of astrophysical interest. Both, FA and AA have already been detected in the interstellar space.[5,6] One of the theories of formation of life on Earth believes that the known interstellar organic molecules could have been important in prebiotic synthesis once delivered to the early Earth by impact with asteroids and comets. Conformational analysis is also important in this active field of search for the presence in the interstellar space of larger organic molecules. One should know which conformer to look for and how the possible stable geometries of the searched molecules can be characterized spectroscopically.[7] Interestingly, IR-absorption spectroscopy of matrix-isolated polyaromatic hydrocarbons has been used by the NASA-Ames Research Group to create a basis set of spectrocopically relevant data to access the presence of this type of molecules in the interstellar space by comparison with astronomic data.

The particular choice of the molecular systems studied takes advantage of the experience of the two research groups participating in this investigation (the Group of

Physical-Chemistry of the University of Helsinki and the Group of Photochemistry and Molecular Spectroscopy of the University of Coimbra) in the characterization of the conformational equilibrium of carboxylic acids and some of their derivatives. Most of these studies result from an independent research of the two groups [8-27] but some were already born from an earlier collaboration between them.[28-31]

1.1 Conformational properties of carboxylic acids

It is widely acknowledged that both the carboxylic and the ester groups adopt preferentially a planar geometry, with two stable arrangements differing by internal rotation about the C-O bond, as represented in Fig.1.1. Generically, for carboxylic acids and esters, these two stable arrangements can be denoted by *trans* and *cis*, for R_1-C-O-R_2 dihedral angles of 180º and 0º, respectively. Unless specific interactions like intramolecular hydrogen bonding or strong electrostatic interaction between the R groups are active, the conformational ground state exhibits a *trans* arrangement. An illustrative example of specific interactions stabilizing the *cis* arrangement can be found in some dicarboxylic acids, where strong intramolecular hydrogen bonds make of the *cis* arrangement the conformational ground state.[12,27,29-31,IV]

The origins of the energy difference and internal rotational barriers in carboxylic acids and esters have been analysed to some extent by theoretical studies. The computationally predicted relative energies and energy barriers between the two arrangements are similar for simple carboxylic acids and esters, where the R groups are either hydrogen or small alkyl groups. The *cis* arrangement is predicted to be higher in energy by 1700-3000 cm^{-1} (20-35 kJ/mol)* and the barrier heights lay within the 4300-4600 cm^{-1} (50-55 kJ/mol) range.[32-35] It is believed that the main reason for the lower energy of the *trans* arrangement lays in the stabilizing effect of a nearly antiparallel alignment of the C=O and O-R_2 bond dipoles and the existence of more

* 1kJ/mol= 83.5935 cm^{-1}

relevant steric and electrostatic repulsions between the R groups destabilizing the *cis* arrangement. The relevance of these two factors can be supported by the lower total dipole moments and the smaller R_1-C-O angles for the *trans* as compared to the *cis* arrangement.[32] The possibility of a stabilizing effect due to intramolecular hydrogen bonding for the *trans* arrangement in the carboxylic acids (C=O…HO) is not supported by the similar relative energies in acids and esters.

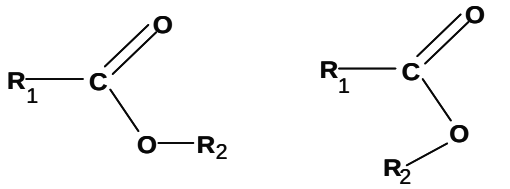

trans (R_1-C-O-R_2 = 180º)

cis (R_1-C-O-R_2 = 0º)

Fig. 1.1 – Stable arrangements of the carboxylic (R_2= H) and ester groups with respect to rotation around the C-O bond.

Electronic delocalization within the O=C-O-R fragment (mesomerism O=C-O-R ↔ $^-$O-C=O-R^+) has also been pointed out as an important stabilizing effect of planar conformations, being more relevant for the *trans* arrangement.[8,20,24,33] However, K. B. Wiberg, who has paid great attention to the computational study of barriers to rotation adjacent to double bonds,[32,36-39] believed that electronic delocalization was not an important factor because the C=O and C-O bond lengths maintained, respectively, their double and simple bond character during rotation about the C-O axis. Giving the example of AA in one of his most relevant papers, Wiberg admits the existence of important changes in the length of the C-O bond, but considers the C=O bond as hardly affected by internal rotation.[32] However, the results obtained by higher level ab initio calculations show that the effect of electronic delocalization is

by no means irrelevant, as pointed out in several studies. [8,20,24,33] For AA, it can be seen in Fig. 1.2 that both C=O and C-O bond lengths are affected by isomerization. Even thought the relative changes are higher for the C-O bond, the changes in the C=O bond length should not be neglected. Indeed, the potential energy curve for the C-O internal rotation in AA nicely follows the difference in the C=O and C-O bond lengths (Fig. 1.2). As the length of these two bonds become closer the conformational energy decreases. In fact, the use of a higher level of theory brings very little changes to the numerical data obtained, but the interpretation here made supports a significant effect of the electronic delocalization within the O=C-O-R fragment, in opposition to the interpretation made before by Wiberg based on calculations at a lower level of theory. Qualitatively similar results are obtained for FA.

The small molecular size of FA and AA makes them specially attractive to computational modelling. FA is particularly interesting because it is the simplest organic acid exhibiting rotational isomerism. Computationally, both FA and AA are equally well characterized. The calculation of energies, structures and fundamental vibrational modes of the two conformers have been reported using fairly sophisticated methods [e. g. Configuration Interaction with Single and Double excitation (CISD)[40] and Møller-Plesset to the forth order (MP4)[41]] with relatively large basis sets. When compared to FA, AA has one more internal rotational degree of freedom in addition to C-O rotation, the C-C rotation. However, there is only one stable arrangement with respect to the C-C bond, which has the in-plane hydrogen atom of the methyl group eclipsed with the carbonyl bond (see Fig. 1.3).[41] The characterization of the conformational system of these two molecules by experimental methods has not been so successful. The *trans* conformer of both molecules has been exhaustively studied experimentally, but very little is known about the *cis* conformer. In fact, *cis*-AA was experimentally detected for the first time in the present work.[V]

There have been many unsuccessful attempts to detect *cis*-FA; some of them have been reported.[42] The first unequivocal identifications of *cis*-FA were made by Hockings and Bjarnov using microwave spectroscopy.[43,44] From these studies a

relative energy of 1365 cm^{-1} and a barrier height as seen from the bottom of the *trans* potential well (*trans* → *cis*) of 4852 cm^{-1} have been estimated. The lack of experimental data on the *cis* conformers is not surprising, considering that their

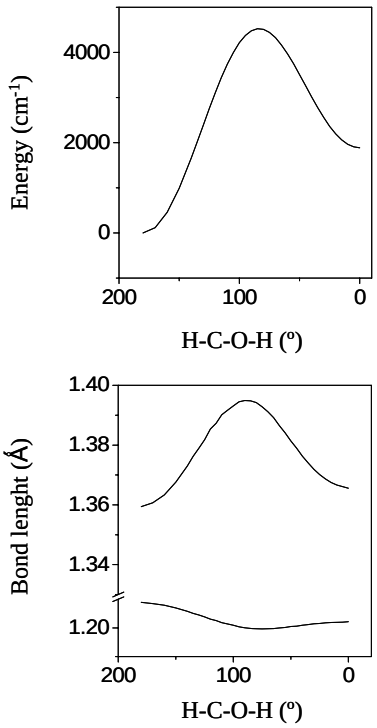

Fig. 1.2 - Potential energy curve for rotational isomerization within the carboxylic group (upper plot) and variation of the C=O and C-O bond lengths along the isomerization path (lower plot). Results obtained for AA at the MP2/6-311G(2d,2p) level of theory.

relatively high conformational energies lead to Boltzman population ratios at room temperature of P_{cis}:P_{trans} ~ 10^{-3}. Thermal decomposition at moderately high temperatures may complicate to some extent thermal population of the higher energy

conformer.[45-48] However, the true reason why it has been so difficult to observe the *cis* conformers might have been revealed by a study of conformational isomerization of FA isolated in rare-gas matrices induced by narrowband NIR irradiation.[10] In that work, *cis*-FA was produced from excitation of the O-H stretching overtone (2νOH) of *trans*-FA isolated in low-temperature argon matrices.[10] IR-absorption spectroscopy was used to identify 8 out of the 9 IR-active fundamentals and a few overtones of *cis*-FA, based on ab initio calculated vibrational frequencies. More importantly, it was found that *cis*-FA was rapidly converting back to the conformational ground state in dark, even at the very low temperatures used (15 K). Since the mechanism for internal rotation within the carboxylic group can be expected to be similar for the three molecules considered in the present work (rotation about the C-O axis, involving mainly motion of the light hydrogen atom), the *cis* $\rightarrow$ *trans* tunneling appears as a possible limiting phenomenon for the study of the higher-energy *cis* conformers in the targeted carboxylic acids.

Conformational isomerization in PA has also deserved some attention from the computational point of view.[33,34,36] As for FA and AA, PA is expected to have two stable geometrical arrangements with respect to the C-O bond. Additionally, PA is expected to exhibit rotational isomerism around the C_α-C bond.[33,34,36] Two stable arrangements with respect to the C_α-C bond are predicted, the *trans* and *gauche* arrangements (C-C-C-O dihedrals of 180º and *ca.* ±60º, respectively), with relatively low energy differences (300-500 cm^{-1})[33,36] and small energy barriers (400 cm^{-1})[34,36] separating them. All together, PA should have four non-degenerated conformers, build up from the combination of the two possible stable arrangements around the C-O and C_α-C bonds, as shown in Fig. 1.3. To the best of our knowledge, the vibrational characterization of the conformational equilibrium by computational methods was not reported hitherto. Experimentally, only one conformer of monomeric PA has been unequivocally characterized, the conformer T_t in Fig. 1.3.[49-51] Both gas-phase electron diffraction and microwave spectroscopy studies have shown that this conformer exhibits a planar heavy-atom backbone, with a staggered arrangement around the

C_β-C_α bond and *trans* arrangements around the C_α-C and C-O bonds (C-C-C-O and C-C-O-H dihedral angles of 180º).[49-51] Moreover, the electron diffraction results suggested that, in addition to the identified conformer, structures bearing a non-planar heavy-atom skeleton should also contribute to the equilibrium conformational distribution in the gas phase, with an estimated population of *ca.* 40% (at T= 488 K).[49]

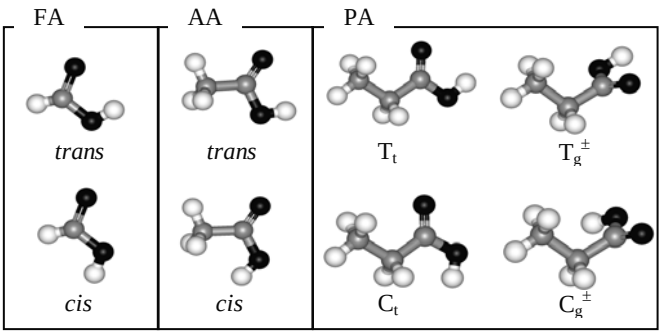

Fig. 1.3 – Conformers of FA, AA and PA.

From the above mentioned, it can be concluded that a convenient approach to the experimental study of conformational isomerization in the targeted carboxylic acids is to use rare-gas matrix isolation as sampling technique, combined with narrowband vibrational excitation to produce the higher energy species from the lower energy forms and IR-absorption spectroscopy to probe changes in the conformational distribution. Ab initio calculations of vibrational frequencies can be used to support the interpretation of the experimental data. In the present study, the approach just described will be applied to the structural and vibrational characterization of the conformational equilibria and, most importantly, to improve our knowledge on the dynamics behind conformational isomerization either induced by vibrational excitation or taking place due to tunneling. Finally, the conformational-selective photochemistry, namely UV-photolysis, will be studied once we know how to control to the conformational distribution.

1.2 Rare-gas matrix isolation

Matrix isolation is now a well established sampling technique, where the molecules of the compound to be studied (guests) are preserved at very low temperature and concentration in a solid medium (host). The idea of investigating atoms and molecules in inert cryogenic matrices emerged in the 50's by Pimentel and coworkers.[52] By then the emphasis was on the spectroscopic investigation of transient species isolated in rare-gas matrices (*e. g.* Ne, Ar, Kr, Xe). The effective transparency to radiation of rare-gas matrices, going from the far-IR to vacuum-ultraviolet (VUV), combined with the lack of appreciable diffusion of the isolated species at the low work temperatures, suppressing bimolecular reactions, and the relatively weak guest-host interactions fuelled the use of this technique in the study of transient species. Molecules with very short lifetimes in fluid conditions were now stable in rare-gas matrices in their ground electronic state and could be studied by a variety of spectroscopic methods. Several reviews and books have been published where the reader can find references to many interesting applications of matrix-isolation spectroscopy, [8,53-59] and even all the practical details necessary to build a matrix-isolation laboratory from scratch.[60]

Soon it was realised that rare-gas solids do not really constitute an inert medium. It is true that on average the perturbations suffered by the trapped species are relatively small, as illustrated by the shift between the matrix vibrational frequencies and the gas phase data (typically of 2%), but by no means negligible. These matrix induced shifts can be very significant for vibrational modes of high transition dipole moment.[13,56] Furthermore, inhomogeneities of the local environment experienced by the isolated molecules cause the so called site-splitting effect, which splits the vibrational bands into multiplets due to slightly different local surroundings (matrix-sites).[61-66] These differences in the probed local environment can be due to different

orientations of the guest within a particular matrix cage, the existence of more than one type of cage or the occupation of cages including guest molecules as nearest or next-nearest neighbours.[66] The importance of the guest-host interactions is so that in cases where the energy difference between the conformers is very small this "solvation term" can cause an inversion of the relative stabilities in comparison with those expected for the molecule in the gas phase.[67,68] Gradually, scientists became more and more interested in the nature of guest-host interactions and started to approach this medium as a prototype solvent for the study of photochemistry and photophysics in the condensed phase.

The non-inertness of rare gases is ultimately demonstrated by the active research in rare-gas chemistry born after Bartlett's synthesis of the first compound containing a rare-gas atom, $Xe^{+}[PtF_6]^{-}$, in 1962.[68] Recent developments in several directions, among which the synthesis of novel rare-gas compounds, have triggered the renaissance of rare-gas chemistry during the last decade.[69,70] Many of these novel compounds have been produced in rare-gas matrices and they fall into two categories: *(1)* rare-gas hydrides of general formula HRgY [where Rg can be Xe, Kr or Ar and Y is an electronegative fragment (*e. g.* I, Br, Cl, F, CN, NC, SH, OH) [71-73]] and *(2)* insertion compounds of rare gases into unsaturated hydrocarbons (*e. g.* $HXeC_2H$, $HKrC_2H$, $HXeC_4H$ and $HKrC_4H$).[74,75] From the lighter rare gases (He, Ne and Ar) HArF is up to date the only experimentally known compound, meaning that they are far more inert than Kr, Xe or Rn.

Vibrational spectroscopy in low-temperature rare-gas matrices is a very commonly used method in the study of conformational isomerization due to the possibility of trapping the less stable conformers by preventing thermal reactions and molecular encounters. The rigidity of the matrix cage has an additional advantage for vibrational spectroscopy, connected with the suppression of rotational motion for most of the molecules bigger than water. Elimination of the rovibrational structure simplifies the spectra in comparison with gas-phase spectra and makes their interpretation easier when based on commonly available spectral simulation tools. The

narrower bandwidths of the spectra recorded in low-temperature matrices allow to resolve absorptions arising from different conformers even when they differ by only a few wavenumbers, which can be a non-trivial or even impossible task in the gas phase or in solution.

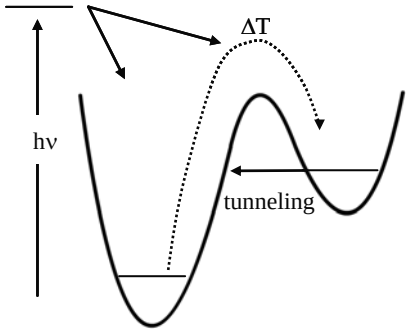

Fig. 1.4 – Representation of possible mechanisms of rotamerization within the carboxylic group: thermal (ΔT) and photochemically (hν) induced processes and rotamerization by tunneling.

A matrix isolation sample can be prepared by deposition of a pre-mixed gaseous mixture or by co-deposition of the species to be studied (or a suitable precursor) and the support gas. In both situations the gas flux is directed towards a cold window kept at very low pressure (10^{-8}-10^{-10} atm) and temperature (4-60 K) inside a cryostat. Most frequently, the deposition procedure freezes instantaneously the sample and suppresses thermal reactions with significant activation energy (E_a > 400 cm^{-1}), hence enabling stabilization of the higher energy conformers already present in the gas phase. Thus, the conformational distribution of the gaseous sample is trapped in the matrix. However, the population of the higher energy conformers can be very low even in the room-temperature gaseous sample. Both thermal and photochemical excitations (IR or UV irradiation) have been exhaustively used to increase the population of the higher energy conformers. A rather unusual

phenomenon that will be also addressed in this work is isomerization by tunneling. As mentioned before, the spontaneous isomerization within the carboxylic group from the higher energy arrangement into the lower energy one is expected to take place for all the studied molecules. A schematic representation of the possible mechanisms of conformational interconversion is shown in Fig. 1.4 for a one dimensional torsional potential featuring internal rotation within the carboxylic group.

1.3 Thermally induced conformational isomerization

Thermal excitation can take place in the gas-phase sample prior to deposition or in the matrix after sample deposition. In the first situation, increasing the temperature will increase the population of the higher energy conformers.[15,76-78] The thermally induced changes in conformational distribution (typically following a Boltzmann distribution[†]) are more evident for lower energy differences among the conformers or strong thermal excitation, which frequently causes thermal decomposition as well.[79] Note that, in the best case scenario, for the carboxylic acids studied in this work ($\Delta E \sim 1700\text{-}3000$ cm^{-1}) it would be necessary to increase the temperature up to 800 K in order to have a detectable amount of the higher energy conformer in the gas phase. At those temperatures, the presence of decomposition products would most probably overshadow the identification of the higher energy conformers. Alternatively, annealing the matrix (heating the sample to a specific temperature and decreasing the temperature back to its initial value) can potentially promote dramatic changes in the metastable distribution of conformational states initially isolated in the matrix, which is assumed as characteristic of the temperature of the gaseous mixture before deposition.[80] The annealing process decreases the matrix

[†] $P_i / P_j = g_i / g_j \; exp\left(-\Delta E / RT\right)$, where i and j are different conformational states, P refers to population, g to degeneracy, ΔE is the relative energy, R is the rare gas constant and T refers to temperature.

rigidity, allowing for the metastable gas-phase equilibrium to be relaxed towards the effective low-temperature equilibrium. That is to say that the population of the conformational states of higher energy will be transferred into the lower energy states. This is exactly the opposite behaviour to that expected upon heating the gaseous mixture. It is evident that these conformational changes are only relevant if the higher energy forms are already present in the gas phase. Furthermore, since the higher temperatures available to perform annealing are limited by sublimation of the host (*e. g.* ~60 K in Xe), it has been shown that thermally induced isomerization can only take place at matrix temperatures for quite low barrier heights (E_a < 1700 cm^{-1} for rare-gas matrices).[56]

From the discussion above it can be concluded that thermal excitation promotes relevant conformational changes if the activation energy is higher than 400 cm^{-1}, so that the gas phase conformational equilibrium is efficiently trapped in the matrix, and lower than 1700 cm^{-1}, so that rotational isomerization can be induced upon annealing of the matrix. What happens if the activation energy falls outside this limited interval? For rotational isomerization processes with very low activation energies, a significant conformational cooling takes place during sample deposition and the conformational distribution in the solid sample approaches the one typical of the low matrix temperatures.[56,81] The extent of conformational cooling depends on the barrier height, relative energies and dipole moments of the conformers involved, and nature and temperature of the substrate.[68] Although conformational cooling seems to be an exception rather than a rule, exploitation of this phenomenon turned out to be a very interesting approach to the study of conformational isomerization of certain systems like glycine and dimethylglycine, glycolic and cyanoacetic acid, methyl cyanoacetate and dimethyl sulfite.[68,82-86] For internal rotation processes with higher activation energies, the only alternative to promote an efficient conformational isomerization is photochemical excitation.

1.4 Photochemically induced conformational isomerization

There are many examples of UV-induced conformational isomerization in the literature.[19,28,87-89] However, the high energies available upon UV excitation bear a great disadvantage over IR excitation. Frequently, upon UV excitation other unimolecular reaction channels became accessible (decomposition and molecular rearrangements involving bond breaking and bond forming processes) strongly competing with conformational isomerization.[88] This is the main reason why IR excitation has definitely became the excellence method for studies of photoinduced conformational isomerization.

A considerable number of studies have been dedicated to IR-induced rotamerization in low temperature-matrices since the pioneer studies on HONO by Pimentel and coworkers in the early 60's .[10,13,29-31,82,90-104] The earlier studies used broadband excitation together with filters to narrow the irradiation bandwidth, which only in the most favourable cases allowed to excite selectively one conformer. The selectivity of this approach is severely conditioned by the similarities between the vibrational spectra of different conformers. From the most recent studies, it is evident that narrowband tuneable laser light sources have opened a new world of opportunities for the study of photochemical processes. In the case of IR-induced conformational isomerization, they allowed for an extraordinary selectivity. It is now possible to choose the vibrational mode, the conformational state and even in which particular local environment within an inhomogeneous matrix to excite the targeted conformer. However, only a few examples are known in which narrowband irradiation was involved.[10,13,29-31,99-104] Indeed, even nowadays the access to expensive tunable IR sources is partially responsible for the limited number of systematic studies published concerning isomerization induced by vibrational excitation at relatively low energies.

Conformational isomerization takes place when enough energy is deposited into the reaction coordinate so that the system can overcome the energy barrier and pass into the products valley. The reaction coordinate for internal rotation around a

simple bond connecting two conformers is essentially described by the torsional mode associated with that particular bond. Frequently, direct excitation of the relevant torsional mode above the reaction barrier is not feasible because its absorption cross section is very low. Alternatively, the energy needed to overcome the isomerization barrier is introduced in the molecule by excitation of a more suitable vibrational mode (fundamental vibration or lower order overtone with appreciable absorption cross section). The excitation energy is later on partially transferred to the reaction coordinate. It can be anticipated that the quantum efficiency of the photoinduced isomerization process (isomerization quantum yield) reflect the dynamics of vibrational energy transfer.

1.4.1 Vibrational energy transfer

Molecular energy flow is a subject that has been reviewed extensively many times for both gas and condensed phases.[105-112] In contrast with the gas phase situation,[113] a quantitative understanding of dynamics of vibrational energy transfer in the condensed phase is still missing. For the isolated gas phase molecule (absence of collisions), the population of the initially excited state is redistributed to other intramolecular vibrational states maintaining the total energy constant. On the other hand, vibrational energy transfer in the condensed phase is ultimately a dissipative process, where the population of the vibrationally excited states is relaxed in a series of steps involving energy removal from the molecule by the solvent (population and energy relaxation).

Gas-phase and condensed-phase photochemistry are expected to differ quite much in many situations. Particularly relevant is the fact that for strong solute-solvent interactions, the potential energy surface for the isolated and solvated molecule can differ quite much, allowing processes to occur in one case that are not possible in the other.[111] Even in the case of photoisomerization in solid rare gases some environment induced effects can affect in a determinant way the efficiency of the process. This is the case of IR-induced isomerization of HONO that was shown to have a very high

quantum yield for the matrix isolated molecule (Kr, Ar, N_2) whereas it has not been reported in the gas phase so far.[13,91,114]

On the other hand, recent studies suggest that earlier times vibrational energy transfer can be very little affected by the solvent, being dominated by pure *intra*molecular vibrational energy *redistribution* (IVR)[‡].[112,115-118] For the isolated molecules in the gas phase, it is widely accepted that the lifetime of a given excited state depends on the mean-squared couplings of the excited state (also known as bright state) with the other vibrational modes (bath states) and the density of coupled states.[106] Thus, pure IVR dynamics is dominated by strong couplings involving nearly resonant vibrational states that can interact with the bright state through relatively low order terms of the intramolecular potential energy surface. To avoid a bottleneck in the energy flow, these states have to be in turn well coupled to additional near-degenerate states and so on. This hierarchical picture of pure IVR in the gas phase is known as the tier model because the energy redistribution proceeds via successive tiers of states coupled via specific low order anharmonic interactions.[106,110]

For a medium size molecule at low excitation energies the vibrational states that could be involved in the redistribution process are far from resonance. In this case, for the molecule in the condensed phase, pure IVR is expected to be less probable than in the high excitation energy regime, which is characterized by very high state densities (10-100 cm^{-1}).[106,110] The solvent vibrational modes (intramolecular or intermolecular modes, such as vibrons or lattice phonons) are expected to participate in the energy relaxation mechanism by compensating the energy mismatch between intramolecular vibrational states.[107,108] The mechanism of vibrational energy transfer described will be referred to as solvent-assisted IVR (phonon-assisted IVR for rare-gas isolated molecules). Additionally, pure *inter*molecular vibrational energy relaxation where all the excitation energy is transferred into the solvent can also take

[‡] The IVR acronym as been used in the literature indistinctively to designated both intramolecular vibrational energy *relaxation* and *redistribution* process. In this work pure IVR implies redistribution while solvent assisted IVR implies relaxation and the simple use of IVR refers to an undetermined process that can involve both relaxation and redistribution.

place. On the other hand, for the molecules isolated in solid rare gases at very low concentrations, intermolecular energy transfer pathways involving more than one solute molecule are very unlikely.

Diatomics in condensed phase are ideal systems to study solvent-assisted relaxation processes, since they constitute the prototypal case of an isolated excited mode. The reported excited state lifetimes measured for diatomics in rare gases generically agree with the theory of multiphonon relaxation[107,119] This theory leads to the "energy gap law" that predicts an exponential decrease in the relaxation rates with increasing energy mismatch between the molecular levels involved in the process, as a consequence of the increasing number of phonons needed to account for the energy gap. For small neutral solutes with little spectral overlap between solute and solvent, the excited state lifetime tends to be long (ns to s).[109,111] Relaxation rates for molecules like NO, CO or CN in rare-gas solids are often controlled by radiative processes due to the large number of phonons involved (high order phonon process).[105] On the other hand, for those diatomic molecules where the vibrational frequency approaches the Debye frequency of the lattice (< 100 cm^{-1}) the energy relaxation process can be extremely fast (ps to subpicosecond for Ca_2, I_2 and Cl_2).[109]

However, not even the case of diatomics in a rare-gas lattice can be simply reduced to the evaluation of energy gaps. For small molecules, the participation of rotational or librational (hindered rotation) energy levels may open additional relaxation channels.[109] Furthermore, the coupling of vibrational modes with rotational degrees of freedom is expected to be stronger than vibrational-phonon coupling due to the fact that the rotational quanta are in general larger than the lattice phonons. Therefore, coupling to rotational or librational states is frequently a lower-order process than vibrational-phonon coupling.[109]

For polyatomic molecules, the energy transfer process in the condensed phase is far more complicated due to the huge number of possible relaxation pathways. However, relaxation of the lowest frequency vibrational mode of a polyatomic molecule should not differ much from that of a diatomic with similar frequency.

Relaxation at moderate excitation energies should additionally reflect the intramolecular anharmonic couplings. At very high excitation energies, when the spacing between intramolecular levels is much lower than the phonon frequencies, vibrational energy transfer approaches a pure IVR phenomenon that can still be affected to some extent by the solid host via modulation of the intramolecular potential. In rare-gas solids, the size of the rare-gas atoms, polarizability and geometry of the matrix site can potentially affect the guest-host interaction potential and consequently the vibrational energy relaxation/redistribution dynamics.[92,105,109] The importance of these factors to the dynamics of energy transfer in the condensed phase is not yet completely understood. Despite the fact that the lifetimes of excited vibrational states of polyatomic molecules are now available in the condensed phase (particularly in solution) for a significant number of polyatomic molecules much less is known about the mode specific relaxation mechanism. [112,115-118]

1.4.2 Isomerization quantum yield

In order to illustrate the complexity of the process, a rough scheme showing how the selective excitation of a vibrational mode other than the torsional mode could lead to conformational isomerization is shown in Fig. 1.5. From the initially excited vibrational mode (ν_{exc}) the energy is transferred into other vibrational modes of the guest molecule (ν_{bath}) coupled to the excited mode. The host lattice is expected to participate in this process by absorbing or emitting phonons that will compensate for the energy gap between the intramolecular states involved. The lattice represents a quasi-continuum of energy levels that constitute an external thermal bath capable of dissipating part of the excitation energy. Eventually, during this complex relaxation mechanism part of the excitation energy is transferred into some excited torsional state (ν_{tors}), that is to say that it is transferred into the reaction coordinate. The classical view is that if the excitation energy reaches the reaction coordinate at energies above the isomerization barrier then conformational isomerization will take place. Later it will be shown that one of the results of the present work reveals the importance of

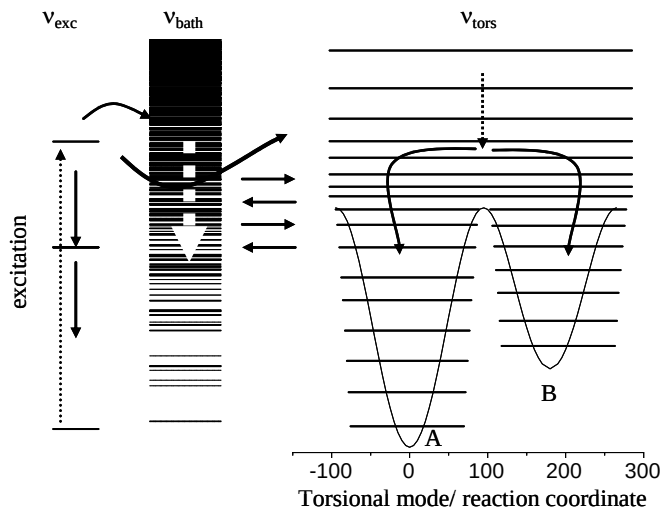

Fig. 1.5 – Schematic representation of the possible energy relaxation pathways following excitation of a specific vibrational mode (ν_{exc}), with special emphasis on those pathways that transfer energy into the reaction coordinate for internal rotation (ν_{tors}). The bath states (ν_{bath}) are constituted by all the other intramolecular vibrational states. The lattice phonons are assumed to constitute a quasi-continuum of intermolecular bath states and are not explicitly represented in this figure.

isomerization below the barrier to fully understand the process of internal rotation within the carboxylic group.

Clearly, the conformational isomerization quantum yield depends on the probability of energy transfer from the excited vibrational level to the reaction coordinate. Thus, the isomerization quantum yield depends on the balance between the efficiency of reactive and non-reactive energy transfer channels, determined by the dynamics of energy transfer.

Several studies of the IR-induced conformational isomerization quantum yields determined after narrowband irradiation of matrix-isolated molecules have been already reported. For matrix-isolated 2,3-difluoropropene ($H_2FC\text{-}CF\text{=}CH_2$), the

quantum yield for isomerization around the C-C bond was shown to depend on the excitation energy, host matrix, and also on the nature of the excited mode, ranging from 10^{-4}-10^{-7}.[100] For CH_2D-CH_2D in solid Kr, the effect of the nature of the excited vibrational mode on the isomerization efficiency was studied by resonant excitation of a number of vibrational states of the *gauche* and *trans* conformers. [102] It was concluded that the quantum efficiency for internal conversion increases with the excitation energy (varying by two orders of magnitude from 1000 cm^{-1} to 3000 cm^{-1}).[102] In this study, the observed deviations (as high as one order of magnitude) from the underlying monotonous increase of the quantum yield with excitation energy were attributed to specific intramolecular interactions controlling the dynamics of the energy relaxation.[102] This study also supports a strong effect of the environment over the isomerization quantum yield, increasing in the series Ar, Kr, Xe.

For HONO isolated in solid Kr, the photoinduced isomerization exhibits mode specific behaviour, with the efficiency of both *cis* $\rightarrow$ *trans* and *trans* $\rightarrow$ *cis* isomerization processes being ~ 2.5 times higher for excitation of the OH stretching fundamental (νOH at 3550 cm^{-1}) as compared with the first N=O stretching overtone (2νN=O, 3340 cm^{-1}),[13] despite the similar energies of these modes. Furthermore, for excitation of the νOH of HONO, the *cis* $\rightarrow$ *trans* isomerization quantum yield approaches unity while it is roughly seven times smaller for the reverse reaction.[13] A quantitatively similar result was also obtained from earlier studies of the molecule isolated in N_2, which seems to indicate that the environment has very little influence over the isomerization quantum yield, in contrast with the observed behaviour for the other two molecules referred above.[91] Studies on conformational isomerization of 1,2-ethanediamine in solid Ar ($NH_2CH_2CH_2NH_2$), induced by mode selective excitation (CH_2 and NH_2 stretches) using narrowband pass filters, also reported contradictory results by claiming that the quantum yield is independent of the excited vibrational mode.[98]

Interestingly, site-selective excitation (excitation of molecules isolated in specific sites) of HONO and oxalyl fluoride (FOC-COF) have demonstrated quite

clearly that the isomerization process is localized at the excited site, therefore suggesting that the matrix cage has a small participation in the isomerization process and intermolecular energy transfer among molecules isolated in different sites is negligible.[13, 104]

The brief overview just presented concerning conformational isomerization shows that systematic studies are needed in order to improve the present understanding of IR-induced conformational isomerization in the condensed phase. The results reported so far seem to be contradictory in many aspects. It is believed that the contribution of the present study can be very relevant to this topic.

1.5 Conformer-selective photochemistry

Although far from being a consensual subject, there are now many studies supporting the local nature exhibited by vibrational energy transfer, even in the condensed phase. The non-statistical behaviour of vibrational energy flow is a great stimulus to the possibility of laser control of chemical reactivity. This control is possible if the rates of vibrational energy transfer can be manipulated to allow for long-lived, bond-localized excitations. Two different approaches have been applied so far: molecular and laser pulse engineering. In the first case the molecules should be modified to have groups that freeze the energy transfer process so as to enhance reactivity towards some pre-determined reaction channel connected to excitation at a specific site.[111, 112] In the second case, tailored pulses and multiple pulse trains have been used to drive the system into the desired pathway, frequently based on an *a priori* detailed knowledge of the molecular Hamiltonian.[120,121]

Recently, the state-of-the-art in laser technology has allowed the scientists to turn into a new paradigm in the optical control of reactivity, known as optimal control. This approach assumes that there is an optimal electric field needed to achieve a specific target, which can be determined by computer algorithms based on statistical

methods operating on a trial and error basis.[122-125] The optimal control methodology claims the great advantage that the molecular Hamiltonian does not need to be known. Evidently, most of the work in this field is focused on isolated molecules in the gas phase, where the phenomena of vibrational energy transfer is relatively well understood and the complications of solvent interactions are not present.

In this work, a much simpler and modest approach to laser control of chemical reactivity exploring the possibility of conformer selective photochemistry will be tested. Exercising control over the conformational structure is a potential way to affect the product distribution of subsequent reactions where a well-defined nuclear arrangement is required to enter a given reaction path.

1.6 Conformational isomerization by tunneling

The case of intramolecular tunneling through a symmetric double-well potential has been extensively studied using supersonic expansion techniques and even matrix isolation combined with various spectroscopic methods that allow to measure the tunneling induced splitting of energy levels. The exhaustive investigation of intramolecular tunneling in symmetric double-well potentials contrast with the lack of extensive experimental evidence of tunneling for asymmetric double-well potentials of considerably high barriers. The fundamental difference between these two situations is that in the symmetric potential case the energy levels involved in the tunneling are resonant while in the asymmetric case they are off-resonance. It is believed that even small departures from symmetry can have dramatic effects on the tunneling probability.

The tunnel effect is a consequence of a non-vanishing probability for quantum–mechanical particles to cross a finite potential barrier even when their total energy is lower than the energy barrier. Since the manifestation of the wavelike properties are inversely related to the particle mass, the tunnel effect is usually

recognized experimentally by a strong decrease of the reaction rate due to substitution of the tunneling particle by an heavier isotope. Deviations from the Arrhenius equation[§] at low temperatures determined by apparently lower activation energies (E_a) and higher pre-exponential factors (A) than those predicted for the classical system are also indicative of appreciable tunnel effect.[126]

The study of tunneling in the condensed phase is a very active area of research. The theoretical investigations are now reaching the stage where comparison with experimental data is becoming possible.[127-129] However, the lack of consistent systematic experimental studies addressing the importance of some of the factors affecting the tunneling in condensed media (e. g. temperature and environment) prevents a clear understanding of the mechanism.

Conformational isomerization within the carboxylic group involves essentially the motion of the hydrogen atom. Thus, the tunnel effect can be quite important at the low temperatures used in rare-gas matrix-isolation studies. Stimulated by the observation of tunneling in FA reported earlier, [10] one of the goals of the present work was to investigative in detail the intramolecular tunneling mechanism in carboxylic acids isolated in low-temperature rare-gas matrices. The studied systems can be regarded as prototype for intramolecular tunneling in asymmetric double-well potentials of considerably high barriers. Curiously, by the time the first manuscript on the subject was under preparation,[III] Akai *et al* reported the observation of tunneling of hydroquinone (HYQ) in solid Ar and Xe, which was interpreted as a case of isomerization by tunneling through a nearly-symmetrical double-well (measured conformational energy differences of ~16 cm^{-1} in solid Xe).[130] Shortly after that, the same authors reported, almost simultaneously with the publication of the paper on FA tunneling,[III] the observation of conformational isomerization by intramolecular tunneling through a truly asymmetrical double-well potential (ab initio conformational

---

[§] $k(T) = A\exp\left(-E_a / k_B T\right)$, where A is the pre-exponential factor, E_a the activation energy, k_B the Boltzmann constant and T refers to temperature.

energy difference of 1800 cm^{-1}).[131] It is also relevant to mention the studies of tautomerization (thiol→thione and selenol→selenone) by proton transfer through an extremely high energy barrier (~ 8000 cm^{-1}) recently reported for thiourea, dithiooxamide and selenourea in low-temperatures rare-gas matrices.[132-134]

As mentioned before, for tunneling of a bound particle in an asymmetrical double well potential, the intramolecular energy levels involved in the process are not resonant.[135] Thus, the observation of a fast *cis* → *trans* isomerization of FA in solid Ar by tunnel effect suggests that the phonon modes are participating in a dissipative tunneling mechanism similarly to the mechanism of relaxation of vibrational energy in a condensed environment.[128,129,136-139] The tunneling rates may depend on the temperature, if thermally populated excited states of the torsional coordinate have a relevant participation as initial tunneling states.[126,140] On the other hand, in the condensed media various mechanisms have been proposed to be responsible for a thermally assisted tunneling, even for a process starting from one specific vibrational level (e. g. energy exchange of the tunneling system with phonons or barrier modulation due to intermolecular vibrations along the tunneling direction).[128] The magnitude of this thermal effect depends on the strength of the solute-solvent interactions. Therefore, a dissipative tunneling mechanism is supposed to depend on the environment as well as on the temperature. However, particularly for the case of H-atom tunneling, the solvent dependence of the tunneling mechanism is still an unclear aspect. There are many examples from studies of intramolecular H-atom tunneling in condensed media of tunneling rates and isotopic effects insensitive to the solvent.[126, 141-144]

2. Methods

2.1 Experimental details and methodology

2.1.1 Sample preparation

The gaseous samples were prepared by mixing the carboxylic acids (>99%), degassed by several freeze-pump-thaw cycles, with high purity rare gases (99.9999%), in the 1:500 to 1:2000 ratio. Exceptionally, the hydroxyl-deuterated PA isotopologue (PA-OD) and the methyl-deuterated isotopologue of AA (AA-CD_3) were obtained from fully-hydrogenated PA (PA-OH) and perdeuterated AA (AA-D_4) by H/D exchange on the inner surface of the sample container and the deposition line saturated with D_2O and H_2O, respectively.[VI,VIII] The gaseous mixtures were deposited onto a CsI substrate kept at 15 K (Ar), 25 K (Kr) or 35 K (Xe), in a closed-cycle helium cryostat (APD, DE 202A) and subsequently cooled down to 8 K.

2.1.2 IR absorption measurements

The FTIR absorption spectra (7900 – 400 cm^{-1}) were measured with a Nicolet SX-60 FTIR spectrometer. A liquid-nitrogen-cooled MCT detector and a Ge/KBr beamsplitter were used to record the MIR absorption spectra, with spectral resolution from 0.25 to 1.0 cm^{-1}. A liquid-nitrogen-cooled InSb detector and a quartz beamsplitter were used to record the NIR absorption spectra, with spectral resolution of 0.5 cm^{-1}. Typically 100 to 500 interferograms were co-added.

In the case of FA, it was realized that the spectrometer radiation source was affecting the isomerization equilibrium. The use of an interference filter blocking glowbar radiation above ~ 1500 cm^{-1} (F_1 in Fig. 2.1) allowed to suppress processes induced by the spectrometer radiation source, leaving an open spectral window sufficiently wide to monitor the conformational distribution of the sample.[II] This procedure was used during the measurements performed to determined the FA

quantum yields and tunneling kinetics for isomerization within the carboxylic group (C-O isomerization).[II,III] Additionally, in some experiments (measuring pumping kinetics, evaluating conformational distribution under pumping and recording high resolution spectra of unstable conformers) it was necessary to record the IR spectra during irradiation.[I,VI,VIII] In order to do that, the pumping beam was quasi-collinear with the spectrometer beam, and interference filters (F_2 in Fig. 2.1 transmitting in the 7900-4000 cm^{-1}, 3650-3400 cm^{-1}, 2000-500 cm^{-1} or 3300-1100 cm^{-1} regions) were placed in front of the detector to prevent its exposure to the pumping radiation while recording spectra. [I,VI,VIII]

2.1.3 IR and UV irradiation

A schematic picture of the setup used for the irradiation experiments is presented in Fig 2.1. Tunable pulsed IR radiation provided by an optical parametric oscillator (Continuum, OPO Sunlite with IR extension, operated by Leonid Khriachtchev) was used to excite vibrations of the studied molecules. The pulse duration was ~ 5 ns, the spectral linewidth ~ 0.1 cm^{-1} and the repetition rate 10 Hz. The pulse energy of the OPO was measured at the sample position with a pulse energy meter (Molectron) to be ~ 0.1 mJ in the 3000-3700 cm^{-1} and ~ 0.4-0.6 mJ in the 4000-7000 cm^{-1} spectral region. The OPO radiation frequency was measured with a Burleigh WA-4500 wavemeter providing an absolute accuracy better than 1 cm^{-1} for the IR pumping radiation.

Photolysis of FA and AA was achieved using the 193 nm radiation of an excimer laser (MPB, MSX-250) operating at 10 Hz with pulse energy of ~ 5 mJ/cm^2 (FA)[IV] or 1-3 Hz with typical pulse energy of 16 mJ/cm^2 (AA).[VI] For FA, the conformationally selective data were obtained by comparison between the results obtained from photolysis of a sample containing only the conformational ground state and those of photolysis of a sample containing a 1 : 1 mixture of both conformers.[IV] In the case of AA, photolysis of the AA-D_4 species was studied instead of the fully-hydrogeneted isotopologue (AA-OH), because the amount of the high-energy *cis*

conformer of AA-OH that could be isolated in the matrix (produced from IR-excitation of the *trans* conformer) was very small.[VI] For both conformers of perdeuterated AA, an almost conformationally pure sample could be excited with UV light. However, a significant amount of the *cis* conformer appeared as one of the products of UV-photolysis of *trans*, and vice versa. Thus, in order to minimize the effect of UV-induced rotamerization, UV-photolysis of each conformer was undertaken while pumping the other conformer with resonant IR radiation.[VI] In this case, the M_1 mirror in Fig. 2.1 was moved horizontally in order to allow for an IR beam quasi-collinear with the UV beam.

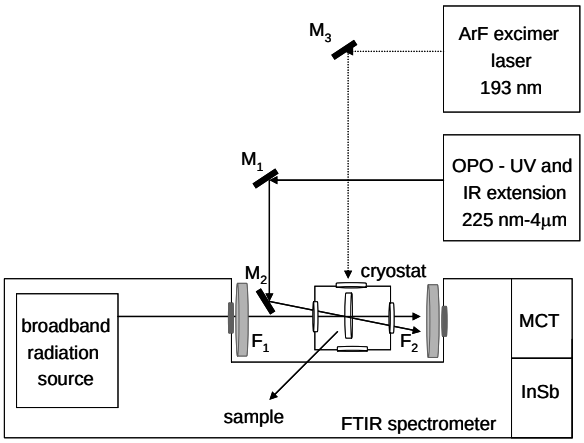

Fig. 2.1 – Irradiation setup used in the studies of IR-induced conformational isomerization and UV-photolysis. M and F are mirrors and interference filters, respectively. In situations where IR and UV excitation were performed simultaneously mirror M_1 was dislocated so as to allow for an IR beam quasi-collinear with the UV beam. The sample holder can be rotated so as to face any of the outer windows of the cryostat.

2.1.4 Quantum yield determination

The quantum yields of the rotamerization processes, $\phi(\nu)$, were extracted from the following equation:

$$\phi(\nu) = \frac{k_p(\nu)}{\sigma^i(\nu) I(\nu)} \tag{2.1}$$

where $k_p(\nu)$ (in s^{-1}) is the averaged isomerization rate upon pumping at the frequency ν, σ (in cm^2) is the absorption cross section of mode *i* at the excitation frequency, and *I* (in $s^{-1}cm^{-2}$) is the averaged photon intensity of the pumping beam. The averaged photon intensity is given by the measured intensity of the laser beam and the irradiated area, which was restricted to a hole with a diameter of 4 mm by using a radiation shield. The cross section is obtained using the measured IR absorption at the excitation frequency, the estimated concentration of molecules in the excited matrix site, and the matrix thickness.

Two methodologies have been applied to determine the pumping rate, k_p in equation (2.1). The most straightforward approach employs the IR-induced formation kinetics of the conformers. The fitting of the time dependent concentration of the photoproducts to an exponential growth curve allows to extract the value of the pumping rate.[III,VII] To minimize errors in the determination of the pumping rates caused by reverse isomerization processes (e.g., processes taking place by tunneling or an eventual simultaneous pumping of the reactant and product conformers), only the kinetic points obtained during the first minutes of irradiation were considered. As an example, Fig. 2.2 shows the IR-induced formation kinetics for two conformers of AA-OD (*trans* and *cis*) and PA-OD (T_t and C_t).

The kinetics based methodology could only be used when the reverse isomerization is relatively slow, which is the case of C-O isomerization of AA-OD, internal rotation around the C_α-C axis (C_α-C isomerization) of PA-OH and both C_α-C and C-O isomerization of PA-OD.[VII,IX] For C-O isomerization from the conformational ground state (*trans*) to the higher energy form (*cis*) of the fully-hydrogenated species, the back reaction taking place by tunneling is too fast to follow reliably the pumping

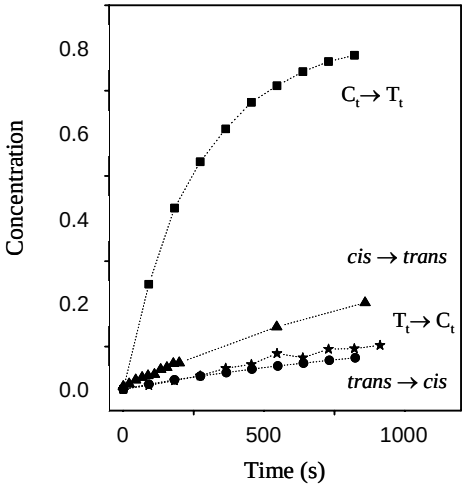

Fig. 2.2 - Pumping kinetics measured for hydroxyl-deuterated AA and PA. The concentrations of the photoproducts are normalised by the initial concentrations of the pumped conformer. The pumping rates are extracted from a linear fit of the beginning of the kinetic curves. For AA, the pumping rates for the *trans* → *cis* (●) and *cis* → *trans* (▲) processes differ by a factor of ~3, whereas for PA, the rates for the $T_t \rightarrow C_t$ (★) and $C_t \rightarrow T_t$ (■) processes differ by a factor of ~25. The lines are merely guides.

kinetics.[III,VII,IX] In this case, as a result of competition between the photoinduced reaction and the reverse tunneling process a stationary state is established under IR-excitation. At the equilibrium, the pumping and tunneling rates are equal and the following relationship applies:

$$k_p(\nu)[trans]_{eq} = k_t(T)[cis]_{eq} \qquad (2.2)$$

where $k_t(T)$ is the tunneling rate coefficient at the temperature *T*. Hence, the pumping rate can be determined from the measured tunneling rate and the ratio of the *trans* and *cis* equilibrium concentrations.[II] The concentration ratio at the equilibrium can be extracted from the changes in integrated absorptions upon pumping and the tunneling

rate coefficient can also be determined by FTIR spectroscopy, as explained later.[II,III]

Another approach was used to estimate the quantum yield in order to compare results obtained from different methodologies and evaluate the reliability of the methods used.[IX] The quantum yield is a ratio of the number of molecules that undergo isomerization (N_{iso}) to the number of absorbed photons (N_{abs}):

$$\phi(\nu) = \frac{N_{iso}}{N_{abs}} \tag{2.3}$$

The value of N_{abs} per unit time is estimated from the absorbance at the excitation frequency, A_{exc}, the intensity of the incoming beam (in $cm^{-2}s^{-1}$), I_0, and the irradiated area, S, as follows:

$$N_{abs} = \left(1 - 10^{-A_{exc}}\right) I_0 S \tag{2.4}$$

The number of isomerization events per unit time is calculated as follows:

$$N_{iso} = \frac{\left(\frac{\Delta A}{A_0}\right) n}{\Delta t} \tag{2.5}$$

where Δt is the short irradiation time, n is the total number of molecules of the excited conformer, A_0 and ΔA are the initial integrated absorption and the change in integrated absorption for a given vibrational mode of the pumped conformer. ΔA is thus related to isomerization induced in a specific site, and it is measured directly from the difference IR absorption spectra. Note that ΔA for a given pumping time can be estimated only if the pumping kinetics is followed in real time, and N_{abs} can only be estimated if the NIR spectrum is measured before pumping. In the cases where the quantum yields obtained by different methods could be compared the values were equal within the estimated experimental error.[IX]

2.1.5 Tunneling kinetics

For all the studied molecules, isomerization from the higher energy *cis* arrangement of the carboxylic group to the lower energy *trans* arrangement is shown

to proceed also by tunneling in dark.[III,VII,IX] Here "dark" is generally used to refer to a process that is not affected by radiation. Even though, in some situations, glowbar radiation (filtered or unfiltered) could be incident at the sample it was assumed not to affect the isomerization process.[III,VII,IX] For the slower tunneling processes (FA, AA-OD, PA-OD), the tunneling kinetics was measured while blocking glowbar radiation above 1500 cm^{-1} to ensure that glowbar is not interfering with the measurements. [III,VII,IX]

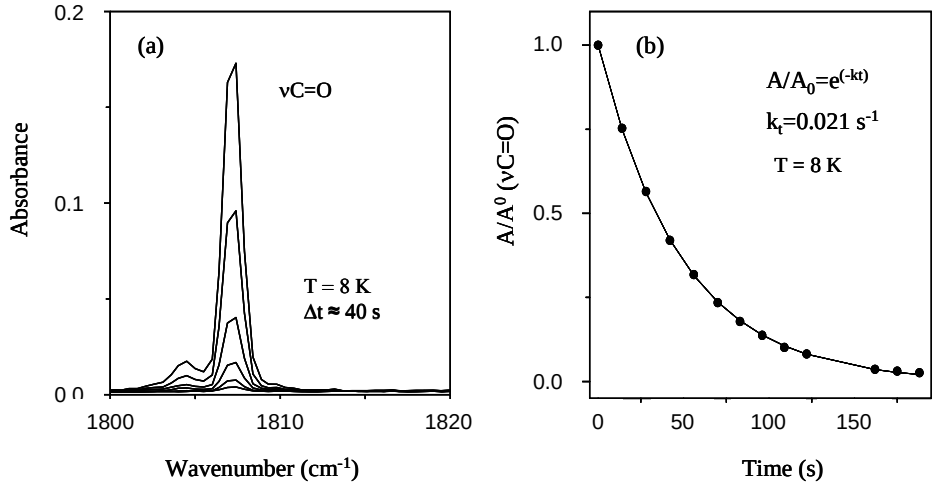

Fig. 2.3 – Tunneling kinetics for the *cis* → *trans* isomerization of AA-OH in solid Ar at 8 K: (a) time decay of the stretching C=O (νC=O) band of *cis*-AA and (b) exponential fit of the time-dependent integrated intensity of this band.

The tunneling kinetics for C-O isomerization from *cis* → *trans* was followed by FTIR spectroscopy by measuring the intensity decrease of a suitable absorption of the reactant conformer, as illustrated for AA in Fig 2.3. An exponential fit to the reactant intensity decay in dark allows to extract the tunneling rate coefficient. The effect of temperature and medium on the dark *cis* → *trans* isomerization of FA-OH, FA-CD (DCOOH) and AA-OH were evaluated by following the tunneling kinetics at

various temperatures and in different rare-gas matrices (Ar, Kr and Xe).[III,VII] For PA, the low concentrations of the high-energy *cis* forms (C_t and $C_g^{\pm}$ in Fig. 1.3) did not allow for such an exhaustive study.

2.2 Computational details and methodology

2.2.1 Ab initio calculations

The structure, energetic and vibrational properties of the conformational systems studied were obtained by ab initio calculations performed using the GAUSSIAN98 package of programs.[145] Generally, these calculation were performed using Møller-Plesset second order correction (MP2) to the Hartree-Fock energy, which adds some contribution from electron correlation.[146,I,VI,VIII] Standard basis sets where the molecular orbitals are defined by liner combinations of Gaussian-type atomic functions were used. The 6-311++G(2d,2p) basis function was the most frequently used.[146] This is a triply split basis (each valence atomic orbital is split in a more compact inner shell and a more diffuse outer shells), e. g. “6-311” means that the core orbital is represented by 6 Gaussians, the inner valence orbital is represented by three Gaussians, and middle and outer orbitals are represented as single Gaussians. Additionally this basis set has polarization functions (d-type orditals and p-type orditals are used to describe the non-hydrogen and hydrogen atoms, respectively) and diffuse functions that allow the orbitals to extent over regions of space considerably far apart from the nucleus.

2.2.2 Normal coordinate analysis

The ab initio geometries and Cartesian harmonic force constants were used to evaluate the potential energy distribution (PED) associated with each normal vibrational mode under the harmonic assumption.[I,VI,VIII] Transformation of the Cartesian harmonic force constants to the molecule-fixed internal coordinates system

allows for a normal coordinate analysis using BALGA program as described by Schachtschneider.[147]

2.2.3 Tunnel Effect

Two approaches were consider regarding the tunnel effect on the conformational isomerization within the carboxylic group: evaluation of the barrier permeability within the semi-classical Wentzel-Kramers-Brillouin (WKB) approximation for tunneling from torsional excited states near the bottom of the potential well and evaluation of the extent of delocalization of the torsional wavefunction for states with energies below the barrier but close to the barrier top. These two approaches were used to evaluate tunneling in the dark and tunneling upon vibrational excitation at energies below the barrier top, respectively.[III,V,148]

To account for the *cis* → *trans* tunneling observed for both FA and AA in dark, the permeability (*G*) of the C-O isomerization barrier from the *cis* torsional well was estimated according to the WKB approximation,[126] using the ab initio torsional potential (*V*) and the energy levels (*W*) of the reactant conformer, as follows:

$$G = \left\{ 1 + exp\left[\frac{2\sqrt{2\mu}}{\hbar} \int_{x1}^{x2} (V - W)^{1/2} \partial x \right] \right\}^{-1} \qquad (2.6)$$

where μ is the reduced mass for the torsional mode (taken from the ab initio calculation) and the integral is the area under the isomerization barrier (integrated barrier height) for tunneling from a given torsional level of the reactant, as shown in Fig. 2.4. This integral was evaluated numerically. Equation (2.6) was derived for a generic one-dimensional potential of the type represented in Fig. 2.4.

The torsional energy levels of the reactant conformer (ground vibrational state, ν_0, first, ν_1, and second, ν_2, excited states) were estimated experimentally from the observed vibrational transitions of *cis*, namely the torsional fundamental (ν=0 → ν=1) and first overtone (ν=0 → ν=2).[149,I] The tunneling rates from each torsional state of the reactant conformer (k_n) are given by multiplying the correspondent barrier

permeability, *G*, by the frequency with which the particle hits the barrier (the torsional frequency in this case). [III,V] A thermally activated nature of tunneling emerges naturally by calculating the total rate constant as a weighted sum over the rate from each torsional level, as follows:

$$k_t(T) = \left(\sum_{i=1}^{n} e^{-h\nu/k_B T} \right)^{-1} \sum_{n=0}^{N} k_n e^{-nh\nu/k_B T} \tag{2.7}$$

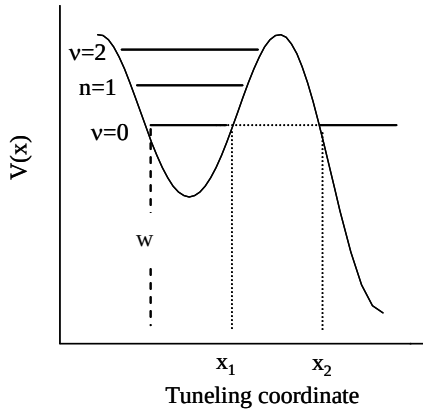

Fig. 2.4 - Tunneling in a system with a single potential well.

Strictly speaking, this is a crude approach to determine the tunneling rates for unsymmetrical double-minimum potentials like those associated with internal rotation in FA and AA, because it does not take into account that discrete sets of energy levels are found in both sides of the barrier. Indeed, it considers only the quantization of energy levels on the reactant side. Although the WKB results are to be taken into account with modest expectations, it should be remembered that the observed tunneling is a dissipative phenomenon, and thus any quantum mechanical evaluation of the tunneling probability that does not takes into account the environment

contribution is equally unrealistic. The theoretical studies of tunneling transitions in condensed media are still of difficult implementation as a predictive tool. This is essentially due to the multidimentional nature of the process, determined not only by the participation of solvent modes but also by the participation of other intramolecular vibrational modes as final states in the tunneling process.

The observation of conformational isomerization induced by excitation energies lower than the reaction barrier suggested that the tunnel effect was also important in the photoisomerization mechanism. In order to get some insight into the mechanism of photoisomerization at energies below the reaction barrier, the unsymmetrical torsional potential of FA extracted from the ab initio calculation was used to calculate the torsional wavefunctions. Due to the magnitude of the excitation energies involved (>2900 cm^{-1}), the most relevant torsional states considered are those near the barrier top. The aim was to evaluate the relative probability of finding the molecule in the *trans* or *cis* well for those states, which was extrapolated from the delocalization of the corresponding torsional wavefunction. Briefly, the MP2/aug-cc-pVTZ torsional potential of FA was fitted with a cosine series of the type:

$$V = \frac{1}{2}\sum_{1}^{n} V_n\left(1 - cos\, n\phi\right) \tag{2.8}$$

Then the vibrational Shrödinger equation was solved variationally in the free rotor basis set (expressed in terms of sine and cosines bases) using the Hamiltonian by Lewis et al.[150] The inertial constants as a function of the torsional angle needed for the calculation were obtained using the method of Pitzer,[151] and the resulting data set was also fitted with a cosine series to be used in the vibrational analysis. The geometries used in the estimation of the inertial constants were taken from the ab initio calculations.

In order to clarify the contribution of the author to the analysis of the tunnel effect, it should be mentioned that the author performed all the calculations involved in closer collaboration with the researcher Mika Pettersson.

2.2.4 Anharmonic couplings, hindered rotation and solvation of formic acid

The smaller size of FA allowed for a more throughout computational investigation of its conformational system. Namely, the accuracy of the correlation-corrected vibrational self-consistent field method (CC-VSCF) was evaluated by comparing the anharmonic vibrational properties of FA calculated by Jan Lundell with the spectroscopic data obtained experimentally.[I]

Also for FA, a crude analysis of the medium effect on the potential energy surface was undertaken based on Polarized Continuum Model (PCM) calculation available from the GAUSSIAN98 package of programs.[145] As the name itself indicates, in the PCM calculations the solvent is treated as a continuum and individual solvent molecules cannot be recognized.[152-154] Using the calculated isolated gas-phase structures of the studied molecules and dielectric constants of the rare gases, the solvation energies and solvated barrier heights could be determined within the PCM method.[III]

Additionally, a FORTRAN 90 code was written by Jonas Jusselius and Mika Pettersson that allowed to investigate hindered rotation of matrix isolated FA according to a previously developed formalism.[155,156] This program uses as input the gas-phase rotational constants, temperature and three parameters describing the lattice potential, which are determined by fitting the calculated rovibrational spectrum to the observed spectrum.[II] Some of the bands observed in the absorption spectra of FA were assigned on the basis of the results obtained from this program.

3. Results

3.1 Characterization of higher energy conformers

As mentioned in *Section 1.1*, from the studied molecules PA is the only one presenting some challenge from the point of view of theoretical characterization of the conformational equilibrium. The previously reported studies on PA used generally a low level of theory and lack a systematic investigation of the two possible isomerization processes (C-O and C_α-C isomerization).[VIII] As expected based on the early studies, the more accurate ab initio calculations performed in this work predicted the four non-equivalent minima on the potential energy surface of PA shown in Fig. 1.3.[VIII] The nomenclature that will be used to designate these stable geometrical arrangements is that defined in VIII. In analogy with previous theoretical results on FA and AA, the most stable structures are those exhibiting a *trans* arrangement of the carboxylic group (T_t and $T_g^{\pm}$) while those with a *cis* arrangement (C_t and $C_g^{\pm}$) are separated from the first ones by an energy difference of 1700-1900 cm^{-1}.[VIII] Among the structures differing by rotation around the C_α-C bond, those with a *trans* arrangement (T_t or C_t) are more stable than the corresponding degenerate *gauche* arrangement ($T_g^{\pm}$ or $C_g^{\pm}$, respectively) by 300-500 cm^{-1}.[VIII]

The ab initio potential energy along the C-O isomerization coordinate calculated for the three studied molecules at the same level of theory are very similar.[III,VII,VIII] Table 3.1 compares the calculated relative energies and barrier heights for C-O isomerization in FA, AA and PA. For PA, the barrier height for C_α-C isomerization was found to be much smaller (405 cm^{-1} for $T_t \rightarrow T_g^{\pm}$ and 559 cm^{-1} for $C_t \rightarrow C_g^{\pm}$) than the C-O isomerization barrier.[VIII]

For all the studied molecules, only the conformational ground state was significantly populated in the rare-gas matrices.[I,VI,VIII] The MIR spectra of freshly

deposited Ar matrices containing FA and AA agreed well with the experimental spectra previously reported for the *trans* conformers isolated in solid Ar.[10,157,158] As for PA, the exclusive presence of the T_t form in an Ar matrix was supported by comparison between the experimental and the ab initio spectra predicted for the four conformers.[VIII] However, in this case, in addition to the ground conformational state, the $T_g^{\pm}$ form was also expected to be present in the gas phase, taking into consideration the available electron diffraction data (*Section 1.1*)[49] and the calculated small energy difference between these two forms. The absence of the $T_g^{\pm}$ form in the matrix, expected to account for 27% of the total conformational population in the gas phase at room temperature,[VIII] is explained by a fast $T_g^{\pm} \rightarrow T_t$ conversion even at the low deposition temperature. The conformational cooling observed in the matrix is supported by the small C_α-C isomerization barrier predicted (~60 cm^{-1} for $T_g^{\pm} \rightarrow T_t$) and by the later observation that the conversion of $T_g^{\pm}$ (photoproduced in the matrix at 8 K) into T_t in solid Ar shows a strong temperature dependence as expected for over-barrier reactions.[VIII]

Table 3.1 – Relative energies (ΔE) and barrier heights (E_a) for C-O isomerization in FA, AA and PA.

C-O isomerization (cm^{-1})	FA	AA	PA
$\Delta E_{cis-trans}$	1418	1831	1733
$E_{a\ trans \rightarrow cis}$	4093	4141	4025

Contributions from the Zero Point Vibrational Energy (ZPVE) extracted directly from the calculations [MP2/6-311++G(2d,2p)] were taken into consideration. The barrier heights were calculated at an optimized transition state structure.

The NIR spectra of freshly deposited FA, AA and PA samples in excess Ar revealed a set of absorptions of the conformational ground states that could be excited to promote isomerization (listed in Table 2 of I for FA and Table I of VII for AA). For PA-OH, the NIR spectrum is shown in Fig. 3.1.

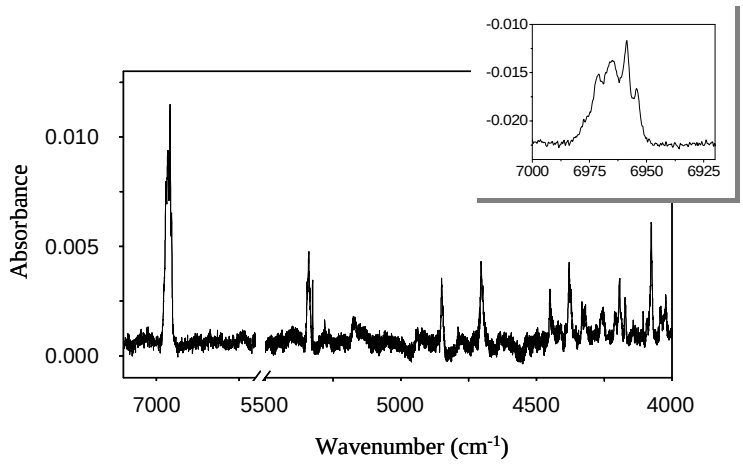

Fig. 3.1 – NIR (7100-4000 cm^{-1}) spectrum of PA-OH isolated in Ar at 8 K. A blow-up of the 2νOH bands is shown in the right corner of the figure in order to illustrate the site splitting effects.

The splitting of the absorption bands observed in both the MIR and NIR spectra of matrix-isolated FA and PA indicate that there are two predominant sites for FA and at least four sites significantly populated for PA. As an illustrative example see the bands of the νOH and 2νOH modes in Figs 2 and 3 of I (FA) and Fig. 3 of VIII (PA), in addition to Fig. 3.1. Site selective vibrational excitation of FA and PA leads to site selective conformational isomerization, [I, VIII] as reported before for other systems. This aspect was studied in greater detail for FA (reported in I and II) and it is illustrated in Fig. 3.2. This figure shows two plots of the isomerization rates determined from the equilibrium concentration of the *trans* and *cis* forms in a specific site against the excitation wavenumber, in comparison with the absorption spectrum. In general, excitation of the lower frequency doublet of a given mode affects exclusively the molecules in the so called site 1 while excitation of the higher frequency doublet promotes conformational isomerization of the molecules isolated in site 2.

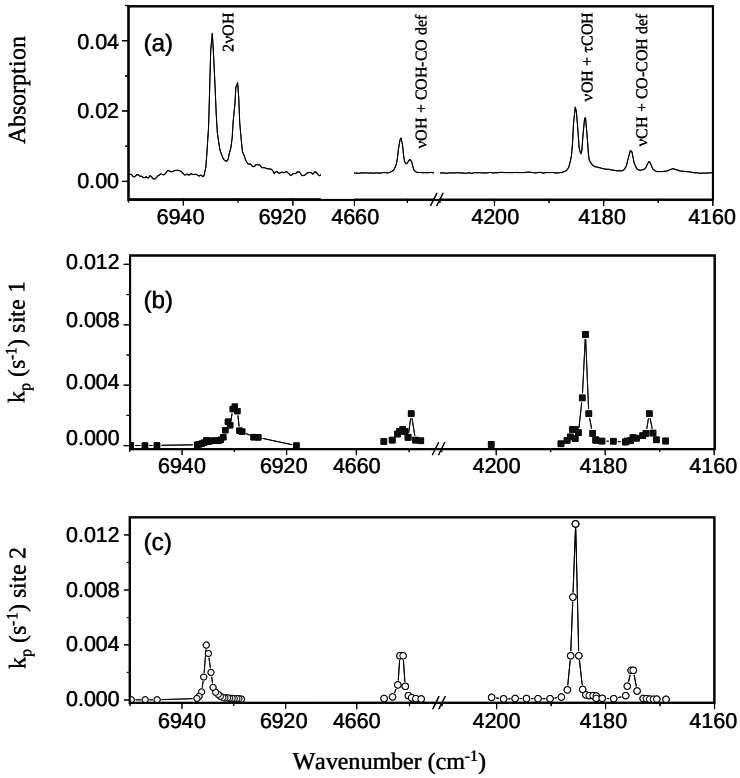

Fig. 3.2 – Absorption spectrum showing the doublet structure of the bands of each vibrational mode of FA in solid Ar (a) and plot of the rate of conformational isomerization in site 1 (b) and site 2 (c) as a function of the excitation wavenumber (also called Reactive-Vibrational-Excitation spectrum, RVE).

Apart from the site-selective nature of the excitation and isomerization processes, Fig. 3.2 also shows that all the excited modes were active in promoting the conformational isomerization of FA. Indeed, for both FA-OH and AA-OH a number of vibrational modes absorbing in the 7000-2900 cm^{-1} spectral region were excited and all of them were shown to be successful in promoting conformational isomerization.[I,II,VII] In view of the consistency of the results, i. e. conformational isomerization is successfully induced irrespectively of the nature of the excited

vibrational mode, for PA-OH the only mode used to promote conformational isomerization was the 2νOH mode. This mode was chosen due to its relatively high energy, large absorption cross section and its well defined site structure. Furthermore, only a restricted number of sites were investigated in detail, chosen to be the ones were isomerization is most clearly observed.[VIII, IX]

For the fully hydrogenated molecules, excitation of the 2νOH mode (7000-6800 cm^{-1}) of the conformational ground state leads to the *trans* → *cis* isomerization within the carboxylic group, as shown in the difference spectra of Fig. 3.3. The difference spectra, generally obtained by subtracting the spectra taken *after* irradiation or *upon* irradiation from that recorded immediately *before* irradiation, have shown to be an extremely sensitive tool to discriminate the spectral signature of different conformers and different sites. Identification of conformers with each of the two possible arrangements within the carboxylic acid group by matrix-isolation vibrational spectroscopy is expected to be a straightforward task based on two absorptions alone that are very sensitive to the carboxylic group conformation, the νOH/νOD [νOH(D)] and νC=O modes. They are systematically predicted by the calculations to appear blueshifted in the *cis* conformation by 40-80 cm^{-1} for νOH(D) (observed 40-70 cm^{-1}) and by 30-40 cm^{-1} for νC=O (observed 16-40 cm^{-1}).[I,VI,IX]

Excitation of the 2νOH of the conformational ground state of FA-CD and AA-CD_3 was equally shown to be effective in promoting isomerization within the carboxylic group,[I,VI] as well as excitation of the 2νOD (5200-5100 cm^{-1}) mode in the hydroxyl-deuterated forms studied (FA-OD, AA-OD, AA-D_4 and PA-OD).[III,VI,VIII]

Additionally, for PA (PA-OH and PA-OD), excitation of the 2νOH(D) mode of the conformational ground state induces the C_α-C isomerization ($T_t \rightarrow T_g^{\pm}$). Although partially overlapping, the spectral subtraction tool also allows for a clear discrimination between the bands of the νOH(D) and νC=O modes corresponding to the T_t (excited) and $T_g^{\pm}$ (photoproduct) conformers (see Fig.3.3). However, the best spectral region to observe non-overlapping bands of the two C_α-C conformations is

obviously that were the modes involving a significant skeletal motion absorb, the 2000-500 cm^{-1} region (see Fig. 5 of VIII, where the bands of T_t are shown to differ significantly from those of $T_g^{\pm}$, and Fig. 4 of VIII, where the bands of C_t can be clearly distinguished from those of $C_g^{\pm}$).

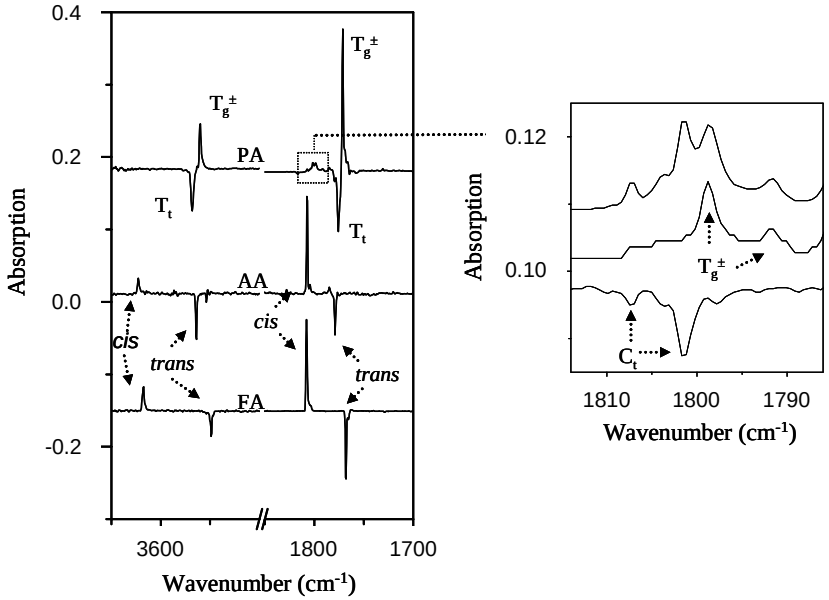

Fig. 3.3 – Difference spectra showing the result of excitation of the 2νOH mode of FA, AA and PA in solid Ar (left panel) and the result of a subsequent period in dark for PA (right panel). The difference spectra in the left panel were obtained by subtracting the spectra recorded after pumping (FA and AA) or during pumping (PA) from those recorded before pumping. In the right panel, the upper plot is a blow-up of the spectra of PA in the left panel, the middle difference spectrum shows the result of a dark period after pumping (spectrum recorded after waiting in dark for a couple of minutes after pumping *minus* spectrum recorded before pumping), the lower difference spectrum shows the net result of the dark period after pumping (spectrum recorded after waiting in dark for a couple of minutes after pumping *minus* spectrum recorded during pumping).

Note that in Fig. 3.3 the spectral subtraction uses the spectrum taken *after* irradiation in the case of FA-OH and AA-OH but it uses the spectrum taken *under* irradiation for PA-OH. This is so because the amount of photoproduced *cis* conformer (C_t) from the T_t conformer of PA-OH is so small that it does not survive to the $C_t \rightarrow T_t$ tunneling decay in dark long enough for a spectrum to be recorded at some decent resolution. The right panel of Fig 3.3 shows a blow-up of the region where the νC=O mode of C_t absorbs. Here, the upper trace shows the bands of C_t appearing under pumping of T_t as a result of C-O isomerization, together with bands of $T_g^{\pm}$ resulting from C_α-C isomerization. The middle trace shows the bands that remain during spectral collection without pumping ($T_g^{\pm}$ bands). Finally, the lower trace shows the net result of this dark period, i. e. the bands of C_t decrease and those of $T_g^{\pm}$ remain unchanged.

The subsequent excitation of the higher energy conformers produced in a first irradiation step from the conformational ground state was also investigated for AA and PA. The increased stability of *cis*-AA and C_t-PA for the hydroxyl-deuterated forms (OD-forms), due to the isotopic effect on the tunneling rates (see *Section 3.2*), allowed for excitation of the conformers with a *cis* arrangement of the carboxylic group. As a result, in both cases, the 2νOD mode was shown to be active in promoting C-O isomerization back to the conformational ground state.[VI,VIII] For PA, excitation of the 2νOH(D) mode of $T_g^{\pm}$ promotes C_α-C isomerization back to the conformational ground state ($T_g^{\pm} \rightarrow T_t$) together with C-O isomerization into the corresponding higher-energy $C_g^{\pm}$ conformer ($T_g^{\pm} \rightarrow C_g^{\pm}$).[VIII]

For the molecules with a simple biconformational framework (FA and AA), identification of the full spectrum of each conformer is straightforward based on the comparison of spectra recorded before and after conformational isomerization.[I,V,VI] The task is less trivial in the case of PA where two sets of bands appear simultaneously upon vibrational excitation. For PA-OH, the bands emerging upon excitation of T_t (C_t and $T_g^{\pm}$) or excitation of $T_g^{\pm}$ ($C_g^{\pm}$ and T_t) are essentially

discriminated by their behaviour in dark. As mentioned before, the bands of C_t and $C_g^{\pm}$ could only be observed during pumping due to a fast dark decay into T_t (e. g. the $C_t \rightarrow T_t$ rate coefficient is ~ 6 x 10^{-2} s^{-1}). Thus, a couple of minutes in dark are sufficient to eliminate from the spectrum the contribution of C_t or $C_g^{\pm}$ whereas the bands of $T_g^{\pm}$ are much more stable (the $T_g^{\pm} \rightarrow T_t$ rate coefficient is ~ 10^{-6} s^{-1}) and those of T_t are completely stable (see Fig. 4 of VIII).

On the other hand, for PA-OD, the two conformers produced by excitation of the T_t and $T_g^{\pm}$, are quite stable at 8 K. In fact, when compared to PA-OH, the $C_t \rightarrow T_t$ dark conversion slows down by ~ 4 orders of magnitude. The $C_g^{\pm} \rightarrow T_t$ is also much slower in PA-OD than in PA-OH (roughly by two orders of magnitude). Nevertheless, the spectral signatures of the photoproduced conformers are also reliably separated for the PA-OD isotopologue based on photochemically induced events. Firstly, the emerging bands of C_t and $T_g^{\pm}$ under excitation of T_t grow at different rates when pumping at different frequencies within the 2νOD absorption envelope [high-frequency pumping (HF) at ~5175 cm^{-1} and low-frequency pumping (LF) at 5170 cm^{-1}].[VIII, IX] Secondly, the subsequent conformationally selective excitation of either C_t or $T_g^{\pm}$ affects exclusively the concentration of the irradiated conformer (see Fig. 5 of IX showing the result of excitation of C_t).

Nevertheless, similarly to PA-OH, dark isomerization processes (tunneling or thermally assisted) can also be used to discriminate among the conformers of PA-OD. The $T_g^{\pm} \rightarrow T_t$ isomerization at 15 K is faster by at least two orders of magnitude than the $C_t \rightarrow T_t$ process, allowing for a clear separation of the spectral signature of $T_g^{\pm}$ and C_t, both produced from excitation of T_t (see Fig. 7 of VIII). Conversely, for the emerging conformers upon excitation of $T_g^{\pm}$ (T_t and $C_g^{\pm}$), the T_t conformer is completely stable in dark while $C_g^{\pm}$ slowly decays into T_t. Most importantly, the bands of $C_g^{\pm}$ are naturally separated from those of T_t, because the first conformer is only observed after the pumping experiments while T_t is the only form isolated in the matrix before any vibrational excitation experiment.

To close the description of the conformational isomerization events, it is worth noting that no evidence was found able to support any efficiently photoinduced concerted C_α-C and C-O isomerization, which would lead to the observation of the $T_t \rightarrow C_g^{\pm}$ or $T_g^{\pm} \rightarrow C_t$ processes. This result is interesting, considering that excitation of the 2νOH(D) modes introduces an energy in the molecules higher than the computationally predicted concerted isomerization barriers (<4800 cm^{-1}).[VIII] Nevertheless, the $C_g^{\pm} \rightarrow T_t$ conversion, involving both rotation along the C_α-C and C-O bonds (ab initio barrier of ~2540 cm^{-1}) was observed *in dark*. This process was slowed down by deuteration of the hydroxyl group as it would be typical of a process taking place below the reaction barrier. A stepwise process involving conversion of $C_g^{\pm}$ into a vibrationally excited $T_g^{\pm}$ (C-O isomerization) by tunneling and a subsequent partial dissipation of the excitation energy into the C_α-C rotational coordinate (above the C_α-C isomerization barrier) finally leading to C_α-C isomerization was tentatively proposed in VIII.

The above described isomerization processes allowed for an unequivocally experimental identification and vibrational characterization of the higher energy conformers of AA (*cis*)[V,VI] and PA ($T_g^{\pm}$, C_t and $C_g^{\pm}$).[VIII] This task was accomplished based on the comparison of difference spectra showing the effect of vibrational excitation with the ab initio spectra of the conformers. The vibrational characterization of the already known conformers was also significantly improved.[I,VI,VIII] A very good agreement was generally found between the experimentally obtained difference spectra and those simulated by ab initio calculations. This good agreement, together with the normal mode analysis based on the calculated harmonic vibrational frequencies and force constants, allowed for an exhaustive vibrational assignment of the spectra of the observed conformers for the studied molecules, discussed in detail in papers I,VI and VIII.

Additionally, a very interesting finding connected with the analysis of the absorption spectra was reported for FA. The magnification of the RVE spectra in

Fig.3.2 shows satellite bands on the high frequency side of intramolecular vibrations, such as the O-H stretching fundamental and first overtone and the νOH + τCOH (~ 4180 cm^{-1}) combination modes, extending over 40 - 65 cm^{-1} away from the absorptions of the main bands (see Fig. 5 in II). These satellite bands have been detected both for FA-OH and AA-OH. The broad satellites are very well defined in the RVE spectra but they are not detected in the absorption spectrum. Thus, the conformational isomerization could be induced even when pumping far away from obvious absorption bands. Note that the RVE spectra can be very sensitive to low cross section absorptions that are active to photoisomerization, because the presence of this absorptions are detected from the emergence of product bands selected on the basis of their high absorption cross section.

The broad satellites in the RVE spectra have been identified as phonon sidebands of intramolecular vibrations resulting from the simultaneous excitation of a lattice phonon and an intramolecular mode by one photon. Phonon sidebands are a common observation in pure molecular solids and are not uncommon also for electronic transitions.[159-162] On the contrary, this phenomenon is rarely observed in the vibrational spectra of molecules in solid rare gases, due to much lower coupling strengths between the lattice and intramolecular vibrational modes, as compared to the electron-phonon coupling in electronic transitions. The ratio of intensity of the phonon wing relatively to the zero-phonon line (pure intramolecular absorption) gives an indication of the relative coupling strengths. For pure vibrational transition the estimated ratio was ~ 0.08 (FA-OH in solid Ar)[II] while values as high as 3.5 have been reported for vibronic transitions (Cl_2 in solid rare gases).[161]

3.2 Isomerization by tunneling

The C-O isomerization taking place by tunneling is discussed in detail in the originals publications III, VII (Section B) and IX (Section 3.2).

The spontaneous conversion from the high-energy *cis* arrangement of the carboxylic group into the low-energy *trans* arrangement was first observed to take place in a timescale of minutes for FA isolated in an Ar matrix at 15 K.[10] According to the Arrhenius formula, a negligible overbarrier isomerization rate is predicted at this temperature, based on the relatively high *cis* → *trans* isomerization barrier (~2700 cm^{-1} according to our calculation) and using the torsional frequency of *cis* (~500 cm^{-1})[I] as the pre-exponencial factor (see solid line in Fig. 3.4).[III] The overbarrier reaction rate should become measurable only above 100 K (k ~ 10^{-5} s^{-1}). Thus, the observed fast decay of *cis*-FA was assumed to take place below the barrier.

The first task of the present study was to show that this earlier observation could be unequivocally attributed to the *cis* → *trans* tunneling. As mentioned in *Section 1.6*, the tunnel effect is usually recognized by a non-linear temperature dependence of the rate coefficient (non-Arrhenius behaviour) and a strong isotopic effect.[126] Therefore, the temperature dependence of the *cis* → *trans* isomerization rate was evaluated in three different rare-gas hosts in a temperature range from 8 K up to 35 K (Ar), 40 K (Kr) or 60 K (Xe), with the higher temperature limit determined by the sublimation rate of the rare-gas host.[III] The effect of substitution of the tunneling particle by a heavier isotope was probed by deuteration of the hydroxyl group.

The temperature dependence of the dark *cis* → *trans* conversion is shown to be clearly non-linear in all the probed hosts.[III] As an illustrative example, Fig. 3.4 shows the observed behaviour in solid Ar in comparison with the expected linear dependence for an overbarrier reaction (solid line). Evaluation of the isotopic substitution effect upon deuteration of the carboxylic hydrogen showed that the tunneling rate for FA-OD is ~ 3 orders of magnitude slower than for FA-OH, which constitutes the ultimately proof that the *cis* → *trans* dark isomerization in FA takes place by tunnel effect.[III]

As anticipated before, in addition to FA-OH and FA-OD, the spontaneous decay of the photoproduced *cis* arrangement of the carboxylic group into the *trans* arrangement was observed in dark for all the studied isotopologues of the three

molecules isolated in solid Ar, even at the lowest working temperatures (8 K).[III,VII, IX,] The measured dark decay rates under such experimental conditions are presented in Table 3.2. Similarly to FA, the much slower dark isomerization rates for the OD-forms (~ 4 orders of magnitude slower) as compared to the corresponding OH-forms corroborate the tunnel effect in the AA and PA dark conversion. For PA, the subsequent discussion will focus exclusively on the $C_t \rightarrow T_t$ dark decay due to the fact that the $C_g^{\pm} \rightarrow T_t$ decay is not a pure tunneling process, as discussed earlier.

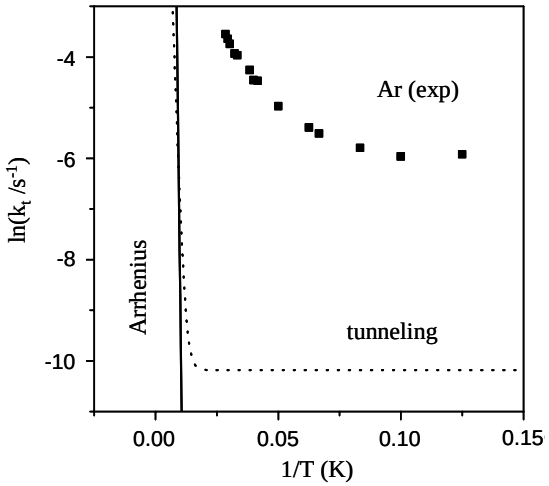

Fig. 3.4 – Arrhenius plot (—) ($k = Ae^{\left(-E_a/RT\right)}$, with A = 1.5×10^{13} s^{-1} and E_a= 2700 cm^{-1}), thermally activated tunneling rate (...) predicted according to equations 2.6 and 2.7 for the *cis* $\rightarrow$ *trans* isomerization rate of FA-OH, and experimentally observed *cis* $\rightarrow$ *trans* isomerization rate of FA-OH in solid Ar (■).

For the OH-isotopologues, the tunneling rate increases with the decreasing *cis* $\rightarrow$ *trans* barrier height in the series FA > AA > PA. The order of magnitude difference in the tunneling rates observed in Ar at 8 K between FA and both AA and

PA (Table 3.2) seem to reflect the calculated relative barrier heights (calculated *cis* → *trans* isomerization barriers of ~2700 cm^{-1} for FA and ~2300 cm^{-1} for both AA and PA)[IX] . On the other hand, as shown graphically in Fig. 3.5, the deuteration effect is stronger for the lower reaction barrier, which is in contradiction with the expected trend for the penetration probability according to the semi-classical WKB approximation (equation 2.6). The tunneling rates for the OD-isotopologues are virtually unchanged irrespectively of the relative barrier heights. This is one of the observations made in this work suggesting that the tunneling rates depend essentially on additional factors to the reaction barrier. However, it should be noted that this apparent contradiction could be biased by two aspects: the solvation effects on the relative energies of the conformers and on the isomerization barriers and, most importantly, the accuracy of the experimental measurements in extracting the rate coefficients for very slow or very fast processes.

Table 3.2 – Tunneling rate coefficients measured for isomerization within the carboxylic group from the *cis* to *trans* arrangement ($C_t \rightarrow T_t$ in PA) in solid Ar at 8 K.

FA	k_t (s^{-1})	AA	k_t (s^{-1})	PA	k_t (s^{-1})
FA-OH	2×10^{-3}	AA-OH	2×10^{-2}	PA-OH	5×10^{-2}
FA-OD	7×10^{-7}	AA-OD	7×10^{-7}	PA-OD	8×10^{-7}
FA-CD [a]	5×10^{-3}	$AA\text{-}CD_3$	7×10^{-2}		
		$AA\text{-}D_4$	1×10^{-6}		

[a] Average between the values measured for molecules isolated in two matrix sites (4×10^{-3} and 6×10^{-3} s^{-1}).[III]

For PA-OH, the concentration of *cis* in the Ar matrices is relatively low due to a faster tunneling rate and a less efficient IR-induce isomerization as compared with FA-OH and AA-OH. The concentration of *cis*-PA is limited *a priori* by the fact that the narrowband radiation allows to excite selectively a limited number of sites and PA exhibits a wider site distribution in comparison with FA and AA. Thus, the analysis of the tunnel effect in PA is limited to the evaluation of the heavy isotope effect in Ar

matrices at 8 K. On the contrary, for FA-OH and AA-OH a sufficient amount of the *cis* conformer could be produced in rare-gas matrices, allowing for a detailed study of the environment and temperature effects in the tunneling rates. Fig. 3.6 shows the comparison of the Arrhenius-like plots for the tunneling rate coefficients measured for FA-OH and AA-OH in solid Ar, Kr and Xe.

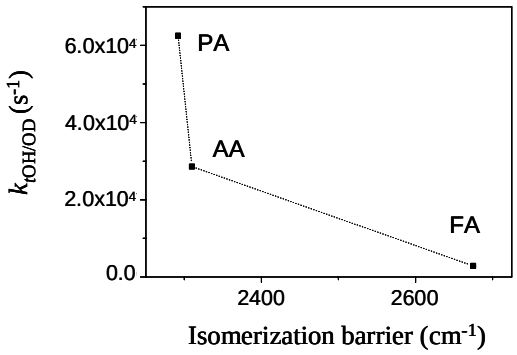

Fig. 3.5 – Ratio between the tunneling rates observed at 8 K in Ar matrices for the OH- and OD-isotopologues of FA, AA and PA as a function of the calculated isomerization barrier (Table 3.1). A dotted line guides the eyes.

A detailed evaluation of the observed temperature dependence of the tunneling rate might be useful to get some insight on the type of mechanism involved in the process. The explicit dependence of the tunneling probability on the width and barrier height leads to the possibility of a thermally activated process when excited vibrational levels of the reaction coordinate (C-O torsion) or other low-energy vibrational modes (lattice modes or intramolecular vibrational modes of lower quanta) participate in the tunneling process.[126] The thermal population of higher energy vibrational levels may lead to a faster tunneling rate, because the barrier becomes lower and narrower while moving up from the bottom of the potential well. Thus, the

relevance of the torsional excited states of the *cis* conformer to the tunnel effect should be evaluated.

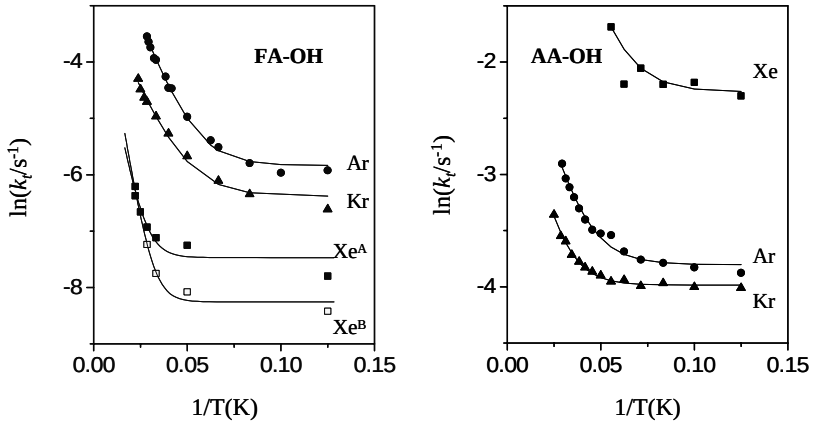

Fig. 3.6 – Arrhenius-like plots for the *cis* $\rightarrow$ *trans* tunneling of FA-OH and AA-OH in various matrices. For FA-OH the tunneling kinetics was measured for molecules isolated in two different matrix sites in all matrices (labeled A and B for Xe matrices), exhibiting a significant site effect only in Xe matrices.[III] The lines were obtained from the fitting of the experimental values (■/□, Xe; ▲, Kr and ●, Ar) to a temperature dependent rate constant of general formula $k_t(T) = k_0 + k_1 \exp(-E_a / RT)$.[VII]

According to the WKB calculations described in *Section 2.2.3*, the tunneling rate from the first excited torsional state of *cis* becomes meaningful only above the highest temperatures probed in this study (above 60 K for FA-OH and 50 K for AA-OH), as illustrated by the dotted line in Fig. 3.4 for FA-OH. Indeed, for both molecules, the barrier permeability is ~ 4 orders of magnitude higher from the first excited state when compared to the ground torsional state, but the estimated population of the excited state is lower than ~10^{-5} even at the highest temperatures probed. Within the limitations of the approximation used, the participation of the excited torsional states would lead to a sudden change in the tunneling rate at 50-60 K, in definite contrast with the smooth temperature-dependence observed (Fig. 3.4).

Thus, it can be safely assumed that the observed *cis* $\rightarrow$ *trans* tunneling for FA-OH and AA-OH in all hosts takes place mainly from the torsional ground state.

On the other hand, the smooth increase with temperature exhibited by the dark *cis* $\rightarrow$ *trans* rate coefficient in all hosts suggests the participation of lower energy quanta than the torsional quanta in the tunneling mechanism.[126,128,138,139] The observed tunneling kinetics is reasonably well described by a generic expression for a temperature-dependent rate coefficient of the type $k_t(T) = k_0 + k_1\, exp(-E_a / RT)$. The k_0 parameter accounts for a temperature-independent rate constant for tunneling exclusively from the ground vibrational level at very low temperatures, while the exponential term in this expression accounts for reaction from a continuous Boltzman distribution of energies. Fig. 3.7 shows in detail the good agreement between the experimental data and the data obtained from this fitting procedure for FA-OH isolated in Ar matrices. In Fig. 3.6 the data obtained from the fitting is shown as an Arrhenius-like plot in comparison with the experimental data for FA-OH and AA-OH in all the probed hosts. In general for FA-OH and AA-OH in all the probed hosts, the fitting allows to extract apparent activation energies of 50-140 cm^{-1} with k_0 values differing on average from the measured rate coefficients at 8 K by 15% and k_1 values higher than k_0 by 1-2 orders of magnitude.[VII]

The simplified nature of the model prevents any serious attempt of understanding the details of the tunneling mechanism based on the fitting parameters. However, it is interesting to note that the obtained values for the apparent activation energy are consistent with the participation of lattice phonons in the tunneling mechanism for all the studied hosts, where the Debye frequency range from 40 to 90 cm^{-1}.[163] For AA-OH the low activation energy could also be accounted by the participation of intramolecular vibrational modes of lower energy as it is the case of the τCH_3 mode (predicted by the calculations at 80-100 cm^{-1}; see Table 1 in VI). [VII] Indeed, for most of the medium size to large molecules, the lowest energy vibrational modes should be able to compete with the lattice modes in accommodating small energy gaps between the vibrational levels involved in the tunneling process on both

sides of the barrier. Furthermore, intramolecular couplings are expected to be stronger than couplings of intramolecular modes with lattice modes.

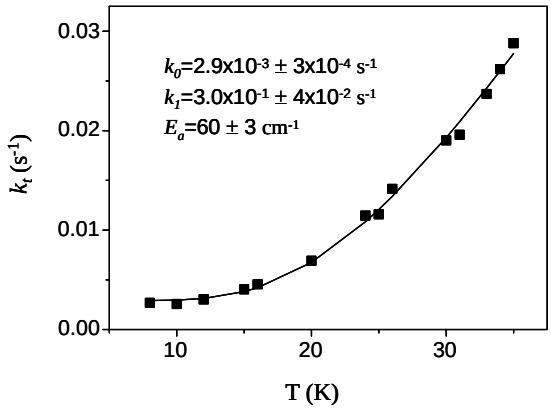

Fig. 3.7 - Fitting of the observed tunneling kinetics of FA-OH in solid Ar with a temperature dependent rate coefficient of the type $k_t(T) = k_0 + k_1\, exp(-E_a / RT)$.

After analysing the temperature effect on the tunneling kinetics, in the following paragraphs the other factors that might affect the tunneling mechanism will be addressed, namely the effect of the rare-gas host, local environment and isotopic substitution of atoms that are not expected to have significant contributions to the reaction coordinate.

The common observation regarding the solvent effect on the tunneling mechanism is that for intramolecular hydrogen atom transfer this effect is negligible, especially in the case of non-polar solvents.[126] The tunneling rates have also been reported to be unaffected by the change from solution to solid matrix.[142,143] However, in contradiction with these observations, guest-host interactions have been used to postulate small host-induced changes in the reaction potential that would either induce tunneling in slightly asymmetric double-well potentials or reduce the tunneling rate in

the condensed phase when compared to the gas phase for symmetrical double-well potentials.[130,164,165] Indeed, our present observations support an appreciable solvent effect on the tunneling mechanism. From the host dependence of the *cis* → *trans* tunneling rates shown in Fig. 3.6, the first thing to note is that, even in a case of weakly interacting media such as rare-gas matrices, the environment has a strong effect in the tunneling rate. For FA-OH the tunneling rate changes by one order of magnitude from Ar to Xe ($k_t^{Ar} > k_t^{kr} >> k_t^{Xe}$) at 8 K. For AA-OH, the measured tunneling rates are larger by at least one order of magnitude (in all probed hosts at 8 K) than the tunneling rates observed for FA-OH. However, roughly the inverse host dependence is observed for this molecule ($k_t^{Xe} >> k_t^{Ar} > k_t^{kr}$), i. e. the tunneling rate is faster in Xe than in Ar by a factor of ~ 5. This reversed environment effects for FA and AA suggests that, in addition to the barrier height, the tunneling rate exhibits a very specific dependence on the solute-solvent interactions in the studied systems. This specificity is supported by the calculations of the solvated barrier height (see *Section 2.2.4*) for the *cis* → *trans* conversion of FA-OH in the various matrices. The calculations predict a systematic increase of the barrier height by ~ 40 cm^{-1} from both Ar to Kr and Kr to Xe, [III] which cannot be directly correlated with the observed relative tunneling rates for FA-OH. Furthermore, the similarity of the isomerization potential and relative dipole moments of *cis* and *trans* for FA and AA are expected to lead to similar solvation effects on the tunneling rates in both molecules if the barrier height was the sole factor to be considered.

A better qualitative understanding of the factors affecting the tunneling mechanism was attempted for the simplest molecule studied. For FA, the calculated solvation energies and the observed fundamental transitions were used to represent the vibrational level structure of *trans* (FA-OH and FA-CD in Ar and FA-OH in Xe) relatively to the torsional ground state of *cis* (see Fig. 4 in III). The relevance of this representation to the understanding of the relative tunneling rates is based on the fact that the final state involved in the tunneling process is not necessarily a torsional excited state of *trans*. Indeed, for the three guest-host systems analysed, the

vibrational state of *trans* closer in energy to the torsional ground state of *cis* is not a torsional state. Fig. 4 in III shows changes in the nature of the nearest vibrational state and in the energy gaps separating these two states within the three guest-host systems analysed in detail. The nature of the nearest state of *trans* to the ground torsional state of *cis* might affect the anharmonic couplings between the levels involved in the tunneling process, while the energy gaps are expected to affect the order of the phonon process involved in the dissipative mechanism. For instance, for FA-OH, the energy gap separating the torsional ground state of *cis* from the nearest mode of *trans* increases from Ar to Xe in a way that a one-phonon emission process is enough to accommodate the energy mismatch in Ar but not in Xe, where a high-order phonon process is required.[III] Accordingly, the tunneling rate at 8 K is faster in Ar than in Xe. Unfortunately, any attempt to predict the effect of the changing nature of the *trans* state involved in the tunneling is prevented by the unknown magnitude of the anharmonic couplings.

With respect to the environment effect on the tunneling rate it is worth mentioned that the site effect on the tunneling rate was shown to be remarkable in Xe matrices, for both FA-OH and FA-CD (see Fig. 3 in III).[III] On the other hand, in the Ar and Kr matrices, the tunneling rates measured for FA-CD exhibit a somewhat weaker but significant site effect, while for FA-OH this effect is negligible (see Fig. 3 in III). The site effect on the tunneling rate should be understood in a similar way as the host effect. In principle, the solvation energy and solvated isomerization barriers can be affected by the local matrix morphology, which will also affect the intramolecular level structure near the torsional ground state of *cis* (initial tunneling state).

Interestingly, for FA and AA, isotopic substitution of the hydrogen atoms that are not involved in the tunneling process was shown to have an opposite effect in the *cis* $\rightarrow$ *trans* tunneling rate to that observed upon deuteration of the hydroxyl group. The tunneling rate increases by a factor ~ 2 from FA-OH to FA-CD and by a factor of 2-3 from AA-OH to AA-CD_3 and AA-OD to AA-D_4, as measured in solid Ar at 8 K (Table 3.2). Once again this effect can be due to specific changes in vibrational

couplings and intrinsic level structure brought about by the deuteration. However, tempted by the apparent systematic nature of this effect it was proposed that, additionally, the vibrational modes of relatively lower energy quanta of the CD/CD_3 groups could better accommodate the energy gaps involved in the tunneling mechanism in comparison to those of the CH/CH_3 groups.[VII] The lower energy quanta of the CD/CD_3 groups could increase the number of intramolecular modes participating in the cascading energy dissipation process within the *trans* well, thus increasing the number of successful tunneling attempts.[VII] An increasing number of vibrational modes of *trans* with frequencies below the torsional ground state of *cis* is, indeed, a consequence of deuteration of the CH/CH_3 group. Note that in Fig 4 of III, there are four vibrational levels of *trans* between the torsional ground states of *trans* and *cis* in the case of FA-CD and only three in the case of FA-OH in solid Ar. The density of vibrational levels of *trans*-AA with energies below that of the torsional ground state of *cis* is also expected to be generally increased by deuteration of the methyl group.[VII] For the methyl-deuterated analogues, the methyl in-plane and out of plane bending modes appear redshifted by ~ 400 cm^{-1} and 150 cm^{-1} (absorbing in the 1000-800 cm^{-1} region, see Tables 1 and S2 in VII) and the τCD_3 mode is predicted to be redshifted by ~ 20 cm^{-1} with respect to the τCH_3 mode (predicted by ab initio calculation at ~ 80 cm^{-1})[VI].

The final conclusion from this section is that any interpretation of the relative tunneling rates observed for the three systems should be based on the intrinsic vibrational level structure and relevant intra and intermolecular couplings of the system, in addition to the barrier heights.

3.3 Isomerization quantum yield

The quantum yields for vibrationally induced conformational isomerizations have been discussed in detail in papers II, VII and IX. The most recent paper is also a

review on the subject, where the quantum yields obtained for PA are discussed in comparison with the earlier results on FA and AA. The obtained quantum yields are presented in Table 3.3.

3.3.1 Trans→ cis C-O isomerization

As sown in Table 3.3, the isomerization quantum yields for the *trans → cis* internal rotation within the carboxylic group have been determined for a number of vibrational modes absorbing in the 2900-7000 cm^{-1} region for both FA-OH and AA-OH in Ar matrices at 8 K and also in Kr matrices for AA-OH.[VII, IX] The data collected allowed an evaluation of the effects of excitation energy and nature of the excited mode on the quantum yields. The quantum yields for vibrationally induced conformational isomerization have been reported before to depend more or less linearly on the excitation energy, with the nature of the excite mode manifesting itself as strong deviations from a linear behaviour.[102] For FA-OH and AA-OH the importance of these two factors is perhaps better illustrated in Fig. 3 of VII, where the obtained C-O isomerization quantum yields are plotted as a function of the excitation energy. The two plots shown in the figure are quite similar. The results can be separated in two distinct regions according to the quantum yield dependence on the excitation energy.

At excitation energies above the ab initio predicted isomerization barriers (3900-4200 cm^{-1} for FA-OH and 4100-4400 cm^{-1} for AA-OH, the intervals establish according to our calculations and literature data),[40,41,148] the quantum yields are relatively insensitive to the nature of the excited modes as well as to the excitation energy. The most dramatic effect of the nature of the excited mode is observed for the 2νOH and νOH + τCOH modes of FA-OH, where the quantum yields differ by a factor of ~ 6. However, it should be noted that the value obtained for the 2νOH is not as reliable as those obtained for the other probed vibrations due differences in the experimental conditions. Excluding the 2νOH mode, the quantum yield changes by as much as a factor of 3 for FA-OH, which can still be accounted for by the

Table 3.3 – Quantum yields[a] for the IR-induced *trans* → *cis* isomerization of FA, AA and PA in rare-gas matrices.

Excited mode/ Energy (cm^{-1})		Ar	Ar
FA-OH		(site 1)	(site 2)
νCH	2955	1.4×10^{-4}	8.4×10^{-5}
2νC=O	3516	-	5.1×10^{-2}
νOH	3550	-	3.9×10^{-2}
νOH + lid [b]	3555	5.0×10^{-2}	1.2×10^{-1}
νCH + CO-COH def	4173	2.5×10^{-1}	2.0×10^{-1}
νOH + τCOH	4184	2.1×10^{-1}	4.1×10^{-1}
νOH + COH-CO def	4650	1.5×10^{-1}	2.1×10^{-1}
2νOH	6932	1.7×10^{-1}	0.7×10^{-1}
Excited mode/ Energy (cm^{-1})		**Ar**	**Kr**
AA-OH			
νOH[c]	3554	1.4×10^{-4}	1.5×10^{-4}
νOH + γC=O	4090	2.6×10^{-3}	3.2×10^{-3}
νOH + τCO	4195	2.7×10^{-3}	8.4×10^{-3}
νHCH_2 + δCH_3	4406	3.0×10^{-3}	-
νOH + δCH_3	4866	-	2.2×10^{-2}
νOH + νC=O	5326	-	2.9×10^{-2}
2νOH	6944	2.2×10^{-2}	2.6×10^{-2}
AA-OD			
2νOD	5170	3.6×10^{-3}	
AA-CD_3			
νOH + νC=O	5335	8.5×10^{-2}	
2νOH	6958	1.5×10^{-1}	
AA-D_4			
νOD + νC=O	4392	1.6×10^{-2}	
2νOD	5168	1.1×10^{-2}	
Excited mode/ Energy (cm^{-1})		**Ar**	
PA-OH			
2νOH	6960	1.4×10^{-2}	-
PA-OD		site HF	site LF
2νOD	5172	3.2×10^{-3}	5.0×10^{-3}

[a] The relative error has been estimated as 50% of the quantum yield value. Where relevant, the excitation wavenumbers correspond to average values for two sites (FA-OH and PA-OD)[I, IX] or for two matrices (AA-OH).[VII] [b] See paper II for discussion on the assignment of this mode. [c]The quantum yield determined for pumping at the 2νOH mode of the molecule isolated in solid Xe is $3.5\text{x}10^{-2}$. Symbols: ν, stretching; δ, bending; τ, torsion and γ, rocking.

experimental accuracy. The same conclusions apply to AA-OH, where the three vibrations probed with energies well above the barrier height differ by less than a factor of 2. Note that the observed fluctuations of the C-O isomerization quantum yields with the nature of the excited state (~ 20-40% and ~ 2-3 % for FA-OH and AA-OH, respectively) are very small when compared with the order of magnitude changes observed for other molecules.[100,102]

Interestingly, the picture changes quite much for pumping below the isomerization barrier, where the quantum yield seems to be greatly affected by the excitation energy (Fig. 3 of VII). The observation of photoinduced isomerization for excitation energies below the barrier height is surprising in itself. It shows clearly that the tunnel effect is also involved in the isomerization mechanism triggered by vibrational excitation. For both FA-OH and AA-OH, note that next to the barrier top the quantum yields are lower but comparable to those observed at higher energies, decreasing strongly (2-3 orders of magnitude) at lower energies (Table 3.3). This behaviour is completely understandable on the basis of an expected higher tunneling probability from torsional state of *trans* next to the barrier top (populated by IR excitation) as compared to those further away from it.

The relative tunneling probability from the torsional states of *trans* near the barrier height can be roughly evaluated by looking at the extent of delocalization of the wave functions over the *trans* and *cis* potential wells. For FA, the estimated torsional wavefunctions are shown in Fig. 3.8. The wavefunctions immediately below the barrier top are strongly delocalized over the two wells while those wavefunctions located at ~ 900 cm^{-1} below the barrier top are already strongly localized in either wells. The highest torsional states of *trans* that could be populated upon excitation of the νCH mode (~2950 cm^{-1}) are strongly localized states more than 1000 cm^{-1} below the isomerization barrier, which is in qualitative agreement with the extremely low quantum yield obtained upon excitation of the νCH mode (~10^{-4}). The quantum yield for excitation of the νOH mode at ~3550 cm^{-1} (~ 10^{-2}), which is capable of populating trosional states closer to the barrier top, is roughly 2 orders of magnitude higher than

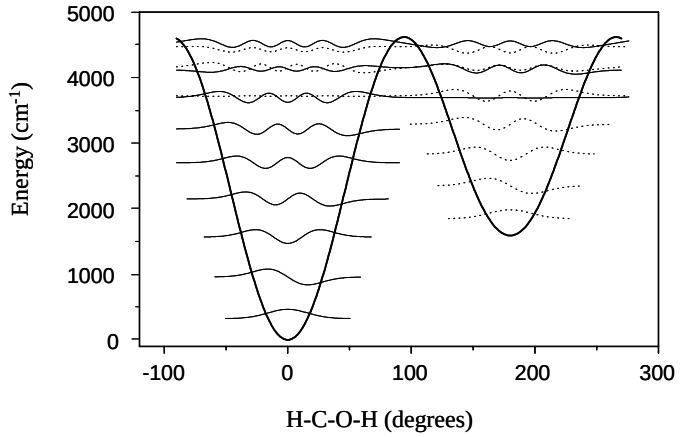

Fig. 3.8 – Calculated torsional potential of FA-OH at the MP2/aug-cc-pVTZ and torsional wavefunctions from the variational calculations described by Lewis et al (see Section 2.2.3)[150]. The solid and dotted curves refer to *trans* and *cis* wavefunctions, repectively.

for excitation of the νCH mode. For a more detailed discussion on this topic see ref. 148, keeping in mind that the energy relaxation mechanism that channels part of the excitation energy into the reaction coordinate is certainly too complex to allow for a quantitative analysis of the results.

Below the barrier height a roughly linear increase of the quantum yield with the excitation energy is observed for both FA-OH and AA-OH. That is to say that also in this region the nature of the excited vibration seems to be quite irrelevant. However, for FA-OH, a satellite band to the νOH assigned to the combination of the νOH mode with the librational motion (hindered rotation) of the molecule (νOH + lib., see paper II, Section C, for a detailed discussion on the assignment of this satellite) seems to have a higher quantum yield (factor of 3) than the corresponding νOH fundamental. This small difference is here evidenced because there are some indications suggesting specific energy relaxation mechanisms for each of the two modes that could explain

qualitatively the observed differences in the quantum yields.[166,167] Namely, it has been previously suggested, in connection with investigation of conformational isomerization of HONO, that the presence of angular momentum could enhance the energy transfer to the torsional mode.[166] However, despite of these indications the observed quantum yield difference between the two modes is still within the limits of our experimental error.

For PA-OH, the *trans* $\rightarrow$ *cis* C-O isomerization quantum yield was exclusively determined for the 2νOH mode (6980-6960 cm^{-1}) in Ar matrices at 8 K .[IX] Comparison of the data obtained for the hydrogenated isotopologues of the three molecules under investigation allow us to get some insight into the effect of the molecular size. One order of magnitude difference is observed between the 2νOH quantum yield determined for FA-OH (10-20%) and those for AA-OH and PA.OH (2%). Note that this difference cannot be connected with the *trans* $\rightarrow$ *cis* isomerization barrier, which changes systematically by ~ 100 cm^{-1} in the order PA < FA < AA (Table 3.1). Furthermore, such a barrier effect is also not supported by our previous observations of relatively unaffected quantum yields by the excitation energies for pumping above the barrier height. The overall density of vibrational states at the excitation energy does not seem to be a determinant factor either or else some differences should be observed between the values obtained for AA-OH and PA-OH. In this series of carboxylic acids, an increasing molecular size corresponds to a global increase of the vibrational level density due to the increasing number of large amplitude and lower energy modes.

Alternatively, the observed difference between the quantum yields obtained for FA-OH and the much lower values for AA-OH and PA-OH was explained in terms of the participation of the intramolecular energy levels associated with the lower energy modes in the mechanism of energy flow. In particular, large amplitude vibrations such as the torsional modes are usually very anharmonic and strong couplings between internal rotors can be expected. These couplings can lead to deactivation of the reaction coordinate through dissipation of its excitation energy into

the bath of low-quanta intramolecular modes and/or lattice modes. Both AA-OH and PA-OH have torsional modes of lower quanta than the τC-O (500-700 cm^{-1}),[I,VI,VIII] in opposition to FA-OH where the τC-O is the lowest energy mode. The vibrational quanta associated with the torsional modes of AA-OH and PA-OH (τCH_3, predicted at ~ 80 cm^{-1} for AA and ~ 220 cm^{-1} for PA, and τC_α-C, predicted at ~ 60 cm^{-1} for PA) are of the same order of magnitude of the Debye frequency for solid Ar (~ 60 cm^{-1}), which can favour energy transfer from the intramolecular modes into the lattice phonons. This could limit the isomerization quantum yield by favouring dissipation within the *trans* well.

Interestingly, among AA and PA, the size of the group attached to the carbonyl carbon (-CH_3 or –CH_2CH_3) seems to have little influence on the C-O isomerization quantum yield, which changes by less than a factor of two. It could be speculated that the τCH_3 in PA is not so efficient in deactivating the reaction coordinate as in AA due to the fact that the methyl group lays further away from the excited coordinate, and thus it is expected to be relatively uncoupled to the τC-O mode. For gas-phase isolated molecules, evidences have been reported that show that the participation of large-amplitude motions in the pure IVR mechanism depends on the distance between the excited bond and the internal rotor.[168] On the other hand, it is clear that the τC_α-C mode participates in the mechanism of energy flow upon excitation of the 2νOH mode of PA, based on the observation of the $T_t \rightarrow T_g^{\pm}$ conversion resulting from internal rotation around the C_α-C bond. The quantum yield for the C_α-C isomerization (1.4×10^{-2}) is similar to that estimated for the C-O isomerization (see Table 3.3). For PA, the balance between the less efficient participation of the τCH_3 mode in deactivation of the C-O isomerization coordinate and the additional competing C_α-C isomerization channel could result in a ratio of reactive to non-reactive energy relaxation pathways towards the C-O isomerization similar to that of AA. However, it should be noted that the complexity of the energy relaxation mechanism prevents an unquestionable analysis of the results that should be

preferably based on the vibrational level structure derived from a reliable anharmonic analysis.

The environment effect on the *trans*→ *cis* isomerization quantum yield was probed by two different approaches: investigation of the matrix site effect and analysis of the effect of varying the rare-gas host.

The site selectivity of the C-O isomerization quantum yield was studied for the two major matrix sites of FA-OH in Ar matrices.[II] As shown in Table 3.3, at most the quantum yields associated with a specific vibrational mode for molecules isolated in different matrix sites differ by a factor of ~ 2 (see Table 3.3 and Fig. 4 of II). Thus, the quantum yields for this particular isomerization process are shown to be rather insensitive to the matrix site.

The effect of the nature of the rare-gas host was evaluated by analysing the C-O isomerization quantum yield for the 2νOH of AA-OH in Ar, Kr and Xe matrices at 8 K.[VII] The obtained values are equal within the estimated experimental error (2.2%, 2.6% and 3.5% in Ar, Kr and Xe, respectively).[VII] The same conclusion applies to the quantum yields determined for AA-OH in Ar and Kr matrices at various excitation energies below the barrier height. This observation suggests that the role of the phonon modes as a thermal bath in the energy flow mechanism is similar in all matrices and it does not shown any mode specificity.

Isotopic substitution effects on the C-O isomerization quantum yield were evaluated for AA and PA.[VII, IX] In the first case, the quantum yields were determined upon excitation of the 2νOH(OD) mode of the AA-OD, AA-CD_3 and AA-D_4 isotopologues and the νOH(OD) + νC=O mode of AA-CD_3 and AA-D_4.[VII] The 2νOD quantum yields were also estimated for PA-OD.

For both AA and PA, the isomerization quantum yield for excitation of the 2νOH mode is significantly reduced upon deuteration of the hydroxyl group (~ 2%→0.4% in AA and ~1%→0.3% in PA). This observation should not be connected with the lower energy introduced by excitation of the 2νOD mode as

compared with the 2νOH, because it was shown previously that the excess energy with respect to the barrier height cannot account for fluctuations of one order of magnitude in the quantum yield. The role of the lower anharmonicity of the 2νOD mode as compared to the 2νOH mode is unclear, because it can, in principle, influence the quantum yield in opposite directions. A lower anharmonicity may favour the energy relaxation within the vibrational envelope of the excited mode, reducing the possibilities of energy transfer into the reaction coordinate, but it may also increase the lifetime of the excited states, increasing the importance of weak anharmonic couplings with the torsional coordinate.

A reasonable explanation for the decrease in the quantum yield of the OD-forms has to do with the magnitude of the energy quanta associated with the reaction coordinate, which is lower in the OD-forms.[II,VI] If we consider the ratio between the frequency of the excited mode and the frequency of the torsional mode for both isotopologues (~ 11 for the OH-forms and ~ 12 for the OD-forms)[VI] a lower-order direct coupling could be anticipated between the two modes in the OH-forms. It can be argued that such a high-order coupling is highly unlikely. However, even more relevant changes in the coupling orders should be expected between the torsional modes and those intermediate modes excited in the cascading relaxation that are not significantly affected by the isotopic substitution, always with higher order couplings for the OD-forms. Establishing a parallelism with the gas phase studies of IVR,[106] the higher the coupling order the weaker the magnitude of the coupling. Therefore a lower probability of energy transfer into the reaction coordinate is expected for the OD-forms. A less significant contribution of the tunnel effect to the photoinduced C-O isomerization could also be determinant for a lower quantum yield in the OD-forms as compared to the OH-forms.

On the other hand, deuteration of the methyl group increases de quantum yield by a factor of 3-7, as seen from comparison of the values estimated for the 2νOH(OD) modes of AA-OH and AA-CD_3 or AA-OD and AA-D_4, shown in Table 3.3.[VII] The significant effect of the methyl deuteration indicates that the methyl rotor has an

important participation in the mechanism of energy flow. Once again, this effect has to be understood on the basis of the intrinsic level structure and specific intramolecular couplings. The methyl-deuteration effect can be analogous to the hydroxyl-deuteration effect bearing in mind that now the isotopic substitution acts essentially on the intermediate excited states. The higher vibrational quanta of the CH_3 modes compared with the CD_3 modes can participate in lower energy couplings with the initially excited mode increasing the rate of energy flow out of this mode. At the same time, due to their higher vibrational quanta, the CH_3 modes will be further away from the τC-O mode, thus higher order couplings with the reaction coordinate can be anticipated. Under this assumption the quantum yield would be lower for the isotopologues bearing the fully-hydrogenated methyl group, as observed.

3.3.2 Cis → trans C-O isomerization

The increased stability of the *cis* arrangement of the carboxylic group in the OD-forms allowed for a more detailed study of the corresponding conformers bearing this arrangement. Therefore, the C-O isomerization quantum yield was also investigated for the reverse *cis → trans* photoisomerization in AA-OD, AA-D_4 and PA-OD ($C_t \rightarrow T_t$). [VII, IX] The *cis → trans* isomerization quantum yields estimated upon excitation of the 2νOD mode of the *cis* conformer are systematically higher than those of the reverse processes (by factor of 3 in AA-OD and by a factor of 40 in AA-D_4 and PA-OD).[VII,IX]

Several reasons can be enumerated to support the fact that the lower *cis → trans* isomerization barrier with respect to the reverse *trans → cis* process (Table 3.1) is not the determinant factor affecting the quantum yield ratio. Firstly, the results discussed previously suggest that the excess energy with respect to the barrier height has very little effect on the isomerization quantum yield. Secondly, a significant difference in the quantum yields for the direct and reverse isomerization process have been observed before in HONO, where the barrier height is nearly equal in both directions (difference of ~ 130 cm^{-1}).[13] Finally, the barrier height in both directions are

nearly unaffected for all the isotopologues (ab initio calculated differences of less than 40 cm^{-1})[**] but the quantum yield ratio between the *cis* → *trans* and *trans* → *cis* processes change from ~ 3 in AA-OD to 40 in AA-D_4.[VII] For the moment, the true nature of the factors determining a systematically higher quantum yield for the exothermic process remains unknown.

3.3.3 C_α-C isomerization vs C-O isomerization

For PA, the relative quantum efficiency of the two competing rotational isomerization processes (C-O and C_α-C isomerization) was studied.[IX] For PA-OD, the site selectivity of the branching ratio was also investigated by exciting the envelope of the 2νOD absorption at two different frequencies.[IX] Table 3 in IX shows the estimated quantum yield for the C-O ($T_t \rightarrow C_t$) and C_α-C ($T_t \rightarrow T_g^{\pm}$) isomerization for the two pumping experiments of PA-OD.

For PA-OH, the estimated C-O and C_α-C isomerization quantum yields are equal within our experimental error (1.4×10^{-2}). On the other hand, for PA-OD, the branching ratio for the C-O and C_α-C isomerization changes from 2 (HF site) to 12 (LF site), in favour of the C-O internal rotation (Table 3 in IX). For this branching ratio contributes a change in the C_α-C isomerization quantum yield of a factor of ~ 4 (0.16% and 0.042%)[IX] depending on the excitation frequency, while the C-O isomerization quantum yields are not significantly affected by local inhomogeneities of the matrix (0.32 and 0.5% depending on the excited site).[IX]

The results obtained for the C-O isomerization are in agreement with those obtained for FA-OH. On the other hand, the apparent site-selectivity of the quantum yield for the C_α-C isomerization observed for PA-OD is in agreement with the fact that the C_α-C rotation qualifies as a possibly restricted process by the rigidity of the

[**] The barrier heights were estimated accounting for the ZPVE correction. This correction was extracted from the ab initio vibrational frequencies scaled by two multiplying factor (0.94 and 0.97 for frequencies above and below 2000 cm^{-1}, respectively) in order to achieve a better fitting with the experimentally observed fundamentals.[VIII]

matrix cage. Indeed, due to the motion of the heavy atoms, this process requires a larger reaction volume in comparison with the C-O isomerization. However, as discussed earlier (see *Section 3.1*), there are some experimental indications of a low barrier for the $T_t \rightarrow T_g^{\pm}$ process in the matrix, which do not support a C_α-C rotation restricted by the matrix cage. Alternatively, site specific pathways for the energy flow leading to site seletive isomerization branching ratio cannot be ruled out. The motion of the heavy atoms within the matrix cage might enhance the coupling of the intramolecular modes with the lattice phonons and thus the C_α-C isomerization could be more affected by the matrix cage than the C-O isomerization.

On the other hand, it should be noted that it is difficult to understand if we are really on the presence of a truly site selective branching ratio or if these site effects on the isomerization quantum yields for the C_α-C rotation are not a consequence of some overlap between the absorptions of the reactant (T_t) and product conformers ($T_g^{\pm}$). Note that the lower C_α-C quantum yield is the one estimated for pumping the 2νOD mode at lower frequencies within its absorption envelope (LF site), where some overlap is expected between the absorptions of T_t and $T_g^{\pm}$ (see Fig 3 of VIII showing the 2νOH absorption of both conformers for the PA-OH). This overlapping is expected to be considerably smaller for the sites where the 2νOD mode absorbs at higher frequencies (HF site). Additionally, we have failed to observe the C_α-C isomerization for excitation of the C_t conformer isolated in the LF site[‡]. Also here, the absence of $C_g^{\pm}$ resulting from C_α-C isomerization could be explained by an overlap of the 2νOD absorption of the C_t and $C_g^{\pm}$ conformers, similarly to that observed for the T_t and $T_g^{\pm}$ conformers of PA-OH.[VIII]

[‡] C_t conformer produced simultaneously with the $T_g^{\pm}$ form upon the LF pumping of the 2νOD mode of T_t.

3.4 Conformationally selective photolysis

The effect of the conformation of the carboxylic group on the UV induced decomposition was investigated for FA and AA isolated in Ar matrices at 8 K. Photolysis of the *trans* form of FA and AA has been studied extensively in the gas phase.[169-177] Additionally for *trans*-FA, a study of the process in rare-gas matrices was also reported.[178] In the present work, the control of the conformational distribution of the sample, possible thanks to the narrowband IR irradiation setup, allowed for the study of photolysis of the two conformers of FA and AA. In the case of FA, a sufficiently large amount of the *cis* conformer could be produced from IR-excitation of *trans* for FA-OH. However, for AA, due to the increased *cis* $\rightarrow$ *trans* tunneling rate, the AA-D_4 isotopologue was used instead of AA-OH to produce enough *cis* conformer in the matrix. In general, the photolysis was induced by 193 nm excitation in Ar matrices at 8 K. This excitation wavelength is associated with the $n \rightarrow \pi^*$ transition of the carbonyl group. The results of this study have been reported in the attached papers IV, VI and ref.179.

For FA, the photolysis mechanism was shown to depend on the initially excited conformer. Recently, experimental evidence of photodissociation channels specific to rotational isomers have also been reported for the gas phase cation 1-$C_3H_7I^+$.[180] On the other hand, for AA a similar product distribution was obtained irrespectively of the excited conformer. Several factors can be pointed out as possible explanation for the difference in the conformational selectivity of photolysis of FA and AA. The effect of the ratio between the isomerization and decomposition rates in the excited states and the nature of the primary dissociation steps (radicals or stable molecules) have been considered in particular.

Five photolysis channels have been proposed earlier for FA, two molecular elimination channels (1-2), one channel leading to OH radical formation (3) and two bond-fission channels leading to H-atom elimination (4-5)[176]:

$$HCOOH + h\nu \rightarrow H_2 + CO_2 \quad (1)$$
$$\rightarrow H_2O + CO \quad (2)$$
$$\rightarrow HCO + OH \quad (3)$$
$$\rightarrow H + COOH \quad (4)$$
$$\rightarrow HCOO + H \quad (5)$$

The number of channels available for decomposition increases with the excitation energy. According to theoretical studies, the decomposition into stable molecules is the only process available for the electronic ground state, while channels 3-5 became accessible both from the S_1 and T_1 surfaces.[170] The available experimental results on UV-photolysis of *trans*-FA arrive to somewhat controversial conclusions. Earlier gas-phase studies favoured molecular elimination channels in the spectral region of 220-260 nm while a high quantum yield for hydroxyl radical formation (0.7-0.8) is pointed out by more recent studies in the same region.[176] The formation of hydrogen atoms was suggested to be significant only at lower excitation wavelengths (<220 nm).[181,182]

Interestingly, a recent study of the 193 nm photolysis of *trans*-FA in the gas phase claims that despite the relatively high excitation energies (enough to excite the S_1 state at 250-270 nm),[169,170] the main primary products observed are the molecular elimination products with a CO/CO_2 branching ratio of 11.[169] This result was explained in terms of dissociation in the vibrationally excited S_0 state from a *trans*-like structure resembling geometrically the transition state for dissociation into CO and H_2O. For fragmentation to take place from a *trans*-like geometry in the vibrationally excited S_0 state the internal conversion (IC) from the initially excited S_1 state is assumed to take place before rotational isomerization.[169,170]

Similar results were reported upon 193 nm photolysis of *trans*-FA in Ar and Kr matrices with an estimated CO/CO_2 branching ratio of ~ 4-5.[178] However, conversely to the 193 nm photolysis in the gas phase, the formation of CO and H_2O in the matrix was suggested to result from cage-induced recombination of HCO and OH radicals formed in a primary decomposition step. Formation of CO_2 and H_2 was

interpreted as resulting from an intersystem crossing (ISC) from the S_1 state into a dissociative triplet state induced by external heavy-atom effect. This heavy-atom effect was supported by a decrease in the CO/CO_2 ratio in Xe matrices or Xe-doped Ar matrices relatively to the observed ratio in pure Ar matrices.[178]

In the present investigation, the products observed upon 193 nm photolysis of of FA in Ar matrices for both *trans* and *cis* conformers were isolated stable molecules (CO_2) or molecular complexes (1:1 complexes of $CO : H_2O$ and $CO_2 : H_2$). [IV,179] The formation of complexes is a common effect in solid-state photolysis.[183-186] Except for the smaller fragments,[187] the species formed upon photolysis do not have enough energy to escape the matrix cage. The molecular entities formed upon dissociation are kept in close contact, which favours the formation of stable van der waals complexes within the cage.

However, while the channel (2) dominates photolysis of *trans*-FA (estimated CO/CO_2 branching ratio of ~ 4 in good quantitative agreement with the earlier study on photofragmentation of *trans*-FA in solid Ar),[178] channel (1) dominates photolysis of *cis*-FA (estimated CO/CO_2 branching ratio of ~ 0.4). [IV,179] Fig. 6 in paper IV illustrates the differences in the photolysis products of *trans*- and *cis*-FA. Note that the branching ratio changes one order of magnitude depending on the initially excited conformer. This remarkable change in the photolysis branching ratio from the *trans* to *cis* conformer represents a clear evidence of the conformational selectivity of the photoinduced dissociation upon 193 nm excitation in solid Ar. The question is which of the previously proposed mechanisms could explain the observed conformational selectivity: *(i)* primary radical decomposition in the excited state surfaces followed by recombination or *(ii)* fast IC to the S_0 surface followed by decomposition prior to conformational isomerization.

Prior to any consideration on the photolysis mechanism, it should be stressed that the main contribution from this work is the experimental evidence of a conformationally selective decomposition pathway for FA isolated in Ar matrices. The lack of thorough theoretical studies on the profile of the accessible electronic surfaces

from excitation of *trans*- and *cis*-FA prevents a clear understanding of the photolysis mechanism. Nevertheless, an analysis of the experimental observation in light of the two interpretations suggested in previous works was attempted.[169,178]

Theoretical studies of the ground state decomposition of FA have shown that the transition state for decomposition into CO + H_2O is geometrically connected with the *trans* conformer while that for decomposition into CO_2 + H_2 is most readily visualized as arising from the *cis* conformer (Fig 2 in IV illustrates this aspect).[40] Therefore, there is some theoretical basis to expect for conformationally dependent ground state decomposition channels. Indeed, a CO/CO_2 ratio of ~ 10 was previously reported for thermal decomposition of *trans*-FA. This is a surprising observation due to the fact that similar barriers have been predicted in the S_0 state for decomposition into molecular products via channels (1) and (2) (~ 23 000 cm^{-1}/430 nm).[40] Thus, the unexpected dominance of channel (2) suggests that there is some determinant dynamic factor to the decomposition mechanism in agreement with the theoretical predictions. Conformational isomerization in the vibrationally excited S_0 state seems to be a slower process when compared to decomposition, despite of its lower reaction barrier (~ 4100 cm^{-1}/ 2400 nm for the *trans* $\rightarrow$ *cis* conversion).

The similarities between the product distribution for photolysis of *trans*-FA (193 nm excitation in the gas phase and Ar matrix) and thermal decomposition support similar decomposition mechanisms. Thus, the observation of conformational memory in the photochemically induced decomposition could be explained on the basis of a mechanism that allows for relaxation into a vibrationally excited S_0 state with a geometry not far from the Frank-Condon geometry.

Furthermore, recent theoretical studies on the photodissociation of *trans*-FA give some support to an extensive decomposition in the S_0 surface even after 193 nm excitation.[170] From the initially excited S_1 state, mainly three processes are energetically accessible upon 193 nm irradiation: direct dissociation via reaction (3) (transition state at 42 000 – 45 000 cm^{-1}/ 240-220 nm), ISC to the T_1 state and IC to S_0 (Fig. 6 in ref. 169 is a good illustration of the dissociative profiles of the S_0, S_1 and T_1

surfaces). For *trans*-FA, the IC to S_0 via an S_0/S_1 conical intersection was suggested to take place with considerable efficiency prior to isomerization in the S_1 state,[170] meaning that there is some probability for the molecule to return to the S_0 state with an unrelaxed structure similar to that of the initially excited conformer. Although there is no detailed theoretical study of photolysis from excitation of the *cis* conformer, the conformational selectivity of the process seems to support a similar mechanism of dissociation in the S_0 surface as that proposed upon excitation of *trans*-FA.

On the other hand, partial isomerization in the S_0 or S_1 states and direct decomposition into radicals in the excited state surfaces could be pointed out as limiting factors of conformational selectivity. In this work, the presence of isolated OH radical (3554 cm^{-1} in solid Ar)[188] upon photolysis was not detected. It can be deduced that either the OH radicals are not formed or that the probability for radical pair recombination back to FA is much higher than for the cage exit of one of the radicals. For the moment, there are no reasons to believe that a radical recombination process could have any conformational preference or that different radicals could be formed from excitation of different coformers. Based on these assumptions, decomposition into radicals would lead to a conformationally independent decomposition process. Indeed, the decomposition of *trans*-FA at lower energies (234 nm) seems to lead to a higher conformational selectivity (CO/CO_2 ~ 6 in Ar matrices),[IV,179] which is in agreement with a lower probability of radical formation.

The lower branching ratio observed for *trans*-FA in the matrix studies, as compared to the gas phase study, is consistent with an increased isomerization rate in the matrix due to the participation of the lattice phonon in the energy relaxation mechanism. The different branching ratios observed for different matrix compositions in ref. 178 can also be rationalized in terms of different contributions from the lattice phonons to the energy relaxation mechanism affecting the ratio between the isomerization rate and the decomposition rate alternatively, or in addition, to the external heavy atom effect on the probability of spin-forbidden processes proposed earlier.[178] Indeed, also in the present study some preliminary indications of a host-

dependent conformational selectivity of 193 nm photolysis were recognized. Namely, the CO/CO_2 ratio was observed to be independent of the composition of the irradiated conformational mixture in Kr matrices and weakly dependent in Xe matrices.

From the discussion above, the conformational selectivity observed for FA in solid Ar suggests an isomerization rate slower than decomposition and a considerable relaxation into the vibrationally excited S_0 state prior to decomposition. Indeed for FA in solid Ar, the amount of conformational isomerization products observed upon 193 nm excitation can be neglected in comparison with the amount of decomposition products. Conversely, for AA, the amount of conformational isomerization products could not be neglected in comparison with those from decomposition in similar experimental conditions. Indeed, a different irradiation setup allowing for simultaneous IR and UV excitation had to be used in order to extract the photolysis products arising exclusively from UV excitation of each of the conformers of AA.[VI] Thus, one of the evident explanations for the lack of conformational selectivity observed in AA is competition between UV induced isomerization and decomposition upon 193 nm irradiation. However, there are other aspects of the photodecomposition of FA and AA that might be relevant to understand the observed differences on the conformational selectivity of the process.

In analogy with FA, the transition states for decomposition of AA have been theoretically connected with specific geometrical structures of the parent molecule.[189] Three molecular channels have been identified upon the gas-phase unimolecular decomposition of AA in the ground state, given by equations (6-8):

$$CH_3COOH \rightarrow CH_4 + CO_2 \quad (6)$$

$$\rightarrow CH_2{=}C{=}O + H_2O \quad (7)$$

$$\rightarrow CH_2C(OH)_2 \rightarrow CH_2{=}C{=}O + H_2O \quad (8)$$

The dominant decomposition products upon thermal excitation of the *trans* conformer are ketene and water (7-8).[190] According to the theoretical calculations, the transition state for reaction (6) is most easily reached from the *cis* well while channels (7) and (8) are most easily reached from the *trans* well.[189] However, despite of the theoretical

indications of conformationally selective decomposition pathways, the predominance of ketene and water upon thermal excitation of *trans*-AA is most readily accounted for by the two possible pathways leading to these same products.

On the other hand, photolysis of AA has been associated with four primary steps (equations 9-12) of radical formation:

$$CH_3COOH + h\nu \rightarrow CH_3CO + OH \quad (9)$$

$$\rightarrow CH_3 + COOH \quad (10)$$

$$\rightarrow CH_3COO + H \quad (11)$$

$$\rightarrow CH_2COOH + H \quad (12)$$

Studies of gas-phase decomposition at excitation energies above 220 nm indicate that the major primary step for AA decomposition is the formation of hydroxyl and acetyl radicals from reaction (9). [171-175] Conversely to FA, there are no indications of production of stable molecular species in primary decomposition steps upon excitation at 193 nm.[171-175]

As for FA, for both conformers of AA, molecular complexes were the main products of 193 nm excitation in solid Ar at 8 K (see ref. VI for a detailed identification of the products). The product distribution arising from photolysis of each of the conformers of AA is exactly the same, as shown in Fig. 2 of VI. The major molecular products were CO, CO_2 and CD_3OD. Somewhat smaller amounts of CD_2=C=O and CD_2=O were also detected.

Importantly, in opposition to FA, the distribution of molecular products arising from photolysis of AA was explained in terms of cage-induced recombination of radicals formed in primary dissociation steps along the excited state surfaces. All the expected molecular products from dissociation in the ground state were also observed upon photolysis of AA in solid Ar (equations 6-8). However, many of the observed decomposition products were exclusively obtained from photolysis in the solid state. Namely, the main product of photolysis of AA was the 1:1 complex between methanol and carbon monoxide. This was the first time that methanol was observed among the decomposition products of AA either induced by thermal or

photochemical excitation in the gas phase. The specificity of the products observed in the matrix supports a significant solid state effect on the photolysis of AA.

Two pathways were proposed to account for the production of methanol in the same cage as carbon monoxide: recombination of the primary acetyl and hydroxyl radical formed on the S_1 or T_1 surfaces (predominant photolysis products in the gas phase) and photolysis of secondary AA decomposition products like ketene in the presence of water. Formaldehyde (complexed with carbon monoxide and hydrogen) is also an exclusive product observed from solid-state photodecomposition of AA. It can be produced from photolysis of secondary products (methanol or ketene in the presence of carbon monoxide and water, respectively).[191-193] A schematic representation of the proposed AA photodecomposition channels in solid Ar is shown in Fig. 4 of VI. As seen in this figure, all the observed molecular complexes are equally explained on the basis of cage-induced recombination of primary radicals or further photolysis of secondary products to yield radicals that, in turn, will react to give different products.

The proposed mechanism for the solid-state photolysis of AA involves essentially decomposition into radicals in the excited state surfaces. Namely, it involves formation of primary radicals from C-O and C-C bond cleavage according to equations (9) and (10). In agreement with the gas-phase photolysis studies, the C-O cleavage was observed to be the dominant step for photolysis in Ar matrices. It accounts for 85-95 % of the observed products depending on the photolysed isotopologues (AA-OH or AA-D_4).[VI] The distribution of photolysis products is in agreement with the fact that the C-C cleavage is supposed to take place only on the T_1 surface while the C-O cleavage occurs both on the S_1 and T_1 surfaces, meaning that it has a higher probability than the C-C cleavage.[177] In a recent theoretical study,[177] it was concluded that although the intersystem crossing from S_1 to T_1 is a spin forbidden process, structural similarities between the crossing point of these two surfaces and the S_1 minimum indicate that this process can happen to a noticeable extent.

The conformational independence of the product distribution for a photolysis

mechanism associated with formation of primary radicals assumes that the branching ratio for radical formation is independent on the geometrical structure of the ground state, as anticipated from the study of FA photolysis. The present experimental investigation of UV-photolysis of the two conformers of FA and AA in solid Ar suggests that the conformational selectivity of the decomposition process is bound by the ratio between conformational isomerization and decomposition and also by the nature of the primary decomposition steps. Even for slow conformational isomerization processes in the excited state surfaces, the decomposition into radicals is expect to lead to the conformational independence of the final stable products. This conclusion is based on the fact that there are no indications that the branching ratio of radical formation in primary dissociation steps could be affected by the conformation of the parent molecule. Furthermore, the energized fragments are not expected to recombine selectively into any of the two possible conformers of the parent molecules.

4. Concluding Remarks

The narrowband IR irradiation of the matrix-isolated conformational ground state of the three molecules studied allowed for the experimental identification and detailed vibrational characterization of the higher energy conformers. The ab initio calculations of the vibrational spectra of the conformers aided the interpretation of the experimental results. The vibrational characterization of the conformational ground state was also significantly improved.

For FA and AA, phonon sidebands to intramolecular vibrations were detected from the observation of IR-induced isomerization processes at energies 40-65 cm^{-1} higher than those associated with pure intramolecular vibrational transitions. The observation of phonon sidebands to intramolecular vibrations in the absorption spectra is very uncommon due to weak vibron-phonon coupling. Nevertheless, this work shows that excitation of phonon sidebands can induce processes over a wide spectral range in an apparently non-resonant way.

Tunneling from the higher energy arrangement of the carboxylic group (*cis*) into the lower energy arrangement (*trans*) was observed in dark for all the studied isotopologues of the three molecules isolated in solid Ar, even at the lowest working temperatures (8 K). The effects of isotopic substitution, temperature and environment on the tunneling rate coefficients were investigated.

As expected for a tunneling process, deuteration of the hydroxyl group was shown to decrease the dark isomerization rates by several orders of magnitude. Isotopic substitution of the hydrogen atoms that are not directly involved in the tunneling coordinate was shown to have the opposite effect in the *cis* $\rightarrow$ *trans* tunneling rate. The effect of deuteration of non-tunneling hydrogen atoms was explained on the basis of deuteration-induced changes in the intrinsic vibrational level structure affecting the nature of the vibrational states and/or the energy gaps involved

in the dissipative tunneling process. The observation of a smooth, non-linear temperature dependence of the tunneling rate coefficients (FA and AA) gave support to an important participation of lower energy quanta (lattice or intramolecular modes) in the studied processes. Regarding the solvent effect, it was shown that even in the case of weakly interacting media such as rare-gas matrices, the environment can have a remarkable effect in the tunneling rate.

The experimental data reported within this work should constitute a relevant contribution to the understanding of the tunnel effect in condensed media and could be useful to validate the theories of dissipative tunneling. A more reliable quantitative estimation of the intrinsic vibrational level structure, intra and intermolecular couplings and barrier heights for molecules isolated in a specific solid environment are needed to fully understand the experimental results obtained.

In the present work, the effects of nature of the excited mode, excitation energy, solid environment, deuteration and molecule size on the quantum yield of vibrationally induced conformational isomerization were also investigated.

For excitation energies *above* the isomerization barrier, the quantum yields were shown to be relatively insensitive to the nature of the excited modes, as well as to the excitation energy. Conformational isomerization was also induced at excitation energies *below* the computational barrier height, showing an important contribution of the tunnel effect also to photochemically induced process. In this energy region, the quantum yield increases with the excitation energy. The observed trend reflects the increased tunneling probability with excitation of the reaction coordinate.

The solid environment (nature of the rare-gas host and matrix site) was shown to have a negligible effect on the quantum yield for isomerization of the carboxylic group. The experimental data is inconclusive regarding the effect of the solid medium on the C_α-C isomerization of PA.

Investigation of the isotopic substitution effect revealed a strong influence on the C-O isomerization. The quantum yield decreases by more than a factor of 4 upon deuteration of the hydroxyl group (AA and PA), while deuteration of the methyl group

increases the quantum yield by a factor of 3-7 (AA). Specific changes in the intrinsic vibrational level structure and in the anharmonic couplings brought about by isotopic substitution were pointed out as possible explanations for the observed deuteration effects. In the case of deuteration of the OH internal rotor, the lower vibrational quanta of the torsional coordinate in the OD-forms was assumed to increase the order of the anharmonic couplings with the excited states, thus decreasing the probability of energy transfer into the reaction coordinate. For the OD-forms, a less significant contribution of the tunnel effect to the photoinduced C-O isomerization could also account for a lower quantum yield as compared to the OH-forms. On the other hand, deuteration of the methyl group was suggested to lead to a less efficient deactivation of the initially excited state, because it is expected to participate in higher-order (less efficient) couplings with the lower energy modes of the deuterated methyl group.

For similar excitation energies and analogous vibrational modes (2νOH), the quantum yield for C-O isomerization was shown to increase by one order of magnitude from FA (10-20%) to AA (2%), while for PA the estimated value is similar to AA (1%). The participation of large amplitude C-C torsional modes of AA and PA in the cascading energy relaxation process was proposed to explain the observed trend. These modes were assumed to be coupled with the reaction coordinate in a way that favours the dissipation of its excitation energy into the bath of lower quanta intramolecular modes and/or lattice modes. This interpretation is supported by the fact that the vibrational quanta associated with the torsional modes of AA and PA are of the same order of magnitude of the Debye frequency of solid rare gases, which can favour energy transfer from the intramolecular modes into the lattice phonons.

On the other hand, the similarity of the C-O isomerization quantum yield estimated for analogous excitation conditions of AA and PA was explained on the basis of a similar ratio of reactive to non-reactive energy relaxation pathways in the two molecules. In this context, it was pointed out that the effect of the competing C_α-C isomerization channel in PA could be cancelled out by a relatively less efficient participation of the τCH_3 mode of PA in the deactivation of the C-O isomerization

coordinate, resulting in similar quantum yields for PA and AA. The fact that the methyl group in PA is further away from the OH rotor than in AA supports a less efficient deactivation of the reaction coordinate by the τCH_3 mode in PA. Similar studies for molecules like propiolic (H-C≡C-C(=O)OH) and 3-butynoic (H-C≡C-CH_2-C(=O)OH) acids could aid evaluation of molecular size and distance of the excitation coordinate from the reaction coordinate on the isomerization quantum yields.

It is worth noting that behind the estimated isomerization quantum yields there is a complex energy relaxation mechanism involving intra and intermolecular energy levels. The method used to probe this mechanism is limited in the sense that it gives information only on the initially excited state and on some of the final states of the relaxation pathways. The lack of information on the nature of the intermediate excited states involved in the cascading relaxation process and on the vibrational level structure of each of the molecules studied determines the speculative nature of the interpretation of the experimental results. Transient absorption techniques should be valuable to improve the knowledge on the energy relaxation mechanism leading to conformational isomerization in carboxylic acids.

One of the most interesting observations of the present work was the conformationally selective photodecomposition exhibited by FA in solid Ar upon excitation at 193 nm. Conversely to FA, for AA the photolysis products are independent on the initially excited structure. The selectivity of the photodecomposition process was assumed to depend on the competition between isomerization and decomposition upon photochemical excitation, as well as on the nature of the primary decomposition steps.

Bibliography

1. Huff, J. B.; Askew, B.; Duff, R. J.; Rebek, J., *J. Am. Chem. Soc.* **1988,** *110*, 5908.
2. Cantor, C. R.; Schimmel, P. R., *Biophysical chemistry*, ed., W. H. Freeman: San Francisco, 1980.
3. Tadayoni, B. M.; Parris, K.; Rebek, J., *J. Am. Chem. Soc.* **1989,** *111*, 4503.
4. Montzka, T. A.; Swaminathan, S.; Firestone, R. A., *J. Phys. Chem.* **1994,** *98*, 13171.
5. Liu, S. Y.; Mehringer, D. M.; Snyder, L. E., *Astrophys. J.* **2001,** *552*, 654.
6. Mehringer, D. M.; Snyder, L. E.; Miao, Y. T., *Astrophys. J.* **1997,** *480*, 71.
7. Snyder, L. E.; Lovas, F. J.; Hollis, J. M.; Friedel, D. N.; Jewell, P. R.; Remijan, A.; Ilyushin, V. V.; Alekseev, E. A.; Dyubko, S. F., *Astrophys. J.* **2005,** to be published.
8. Fausto, R., in *Low temperature molecular spectroscopy*, ed. Fausto, R., Kluwer Academic Publishers, Dordrecht, 1996.
9. Murto, J.; Raaska, T.; Kunttu, H.; Räsänen, M., *Theochem-J. Mol. Struc.* **1989,** *59*, 93.
10. Pettersson, M.; Lundell, J.; Khriachtchev, L.; Räsänen, M., *J. Am. Chem. Soc.* **1997,** *119*, 11715.
11. Nieminen, J.; Pettersson, M.; Räsänen, M., *J. Phys. Chem.* **1993,** *97*, 10925.
12. Nieminen, J.; Räsänen, M.; Murto, J., *J. Phys. Chem.* **1992,** *96*, 5303.
13. Khriachtchev, L.; Lundell, J.; Isoniemi, E.; Räsänen, M., *J. Chem. Phys.* **2000,** *113*, 4265.
14. Borba, A.; Gomez-Zavaglia, A.; Lapinski, L.; Fausto, R., *Phys. Chem. Chem. Phys.* **2004,** *6*, 2101.
15. Reva, I. D.; Jarmelo, S.; Lapinski, L.; Fausto, R., *Chem. Phys. Lett.* **2004,** *389*, 68.
16. Reva, I. D.; Stepanian, S. G.; Adamowicz, L.; Fausto, R., *J. Phys. Chem. A* **2003,** *107*, 6351.
17. Jarmelo, S.; Fausto, R., *Phys. Chem. Chem. Phys.* **2002,** *4*, 1555.
18. Fausto, R.; Maçôas, E. M. S.; Kulbida, A., *J. Mol. Struct.* **1999,** *481*, 83.
19. Fausto, R.; Kulbida, A.; Schrems, O., *J. Chem. Soc. Faraday Trans.* **1995,** *91*, 3755.
20. Kulbida, A.; Fausto, R., *J. Chem. Soc. Faraday Trans.* **1993,** *89*, 4257.
21. Fausto, R.; Teixeira-Dias, J. J. C.; Gil, F. P. S. C., *J. Chem. Soc. Faraday Trans.* **1993,** *89*, 3235.
22. de-Carvalho, L. A. E. B.; Teixeira-Dias, J. J. C.; Fausto, R., *Theochem-J. Mol. Struct.* **1990,** *67*, 109.
23. Fausto, R.; de-Carvalho, L. A. E. B.; Teixeira-Dias, J. J. C., *Theochem-J. Mol. Struct.* **1990,** *66*, 67.
24. Fausto, R.; de-Carvalho, L. A. E. B.; Teixeira-Dias, J. J. C.; Ramos, M. N., *J. Chem. Soc. Faraday Trans. 2* **1989,** *85*, 1945.
25. Fausto, R.; Teixeira-Dias, J. J. C., *J. Mol. Struct.* **1986,** *144*, 225.
26. Fausto, R.; Teixeira-Dias, J. J. C., *J Mol. Struct.* **1986,** *144*, 241.
27. Reva, I. D.; Stepanian, S. G.; Adamowicz, L.; Fausto, R., *J. Phys. Chem. A* **2001,** *105*, 4773.
28. Kulbida, A.; Ramos, M. N.; Räsänen, M.; Nieminen, J.; Schrems, O.; Fausto, R., *J. Chem. Soc. Faraday Trans.* **1995,** *91*, 1571.
29. Maçôas, E. M. S.; Fausto, R.; Lundell, J.; Pettersson, M.; Khriachtchev, L.; Räsänen, M., *J. Phys. Chem. A* **2000,** *104*, 11725.
30. Maçôas, E. M. S.; Fausto, R.; Lundell, J.; Pettersson, M.; Khriachtchev, L.; Räsänen, M., *J. Phys. Chem. A* **2001,** *105*, 3922.
31. Maçôas, E. M. S.; Fausto, R.; Pettersson, M.; Khriachtchev, L.; Räsänen, M., *J. Phys.*

Chem. A **2000,** *104*, 6956.
32. Wiberg, K. B.; Laidig, K. E., *J. Am. Chem. Soc.* **1987,** *109*, 5935.
33. Teixeira-Dias, J. J. C.; Fausto, R., *J. Mol. Struct.* **1986,** *144*, 199.
34. Lii, J. H., *J. Phys. Chem. A* **2002,** *106*, 8667.
35. Allinger, N. L.; Chang, S. H. M., *Tetrahedron* **1977,** *33*, 1561.
36. Wiberg, K. B., *J. Am. Chem. Soc.* **1986,** *108*, 5817.
37. Wiberg, K. B.; Martin, E., *J. Am. Chem. Soc.* **1985,** *107*, 5035.
38. Wiberg, K. B.; Murcko, M. A., *J. Comput. Chem.* **1988,** *9*, 488.
39. Wiberg, K. B.; Schreiber, S. L., *J. Org. Chem.* **1988,** *53*, 783.
40. Goddard, J. D.; Yamaguchi, Y.; Schaefer, H. F., *J. Chem. Phys.* **1992,** *96*, 1158.
41. Senent, M. L., *Mol. Phys.* **2001,** *99*, 1311.
42. Hisatsun.Ic; Heicklen, J., *Can. J. Spectrosc.* **1973,** *18*, 135.
43. Hocking, W. H., *Z Naturforsch A* **1976,** *31*, 1113.
44. Bjarnov, E.; Hocking, W. H., *Z Naturforsch A* **1978,** *33*, 610.
45. Blake, P. G.; Jackson, G. E., *J. Chem. Soc. B* **1969**, 94.
46. Blake, P. G.; Jackson, G. E., *J. Chem. Soc. B* **1968**, 1153.
47. Blake, P. G.; Davies, H. H.; Jackson, G. E., *J. Chem. Soc. B* **1971**, 1923.
48. Blake, P. G.; Hole, K. J., *J. Chem. Soc. B* **1966**, 577.
49. Derissen, J. L., *J. Mol. Struct.* **1971,** *7*, 81.
50. Stiefvater, O. L., *J. Chem. Phys.* **1975,** *62*, 233.
51. Stiefvater, O. L., *J. Chem. Phys.* **1975,** *62*, 244.
52. Whittle, E.; Dows, D. A.; Pimentel, G. C., *J. Chem. Phys.* **1954,** *22*, 1943.
53. Perutz, R. N., *Chem. Rev.* **1985,** *85*, 77.
54. Perutz, R. N., *Chem. Rev.* **1985,** *85*, 97.
55. *Chemistry and physics of matrix-isolated species*, ed. Andrews, L. and Moskovits, M., Elsevier Science Pub. Co., Amsterdam, 1989.
56. Barnes, A. J., *J. Mol. Struct.* **1984,** *113*, 161.
57. Tasumi, M.; Nakata, M., *J. Mol. Struct.* **1985,** *126*, 111.
58. Almond, M. J., *Annu. Rep. Prog. Chem. Sec. C* **1997,** *93*, 3.
59. Klaeboe, P.; Nielsen, C. J., *Analyst* **1992,** *117*, 335.
60. Dunkin, I. R., in *Matrix-Isolation Techniques: A Practical Approach*, Oxford University Press, Oxford, 1998.
61. Hallamasek, D.; Babka, E.; Knozinger, E., *J. Mol. Struct.* **1997,** *408*, 125.
62. Swanson, B. I.; Jones, L. H., *J. Mol. Spectrosc.* **1981,** *89*, 566.
63. Swanson, B. I.; Jones, L. H., *J. Chem. Phys.* **1981,** *74*, 3205.
64. Jones, L. H.; Swanson, B. I.; Fry, H. A., *Chem. Phys. Lett.* **1982,** *87*, 397.
65. Swanson, B. I.; Jones, L. H.; Foltyn, E. M.; Asprey, L. B., *J. Phys. Chem.* **1982,** *86*, 3522.
66. Downs, A. J., in *Low temperature molecular spectroscopy*, ed. Fausto, R., ASI Series, Kluwer Academic Publishers: Dordrecht, 1996.
67. Barnes, A. J.; Lomax, S.; Vanderveken, B. J., *J. Mol. Struct.* **1983,** *99*, 137.
68. Reva, I. D.; Stepanian, S. G.; Adamowicz, L.; Fausto, R., *Chem. Phys. Lett.* **2003,** *374*, 631.
69. Gerber, R. B., *Annu. Rev. Phys. Chem.* **2004,** *55*, 55.
70. Christe, K. O., *Angew. Chem. Int. Edit.* **2001,** *40*, 1419.
71. Khriachtchev, L.; Pettersson, M.; Runeberg, N.; Lundell, J.; Räsänen, M., *Nature* **2000,** *406*, 874.
72. Pettersson, M.; Lundell, J.; Räsänen, M., *Eur. J. Inorg. Chem.* **1999**, 729.

73. Pettersson, M.; Lundell, J.; Khriachtchev, L.; Isoniemi, E.; Räsänen, M., *J. Am. Chem. Soc.* **1998,** *120*, 7979.
74. Khriachtchev, L.; Tanskanen, H.; Lundell, J.; Pettersson, M.; Kiljunen, H.; Räsänen, M., *J. Am. Chem. Soc.* **2003,** *125*, 4696.
75. Tanskanen, H.; Khriachtchev, L.; Lundell, J.; Kiljunen, H.; Räsänen, M., *J. Am. Chem. Soc.* **2003,** *125*, 16361.
76. Albinsson, B.; Teramae, H.; Downing, J. W.; Michl, J., *Chem. Eur. J* **1996,** *2*, 529.
77. Albinsson, B.; Michl, J., *J. Phys. Chem.* **1996,** *100*, 3418.
78. Bodenbinder, M.; Ulic, S. E.; Willner, H., *J. Phys. Chem.* **1994,** *98*, 6441.
79. Blom, C. E.; Gunthard, H. H., *Chem. Phys. Lett.* **1981,** *84*, 267.
80. Kulbida, A.; Nosov, A., *J. Mol. Struct.* **1992,** *265*, 17.
81. Felder, P.; Gunthard, H. H., *Chem. Phys.* **1982,** *71*, 9.
82. Reva, I. A.; Jarmelo, S.; Lapinski, L.; Fausto, R., *J. Phys. Chem. A* **2004,** *108*, 6982.
83. Stepanian, S. G.; Reva, I. D.; Radchenko, E. D.; Rosado, M. T. S.; Duarte, M. L. T. S.; Fausto, R.; Adamowicz, L., *J. Phys. Chem. A* **1998,** *102*, 1041.
84. Reva, I. D.; Plokhotnichenko, A. M.; Stepanian, S. G.; Ivanov, A. Y.; Radchenko, E. D.; Sheina, G. G.; Blagoi, Y. P., *Chem. Phys. Lett.* **1995,** *235*, 617.
85. Reva, I. D.; Plokhotnichenko, A. M.; Stepanian, S. G.; Ivanov, A. Y.; Radchenko, E. D.; Sheina, G. G.; Blagoi, Y. P., *Chem. Phys. Lett.* **1995,** *232*, 141.
86. Gómez-Zavaglia, A.; Reva, I. D.; Fausto, R., *Phys. Chem. Chem. Phys.* **2003,** *5*, 41.
87. Blom, C. E.; Muller, R. P.; Gunthard, H. H., *Chem. Phys. Lett.* **1980,** *73*, 483.
88. *Low temperature molecular spectroscopy*, ed. Fausto, R., NATO ASI Series, Kluwer Academic Publishers, Dordrecht, 1996.
89. Muller, R. P.; Hollenstein, H.; Huber, J. R., *J. Mol. Spectrosc.* **1983,** *100*, 95.
90. Baldeschwieler, J. D.; Pimentel, G. C., *J. Chem. Phys.* **1960,** *33*, 1008.
91. Hall, R. T.; Pimentel, G. C., *J. Chem. Phys.* **1963,** *38*, 1889.
92. Räsänen, M.; Kunttu, H.; Murto, J., *Laser. Chem.* **1988,** *9*, 123.
93. Lotta, T.; Murto, J.; Räsänen, M.; Aspiala, A., *J. Mol. Struct.* **1984,** *114*, 333.
94. Gunthard, H. H., *J. Mol. Struct.* **1984,** *113*, 141.
95. Frei, H.; Pimentel, G. C., *Annu. Rev. Phys. Chem.* **1985,** *36*, 491.
96. Frei, H.; Pimentel, G. C., in *Chemistry and physics of matrix-isolated species*, ed. Andrews, L. and Moskovits, M., Elsevier Science Pub. Co., Amsterdam, 1989.
97. Poliakoff, M.; Turner, J. J., in *Chemical and biochemical applications of lasers*, ed. Moore, C. B., Academic Press., New York, 1980; Vol. 5.
98. Kudoh, S.; Takayanagi, M.; Nakata, M.; Ishibashi, T.; Tasumi, M., *J. Mol. Struct.* **1999,** *479*, 41.
99. Pourcin, J.; Davidovics, G.; Bodot, H.; Abouafmarguin, L.; Gauthierroy, B., *Chem. Phys. Lett.* **1980,** *74*, 147.
100. Knudsen, A. K.; Pimentel, G. C., *J. Phys. Chem.* **1991,** *95*, 2823.
101. Hoffman, W. F.; Shirk, J. S., *Chem. Phys.* **1983,** *78*, 331.
102. Roubin, P.; Varin, S.; Verlaque, P.; Coussan, S.; Berset, J. M.; Ortega, J. M.; Peremans, A.; Zheng, W. Q., *J. Chem. Phys.* **1997,** *107*, 7800.
103. Coussan, S.; Bouteiller, Y.; Perchard, J. P.; Zheng, W. Q., *J. Phys. Chem. A* **1998,** *102*, 5789.
104. Sander, S.; Willner, H.; Khriachtchev, L.; Pettersson, M.; Räsänen, M.; Varetti, E. L., *J. Mol. Spectrosc.* **2000,** *203*, 145.
105. Dubost, H.; Legay, F., in *Chemistry and physics of matrix-isolated species*, ed. Andrews, L. and Moskovits, M., Elsevier Science Pub. Co., Amsterdam, 1989.

106. Nesbitt, D. J.; Field, R. W., *J. Phys. Chem.* **1996,** *100*, 12735.
107. Legay, F., in *Chemical and Biochemical Applications of Lasers*, ed. Moore, C. B., Academic Press, New York, 1977; Vol. II.
108. Bondybey, V. E., *Annu. Rev. Phys. Chem.*, **1984,** *35*, 591.
109. Bondybey, V. E.; Räsänen, M.; Lammers, A., *Annu. Rev. Phys. Chem. Sec. C* **1999,** *95*, 331.
110. Lehmann, K. K.; Scoles, G.; Pate, B. H., *Annu. Rev. Phys. Chem.* **1994,** *45*, 241.
111. Owrutsky, J. C.; Raftery, D.; Hochstrasser, R. M., *Annu. Rev. Phys. Chem.* **1994,** *45*, 519.
112. Assmann, J.; Kling, M.; Abel, B., *Angew. Chem. Int. Edit.* **2003,** *42*, 2226.
113. Zewail, A. H.; Schryver, F. C. d.; Feyter, S. D.; Schweitzer, G., *Femtochemistry*, ed. Wiley-VCH, Weinheim, New York, 2001.
114. Mcdonald, P. A.; Shirk, J. S., *J. Chem. Phys.* **1982,** *77*, 2355.
115. Yoo, H. S.; DeWitt, M. J.; Pate, B. H., *J. Phys. Chem. A* **2004,** *108*, 1348.
116. Yoo, H. S.; DeWitt, M. J.; Pate, B. H., *J. Phys. Chem. A* **2004,** *108*, 1365.
117. Yoo, H. S.; McWhorter, D. A.; Pate, B. H., *J. Phys. Chem. A* **2004,** *108*, 1380.
118. Elles, C. G.; Cox, M. J.; Crim, F. F., *J. Chem. Phys.* **2004,** *120*, 6973.
119. Nitzan, A.; Mukamel, S.; Jortner, J., *J. Chem. Phys.* **1974,** *60*, 3929.
120. Torralva, B. R.; Allen, R. E., *J. Mod. Optic.* **2002,** *49*, 593.
121. Henriksen, N. E., *Chem. Soc. Rev.* **2002,** *31*, 37.
122. Brixner, T.; Gerber, G., *Chemphyschem* **2003,** *4*, 418.
123. Lozovoy, V. V.; Comstock, M.; Dantus, M., *Acs. Sym. Ser.* **2002,** *821*, 61.
124. Kohler, B.; Krause, J. L.; Raksi, F.; Rosepetruck, C.; Whitnell, R. M.; Wilson, K. R.; Yakovlev, V. V.; Yan, Y. J.; Mukamel, S., *J. Phys. Chem.* **1993,** *97*, 12602.
125. Krause, J. L.; Whitnell, R. M.; Wilson, K. R.; Yan, Y. J.; Mukamel, S., *J. Chem. Phys.* **1993,** *99*, 6562.
126. Bell, R. P.,in *The tunnel effect in chemistry*, Chapman and Hall, London, 1980.
127. Kumada, T.; Komaguchi, K.; Aratono, Y.; Miyazaki, T., *Chem. Phys. Lett.* **1996,** *261*, 463.
128. Ivanov, G. K.; Kozhushner, M. A.; Trakhtenberg, L. I., *J. Chem. Phys.* **2000,** *113*, 1992.
129. Ivanov, G. K.; Kozhushner, M. A.; Trakhtenberg, L. I., *Chem. Phys. Lett.* **2000,** *322*, 78.
130. Akai, N.; Kudoh, S.; Takayanagi, M.; Nakata, M., *Chem. Phys. Lett.* **2002,** *356*, 133.
131. Akai, N.; Kudoh, S.; Takayanagi, M.; Nakata, M., *J. Phys. Chem. A* **2002,** *106*, 11029.
132. Rostkowska, H.; Lapinski, L.; Khvorostov, A.; Nowak, M. J., *J. Phys. Chem. A* **2003,** *107*, 6373.
133. Rostkowska, H.; Lapinski, L.; Khvorostov, A.; Nowak, M. J., *Chem. Phys.* **2004,** *298*, 223.
134. Lapinski, L.; Rostkowska, H.; Khvorostov, A.; Yaman, M.; Fausto, R.; Nowak, M. J., *J. Phys. Chem. A* **2004,** *108*, 5551.
135. Flanigan, M. C.; Delavega, J. R., *J. Chem. Phys.* **1974,** *61*, 1882.
136. Basilevsky, M. V.; Davidovitch, G. V., *J. Chem. Phys.* **2001,** *115*, 6072.
137. Basilevsky, M. V.; Davidovitch, G. V., *J. Chem. Phys.* **2001,** *115*, 6083.
138. Suarez, A.; Silbey, R., *J. Chem. Phys.* **1991,** *94*, 4809.
139. Silbey, R.; Trommsdorff, H. P., *Chem. Phys. Lett.* **1990,** *165*, 540.
140. Wittl, F.; Eberlein, J.; Epple, T.; Dechant, M.; Creuzburg, M., *J. Chem. Phys.* **1993,** *98*, 9554.

141. Eisenberger, H.; Nickel, B.; Ruth, A. A.; Alsoufi, W.; Grellmann, K. H.; Novo, M., *J. Phys. Chem.* **1991,** *95*, 10509.
142. Alsoufi, W.; Grellmann, K. H.; Nickel, B., *J. Phys. Chem.* **1991,** *95*, 10503.
143. Brunton, G.; Gray, J. A.; Griller, D.; Barclay, L. R. C.; Ingold, K. U., *J. Am. Chem. Soc.* **1978,** *100*, 4197.
144. Henning, J.; Limbach, H. H., *J. Chem. Soc. Faraday Trans. 2* **1979,** *75*, 752.
145. Frisch, M. J. T., G. W; Schlegel, H. B.; Scuseria, G. E.; Robb, M. A.; Cheeseman, J. R.; Zakrzewski, V. G.; Montgomery, J. A.; Stratmann, R. E; Burant, J. C.; Dapprich, S.; Millam, J. M.; Daniels, A. D.; Kudin, K. N.; Strain, M. C.; Farkas, O.; Tomasi, J.; Barone, V.; Cossi, M.; Cammi, M.; Mennucci, B.; Pomelli, C.; Adamo, C.; Clifford, S.; Ochterski, J.; Petersson, G. A.; Ayala, P. Y.; Cui, Q.; Morokuma, K.; Malick, D. K.; Rabuck, A. D.; Raghavachari, K.; Foresman, J. B.; Cioslowski, J.; Ortiz, J. V.; Baboul, A. G.; Stefanov, B. B.; Liu, G.; Liashenko, A.; Piskorz, P.; Komaromi, I.; Gomperts, R.; Martin, R. L.; Fox, D. J.; Keith, T.; Al-Laham, M. A.; Peng, C. Y.; Nanayakkara, A.; Gonzalez, C.; Challacombe, M.; Gill, P. M. W.; Johnson, B. G.; Chen, W.; Wong, M. W.; Andres, J. L.; Head-Gordon, M.; Replogle, E. S.; Pople, J. A., *GAUSSIAN 98, Gaussian, Inc., Pittsburgh, PA, 1998; Revision A. 9* **1998**.
146. Jensen, F., in *Introduction to computational chemistry*, John Wiley & Sons, Ltd., Chichester, 1999.
147. Schachtschneider, J. H., in *Technical Report; Shell Development Co., Emeryville, CA* **1969**.
148. Pettersson, M.; Maçôas, E. M. S.; Khriachtchev, L.; Fausto, R.; Räsänen, M., *J. Am. Chem. Soc.* **2003,** *125*, 4058.
149. Hollas, J. M., in *Modern spectroscopy*. 4th ed., John Wiley, Chichester, 2004.
150. Lewis, J. D.; Malloy, T. B.; Chao, T. H.; Laane, J., *J. Mol. Struct.* **1972,** *12*, 427.
151. Pitzer, K. S., *.J.Chem.Phys.* **1946,** *14*, 239.
152. Miertus, S.; Tomasi, J., *Chem. Phys.* **1982,** i, 239.
153. Miertus, S.; Scrocco, E.; Tomasi, J., *Chem. Phys.* **1981,** *55*, 117.
154. Cramer, C. J.; Truhlar, D. G., *Chem. Rev.* **1999,** *99*, 2161.
155. Flygare, W. H., *J. Chem. Phys.* **1963,** *39*, 2263.
156. Apkarian, V. A.; Weitz, E., *J. Chem. Phys.* **1982,** *76*, 5796.
157. Berney, C. V.; Redingto.Rl; Lin, K. C., *J. Chem. Phys.* **1970,** *53*, 1713.
158. Reva, I. D.; Plokhotnichenko, A. M.; Radchenko, E. D.; Sheina, G. G.; Blagoi, Y. P., *Spectrochim. Acta A* **1994,** *50*, 1107.
159. Brodyanski, A. P.; Medvedev, S. A.; Vetter, M.; Kreutz, J.; Jodl, H. J., *Phys. Rev. B* **2002,** *66*, 104301.
160. Pettersson, M.; Nieminen, J., *Chem. Phys. Lett.* **1998,** *283*, 1.
161. Bondybey, V. E.; Fletcher, C., *J. Chem. Phys.* **1976,** *64*, 3615.
162. Bondybey, V. E., in *Chemistry and physics of matrix-isolated species*, ed. Andrews, L. and Moskovits, M., Elsevier Science Pub. Co., Amsterdam, 1989.
163. Jodl, H. J., in *Chemistry and physics of matrix-isolated species*, ed., Andrews, L. and Moskovits, M., Elsevier Science Pub. Co., Amsterdam, 1989.
164. Akai, N.; Kudoh, S.; Nakata, M., *J, Phys, Chem, A* **2003,** *107*, 3655.
165. Firth, D. W.; Barbara, P. F.; Trommsdorff, H. P., *Chem, Phys,* **1989,** *136*, 349.
166. Agrawal, P. M.; Thompson, D. L.; Raff, L. M., *J, Chem, Phys,* **1995,** *102*, 7000.
167. Klein, M. V.; Wedding, B.; Levine, M. A., *Phys, Rev,* **1969,** *180*, 902.
168. Bethardy, G. A.; Wang, X. L.; Perry, D. S., *Can. J. Chem.* **1994,** *72*, 652.
169. Su, H. M.; He, Y.; Kong, F. N.; Fang, W. H.; Liu, R. Z., *J. Chem. Phys.* **2000,** *113*,

1891.
170. He, H. Y.; Fang, W. H., *J. Am. Chem. Soc.* **2003,** *125*, 16139.
171. Owrutsky, J. C.; Baronavski, A. P., *J. Chem. Phys.* **1999,** *111*, 7329.
172. Hunnicutt, S. S.; Waits, L. D.; Guest, J. A., *J. Phys. Chem.* **1991,** *95*, 562.
173. Hunnicutt, S. S.; Waits, L. D.; Guest, J. A., *Abstr. Pap. Am. Chem. Soc.* **1990,** *200*, 91.
174. Hunnicutt, S. S.; Waits, L. D.; Guest, J. A., *J. Phys. Chem.* **1989,** *93*, 5188.
175. Peterman, D. R.; Daniel, R. G.; Horwitz, R. J.; Guest, J. A., *Chem. Phys. Lett.* **1995,** *236*, 564.
176. Singleton, D. L.; Paraskevopoulos, G.; Irwin, R. S., *J. Phys. Chem.* **1990,** *94*, 695.
177. Fang, W. H.; Liu, R. Z.; Zheng, X. M.; Phillips, D. L., *J. Org. Chem.* **2002,** *67*, 8407.
178. Lundell, J.; Räsänen, M., *J. Mol. Struct.* **1997,** *437*, 349.
179. Khriachtchev, L.; Macoas, E.; Pettersson, M.; Räsänen, M., *J. Am. Chem. Soc.* **2002,** *124*, 10994.
180. Park, S. T.; Kim, S. K.; Kim, M. S., *Nature* **2002,** *415*, 306.
181. Gorden, R. J.; J., A. P., *J. Phys. Chem.* **1961,** *65*, 1033.
182. Burton, M., *J. Am. Chem. Soc.* **1963,** *58*, 1655.
183. Schatte, G.; Willner, H.; Hoge, D.; Knozinger, E.; Schrems, O., *J. Phys. Chem.* **1989,** *93*, 6025.
184. Lundell, J.; Räsänen, M.; Kunttu, H., *Theochem-J. Mol. Struct.* **1995,** *358*, 159.
185. Lundell, J.; Räsänen, M., *J. Phys. Chem.* **1995,** *99*, 14301.
186. Heikkila, A.; Pettersson, M.; Lundell, J.; Khriachtchev, L.; Räsänen, M., *J. Phys. Chem. A* **1999,** *103*, 2945.
187. Apkarian, V. A.; Schwentner, N., *Chem. Rev.* **1999,** *99*, 1481.
188. Khriachtchev, L.; Pettersson, M.; Tuominen, S.; Räsänen, M., *J. Chem. Phys.* **1997,** *107*, 7252.
189. Moreira, I. D. R., *Theochem-J. Mol. Struc.* **1999,** *466*, 119.
190. Butkovskaya, N. I.; Manke, G.; Setser, D. W., *J. Phys. Chem.* **1995,** *99*, 11115.
191. Glass, G. P.; Kumaran, S. S.; Michael, J. V., *J. Phys. Chem. A* **2000,** *104*, 8360.
192. Wen, Y.; Segall, J.; Dulligan, M.; Wittig, C., *J. Chem. Phys.* **1994,** *101*, 5665.
193. Harich, S.; Lin, J. J.; Lee, Y. T.; Yang, X., *J. Chem. Phys.* **1999,** *111*, 5.

Appendix I

Vibrational spectroscopy of cis- and trans-formic acid in solid argon.

Ermelinda M. S. Maçôas, Jan Lundell, Mika Pettersson, Leonid Khriachtchev, Rui Fausto and Markku Räsänen

J. Mol. Spectrosc. **2003**, *219*, 70-80.

Vibrational Spectroscopy of *cis*- and *trans*- Formic Acid in Solid Argon

Ermelinda M. S. Maçôas[1,2,*], Jan Lundell[1], Mika Pettersson[1], Leonid Khriachtchev[1], Rui Fausto[2] and Markku Räsänen[1]

[1]*Laboratory of Physical Chemistry, University of Helsinki, P.O.Box 55 (A.I. Virtasen aukio 1), FIN-00014 Helsinki, Finland.* [2]*Department of Chemistry (CQC),University of Coimbra, P-3004-535 Coimbra, Portugal.*

Abstract

Absorption spectra of *cis* and *trans* conformers of formic acid (HCOOH) isolated in solid argon are analyzed in the mid-infrared (4000-400 cm^{-1}) and near-infrared (7800-4000 cm^{-1}) regions. The HCOOH absorption spectrum reveals matrix-site splitting for the trapped molecule. Narrowband tunable infrared radiation is used to pump a suitable vibrational transition of the *trans* conformer in order to promote site-selectively the conversion to the *cis* conformer and separate the spectral features of each site group. Several anharmonic resonances are identified for both conformers. The results of anharmonic vibrational *ab initio* calculations (CC-VSCF) for the *trans* and *cis* conformers of formic acid are reported and compared with the experimental spectra.

1. Introduction

Formic acid (HCOOH) is the simplest organic acid exhibiting rotational isomerism with respect to rotation around the single C-O bond. It is a molecule of astrophysical [1] and atmospheric [2] relevance, and has a wide range of industrial applications [3]. Formic acid exists in two stable planar structures, the *cis* and *trans* conformers shown in Fig. 1, with 0º and 180º H-C-O-H dihedral angles, respectively. The *trans* form is the most stable and the predominant one in the gas phase. Gas phase [4-8] and matrix-isolated [9-12] *trans*-formic acid and its isotopomers have been the subject of many spectroscopic studies in the mid-infrared region (mid-IR). Near-infrared (near-IR) spectroscopic data for the gaseous *trans*-HCOOH and its deuterated analogues are also available [13]. Recently, a detailed analysis of the gas-phase vibrational spectrum of *trans*-HCOOH appeared, reporting new overtone and combination data [14]. To the best of our knowledge no near-IR data of matrix-isolated formic acid has been reported yet.

The first reliable identification of *cis*-HCOOH was made in the gas phase by Hocking, where the microwave spectra of isotopically substituted species of *cis*-formic acid were reported [15]. The lack of experimental data concerning this conformer is not surprising considering the relative

* Corresponding author.
E-mail address:emacoas@qui.uc.pt (E.M.S. Maçôas)

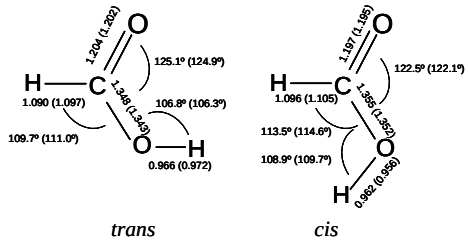

Fig. 1. The two stable conformers of formic acid; *cis*-HCOOH being 1365 cm^{-1} above *trans*-HCOOH [15]. The optimized MP2/6-311++ G(2d,2p) geometrical parameters are given together with the experimental values from [30] in parenthesis. Angles are in degrees and bond length in angstroms.

energy difference of 1365 cm^{-1} between the two conformers [15], leading to a Boltzmann population ratio of P_{cis}:$P_{trans} \approx 10^{-3}$ at 298 K. The thermal decomposition of gaseous formic acid at moderately hightemperatures complicates the thermal enhancement of the population of the *cis* form [16]. The assignment of 8 out of the 9 IR-active fundamentals and a few overtones and combination modes of *cis*-formic acid in an argon matrix have been previously reported [17]. In that work, narrowband tunable near-IR radiation was used to convert the *trans* conformer into the *cis* form by pumping the first OH stretching overtone at ca. 6934 cm^{-1}. This excitation is sufficient to surmount the estimated torsional energy barrier (values ranging from ≈ 4200 to 4800 cm^{-1} [15,18,19]). It was found that in an argon matrix at 15 K *cis*-HCOOH tunnels back to *trans*-HCOOH with a rate of ca. $2x10^{-3}$ s^{-1}, limiting the data collection time [17,20].

Splitting of IR absorption bands of matrix-isolated species is a well-known phenomenon usually called matrix-site effect. This splitting is caused by different local environments of the trapped species and potentially provides a way to study local matrix morphology. In our studies of HONO and $(FCO)_2$ in rare-gas matrices [21,22], it was found that the interconversion of the isomers with narrowband IR pumping is site-selective and no exchange between site groups was seen. This concept of site-selective optical pumping is also used in the present study.

In this work, the mid-IR absorption spectra of *cis*- and *trans*-HCOOH and DCOOH, as well as the near-IR absorption spectra of *cis*- and *trans*-HCOOH, isolated in different sites in argon matrices at 8 K are analyzed. The near-IR spectra of the matrix-isolated *trans*-DCOOH and *trans*-HCOOD isotopomers are also studied. Additionally, the anharmonic vibrational frequencies for both isomers of HCOOH and DCOOH, derived from correlation-corrected vibrational self-consistent-field calculations (CC-VSCF) [23-26] based on the MP2/6-311++ G(2d,2p) computed potential energy surfaces, are reported and the performance of the method is discussed.

2. Experimental

The gaseous samples were prepared by mixing formic acid (KEBO LAB, >99%) or its isotopomers (HCOOD and DCOOD, IT Isotop, 95-98%), degassed by several freeze-pump-thaw cycles, with high purity argon (AGA, 99.9999%), typically in the 1:1000 proportion. The DCOOH species was obtained from DCOOD by exchange with H_2O adsorbed on the inner surface of the sample container and the deposition line. In this way DCOOD : DCOOH ratios of ≈1:5 in the matrix samples were obtained. The gaseous mixtures were deposited onto a cooled CsI substrate kept at 15 K in a closed cycle helium cryostat (APD, DE 202A) and subsequently cooled down to 8 K. The IR absorption spectra (7900–450 cm^{-1}) were measured with a Nicolet SX-60 FTIR spectrometer. A liquid nitrogen cooled MCT detector and a KBr beamsplitter were used to record the mid-IR spectra, with unapodized spectral resolutions from 0.25 to 1.0 cm^{-1}, and a nitrogen cooled InSb detector and a quartz beamsplitter were used for the near-IR spectra, with a spectral resolution of 0.5 cm^{-1}. Typically 128 and 500 interfero-

grams were coadded for the mid-IR and near-IR spectra, respectively.

Tunable (225 nm - 4μm) pulsed IR radiation provided by an optical parametric oscillator (OPO Sunlite, Continuum, with IR and UV extension) was used to induce the *trans*→*cis* isomerization of HCOOH and DCOOH. The pulse duration was ca. 5 ns with a linewidth of ~0.1 cm^{-1}. A Burleigh WA-4500 wavemeter was used to control the OPO radiation wavelength, providing an absolute accuracy better than 1 cm^{-1}. Without pumping, the concentration of the *cis* conformer produced by irradiation of the *trans* form decreases by more than 70 % during the time needed to record the spectra. In order to maintain a sufficiently large concentration of the *cis* conformer during long measurements, the IR absorption spectra were recorded under simultaneous IR pumping. For this purpose the pumping beam was nearly parallel to the spectrometer beam and interference filters were used to prevent the scattered laser radiation from reaching the detector. A band pass filter transmitting in the 7900-4000 cm^{-1} region was used to record the spectrum while irradiating the sample in the OH stretching fundamental region of *trans*-HCOOH (3560-3545 cm^{-1}) whereas the 3650-3400, 3300-1000 and 2000-500 cm^{-1} band pass filters were used to record the mid-IR spectra while pumping near-IR active bands. With these filters no interference of the laser radiation on the interferogram was detected.

3. Computational method

The equilibrium structures and harmonic vibrational frequencies of *trans*- and *cis*-HCOOH were calculated using the second-order Møller-Plesset perturbation (MP2) theory with the 6-311++G(2d,2p) basis set. This basis set has been shown to be able to reproduce the experimental structural and vibrational properties of formic acid with an acceptable accuracy [27,28].

The anharmonic vibrational properties of various isotopomers of *trans*- and *cis*-HCOOH were studied by combining the electronic ab initio code GAMESS [29] with the vibrational self-consistent field (VSCF) method and its extension by corrections via second-order perturbation theory [23-26]. This correlation-corrected VSCF (CC-VSCF) method was used to solve the vibrational Schrödinger equation within the normal-mode coordinate system. This procedure involved representing the wave-function as a product of one-dimensional functions and then solving the resulting equations self-consistently. To make the integrals involved in the CC-VSCF calculation more tractable and to reduce the number of electronic structure computations required, a pairwise coupling approximation was made to the potential in the normal-mode representation [24]. This approxima-tion provided a grid of points in normal-mode coordinates at which the potential energy was calculated. Each pair of normal modes was pictured with a 16-by-16 potential surface grid, leading to a total of 30816 points computed at the MP2/6-311++G(2d,2p) level of theory for each isotopomer.

4. Results and discussion

When the deposited samples are kept at 8 K under broadband globar irradiation it is possible to detect very weak bands belonging to the *cis* conformer for HCOOH, DCOOH and HCOOD. The presence of the less stable conformer in the sample is due to the globar induced isomerization that leads to a photoequilibrium of the *trans*↔*cis* inter-conversion under broadband IR irradiation [22]. The globar induced iso-merization processes are suppressed by blocking the radiation above 2000 cm^{-1}. In this case, the presence of the *cis* form was not detected.

The spectra of formic acid in an argon matrix clearly reveal two predominant trapping sites, here labeled as site 1 and site 2. Pumping formic acid site-selectively allows us to distinguish the spectral features of each site. Figs. 2 and 3 present two regions of the mid-IR and near-IR difference

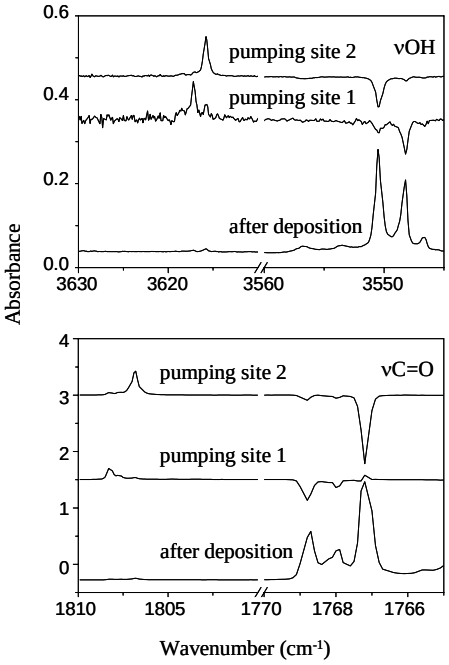

Fig. 2. Fragments of the mid-infrared spectra of HCOOH in solid Ar at 8 K. The as-deposited samples contain the *trans* conformer (lower trace). Pumping of site 1 and site 2 of *trans*-HCOOH gives rise to the *cis* conformer as presented by the difference spectra (middle and upper traces).

spectra demonstrating the results of the site-selective pumping of *trans*-HCOOH. The photo-induced relative population of the *cis* conformers was typically ≈50%.

5. Mid-IR region

The absorptions of *trans*-formic acid detected at 4183.6 cm^{-1} for site 1 and 4185.2 cm^{-1} for site 2 were used to excite vibrationally HCOOH and promote the site-selective rotamerization, enabling the collection of information about the mid-IR spectrum of both sites (Fig. 2). DCOOH was irradiated at 6933.3 and 6937.4 cm^{-1} in order to promote the photo-isomerization reactions in the corresponding sites 1 and 2. Table 1 shows the observed mid-IR absorptions for the two main sites for both conformers of HCOOH and DCOOH in solid argon together with the anharmonic computational predictions for the vibrational frequencies. The assignments made for both conformers of HCOOH and for *trans*-DCOOH agree with those reported in [10,11,17]. The spectral data for *cis*-DCOOH is reported here for the first time. For some modes (e.g. C=O stretching) the band belonging to the same site appear clearly splitted in several components. This is due to solid state perturbations on the vibrational properties of the guest molecule, which can split the absorption bands by coupling the vibrational transitions with libration motion of the molecule or by the equilibrium between different orientations of the molecule in the same site [21]. The presence of accidentally nearly degenerated sites besides the two main sites can also be responsible for the splitting. Since the vibrational bands for the two sites of the same conformer differ only by a few wavenumbers we will limit the following discussion to the assignment of the vibrational bands originating from the molecules isolated in site 2.

Generally, for a carboxylic group displaying an O=C-O-H dihedral angle of 180º the O-H and C=O stretching vibrations occur at higher wavenumbers (νOH ≈ 3616 and νC=O ≈ 1807 cm^{-1} for *cis*-HCOOH) than in the 0º dihedral angle arrangement (νOH ≈ 3550 and νC=O ≈ 1768 cm^{-1} for *trans*-HCOOH). This is due to the different degree of the [O=C-O-H ↔ O^--C=O^+-H] mesomerism in the two conformations, which appears to be slightly less efficient in the higher energy *cis* configuration. This leads to a shortening of the C=O and O-H bond distances and a lengthening of the C-O bond distance, as well as the decrease of the OCO angle in the *cis* configuration when compared to the *trans* form [15,30,31]. The structural differences arising from the

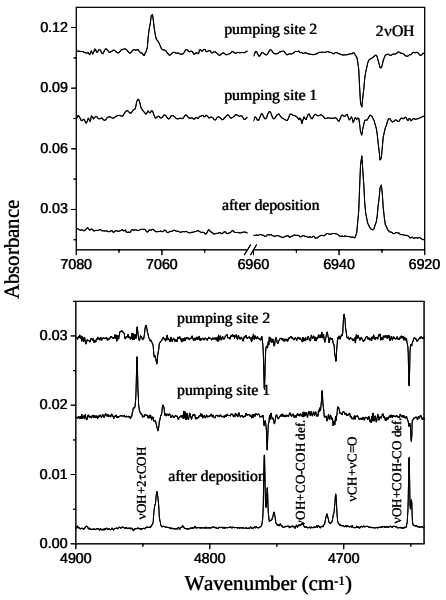

Fig. 3. Fragments of near-infrared spectra of HCOOH in solid Ar at 8 K. The as-deposited samples contain the trans conformer (lower trace). Pumping of site 1 and site 2 of *trans*-HCOOH gives rise to the *cis* conformer as presented by the difference spectra (middle and upper traces).

mesomerism do not have a counterpart on the C-O stretching mode (νC-O) because it is generally a very mixed vibration. The observed νOH and νC=O frequencies for both conformers of HCOOH are reproduced by the anharmonic calculations with an accuracy better than 1%.

The C-H rocking fundamental (γCH) of *trans*-HCOOH appears as a weak band at 1381.0 cm^{-1}, in good agreement with the calculations (1388.7 cm^{-1}). For *cis*-HCOOH the weak band observed at 1391.8 cm^{-1} is assigned to the γCH mode in site 2 while the corresponding mode for site 1 could not be detected. The weak band reported in [17] in this region (1396 cm^{-1}) was not observed in the present experiments.

A Fermi resonance doublet was observed for *trans*-HCOOH at 1305.7 and 1215.8 cm^{-1} involving the CO-COH deformation mode (CO-COH def.) and the first overtone of the COH torsion (2τCOH). This resonance is well known and it has been considered to be responsible for the apparent shift of 2τCOH towards higher wavenumbers in *trans*-HCOOH [8,10,11]. Simultaneously, the CO-COH deformation in this conformer is observed at lower wavenumbers when compared with the *cis* form (although it was predicted by the calculations at higher wavenumbers). In the *cis* conformer, the τCOH overtone is 270 cm^{-1} below the CO-COH deformation mode (≈ 980 cm^{-1}) and there is no analogous Fermi resonance involving these two modes.

A number of overtone and combination bands can be seen in the mid-IR region. The first overtone of the νC=O vibration (2νC=O) of *cis*-HCOOH, predicted by the anharmonic calculations at 3570.9 cm^{-1}, was detected at 3595.4 cm^{-1}. Both conformers of HCOOH exhibit a weak combination band appearing at slightly lower energies from the CH stretching fundamental. The observed band of the *trans* conformer (ca. 2865.6 cm^{-1}) is assigned to the νC=O + COH-CO def. combination in agreement with [14]. On the other hand, the observed band for *cis* (ca. 2753.4 cm^{-1}) is tentatively assigned to the νC=O + 2τCOH combination mode. The first overtone of the γCH mode of the *cis* conformer could also be expected to give rise to a band in this region, but the assignment of the 2753.4 cm^{-1} band to this vibration can be ruled out because this band is more intense than the γCH fundamental. On the other hand, for *cis*-HCOOH the νC=O is the most intense band and the 2τCOH is one order of magnitude higher in intensity than the γCH fundamental.

The band observed for *trans*-HCOOH at 2397.1 cm^{-1} is assigned to the νC=O + τCOH combination mode. In the gas phase spectrum, two bands were detected in a 50 cm^{-1} interval region centered at this value [14]; the bands were assigned to the first overtone of the CO-COH def. mode (≈ 2400 cm^{-1}) and the combination of the carbonyl stretching with the O=C-O bending (νC=O + δOCO ≈ 2376 cm^{-1}). In [14], the

assignment of the CO-COH def. overtone was made without taking into account the shift induced by the involvement of the fundamental in the Fermi resonance interaction mentioned above. For the unperturbed vibrational level we can expect this overtone to occur well above 2400 cm^{-1}. Therefore, we reject the assignment of the 2397.1 cm^{-1} band to the CO-COH def. overtone. Next, we consider the possible assignment of this band to the νC=O + δOCO mode. It can be approximated that the gas-to-matrix shift of the combination mode roughly follows the arithmetic sum of the gas-to-matrix shift of the two fundamentals involved (ΔνC=O= -9.6 and ΔδOCO= +3.3 cm^{-1}). Then the νC=O + δOCO combination is expected to lie in the matrix spectrum at ca. 20 cm^{-1} below the observed frequency. The νC=O + τCOH combination mode is expected to lie at higher wavenumbers than the νC=O + δOCO mode and therefore closer to the observed value in the matrix making this assignment most plausible. No bands were observed in the matrix spectrum that could be ascribed to the 2CO-COH def. or νC=O + δOCO modes.

The CO-COH def. + COH-CO def. combination band was observed for *cis*-COOH at 2342.3 cm^{-1} and calculated at 2305.5 cm^{-1}. The corresponding mode was not detected for the *trans* conformer, in agreement with its predicted lower intensity (four times lower than in the *cis* conformer). The very weak band observed for *cis*-HCOOH at 2198.5 cm^{-1} is ascribed to the overtone of the COH-CO def. mode, which in the *trans* conformer gives rise to the band at 2195.1 cm^{-1} [11].

Following the gas phase assignment [14], the very weak band observed for *trans*-HCOOH at 1844.1 cm^{-1} is tentatively ascribed to the CO-COH def. + δOCO combination. However, its assignment to the CO-COH def. + τCOH mode is also possible. Indeed, for *trans*-HCOOH it is difficult to distinguish the combination modes involving δOCO or τCOH because these two fundamentals appear at similar frequencies. Note that in the case of the *cis* conformer the τCOH and δOCO fundamentals are separated by approximately 155 cm^{-1}, which allows us to reliably distinguish the combination modes involving each vibration.

For DCOOH the C=O stretching mode participates in a very strong Fermi resonance with the first overtone of the CD wagging mode (2ωCD) in both isomers (see Table 1) [10,11]. Therefore, the previously discussed dependency of the νC=O on the conformation is not observed for DCOOH, with both conformers giving rise to bands at similar frequency values. The 2ωCD is predicted to be more than two orders of magnitude lower in intensity than the νC=O for both conformers of DCOOH. However, the observed ratio of intensities (2ωCD : νC=O) is roughly 1:2 and 1:5 for *trans*- and *cis*-DCOOH, respectively, due to the involvement of the two vibrations in the Fermi resonance interaction. Despite the larger intensity ratio of the Fermi doublet for *trans*-DCOOH, the observed frequency splitting between the components is larger for *cis*-DCOOH (ca. 57 and ca. 37 cm^{-1} in *trans*-DCOOH). Accordingly, the Fermi resonance coupling coefficients (W), obtained from a standard perturbative analysis [32], for *cis*- and *trans*-DCOOH are ca. 21 and 18 cm^{-1}, respectively, also pointing to a stronger coupling between the νC=O and the 2ωCD in the *cis* form.

It has been suggested that the COH bending (δCOH) in *trans*-DCOOH is also involved in a Fermi interaction together with the 2τCOH mode (the τCOH fundamental appears at ≈ 626 cm^{-1}) [11]. This is supported by our observation that the δCOH absorption band in *cis*-DCOOH is much higher in energy (1239.4 cm^{-1}) than the corresponding band for *trans*-DCOOH (1200.3 cm^{-1}), although the calculations predict the opposite trend (see Table 1). The Fermi resonance in *trans*-DCOOH shifts the δCOH level down. In *cis*-DCOOH the overtone of the τCOH mode is observed at 995.1 cm^{-1}, which is too low to enable its involvement in a Fermi resonance with the δCOH mode.

Table1
Observed vibrational frequencies(cm^{-1}) in the mid-IR for the two predominant sites of *trans*- and *cis*-HCOOH/DCOOH isolated in Ar at 8K and calculated anharmonic vibrational frequencies (CC-VSCF) for the corresponding molecules in the gas phase.

Assignment [a]	*trans* Observed		Calculated	cis Observed		Calculated
	site1	site 2		site 1	site 2	
HCOOH						
	3553.7 ^{w}	3556.7 ^{vw}		3617.2 ^{m}	3615.9 ^{m}	3635.2
νOH	3548.2 ^{m}	3550.5 ^{m}	3551.6			
	3546.7 ^{w}					
2νC=O	3519.0 ^{w}	3515.7 ^{w}	3596.4		3595.4 ^{w}	3570.9
νCH	2956.1^{m}	2953.1 ^{m}	2951.4	2899.5 ^{w}	2896.3 ^{w}	2863.1
νC=O + COH-CO def		2865.6 ^{vw}	2832.7			2875.5
νC=O + 2τCOH				(2759.9 ^{w})	(2753.4 ^{w})	
νC=O + δCOH	(2397.9 ^{vw})	(2397.1 ^{vw})	2348.1			2329.9
CO-COH def + COH-CO def			2332.3	2340.1 ^{vw}	2342.3 ^{vw}	2305.5
2COH-CO def	2196.1^{w}	2195.1 ^{w}	2117.1	2206.8 ^{vw}	2198.5 ^{vw}	2136.6
CO-COH def + δOCO [b]	(1844.1^{vw})	(1844.1^{vw})				
νC=O	1768.9 ^{vs}	1767.2 ^{vs}	1757.2	1808.0 ^{vs}	1806.9 ^{vs}	1794.9
	1768.3 ^{sh}			1807.8 ^{w}		
	1768.0 ^{m}					
	1764.9 ^{br}					
γCH	1384.4 ^{w}	1381.0 ^{w}	1388.7		1391.8 ^{vw}	1404.2
CO-COH def	^{c}1305.7 ^{w}	^{c}1305.7 ^{w}				
	^{c}1214.8 ^{w}	^{c}1215.8 ^{w}	1267.8	1243.4 ^{s}	1248.9 ^{vs}	1204.3
COH-CO def	1106.8 ^{vw}	1106.9 ^{vw}	1077.5	1107.3 ^{m}	1104.6 ^{m}	1077.6
	1103.9 ^{s}	1103.6 ^{sh}				
	1100.9 ^{br}	1103.2 ^{s}				
	1094.7 ^{vw}					
ωCH	1037.4 ^{w}	1038.5 ^{w}	1034.6			1014.0
2τCOH			1109.8	979.5 ^{w}	982.6 ^{w}	845.1
	638.6 ^{vw}					
τCOH	635.4 ^{s}	635.4 ^{s}	598.4	502.9 ^{m}	505.3 ^{m}	430.8
δOCO	628.0 ^{m}	629.3 ^{m}	621.0	662.3 ^{w}	662.3 ^{w}	647.3
DCOOH						
	3562.5 ^{vw}	3560.9 ^{vw}				
νOH	3549.9 ^{m}	3551.7 ^{m}	3549.6	3617.4 ^{w}	3615.4 ^{m}	3637.8
	3547.2 ^{vw}			3616.0 ^{m}		
2νC=O	3461.3 ^{vw}	3463.5 ^{vw}				
νCD	2225.2 ^{m}	2225.2 ^{m}	2230.8	2183.5 ^{m}		2167.3
				2179.7 ^{sh}		
νC=O	^{d}1761.7^{s}		1726.8	^{d}1778.7 ^{s}		1761.1
	^{d}1761.0 ^{s}			^{d}1778.4 ^{m}		
	^{d}1759.5 ^{vs}			^{d}1777.2 ^{vs}		
	^{d}1759.8 ^{sh}					
	^{d}1758.1 ^{s}					
				^{d}1721.5 ^{m}		
	^{d}1723.7 ^{m}			^{d}1720.9 ^{m}		
	^{d}1722.9 ^{vs}					
ωCD + τCOH				(1370.2 ^{w})	(1372.5 ^{w})	
δCOH	1199.6 ^{w}	1200.3 ^{w}	1255.6	1248.9 ^{vw}	1239.4 ^{vs}	1193.9
				1234.0 ^{vs}		
				1229.1 ^{vw}		
νC-O	1142.1 ^{s}	1141.7 ^{s}	1126.7	1143.4 ^{m}		1125.4
	1144.4 ^{w}					
2τCOH				996.3 ^{w}	995.1 ^{w}	840.5
γCD	976.2 ^{s}	974.1 ^{s}	981.2	961.9 ^{w}	962.9 ^{w}	985.7
	974.9 ^{w}					
ωCD	874.8 ^{w}	875.0 ^{w}	875.8			866.2
	667.7 ^{vw}	667.7 ^{vw}				
	629.8 ^{w}					
τCOH	626.4 ^{m}	625.9 ^{m}	589.4	500.7 ^{w}		425.4
				498.1 ^{w}		
δOCO	622.3 ^{m}	623.5 ^{m}	615.2	655.2 ^{vw}	655.2 ^{vw}	640.8

Qualitative information on intensities is given as superscript: vs, very strong; s, strong; m, medium; w, weak; vw, very weak; sh, shoulder; br, broad. [a]According to [11]: ν, stretching; δ, bending; γ, rocking; ω, wagging, def., deformation. [b]According to [14]. [c] Components of a Fermi resonance doublet between the first overtone of τCOH and the CO-COH def. observed only for *trans*-HCOOH. [d]Components of a Fermi resonance doublet between the first overtone of the ωCD and νC=O modes.Frequency values centered between site 1 and site 2 columns could not be assigned to a specific site due to lack of site selective data. Values in parentheses are tentatively assigned. An explanation about the assignment of several bands to the same mode in the site-selective spectra is given in the text.

Table 2
Observed vibrational frequencies (cm^{-1}) in the near-IR for the two predominant sites of *trans*- and *cis*-HCOOH isolated in Ar at 8 K and calculated anharmonic vibrational frequencies (CC-VSCF) for the corresponding molecules in gas phase.

Assignment	*trans*-HCOOH			Gas phase[a]	Calc.	*cis*-HCOOH		Calc.
	Ar site 1		Ar site 2			Ar site 2	Ar site 2	
2νOH	6930.3^{s}		6934.8^{s}	6968	6943.7	7062.3^{s}	7065.7^{m}	7053.8
2νCH + ωCH				6773				
νOH + νCH				6507	6431.0			6425.6
νCH + 2νC=O		6411.2^{vw}		6440				
		6407.0^{vw}						
2νCH		5803.0^{vw}		5775	5788.3			5604.0
		5797.3^{vw}						
νCH + 2γCH				5592				
νOH + νC=O	5316.4^{m}		5317.2^{m}	5343	5236.2			5347.2
νOH +γCH	4928.7^{m}		4926.1^{w}	4942	4863.5			4960.1
			4841.2^{sh}					
νOH + 2τCOH[b]	(4838.7^{m})		(4839.8^{m})	4857				
νOH + CO-COH	(4757.2^{m})		(4759.4^{m})	4780	4686.1	4847.7^{m}	4854.4^{s}	4704.8
2νC=O + CO-COH			(4752.2^{br})					
?		4712.0						
νCH + νC=O	4707.0^{vw}		4706.0^{m}	4708	4708.3	4704.0^{w}	4700.0^{m}	4666.2
νOH + COH-CO def.	4649.6^{m}		4651.4^{m}	4670	4534.7	4716.2^{m}	4712.5^{w}	4622.6
νOH + ωCH				4600	4517.6			4576.6
2γCH + νC=O		4510.0^{vw}		4515			4553.4^{vw}	
νCH + γCH		4317.0^{w}		4300	4287.4			4219.3
νC=O + 2CO-COH		(4270.4^{w})						
νCH + 2τCOH[b]	(4254.2^{w})		(4252.0^{w})	4242				
νOH + τCOH	(4183.6^{m})		(4185.2^{m})	4209	4102.2	(4110.0^{vw})	(4111.5^{vw})	4130.2
νCH + CO-COH	(4171.8^{w})		(4175.1^{w})		4214.4			4098.7
νOH + δOCO		(4167.4^{vw})		4192	4085.8	4277.3^{vw}	4275.9^{vw}	4195.8
?		4157.7^{vw}						
νCH + COH-CO def.	4059.7^{w}		4055.3^{w}	4043	4026.6			

Qualitative information on intensities is given as superscript: vs- very strong; s, strong; m- medium; w, weak; vw, very weak; sh, shoulder; br, broad. Frequencies in parentheses correspond to tentative assignments.[a]From [14]. ν, stretching; δ, bending; γ, rocking; ω, wagging, def., deformation. [b] Ascribed as components of a Fermi resonance doublet between the combination modes νOH(νCH) + 2τCOH and νOH(νCH) + CO-COH def. of the *trans* conformer.

The τCOH fundamental mode is observed at ≈500 cm^{-1} for the *cis* conformer in both HCOOH and DCOOH. This vibration is shifted ≈130 cm^{-1} towards lower wavenumbers when compared with the same vibration in the *trans* conformer (see Table 1). The repulsive interaction between the C=O and O-H bond dipoles resulting from their nearly parallel alignment and the steric repulsion between the hydrogen atoms lying on the same side of the C-O bond in the *cis* configuration have been pointed out as the major factors responsible for the higher energy of the *cis* conformer when compared with the *trans* form [18]. Indeed, these effects partially destabilize the *cis* planar conformations of this molecule with respect to the non-planar conformations. Thus, it leads to a softer torsional energy profile around this conformer and decreases the force constant of the torsion.

6. Near-IR region

In this section, we analyze the near-IR (7900-4000 cm^{-1}) spectra of the two conformers of formic acid, the discussion

Table 3
Observed near-IR active vibrational frequencies (cm^{-1}) of the *trans* conformer of DCOOH, HCOOD and DCOOD isolated in Ar at 8 K[a] and calculated anharmonic vibrational frequencies (CC-VSCF) for the corresponding molecules in gas phase.

DCOOH				HCOOD				DCOOD			
Assignment	Ar	Gas phase[b]	Calc.	Assignment	Ar	Gas phase[b]	Calc.	Assignment	Ar	Gas phase[b]	Calc.
2νOH	6937.4	6975	6939.4	2νOD	5152.9	5181	5163.6	2νOD	5152.9	5181	5169.1
	6933.3				5149.7				5149.7		
νOH + νCD	5773.2		5708.9	νOH + νCD			5547.2	νOD + νCD			4823.5
2νCD	4401.2	≈4360[e]	4400.8	2νCH			5791.3	2νCD			4398.7
νOH + 2ωCD[c]	(5312.0)			νOD + νC=O	4382.2	4404	4345.8	νOD + νC=O			4318.3
νOH + νC=O[c]	(5273.9)		5205.5		4380.0						
νOH + 2τCOH[d]	(4835.1)	4850									
	(4825.3)										
νOH + δCOH[d]	(4743.3)	4781	4649.5								
	(4740.9)										
νOH + γCD			4451.5								
νOH + ωCD			4356.5								
				νCH + γCH			4275.8				
νCD + 2ωCD[c]	(3974.3)	3980		νCH + νC=O	4723.7	4736	4704.3	νCD + νC=O	3987.1	3981	3949.2
νCD + νC=O[c]	(3937.3)		3953.4		4721.1	4702					
νOH + νCO	4693.2	4701	4593.1	νCH + νCO	4142.6	4144	4114.4				
	4691.7				4141.2	4115					
νOH + τCOH	4175.4		4098.6	νCH + νCH	3990.2		3926.9				
	4173.3				3988.2						
νOH + δOCO	4170.2	4201	4076.2								
	4166.7			νCH + τCOD	3946.2						
				νCH + δCOD			3923.4				

[a]The majority of the modes appear site-splitted. [b] From [13]. [c] Components of a Fermi resonance doublet between the combination modes νOH(νCD) + 2ωCD and νOH(νCD) + νC=O. [d] Fermi resonance doublet between the combination modes νOH + 2τCOH and νOH + δCOH. [e] Band center of the observed doublet ascribed to rotational structure. ν, stretching; δ, bending; γ, rocking; ω, wagging; def., deformation. Frequencies in parentheses correspond to tentative assignments.

being focused on site 2. The OH stretching absorption bands of *trans*-formic acid were used to promote the site-selective rotamerization process (Fig. 3). Table 2 presents the observed vibrational frequencies for both HCOOH conformers and the results of the anharmonic vibrational calculations. Table 3 collects the observed and calculated vibrational frequencies for *trans*-DCOOH, HCOOD and DCOOD omitting site labeling.

The first OH stretching overtone of *trans*-HCOOH is observed at 6934.8 cm^{-1} and predicted by the calculations at 6943.7 cm^{-1}, both of them being in good agreement with the existing gas phase data (6968 cm^{-1} [14]). For *cis*-HCOOH the same mode is predicted by the calculations at 7053.8 cm^{-1} and observed at 7065.7 cm^{-1}. The experimentally determined anharmonicity constant for the OH stretching mode of *cis*-HCOOH is ca. -85 cm^{-1}, which is very close to the values obtained for the *trans* conformer (ca. -83 cm^{-1} and -91cm^{-1}, matrix isolated and gas phase [14], respectively). The νOH + νCH mode, observed in the gas phase for *trans*-HCOOH at 6507 cm^{-1}, was not found in our matrix studies. For *trans*-DCOOH a band appearing at 5773.2 cm^{-1} is assigned to the νOH + νCD mode (predicted by the CC-VSCF calculations at 5708.9 cm^{-1}).

For *trans*-HCOOH, the medium intensity bands observed at 4839.8 and 4759.4 cm^{-1} are here ascribed to the νOH + 2τCOH and νOH + CO-COH def. combination modes. Considering the observed fundamental vibrations, it is reasonable to assign the higher frequency band to a combination mode involving the νOH fundamental and

Table 4
Observed and CC-VSCF calculated anharmonicities and coupling constants[a] for *cis*- and *trans*-HCOOH.

	trans-HCOOH				*cis*-HCOOH		
	Site 1	Site 2	Gas phase[b]	Calc.	Site 1	Site 2	Calc.
Combinations	Coupling constants (x_{ij}, cm^{-1})						
νOH + νC=O	-0.7	-0.5	-1.2	-72.6			-82.9
νOH + γCH	-3.9	-5.4	-3.6	-76.8			-79.3
νOH + CO-COH def.				-	-12.9	-10.4	-134.7
νOH + COH-CO def.	-2.5	-2.3	-1.8	-94.4	-8.3	-8.0	-90.2
νOH + ωCH			-1.0				
νOH + τCOH	(0)	(-0.7)	(-2.2)	-47.8	(-10.1)	(-9.7)	+64.2
νOH + δOCO	(-15.5)		(-4.7)	-86.8	-2.2	-2.3	-86.7
νCH + νC=O	-18.0	-14.3	-5.4	-0.3	-3.5	-3.2	-8.2
νCH + γCH	-23.5	-17.1	-22.1	-52.7			-48.0
νCH + COH-CO def.	-0.3	-1.0	-1.8	-2.3			-7.7
νCH + ωCH			-5.7				
νC=O + COH-CO def.		-4.8	-2.6	-2.0			-3.0
νC=O + τCOH	(-6.4)	(-5.5)		-7.5			-104.2
CO-COH def. + COH-CO def.				-7.0	-10.6	-11.2	-23.6
Overtones	Anharmonicity constants (x_i, cm^{-1})						
2νOH	-83.1	-83.1	-91.2	-79.8	-86.1	-83.1	-108.3
2νCH	-53.1		-52.4	-57.3			-61.1
2νC=O	-9.4	-9.4	-9.3	-9.0		-9.2	-9.5
2COH-CO def.	-5.9	-5.7	-6.6	-19.0	-3.9	-5.4	-9.3
2τCOH				-43.5	-13.2	-14.0	-8.3

[a] $x_{ii} = \nu_{i+i} - \nu_i - \nu_i$; $x_{ii} = (2\nu_i - 2\times\nu_i)/2$.
[b] Gas phase data was taken from [14].
Values in parentheses were calculated based on a tentative assignment. Values centered between site 1 and site 2 columns are average estimates for the two sites.

the overtone of δOCO or τCOH. In both cases, the observed combination mode would be shifted up from the expected value (even without taking into account the anharmonicity). This could be explained by a Fermi resonance coupling with a mode laying at similar wavenumbers. As discussed earlier, in the mid-IR region the 2τCOH and CO-COH def. modes are coupled by Fermi resonance, and it is plausible that the combination mode of each of these vibrations with the same νOH fundamental is also perturbed in a similar way. In the gas phase [14], the band at 4857 cm^{-1} was tentatively assigned to the νOH + 2τCOH combination mode while the band at 4780 cm^{-1} was assigned to the νOH + CO-COH def. combination mode. In [14], the existence of the Fermi resonance coupling between the 2τCOH and CO-COH def. modes was ignored, and the perturbed vibrational levels were used to estimate the position of the combination modes. In *cis*-HCOOH, only one band that can be ascribed to the νOH + CO-COH def. is observed in the 4900-4700 cm^{-1} region (4854.4 cm^{-1}). This is in agreement with the fact that the νOH + 2τCOH combination mode is expected to occur at significantly lower wavenumbers (in the 4600-4500 cm^{-1} region, see Table 1), therefore preventing its involvement in a Fermi resonance of the same type as that

observed for *trans*-HCOOH.

The *cis*-HCOOH absorption band at 4700.0 cm^{-1} is ascribed to the νCH + νC=O combination, observed for *trans*-HCOOH at 4706.0 cm^{-1} (see site 2 data in Table 2). The *cis*-band at 4712.5 cm^{-1} is assigned to the νOH + COH-CO def. combination, observed at a frequency ca. 60 cm^{-1} higher than that of the *trans*-conformer (4651.4 cm^{-1}). The magnitudes of the coupling constants for these two modes seem to be reversed in *cis*-HCOOH (coupling constant $x_{ij}= \nu_{i+j} - \nu_i - \nu_j \approx -3.2$ cm^{-1} and -8.0 cm^{-1} for νCH + νC=O and νOH + COH-CO def., respectively) when compared to *trans*-HCOOH ($x_{ij} \approx -14.3$ cm^{-1} and -2.3 cm^{-1}, respectively). However, the alternative assignment of the lower frequency band to the νCH + νC=O would result in a positive coupling constant for the νCH + νC=O mode, which seems unlikely.

In the 4200-4150 cm^{-1} region few bands are observed for both isomers that are tentatively assigned. Three site-splitted bands are observed for *trans*-HCOOH, ascribed to the νOH + τCOH, νOH + δOCO and νCH + CO-COH def. combination modes (see Table 2). The assignment of these bands follows that made previously in [14]. A very weak band observed at 4111.5 cm^{-1} for *cis*-HCOOH can be due either to the νOH + τCOH combination mode (the sum of the fundamentals gives ca. 4120 cm^{-1}) or the νCH + CO-COH def. vibration (the sum of the fundamentals gives ca. 4144 cm^{-1}). The νOH + δOCO combination band is observed for *cis*-HCOOH at ca. 4276 cm^{-1} as a weakly coupled mode (the sum of the fundamentals is ca. 4278 cm^{-1}). As already mentioned, the difference between the observed frequencies for the τCOH and δOCO fundamentals in *cis*-HCOOH allows us to reliably separate the combination modes involving each one of these vibrations.

For *trans*-DCOOH the bands observed at ≈ 4830 and 4740 cm^{-1} are tentatively assigned to a Fermi resonance doublet involving νOH + 2τCOH and νOH + δCOH, in a similar way to what was found for *trans*-HCOOH. Another Fermi resonance doublet was observed in the *trans*-DCOOH spectrum coupling the νOH + 2ωCD with the νOH + νC=O (see Table 3). The splitting between this Fermi resonance doublet is identical to that observed in the mid-IR for the very strong Fermi resonance doublet involving the 2ωCD and νC=O modes (ca. 37 cm^{-1}). The unperturbed frequencies of the 2ωCD and νC=O vibrations are estimated to be ca. 1746 and 1738 cm^{-1}, respectively. The unperturbed νOH + 2ωCD and νOH + νC=O combination modes are expected at ca. 5297 and 5289 cm^{-1}, respectively, using site averaged values and without taking into account the intermode coupling constant. By comparison of these values with the observed combination bands (5312 and 5274 cm^{-1}), we estimate a Fermi resonance induced shift relative to the unperturbed positions of 15 cm^{-1}, exactly the same as that calculated for the mid-IR active Fermi doublet due to νC=O and 2ωCD.

In Table 4, we present several observed and calculated (CC-VSCF) coupling and anharmonicity constants for *cis*- and *trans*-HCOOH together with the corresponding gas phase data [14]. By comparing the coupling constants obtained for *trans*-HCOOH isolated in argon with the gas phase data, we conclude that the cage potential affects significantly the guest intermode couplings. These changes in the coupling constants are in many cases of similar magnitude as the constants themselves. Moreover, changing of the matrix trapping site leads also to significant effects on the anharmonicity and intermode couplings (see, for example, the constants of either νCH + νC=O or νCH + γCH modes in Table 4). It can then be concluded that the local environment is an important factor to be considered in the processes involving intramolecular vibrational redistribution and relaxation in solid phase. The average difference between the constants estimated for both sites and the gas phase values is approximately the same in both conformers, which means that the local environment perturbs both conformers to a similar extent.

Table 5
Harmonic and anharmonic vibrational frequencies (cm^{-1}) and infrared intensities (in parentheses) of *trans*- and *cis*-formic acid.[a]

	trans-HCOOH					*cis*-HCOOH				
	ν_{harm}		ν_{anh}		ν^{Ar}_{ex}	ν_{harm}		ν_{anh}		ν^{Ar}_{exp}
2νOH			6943.7	(4)	6933 (13)			7053.8	(3)	7064 (10)
2νCH			5788.3	(1)	5800 (<1)			5604.0	(1)	
νOH + νC=O			5236.2	(3)	5317 (2)					
νOH + γCH			4863.5	(1)	4927 (2)					
νOH + CO-COH def.					4758 (2)			4704.8	(37)	4851 (2)
νCH + νC=O			4708.3	(4)	4707 (1)			4666.2	(5)	4702 (2)
νOH + COH-CO def.			4534.7	(11)	4651 (2)			4622.6	(2)	4714 (<1)
νCH + CO-COH def.			4214.4	(2)	4173 (1)			4098.7	(1)	
νOH + τCOH			4102.2	(83)	4184 (5)			4130.2	(39)	4111 (7)
νCH + COH-CO def.			4026.6	(1)	4058 (1)					
νOH	3784.0	(171)	3551.6	(217)	3549 (320)	3851.5	(171)	3635.2	(221	3617 (380
2νC=O			3496.4	(9)	3517 (14)			3570.9	(8)	3595 (15)
3CO-COH def.								3520.8	(11)	
νC=O + γCH			3140.2	(1)						
3COH-CO def.			3108.8	(1)						
νCH	3134.2	(69)	2951.4	(71)	2955 (80)	3046.1	(134)	2863.1	(118	2898 (120
νC=O + COH-CO def.			2832.7	(12)	2866 (6)			2875.5	(6)	
2γCH			2774.4	(1)				2806.4	(2)	
CO-COH def. + COH-CO def.			2338.3	(3)				2305.5	(12)	2341 (17)
2COH-CO def.			2117.1	(13)	2196 (16)			2136.6	(2)	2203 (6)
2ωCH			2077.7	(4)				2035.7	(3)	
νC=O	1788.8	(696)	1757.2	(997)	1768 (1000)	1829.2	(558)	1794.9	(826	1807 (850
COH-CO def. + δOCO			1697.8	(2)						
3τCOH			1616.9	(68)				1457.8	(41)	
COH-CO def. + τOCO			1594.6	(2)						
γCH	1426.5	(3)	1388.7	(13)	1383 (19)	1441.7	(<1)	1404.2	(7)	1392 (2)
CO-COH def.	1316.6	(20)	1267.8	(34)	1215 (53)	1287.2	(615)	1204.3	(749	1246 (933
2τCOH			1109.8	(34)	1306 (17)			845.1	(1)	981 (16)
COH-CO def.	1123.3	(586)	1077.5	(618	1103 (757)	1113.0	(164)	1077.6	(170	1106 (250
ωCH	1065.3	(8)	1034.6	(1)	1038 (11)	1042.9	(<1)	1014.0	(2)	
τCOH	676.8	(298)	598.4	(320)	635 (500)	536.8	(184)	430.8	(156	504 (240
δOCO	631.7	(82)	621.0	(109)	629 (171)	661.2	(24)	647.3	(26)	662 (16)

[a] Calculated infrared intensities (in km/mol) and experimental integrated intensities were normalized so that the most intense band of the trans conformer has an intensity of 1000. After this procedure all the predicted combination and overtone bands with intensities less than 1 are omitted. Experimental band positions correspond to the average value of the observed bands for the molecules isolated in two matrix-sites. The intensities of the anharmonic vibrations were obtained from Hartree-Fock wave functions in the CC-VSCF calculations. [b] Bands involved in Fermi resonance coupling. These bands should not be compared with the calculated values.

7. Anharmonic calculations

The equilibrium structures and harmonic vibrational properties of the conformers of formic acid are rather well reproduced at the MP2/6-311++G(2d,2p) level of theory employed previously in our studies of HCOOH [27,28]. The harmonic and anharmonic vibrational frequencies computed for *trans*- and *cis*-HCOOH are compared in Table 5. The anharmonic effects are most significant for the high-frequency modes, i.e. the OH and CH stretches, for which the anharmonic calculations reduce the obtained frequencies by ≈200 cm^{-1} from the harmonic values. The CC-VSCF calculations give a good reproduction of the experimentally observed positions for most of the fundamental frequencies. Only the skeletal deformation modes (CO-COH def. and COH-CO def.) and the torsional mode seem to be troublesome. For example, the CC-VSCF calculations predict the torsional mode to be

ca. 40 and 70 cm^{-1} below the experimental values of *trans*- and *cis*-HCOOH, respectively (see Table 5). The infrared intensities obtained both in the harmonic and anharmonic calculations are rather similar and both follow qualitatively the experimentally observed data.

The CC-VSCF calculations reveal a rather rich overtone and combination band spectrum for both conformers in qualitative accord with the experimentally observed spectra. However, the numerical agreement between the experimentally found vibrational frequencies and the CC-VSCF ones are not as good as in the case of the fundamental modes. For the first overtones of the OH and CH stretching modes, the calculations give reasonable estimates of the band positions. On the other hand, most of the combination bands and overtones involving one or several skeletal deformation modes seem to be a challenge for the CC-VSCF method. The results of the anharmonic CC-VSCF calculations are compared with the experimental data in Table 4 in the form of computed anharmonicity and coupling constants for the observed overtone and combination bands. The errors made in computing the fundamentals are reflected in the overtones and combination modes, and thus in many cases the coupling constants are overestimated. There can be several reasons for the discrepancy of the observed and computed vibrational frequencies. The CC-VSCF calculations involve an approximation of separability of normal coordinates used to describe the vibrational motions of the molecule [23-25]. Therefore, if strong couplings exist between modes the CC-VSCF calculations are not able to reproduce these motions. Also, the wide-amplitude vibrational modes, like the torsion in formic acid, seem to be hard to describe sufficiently well. Additionally, it must be remembered that the computational level used here (MP2/6-311++G(2d,2p)) could prove less reliable for configurations further away from the equilibrium structure. All in all, the CC-VSCF method is able to reproduce the experimental characteristics of formic acid on a qualitative level and it is more suitable to support experimental identification of molecular species than the standard harmonic vibrational calculations.

8. Conclusions

Vibrational spectroscopic data on matrix-isolated *cis*- and *trans*-HCOOH and DCOOH in different sites is presented. The 7900-4000 cm^{-1} spectral features for *cis*-HCOOH are discussed for the first time. This study also presents for the first time the experimental vibrational spectra of *cis*-DCOOH.

For *trans*-HCOOH all but two of the CC-VSCF predicted binary combinations and first overtones in the 7000-4000 cm^{-1} region were detected. For *cis*-HCOOH about half of the expected modes were observed, in spite of the presence of this conformer in the matrix in a lower concentration. A very strong Fermi resonance between νC=O and 2ωCH, previously reported for *trans*-DCOOH, was also found to be present in the *cis* conformer. The observed combinations of these two modes with the νOH were also found to be involved in Fermi resonance.

From the site-selective data, we conclude that the cage potential affects significantly the guest intermode coupling. The effect of local morphology on the anharmonicity and inter-mode couplings was found to be comparable with the effect of going from the gas phase to the solid rare gas environment. Therefore, we expect an important contribution from the local environment to the dynamics of processes involving intramolecular vibrational redistribution and relaxation in solid phase.

The CC-VSCF calculations reproduce reasonably well the experimentally observed positions of the fundamental frequencies, excluding the skeletal deformation modes and the torsional vibration. The coupling constants are overestimated by the calculations. The absolute shifts from the experimental values for the combination

bands and overtones are twice as high as the ones for fundamentals, nevertheless, the relative error is still small (≈3%). The systematic underestimation of the vibrational frequencies might be an indication that the ab initio potential energy surface used is too ”soft”. Despite of that, the CC-VSCF calculations were shown to be superior to the standard harmonic vibrational predictions, and their ability to contribute to the assignment of overtone and combination modes appears as a valuable tool to aid the experimental work.

Acknowledgments

The Academy of Finland and Finnish Cultural Foundation are thanked for financial support. E.M. and RF acknowledge the Portuguese Foundation for Science and Technology (Ph.D. grant SFRH/BD/4863/2001 and project POCTI743366/QUI/2001). Prof. Benny Gerber and Dr. Galina Chaban are thanked for discussions on the anharmonic vibrational calculations.

References

[1] S.- Y. Liu, D. M. Mehringer, L. E. Snyder, J. Astrophys. 552 (2001) 654-663.
[2] A. Goldman, F. H. Murcray, D. G. Murcray, C. P. Rinsland, Geophys. Res. Lett. 11 (1984) 307-310.
[3] B. Elves, S. Hawkins, M. Ravenscroft, J. F. Rounsaville, G. Schulz (Eds), Ullmann’s Encyclopedia of Industrial Chemistry, vol. A12, fifth ed, VCH, Germany, 1989.
[4] R. C. Millikan, K. S. Pitzer, J. Chem. Phys. 27 (1957) 1305-1308.
[5] I. C. Hisatsune, J. Heicklen, Can. J. Spectrosc. 18 (1973) 135-142.
[6] G. M. R. S. Luiz, A. Scalabrin, D. Pereira, Infrared Phys. & Techn. 38 (1997) 45-49 (1997).
[7] T. L. Tan, K. L. Goh, P. P. Ong, H. H. Teo, J. Mol. Spectrosc. 198 (1999) 110-114, and references therein.
[8] J. E. Bertie, K. H. Michaelian, J. Chem. Phys. 76 (1982) 886-894.
[9] T. Miyazawa, K. S. Pitzer, J. Chem. Phys. 30 (1959) 1076-1086.
[10] R. L. Redington, J. Mol. Spectrosc. 65 (1977) 171-189.
[11] D. O. Henderson, Doctoral Thesis, Texas Technical University, 1987.
[12] F. Madeja, P. Markwick, M. Havenith, K. Nauta, R. E. Miller, J. Chem. Phys. 116 (2002) 2870-2878.
[13] Morita H., S. Nagakura, J. Mol. Spectrosc. 41 (1972) 54-68.
[14] M. Freytes, D. Hurtmans, S. Kassi, J. Liévin, J. Vander Auwera, A. Campargue, M. Herman, Chem. Phys. 283 (2002) 47-61.
[15] W. M. Hocking, Z. Naturforsch 31A (1976) 1113-1121.
[16] P. G. Blake, H. H. Davies, G. E. Jackson, J. Chem. Soc. B (1971) 1923.
[17] M. Pettersson, J. Lundell, L. Khriachtchev, M. Räsänen, J. Am. Chem. Soc. 119 (1997) 11715-11716.
[18] K. B. Wiberg, K. E. Laidig, J. Am. Chem. Soc. 109 (1987) 5935-5943.
[19] J. D. Goddard, Y. Yamaguchi, H. F. Schaefer III, J. Chem. Phys. 96 (1992) 1158-1166.
[20] M. Pettersson, E. M. S. Maçôas, L. Khriachtchev, J. Lundell, R. Fausto, M. Räsänen, J. Chem. Phys. 117 (2002) 9095-9098.
[21] S. Sander, H. Willner, L. Khriachtchev, M. Pettersson, M. Räsänen, E. L. Varetti, J. Mol. Spectrosc. 203 (2000) 145-150.
[22] L. Khriachtchev, J. Lundell, E. Isoniemi, M. Räsänen, J. Chem. Phys. 113 (2000) 4265-4273.
[23] J. O. Jung, R. B. Gerber, J. Chem. Phys. 105 (1996) 10332-10348.
[24] J. O. Jung, R. B. Gerber, J. Chem. Phys. 105 (1996) 10682-10690.
[25] G. M. Chaban, J. O. Jung, R. B. Gerber, J. Chem. Phys. 111 (1999) 1823-1829.
[26] G. M. Chaban, J. O. Jung, R. B. Gerber, J. Phys Chem. A. 104 (2000) 2772-2779.
[27] J. Lundell, M. Räsänen, Z. Latajka, Chem .Phys. 189 (1994) 245-260.
[28] J. Lundell, Chem. Phys. Lett. 266 (1997) 1-6.
[29] M. W. Schmidt, K. K. Baldridge, J. A. Boatz, S. T. Elbert, M. S. Gordon, J. H. Jensen, S. Koseki, N. Matsunaga, K. A. Nguyen, S. J. Su, T. L. Windus, M. Dupuis, J. A. Montgomery, J.Comput.Chem. 14 (1993) 1347-1363.
[30] E. Bjarnov, W. M. Hocking, Z. Naturforsch, 33A (1978) 610-618.
[31] R. Fausto, A. E. Batista de Carvalho, J. J. C. Teixeira-Dias, M. N. Ramos, J. Chem. Soc., Faraday Trans. 2 85 (1989) 1945-1962.
[32] G. S. Devendorf, M-H. A. Hu, D. Ben-Amotz, J. Phys. Chem. A. 102 (1998) 10614-10619.

Appendix II

Reactive vibrational excitation spectroscopy of formic acid in solid argon: Quantum yield for infrared induced trans→cis isomerization and solid state effects on the vibrational spectrum.

Ermelinda M. S. Maçôas, Leonid Khriachtchev, Mika Pettersson, Jonas Juselius, Rui Fausto and Markku Räsänen

J. Chem. Phys. **2003**, *119*, 11765-11772.

Reactive vibrational excitation spectroscopy of formic acid in solid argon: Quantum yield for infrared induced *trans→cis* isomerization and solid state effects on the vibrational spectrum

E. M. S. Maçôas[a)]
Department of Chemistry, University of Helsinki, P.O. Box 55 (A.I. Virtasen aukio 1), FIN-00014 Helsinki, Finland and Department of Chemistry (CQC), University of Coimbra, P-3004-535 Coimbra, Portugal

L. Khriachtchev, M. Pettersson,[b)] and J. Juselius
Department of Chemistry, University of Helsinki, P.O.Box 55 (A.I. Virtasen aukio 1), FIN-00014 Helsinki, Finland

R. Fausto
Department of Chemistry (CQC), University of Coimbra, P-3004-535 Coimbra, Portugal

M. Rasanen
Department of Chemistry, University of Helsinki, P.O. Box 55 (A.I. Virtasen aukio 1), FIN-00014 Helsinki, Finland

(Received 4 June 2003; accepted 17 September 2003)

Formic acid molecules are trapped in two predominant local environments (sites) when isolated in an argon matrix at 8 K. Using narrowband tunable infrared (IR) radiation, we performed site-selective excitation of various vibrational modes of the lower-energy *trans* conformer. For all excited modes, ranging from 7000 to 2950 cm^{-1}, we detected site-selective isomerization to the higher-energy *cis* form. By measuring the IR absorption of a selected band of the *cis* conformer as a function of the excitation frequency, the reactive vibrational excitation (RVE) spectra were obtained. The *trans→cis* isomerization quantum yields for the excited modes were determined. Remarkably, very high absolute values were obtained for the quantum yield (up to 40%) at excitation energies above the reaction barrier. The efficiency of the photoinduced isomerization is essentially independent of the excited vibrational mode in a broad energy interval. Even when the excitation energy was below the reaction barrier, IR-induced rotational isomerization was observed, which indicates tunneling from the vibrationally excited *trans* conformer to the *cis* form. Using the RVE spectra, phonon sidebands were detected on the high-frequency side of the zero-phonon-line of the OH stretching mode of *trans*-formic acid. These weak and broad bands were not observed in the absorption spectra. Additionally, a relatively narrow band blueshifted by 6 cm^{-1} from the OH stretching fundamental mode was assigned to a librational satellite based on simulations using the hindered rotation model for an asymmetric top trapped in an octahedral crystal field. [DOI: 10.1063/1.1624598]

I. INTRODUCTION

Infrared (IR)-induced isomerization reactions in cryogenic matrices have been the subject of many studies since the pioneering work on *cis*- and *trans-HONO* interconversion by Baldeschwieler and Pimentel.[1-3] The possibility of mode-selective chemistry and optical control of reaction pathways has been the motivation for many of these studies. Particularly interesting is the conformer-selective photo-

[a)] Author to whom correspondence should be addressed. Electronic mail: emacoas@qui.uc.pt
[b)] Present address: Department of Chemistry, University of Jyväskylä, P. O. Box 35, FIN-40014 University of Jyväskylä, Finland

chemistry controlled by narrowband IR irradiation.[4] Low temperature rare-gas matrices provide an unique environment for selective photochemistry. The low temperatures suppress thermal reactions with significant activation energy, hence enabling stabilization of high energy conformers once they have been produced by photoinduced isomerization.

The quantum efficiency of the IR-induced rotational isomerization depends on the probability of energy transfer from the excited vibrational level to the reaction coordinate. For an isolated molecule, the strength of the anharmonic couplings and the density of states are the key factors affecting the relaxation process.[5] Many unimolecular reactions are often interpreted assuming complete randomization of the excitation energy among all degrees of freedom. This approach is valid if the intramolecular vibrational energy relaxation (IVR) rates are much faster than the reaction rate. Though the IVR dynamics is not simply related to the density of states, complete randomization of the excitation energy is more probable for high energy excitation where the density of states is higher.[6] On the other hand, if the IVR rates are smaller or comparable with the reaction rate, the reaction efficiency will depend not only on the energy content but also on the initially excited mode.[7] In condensed phase, the mechanisms for energy relaxation depend additionally on the guest-host interactions.[8,9] Usually, photoinduced rotamerization efficiencies are higher in Xe than in Ar matrices, and in solid Kr the efficiencies are intermediate between those two hosts.[10] The solid host compensates the energy mismatch between the intramolecular energy levels involved in the energy relaxation by converting the excess internal energy of the guest molecule into lattice phonons. As an extreme case, one may expect the host to favor the relaxation pathway involving lower number of phonons.[11] For formic acid, the local matrix morphology is expected to influence the dynamics of energy relaxation at low

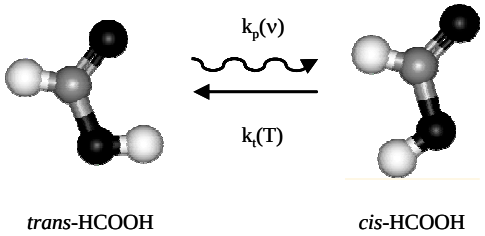

FIG. 1. *Cis* and *trans* formic acid conformers. The *trans*→*cis* isomerization is induced by vibrational excitation while the inverse *cis*→*trans* process occurs in dark via tunneling. The tunneling rate is temperature dependent. The *cis* conformer is higher in energy than the *trans* form by 1365 cm^{-1} as estimated experimentally in the gas phase (Ref. 16).

excitation energies (low density of states) due to its effect on the anharmonicity and intermode coupling constants.[12] Therefore the energy relaxation pathways and consequently photorotamerization efficiencies might depend not only on the rare gas used as host but also on local environment within the same host.

Estimations of quantum yield for narrowband IR-induced rotamerization have been previously reported.[6,13-15] For isomerization of matrix-isolated 2,3-difluoropropene, the quantum yield was shown to depend on excitation energy, on host matrix, and also on the nature of the excited mode.[13] For HONO, the photoinduced isomerization exhibits mode specific behavior with the efficiency of both *cis*→*trans* and the *trans*→*cis* isomerization processes being ≈2.5 times higher for excitation of the OH stretching fundamental as compared to the first N=O stretching overtone,[14] despite the similar energies of these modes. For CH_2D-CH_2D isolated in solid rare gases, the influence of the host and the nature of the excited vibrational mode on the isomerization efficiency were studied by resonant excitation of a number of vibrational states of the *gauche* and *trans* conformers.[6] It was concluded that the conversion efficiencies increase with the excitation energy and the observed deviations from the monotonous behavior were attributed to specific

intramolecular interactions controlling the dynamics of the energy relaxation.

Formic acid is one of the simplest molecules with rotational isomerism. It has two stable planar structures, the *cis* and *trans* conformers, represented in Fig. 1, the *trans* form being the conformational ground state. The gas phase energy difference between these two forms was determined as 1365±30 cm^{-1} (16 $kJmol^{-1}$).[16] Extensive spectroscopic studies have been carried out on *cis* and *trans*-formic acid isolated in solid Ar, including several isotopologues.[12,17-21] In an argon matrix, this molecule is mainly isolated in two slightly different local environments as deduced from the IR absorption spectrum, which reveals characteristic site splitting of the bands.[12]

In this work, the IR-induced *trans*→ *cis* isomerization process of formic acid is studied. The quantum yields for the rotamerization induced by selective excitation of various vibrational modes of the *trans* conformer in the 7000-2950 cm^{-1} region are determined. As a development of our previous work,[22] this article emphasizes local-environment effects on the isomerization quantum yields, and the corresponding results on the OH stretching overtone (2νOH) are added. The solid-state effects on the rotamerization and absorption processes are analyzed. In particular, phonon sidebands and librational satellites of intramolecular vibrational transitions are found using photorotamerization and IR absorption, respectively.

II. EXPERIMENTAL DETAILS AND METHODOLOGY

The gaseous samples were prepared by mixing formic acid (KEBO LAB, >99%), degassed by several freeze-pump-thaw cycles, with high purity argon (AGA, 99.9999%), typically in the 1:2000 proportion. The samples were deposited onto a CsI substrate kept at 15 K in a closed cycle helium cryostat (APD, DE 202A) and subsequently cooled down to 8 K. Typically 60-70 μm thick samples were prepared. The IR absorption spectra (7900-400 cm^{-1}) were measured with a Nicolet SX-60 FTIR spectrometer at 8 K. A liquid-nitrogen-cooled MCT detector and a KBr beamsplitter were used to record the mid-IR spectra, with spectral resolutions from 0.25 to 1.0 cm^{-1}, and a liquid-nitrogen-cooled InSb detector and a quartz beamsplitter were used for the near-IR spectra, with a spectral resolution of 0.5 cm^{-1}. Typically 100-500 interferograms were co-added.

Tunable pulsed IR radiation provided by an optical parametric oscillator (OPO Sunlite, Continuum, with IR extension) was used to excite vibrationally *trans*-HCOOH. The pulse duration was ≈5 ns with a spectral linewidth of ~0.1 cm^{-1} and a repetition rate of 10 Hz. A Burleigh WA-4500 wavemeter was used to control the OPO radiation frequency, providing an absolute accuracy better than 1 cm^{-1} for the IR radiation frequency. A mask with a circular hole of 4 mm in diameter attached on the sample substrate limited the area probed by IR spectroscopy. Since the size of this hole is smaller than both the beam of the spectrometer and the IR pumping beam, the probed area is fully irradiated. The IR radiation energy was measured at the sample position with a pulsed energy meter (Molectron), and it was 0.1-0.6 mJ per pulse for the 2900-7000 cm^{-1} region. The pumping beam was quasicollinear with the spectrometer beam and the interference filters transmitting in the 2000-500 cm^{-1} or in the 3300-1100 cm^{-1} regions attached at the spectrometer detector prevented the pumping radiation from reaching the detector. Another bandpass filter (1500-700 cm^{-1}) placed between the globar source and the sample eliminated globar-induced rotamerization of *trans* formic acid. These filters limited the spectral window of the IR absorption spectra recorded during pumping to the 1500-700 or 1500-1100 cm^{-1} regions.

Photoequilibrium is established under IR pumping of the *trans* conformer as a result of the interplay between *cis*-formic acid generation and its depletion due to tunneling (see Fig. 1). At the equilibrium the pumping

and tunneling rates are equal:

$$k_p(\nu)\,[\,trans]_{eq} = k_t(T)\,[\,cis]_{eq} \qquad (1)$$

Hence, the pumping rate $k_p(\nu)$ can be determined from the tunneling rate $k_t(T)$ and the ratio of the *cis* and *trans* photo-equilibrium concentrations. For solid argon at 8 K, $k_t(T)$ is 2.3×10^{-3} s^{-1} and it is not affected by the local environment.[23] It should be mentioned that the pumping takes place on a time scale (5 ns) which is very short compared with the interval between pulses (100 ms) and thus essentially an averaged pumping rate is measured. Between the pump pulses the concentration of the *cis* conformer is practically constant. The concentration of the *cis* conformer was followed using the integrated absorption of the intense CO-COH deformation (CO-COH def.) mode in the 1250-1240 cm^{-1} region. In the available spectral window to record the IR spectrum during pumping (limited by the filters), there are no bands of *trans*-formic acid that can be used to follow directly the concentration of this form. Instead, we used the ratio of the absorption cross sections of the O-C=O bending of the *trans* form (δOCO observed at ≈630 cm^{-1}) and the CO-COH def. band of the *cis* form to calculate the ratio of the *cis* and *trans* photoequilibrium concentrations as follows:

$$\Delta A_T^{\delta OCO} = \alpha \Delta A_C^{CO-COH def.} \quad , \qquad (2)$$

$$\frac{[cis]_{eq}}{[trans]_{eq}} = \left(\frac{\Delta A_T}{A^o{}_T - \Delta A_T}\right)_{\delta OCO} \quad , \qquad (3)$$

where ΔA is the pumping-induced change of the integrated absorption, A^0 is the initial (before irradiation) integrated absorption, the subscripts *C* and *T* referring to the *cis* and *trans* forms, respectively. The value of α was accurately determined from the change of integrated absorptions of the corresponding bands induced by IR pumping in separate experiments without filters.

The pumping rate is proportional to the quantum yield, $\phi(i)$, of the rotamerization process, the absorption cross section of the excited mode of the *trans* conformer [$\sigma^i_T(\nu)$ in cm^2], and the photon intensity of the pumping (I in s^{-1} cm^{-2}) as

$$k_p(\nu) = \phi(i)\sigma^i_T(\nu)I(\nu) \quad , \qquad (4)$$

where *i* refers to the *i*th excited vibrational mode. The absorption cross section is obtained using the measured IR absorption at a given excitation frequency, the formic acid concentration and the matrix thickness. Equation (4) is used to calculate the quantum yields once the pumping rates were extracted via Eq. (1).

III. COMPUTTIONAL MODEL FOR HINDERED ROTATION

Interaction of molecules with matrix atoms shifts the absorption bands from their gas phase values. The main contribution to the perturbation of the rotational spectra of trapped molecules comes from the electrostatic potential exerted by the lattice atoms, and the coupling of lattice vibrations to the molecular vibration and rotation. The theory of rotation of molecules in condensed phase has been investigated repeatedly.[24-30] In this work, we use the theoretical description of rotational energy levels of a polyatomic molecule isolated in an octahedral field, developed by Flygare.[24] This formulation was previously applied for a symmetric top.[31] In this model, only the electrostatic effects on the rovibrational spectrum are considered and the rotational-translational coupling effects are neglected. Furthermore, quantum effects such as Pauli repulsion due to overlapping electronic wave functions are ignored. This seems to be a good approximation due to the fact that most of the observed vibrations of formic acid isolated in rare-gas matrices are redshifted from the gas-phase values. Although this model is rather simplified, it can provide helpful information for the interpretation of the

experimental data with respect to librational motion of the trapped molecule.

A FORTRAN 90 code was written to calculate the Hamiltonian matrix elements in the free rotor basis set according to Flygare's formalism and to diagonalize this matrix.[24] This FORTRAN 90 code is also used to calculate the dipole-transition moments according to the formulation described in Ref. 31. The program uses as an input three parameters describing the lattice potential (V^J,V^K,V^M), the gas-phase rotational constants,[32,33] and the temperature (T = 8K). The basis set contained 2244 basis functions corresponding to a maximum value of the quantum number $J=15$. The same potential parameters are employed for the fundamental and excited vibrational states. The calculated stick spectrum was displayed using Gaussian functions with a linewidth of 0.6 cm^{-1}. This program was found to reproduce accurately the energy levels of the hindered rotation of linear molecules reported in the literature.[29] The program also reproduced the symmetric top spectral features obtained in Ref. 31 as a function of temperature for several values of the rotational barrier.

IV. EXPERIMENTAL RESULTS

The pumping rate for the photoinduced *trans→cis* conversion of formic acid isolated in solid argon (k_p) was extracted as a function of the excitation frequency as described above. This dependence [$k_p(\nu)$] is hereafter called a "reactive vibrational excitation (RVE) spectrum", in analogy with Ref. 3. This data is presented in Figs. 2 and 3 for the two major sites observed in an argon matrix.[12] It has been shown recently that these sites do not interconvert when the matrix is exposed site-selectively to IR radiation.[12] The molecules with the OH stretching (νOH) absorption at 3548.2 and 3550.5 cm^{-1} are by definition isolated in site 1 and site 2, respectively. An equal absorption cross section was assumed for the same vibrational modes of molecules in the two sites.

Some support for this approximation was obtained by comparing the relative intensities of various vibrational modes for both sites, which were roughly unaffected by the local environment. This led to the estimation of the site distribution as 62% of formic acid molecules in site 2 and 38% in site 1. The absorption spectra are also shown in Figs. 2 and 3 for comparison.

The calculations on formic acid isolated in solid argon lead to an energy difference between the conformers of 1123 cm^{-1} (13 $kJmol^{-1}$) and a *trans→cis* energy barrier of 3810 cm^{-1} (45.6 $kJmol^{-1}$).[23] Thus, the excitation energies used in this study allowed us to obtain the RVE spectra at energies above the torsional barrier [pumping the νOH overtone (2νOH) at 6930 cm^{-1} or the combination of the νOH with the COH-CO deformation mode (νOH + COH-CO def.) at 4650 cm^{-1}] and at energies considerably below the barrier [pumping the CH stretching (νCH) at 2950 cm^{-1}]. All excited modes in this range were found to be active in promoting the *trans→cis* rotamerization (see Figs. 2 and 3). The RVE spectra were used to determine the quantum yields for the excited vibrations and the results are listed in Table I and plotted as a function of the excitation energy in Fig. 4.

The RVE spectra revealed an interesting and important feature: in addition to the *trans→cis* isomerization induced at exact resonance, the process occurs under pumping *at higher energies* from the main absorption band. Broad bands blueshifted from the νOH fundamental and overtone modes appear in the RVE spectra (see Fig. 5). A similar behavior is also observed in the case of the combination mode of the νOH with the C-O torsion (νOH + τCOH at 4184 cm^{-1}). The broadness and low intensities of these sidebands prevent their direct observation in the IR absorption spectra.

As seen in Figs. 2 and 3, the relative peak intensities differ in the RVE and IR absorption spectra. The most significant difference is observed for the CH stretching mode (νCH) whose pumping rate is at least

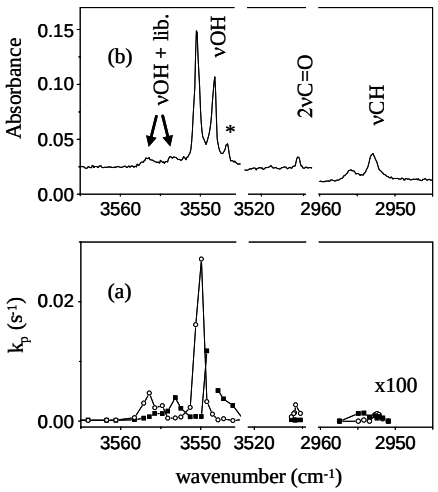

FIG. 2. (a) RVE spectrum for the IR-induced *trans→cis* isomerization of formic acid isolated in solid Ar at 8 K (■, site 1 and o, site 2) and (b) absorption spectrum of *trans*-formic acid in the 3565-2945 cm^{-1} region. The RVE spectrum in the νCH region is magnified by a factor of 10^2. The pumping rate value for the excitation of the νOH in site 1 is omitted due to the low accuracy of the measurements. The band marked with (*) was not assigned.

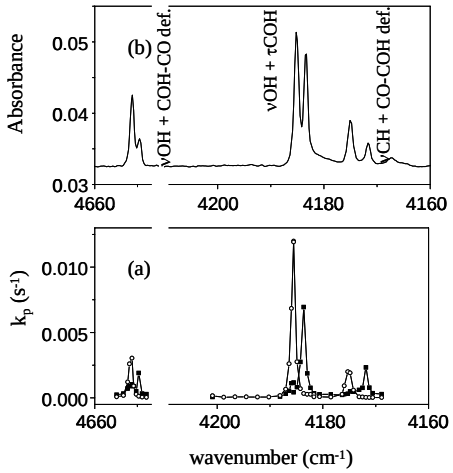

FIG. 3. (a) RVE spectrum for the IR-induced *tran→cis* isomerization of formic acid isolated in solid Ar at 8 K (■, site 1 and o, site 2) and (b) absorption spectrum of *trans*-formic in the 4660-4645 cm^{-1} and 4200-4160 cm^{-1} regions.

2 orders of magnitude lower than for the νOH fundamental or the carbonyl stretching overtone (2νC=O). A reliable difference is also observed in the νOH region for site 2 when comparing the relative intensities of the νOH (3550.5 cm^{-1}) band and the narrow blueshifted satellite band at 3556.7 cm^{-1} (see Fig. 2). For site 2, the IR absorption spectrum of this region is shown in detail in Fig. 6. The narrow blueshifted satellite band is here assigned to a combination between the νOH mode and the librational motion of the molecule (νOH + lib.). As shown in Fig. 6, a similar blueshifted librational satellite band was observed for DCOOH. This assignment is supported by simulations of hindered rotation of the trapped molecule in the matrix cage to be discussed below.

TABLE I. Quantum yield for the IR-induced *trans→cis* rotamerization in formic acid.[a]

	Quantum yield (ϕ)			
Excited mode	Site 1		Site 2	
2νOH	0.17	(6930.3)	0.07	(6934.8)
νOH + COH-CO	0.15	(4649.6)	0.21	(4651.4)
νOH + τCOH	0.21	(4183.6)	0.41	(4185.2)
νCH + CO-COH	0.25	(4171.8)	0.20	(4175.1)
νOH + lib.	0.050	(3553.7)	0.12	(3556.7)
νOH	b	(3548.2)	0.039	(3550.5)
*	0.024	(3546.7)		
2νC=O		(3519.0)	0.051	(3515.7)
	1.4×10^{-4}	(2956.1)	8.4×10^{-5}	(2953.1)

[a]The position of the absorption band of each site is given in parentheses (cm^{-1}). Symbols: *ν*, stretching; def, deformation; τ, torsion; lib., libration.
[b]This value is omitted due to low accuracy of the measurements determined by the very low concentration of *trans*-HCOOH in site 1 in the photoequilibrium. The absorption band marked with (*) is not assigned.

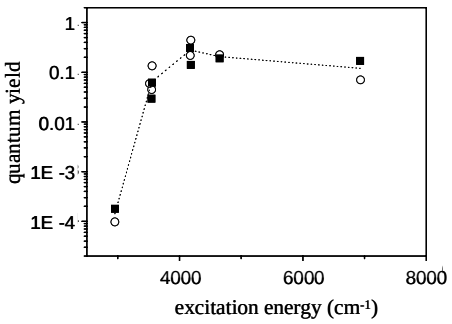

FIG. 4. Quantum yield (in logarithmic scale) for IR-induced *trans→cis* isomerization of HCOOH isolated in Ar at 8 K as a function of the excitation energy (■, site 1 and O, site 2). The points correspond to the following vibrational modes: ~ 6930 cm^{-1}: 2νOH; ~4650 cm^{-1}: νOH + COH-CO def; ~ 4185 cm^{-1}: νOH + τCOH; ~ 4175 cm^{-1}: νCH+CO-COH def; ~ 3550 cm^{-1}: νOH; ~ 3515 cm^{-1}: 2νC=O; ~ 2955 cm^{-1}: νCH. The estimated energy barrier for the reaction is 3810 cm^{-1}. A dotted line guides the eye.

V. DISCUSSION

A. Quantum yield for the *trans→cis* isomerization

Four combination modes of *trans*-formic acid with energies above the isomerization barrier were pumped site-selectively: 2νOH (6932 cm^{-1}), νOH + COH-CO def. (4650 cm^{-1}), νOH + τCOH (4184 cm^{-1}), and νCH + CO-COH def. (4173 cm^{-1}).[12] At these excitation energies, the isomerization quantum yield is ~ 20% (see Table I). The efficiency of the process is rather indepen-dent of the excited modes and no major differences between the trapping sites are observed either (see Fig. 4). Interestingly, the quantum yield values determined for this relatively small molecule are very large when compared to the values reported for $CH_2FC(F)=CH_2$(10^{-7}-10^{-4}).[13] Similarly high quantum yields were previously estimated for the photoisomerization process in the HONO molecule by excitation of the νOH.[14] The high quantum yields imply that the time scale for the *trans→cis* isomerization is shorter than the time scale for vibrational relaxation within the *trans* well. The latter is dictated by the rate of energy transfer to the lattice which, in turn, depends on the energy gaps between the intramolecular vibrational levels. For small molecules, such as formic acid, there may exist large energy gaps acting as bottlenecks for relaxation.

For pumping above the isomerization barrier, there are some fluctuations of the quantum yield values to be noticed in Table I. For example, in site 2, quantum yields for the 2νOH and νOH + τCOH modes differ by a factor of 6. The quantum yield for the νOH + τCOH mode differs by a factor of 2 depending on the site (see Table I). These results could be considered as some limited evidence of site- and mode-specific effects. The observed deviations from the averaged value are rather small compared, for example, with the variations of quantum yield reported for deuterated ethane (order of magnitude).[6] In our experiments, the quantum yield extracted for 2νOH has somewhat larger uncertainty (compared with the other modes) due to experimental reasons.

The quantum yield was also estimated for four vibrations below the predicted torsional barrier: combination of νOH with the librational motion of the molecule (νOH + lib., 3555 cm^{-1}), νOH (3549 cm^{-1}), 2νC=O (3516 cm^{-1}), and νCH (2955 cm^{-1}). The value obtained for the νOH mode in site 2 is lower by a factor of 3 than that for its librational satellite (see Table I). In a study on librational motion of the hydroxyl ion isolated in alkali halide crystals, it was suggested that the excited stretching and stretching-libration combination states should have different decay mechanisms.[34] The enhanced efficiency of the combination mode may be due to the stronger coupling between this mode and the reaction coordinate. For HONO, it was previously suggested that the presence of angular momentum enhances the energy transfer to the torsional mode.[35]

The energy dependence of the quantum yield for excitation below the energy barrier

for the *trans→cis* conversion is attributed to the tunneling between the *trans* and *cis* potential wells.[23] At these excitation energies, the quantum yield is limited by the tunneling probability between the potential wells. On the other hand, there are no such limitations for the quantum yield when the molecule is pumped with energy above the torsional barrier. The energy relaxation mechanism that channels the excitation energy into the reaction coordinate is clearly very complex, and its thorough theoretical investigation is highly desirable.

B. Phonon-sideband excitation

The RVE spectra reveal broad bands at higher energies from intramolecular vibrations (see Fig. 5). Photoinduced processes activated far from obvious absorption bands have been earlier assigned to excitation of two kinds of weak combinations: librational modes of the isolated molecule or lattice phonons with intramolecular vibrations.[36,37] In this work, the broad satellite bands in the RVE spectrum are characteristic of phonon sidebands of intramolecular vibrational transitions observed in pure molecular solids,[38] the zero-phonon-line (ZPL) corresponding to the intramolecular vibration. These phonon sidebands originate from the simultaneous excitation of an intramolecular vibration and a lattice phonon by one photon. Intense phonon sidebands are commonly observed for electronic transitions[39,40] when the most probable vertical transition involves a certain number of lattice phonons.[41] In most of the cases, the vibrational spectra of matrix-isolated species consist mainly of sharp ZPLs showing little indications of phonon sidebands. This difference is due to weaker vibration-phonon coupling compared with electron-phonon coupling.

The calculated one-phonon density of states of pure solid argon is about 70 cm^{-1} broad,[39,42,43] which is in agreement with the ≈65 cm^{-1} wide band observed in the RVE spectrum above the νOH band (3549 cm^{-1}). Pumping at energies below the ZPL is

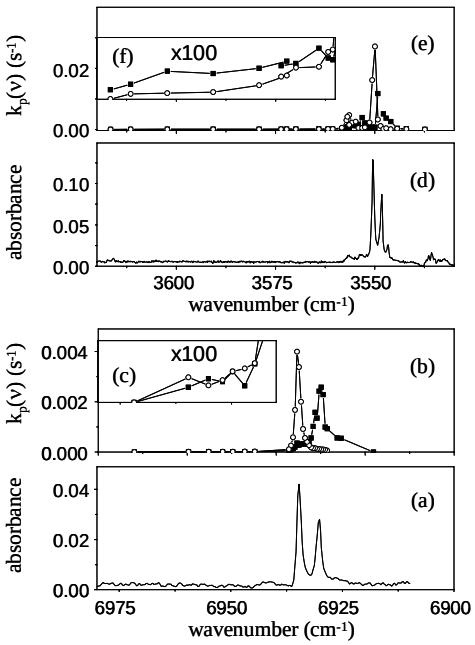

FIG. 5. Spectra of formic acid in the 2νOH (a-c) and νOH (d-f) region showing the presence of the phonon sideband in the RVE spectra (■, site 1 and o, site 2): (a) and (d) IR-absorption spectra, (b) and (e) RVE spectra; (c) and (f) expansion of the RVE spectra. The absorption maxima should not be compared between these two spectral regions because different matrices were used to collect these spectra.

inefficient in promoting isomerization, which is due to the low probability of the anti-Stokes process (when an existing phonon contributes to the vibrational transition) at the matrix temperatures. The ratio of the intensity of the phonon sideband to the ZPL is a measure of the coupling of the involved vibration with the lattice phonons.[39] In the RVE spectra, the measured ratio of the pumping rates for these two bands is ~ 0.08. The actual ratio of the absorption bands may differ from this value if the quantum yield differs between the ZPL and the phonon sideband. As shown in Fig. 5, for the 2νOH the apparently nonresonant excitation was detected up to

40 cm^{-1} from the ZPL. Our sensitivity to probe the phonon sideband of this mode is limited due to the fact that the ZPL is more than one order of magnitude weaker than the ZPL of the fundamental vibration. Nevertheless, some estimation of the coupling efficiency of the 2νOH mode can be made comparing the ratio of the absolute intensities of the ZPL and that of the phonon sideband at ~ 20 cm^{-1} from the ZPL for the νOH fundamental and overtone modes. Within our accuracy, this gives similar coupling efficiency for both modes.

The RVE spectrum appears to be useful to probe phonon sidebands that are in most cases not observed in the IR absorption spectrum. The increase of sensitivity to the weak and broad spectral features in the RVE method as compared with the IR absorption is explained by the essential absence of noisy background. Notice that the signals in the RVE spectra come from the efficiency of a given excited vibration to induce the isomerization reaction. The pumping rate is determined indirectly from the absorption of a certain vibrational mode of the reaction product (*cis*-HCOOH here), which was chosen due to its large absorption cross section in order to maximize sensitivity. In other words, this advantage is analogous to the situation with the high sensitivity of luminescence spectroscopy as compared with absorption spectroscopy. As shown above, a significant part of the oscillator strength can be carried by the phonon sideband. This possibility should be kept in mind when making accurate determinations of the band intensities in solid matrices.[31] In addition, while studying processes promoted by IR light one should be aware that due to phonon sidebands the processes can be induced over a broad spectral range in an apparently nonresonant way.

C. Librational motion

The IR absorption spectrum in the νOH spectral region of HCOOH and DCOOH isolated in solid Ar reveals the presence of narrow bands blueshifted by 6 and 9 cm^{-1} from the fundamental absorptions, respectively. In this section, we will discuss the assignment of these bands to the combination of the librational and vibrational motions of the molecule.

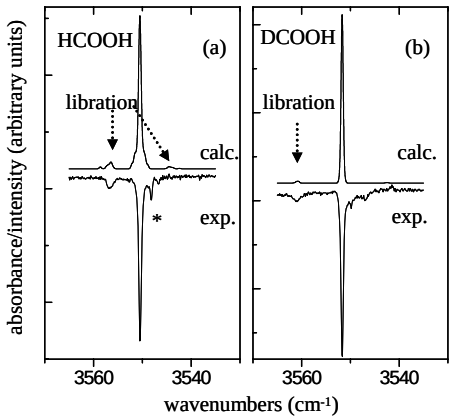

FIG. 6. IR absorption bands observed in the νOH region of HCOOH and DCOOH isolated in site 2 in an Ar matrix at 8 K (downwards) and simulated spectra on the basis of the hindered rotation of the molecule in the matrix (upwards). The experimental spectra are difference spectra showing the result of the site-selective pumping of molecules in site 2. The band marked with (*) belongs to *trans*-HCOOH in site 1 and it is seen here due to the limited site-selectivity caused by the overlap of the absorption bands at the irradiation wavelength. For the simulated spectra, the calculated transitions on the basis of the hindered rotation model (Ref. 24) were plotted with Gaussian bands (FWHM=0.6 cm^{-1}).

For HCOOH, site 2 exhibits one weak blueshifted satellite at 3556.7 cm^{-1} in addition to the main νOH fundamental band at 3550.5 cm^{-1} (see Fig. 6).[12] HCOOH in site 1 shows one main band due to the νOH fundamental mode at 3548.2 cm^{-1} and two weak satellite bands at 3553.7 and 3546.7 cm^{-1}.[12] Simply by summing the fundamental transitions, the combination modes that could explain the observed satellites are the νCH plus OCO deformation (νCH + δOCO ~ 3583 cm^{-1}) and the νCH plus COH torsion (νCH + τCOH ~ 3590 cm^{-1}), which

are 20-40 cm^{-1} higher than the observed bands. For DCOOH, site 2 exhibits one weak blueshifted satellite at 3560.9 cm^{-1} in addition to the νOH main band at 3551.7 cm^{-1} (see Fig. 6).[12] Site 1 of DCOOH shows two weak satellite bands at 3562.5 and 3547.2 cm^{-1} and one main band assigned to νOH at 3549.9 cm^{-1}.[12] The observation of a similar absorption pattern in the νOH spectral region of both isotopologues shows that the weak satellites observed cannot originate from combination modes involving the νCH vibration. No other second order combinations or overtones without involving the C-H bond are expected in this region.

In a recent paper, the rotationally resolved νOH and νCH spectral regions of HCOOH and DCOOH monomers were analyzed in liquid He droplets.[44] In that study, the accidental resonant mixing between the νOH and the νCH + δOCO and νCH + νCOH combination modes was shown to give rise to a triplet at 3571, 3569, and 3566 cm^{-1}. In He droplets, the νOH fundamental couples via Fermi resonance with the νCH + δOCO combination mode that, in turn, interacts with the νCH + τCOH mode via Coriolis coupling.[44] The assignment made for the observed bands in He droplets was supported by the absence of the same spectral pattern in the νOH region of the DCOOH isotopologue. This indicates different origins for the weak blueshifted bands observed in Ar matrix and in He droplets.

The coupling of the νOH mode with the librational motion of the molecule can explain the observed spectrum for the two isotopologues in the νOH region. Several small molecules have been shown to exhibit rotation in rare gas matrices.[8,9,31,45-47] Hindered rotation of a molecule in the matrix cage gives rise to librational motion.

In the simulations, the three components of the rotational barrier [V^J, V^K, V^M] were taken as free parameters to fit the calculated rovibrational spectrum to the observed spectrum in the νOH region for both HCOOH and DCOOH. As expected, for $V^J = V^K = V^M = 0$ cm^{-1} the spectra show the characteristic pattern of free rotation. When the rotational barriers are large enough the hindered rotation gives rise to two satellite bands equally shifted to higher and lower energies from the main band. The shift of the satellite bands from the main band increases and their intensity decrease as the barrier increases. The blueshifted satellite band corresponds to the sum combination while the redshifted band corresponds to the difference combination. The expected lower population of the excited librational levels at the low working temperature (8 K) determines the weaker intensity of the redshifted satellites when compared with the blueshifted ones.

The position of the librational satellite was found to be essentially dependent on the V^J value and rather insensitive to the V^K and V^M values. Reasonably good fits to the experimental values were obtained with V^J = 11 cm^{-1} for HCOOH and V^J = 18 cm^{-1} for DCOOH, irrespectively of the value of V^K and V^M, which were varied independently from 0 to 100 cm^{-1}. As an illustration, in Fig. 6 the spectra obtained with the optimized V^J values for both isotopologues and $V^K = V^M = 0$ cm^{-1} is shown. Some isotopic effect is expected due to the different hexadecapole moments of the two isotopologues arising from the different position of the center of mass for the O-H and O-D forms. As shown in Fig. 6, the hindered rotation model reproduces the position and relative intensity of the blueshifted satellite of the νOH observed for both HCOOH and DCOOH, thus giving confidence to the assignment. The redshifted bands were not experimentally observed, which is also in agreement with the simulations that give a very low intensity for these bands. Though this qualitative explanation of the observed satellites is based on a simple application of Flygare's model, the main features of the experimental spectra are well reproduced. A more detailed theoretical analysis is outside the scope of the present work.

In addition to the blueshifted satellite, for site 1 of HCOOH and DCOOH it is also

possible to observe a band that is about 2 cm^{-1} redshifted from the pure νOH fundamental band (see Fig. 2). This band cannot be associated with a librational band due to its small shift from the fundamental and its higher intensity when compared with the blueshifted librational satellite. Currently we have no explanation for this band.

VI. CONCLUDING REMARKS

The *trans→cis* rotamerization of formic acid in solid Ar was induced site- and mode-selectively by using narrowband IR irradiation in the 7000-2950 cm^{-1} region. All excited modes in this region were active in promoting the isomerization process. Remarkable is the high absolute value of the quantum yield (up to 40%) estimated for this isomerization process. While the details of the isomerization mechanism are currently unknown this very high efficiency should be of interest for theoretical modeling. The energy relaxation is rather independent of both the nature of excited mode and the trapping site. Nevertheless, the observed deviations from the average quantum yield value of 20% for excitation energies above the rotamerization barrier could be an indication of some specific mode and local environment effects. This interpretation has to be considered tentative due to the limited accuracy of the present experiments. Tunneling is an important mechanism involved in the rotamerization of formic acid essentially evidenced by the *trans→cis* isomerization induced by excitation of the νCH mode. Excitation of this mode introduces an energy in the system which is considerably below the energy barrier.

The RVE spectrum reveals the solid state effects on the vibrational spectroscopy of formic acid isolated in an Ar matrix. Broad RVE bands blueshifted from the intramolecular vibrations were assigned to phonon sidebands. In general, such weak and broad bands are not observed in the IR absorption spectra. Additionally, narrower bands blueshifted from the pure νOH band observed both in the RVE and IR absorption spectra of HCOOH were assigned to librational satellites.

ACKNOWLEDGMENTS

The Academy of Finland is thanked for financial support. E.M.S.M. and R.F. acknowledge the Portuguese Foundation for Science and Technology (Ph.D. Grant No. SFRH/BD/4863/2001 and Project No. POC TI/43366/QUI/2001).

[1] J. D. Baldeschwieler and G. C. Pimentel, J. Chem. Phys. **33,** 1008 (1960).
[2] H. Frei and G. C. Pimentel, Annu. Rev. Phys. Chem. **36,** 491 (1985).
[3] H. Frei and G. C. Pimentel, in *Chemistry and Physics of Matrix-Isolated Species*, edited by L. Andrews and M. Moskovits (Elsevier Science, New York, 1989).
[4] L. Khriachtchev, E. Maçôas, M. Pettersson, and M. Räsänen, J. Am. Chem. Soc. **124,** 10994 (2002).
[5] J. Nesbitt and R. W. Field, J. Phys. Chem. **100,** 12735 (1996).
[6] P. Roubin, S. Varin, P. Verlaque, S. Coussan, J.-M. Berset, J.-M. Ortéga, A. Peremans, and W.-Q. Zheng, J. Chem. Phys. **107,** 7800 (1997).
[7] J. Jortner and R. D. Levine, in *Advances in Chemical Physics*, edited by J. Jortner, R. D. Levine, and S. A. Rice (Wiley-Interscience, New York, 1981), Vol. 47.
[S] V. E. Bondybey, M. Räsänen, and A. Lammers, Annu. Rep. Prog. Chem., Sect. C: Phys. Chem. **95,** 331 (1999).
[9] F. Legay, in *Chemical and Biochemical Applications of Lasers*, edited by C. B. Moore (Academic, New York, 1977).
[10] M. Räsänen, H. Kunttu, and J. Murto, Laser Chem. 9, 123 (1988).
[11] V. E. Bondybey, Annu. Rev. Phys. Chem. **35,** 591 (1984).
[12] E. M. S. Maçôas, J. Lundell, M. Pettersson, L. Khriachtchev, R. Fausto, and M. Räsänen, J. Mol. Spectrosc. **219,** 70 (2003).
[13] A. K. Knudsen and G. C. Pimentel, J. Phys. Chem. **95,** 2823 (1991).
[14] L. Khriachtchev, J. Lundell, E. Isoniemi, and M. Räsänen, J. Chem. Phys. **113,** 4265 (2000).
[15] W. F. Hoffman III and J. S. Shirk, Chem. Phys. **78,** 331 (1983).
[16] W. M. Hocking, Z. Naturforsch. A **31A**, 1113 (1976).
[17] M. Pettersson, J. Lundell, L. Khriachtchev, and M. Räsänen, J. Am. Chem. Soc. **119,** 11715 (1997).
[18] T. Miyazawa and K. S. Pitzer, J. Chem. Phys. **30,** 1076 (1959).
[19] R. L. Redington, J. Mol. Spectrosc. **65,** 171 (1977).
[20] D. O. Henderson, Doctoral thesis, Texas Tech.

University, 1987.
[21] F. Madeja, P. Markwick, M. Havenith, K. Nauta, and R. E. Miller, J. Chem. Phys. **116,** 2870 (2002).
[22] M. Pettersson, E. M. S. Maçôas, J. Lundell, L. Khriachtchev, R. Fausto, and M. Räsänen, J. Chem. Phys. **117,** 9095 (2002).
[23] M. Pettersson, E. M. S. Maçôas, L. Khriachtchev, R. Fausto, and M.Räsänen, J. Am. Chem. Soc. **125,** 4058 (2003).
[24] H. Flygare, J. Chem. Phys. **39,** 2263 (1963).
[25] A. Cabana, G. B. Savitzky, and D. F. Hornig J. Chem. Phys. **39,** 2942 (1963).
[26] V. Narayanamurti, Phys. Rev. Lett. **13,** 693 (1964).
[27] B. Wedding and M. V. Klein, Bull. Am. Phys. Soc. **11,** 228 (1966).
[28] A. F. Devonshire, Proc. R. Soc. London, Ser. A **153,** 601 (1936).
[29] H. F. King and D. F. Hornig, J. Chem. Phys. **44,** 4520 (1966).
[30] P. Sauer, Z. Phys. **194,** 360 (1966).
[31] V. A. Apkarian and E. Weitz, J. Chem. Phys. **76,** 5796 (1982).
[32] J. Vander Auwera, J. Mol. Spectrosc. **155,** 136 (1992).
[33] K. L. Goh, P. P. Ong, T. L. Tan, W. F. Wan, and H. H. Teo, J. Mol. Spectrosc. **190,** 125 (1998).
[34] M. V. Klein, B. Wedding, and M. A. Levine, Phys. Rev. **180,** 902 (1969).
[35] P. M. Agrawal, D. L. Thompson, and L. M. Raff, J. Chem. Phys. **102,** 7000 (1995).
[36] S. Fei, G. S. Yu, H. W. Li, and H. L. Strauss, J. Chem. Phys. **104,** 6398 (1996).
[37] W. P. Ambrose and A. J. Sievers, J. Opt. Soc. Am. B **9**, 753 (1992).
[38] A. P. Brodyanski, S. A. Medvedev, M. Vetter, J. Kreutz, and H. J. Jodl, Phys. Rev. B **66,** 104301 (2002).
[39] V. E. Bondybey and C. Fletcher, J. Chem. Phys. **64,** 3615 (1976).
[40] M. Pettersson and J. Nieminen, Chem. Phys. Lett. **283,** 1 (1998).
[41] V. E. Bondybey, in *Chemistry and Physics of Matrix-Isolated Species,* edited by L. Andrews and M. Moskovits (Elsevier Science, Amesterdam, 1989).
[42] *Rare Gas Solids*, edited by M. L. Klein and J. A. Venables (Academic, London, 1976), Vol. 1.
[43] H. J. Jodl, in *Chemistry and Physics of Matrix-Isolated Species,* edited by L. Andrews and M. Moskovits (Elsevier Science, Amesterdam, 1989).
[44] F. Madeja, P. Markwick, and M. Havenith, J. Chem. Phys. **116,** 2870 (2002).
[45] L. H. Jones, S. A. Ekberg, and B. I. Swanson, J. Chem. Phys. **85,** 3203 (1986).
[46] R. M. Bentwood, A. J. Barnes, and W. J. Orville-Thomas, J. Mol. Spectrosc. **84,** 391 (1980).
[47] E. Isoniemi, M. Pettersson, L. Khriachtchev, J. Lundell, and M. Räsänen, J. Phys. Chem. A **103,** 679 (1999).

Appendix III

Cis→ trans conversion of formic acid by dissipative tunneling in solid rare gases: Influence of environment on the tunneling rate.

Mika Pettersson, Ermelinda M. S. Maçôas, Leonid Khriachtchev, Jan Lundell, Rui Fausto and Markku Räsänen

J. Chem. Phys. **2002**, *117*, 9095-9098.

Cis→trans conversion of formic acid by dissipative tunneling in solid rare gases: Influence of environment on the tunneling rate

M. Pettersson[a)]
Laboratory of Physical Chemistry, P.O. Box 55, FIN-00014, University of Helsinki, Finland

E. M. S. Maçôas
Laboratory of Physical Chemistry, P.O. Box 55, FIN-00014, University of Helsinki, Finland and Department of Chemistry-CQC, University of Coimbra, P-3004-535, Coimbra, Portugal

L. Khriachtchev and J. Lundell
Laboratory of Physical Chemistry, P.O. Box 55, FIN-00014, University of Helsinki, Finland

R. Fausto
Department of Chemistry-CQC, University of Coimbra, P-3004-535, Coimbra, Portugal

M. Räsänen
Laboratory of Physical Chemistry, P.O. Box 55, FIN-00014, University of Helsinki, Finlan
(Received 21 August 2002; accepted 23 September 2002)

The relaxation of the higher-energy *cis* conformer of formic acid to the lower-energy trans form by a tunneling mechanism has been investigated in low-temperature rare gas matrices. In the temperature range 8–60 K, the tunneling takes place dominantly from the vibrational ground state of the *cis* form and the temperature dependence of the tunneling rate constant is influenced by the interactions with the environment. The temperature-dependent tunneling rates for HCOOH and DCOOH in solid Ar, Kr, and Xe are measured including data for molecules in different local environments within each host. It was found that the medium and the local environment has a significant influence on the tunneling rate. © 2002 American Institute of Physics.
[DOI:10.1063/1.1521429]

In reaction kinetics, tunneling of atoms is often negligible compared with over-barrier transitions. At very low temperatures, however, the population of energy states above the barrier becomes exceedingly small and tunneling becomes comparatively more important.[1] In a condensed environment, phonons participate in a tunneling reaction and the environment should have some effect on tunneling reactions.[2,3] However, in several previous experiments it was found that the tunneling rate constant was unaffected by the change of solvent.[1,4–6] In this work, we have studied the conversion of *cis* formic acid (HCOOH) to *trans* formic acid in solid rare gases (Ar, Kr, Xe). This reaction is dominated by tunneling from the vibrational ground state at temperatures below 60 K. The results show that the tunneling rate depends strongly on the environment.

[a)] Electronic address: petters@csc.fi

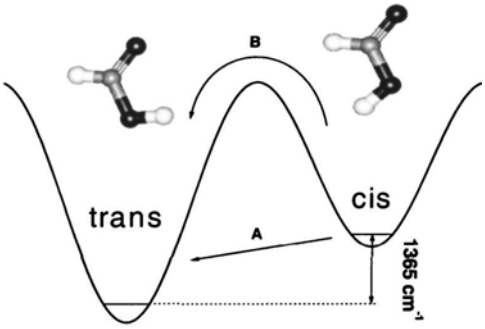

FIG. 1. *Cis* and *trans* formic acid and the torsional potential which connects the two conformers. The energy difference between the conformers is the experimental gas phase result from the Ref. 7. The arrows represent the conformer conversion processes by (A) tunneling and (B) over-barrier reactions.

The samples were made by mixing vapors of formic acid (FA) (KEBO lab, >99%) or its isotopomers (IT Isotope 95%–98% deuteration) with rare gases (Rg) Ar (AGA, 99.9999%), Kr (Air Liquid, 99.95%), Xe (AGA, 99.997%) in the gas phase in a proportion FA/Rg ≈ 1/1000. The gas mixture was deposited on a CsI substrate at 15 K (Ar), 25 K (Kr) or 35 K (Xe) yielding highly monomeric matrices with respect to FA. Thickness of the sample was typically about 100 μm. After deposition, the samples were cooled to ~ 8 K which was the lower limit for the cryostat (APD DE 202 A). The spectra were measured with a FTIR spectrometer (Nicolet 60 SX) with a resolution of 1 or 0.25 cm^{-1}.

FA has energy minima in two planar forms differing by orientation of the hydroxyl group as shown in Fig. 1. The interconversion of the conformers involves mainly the torsional motion of the hydroxyl group. In the gas phase, *cis*-FA is 1365 ± 30 cm^{-1} higher in energy than *trans*-FA.[7] The barrier from *trans* to *cis* has been calculated to be ~ 4200 cm^{-1}.[8] In this work, *cis*-FA was prepared by exciting the vibrational transitions of *trans*-FA in rare-gas matrices with narrowband infrared radiation of an optical parametric oscillator (Sunlite, Continuum, FWHM ~ 0.1 cm^{-1}). The excitation energy flows into the torsional coordinate inducing the conformer conversion.[9] The IR spectra of *cis* and *trans* FA differ significantly from each other making it possible to distinguish them easily in rare-gas matrices.[9] FA is trapped in several sites corresponding to different local environments and the corresponding IR absorption frequencies differ typically a few cm^{-1} as illustrated in Fig. 2 for *cis*-FA in solid Xe. *Cis*-FA was generated site-selectively by irradiating molecules in a separate site at a time similarly to our matrix-isolation studies on HONO.[10] In this way, the tunneling kinetics of FA in different sites could be investigated. There was no interconversion between different site groups either in IR pumping or in relaxation by tunneling.

Once formed, *cis*-FA converts back to *trans*-FA in a timescale of minutes even below 20 K.[9] At these temperatures, this reaction occurs purely via tunneling. Indeed, according to the ab initio calculations, the barrier (E_a) for the *cis*→*trans* isomerization is ~ 2800 cm^{-1},[8] which gives, according to the Arrhenius formula $k=A*exp(-E_a/kT)$ and using the torsional frequency for the pre-exponential factor *A*, a rate constant of

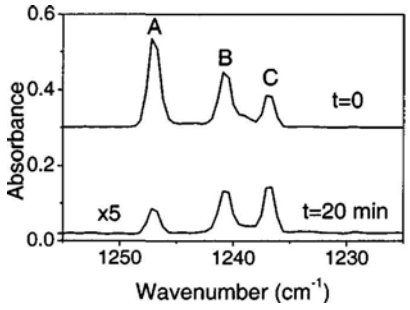

FIG. 2. IR absorption of *trans*-HCOOH in the CO-COH deformation fundamental region in solid Xe at 8 K. A, B, and C denote the absorptions corresponding to various sites (local environment). The lower trace was measured 20 min after the upper trace showing the different tunneling rates for the three sites.

~10 $^{-16}$ s^{-1} even at 60 K. This rate is more than 13 orders of magnitude smaller than what is observed in our experiments. The over-barrier reaction should become significant at temperatures only above ~110 K. The torsional mode, which mainly corresponds to the tunneling coordinate, is the lowest frequency vibration in *cis*-FA at ~500 cm^{-1}.[9] It follows that, at the highest temperatures of our experiments (60 K) the population of the first excited torsional level is <10^{-5}. We have estimated by using the WKB approximation[1] for the penetration probability and ab initio calculated (MP2/6-311++G(2d,2p), GAUSSIAN 98)[11] torsional potential that the permeability of the barrier from the first excited torsional level is ~ 4 orders of magnitude higher than from the ground state. Therefore, at low temperatures the tunneling reaction takes place essentially from the ground vibrational state of *cis*-FA and the tunneling from the thermally excited vibrational states may become important only at temperatures above 60 K. In this respect, FA is an ideal system to study the effect of the environment on tunneling.

The kinetics of the tunneling reaction was measured by FTIR spectroscopy after the *trans*→*cis* IR pumping was stopped by following the decrease in intensity of the CO-COH deformation absorption band of *cis* FA at ~1250 cm^{-1} (see Fig. 2). As an additional complication, it was found that the spectrometer glowbar radiation increases the rate of the *cis*→*trans* conversion significantly. By using an interference filter that blocks the radiation above ~ 1500 cm^{-1}, the effect of glowbar was suppressed and tunneling rates could be reliably measured. It was also estimated that the room temperature blackbody radiation from the cryostat windows did not affect the results. The Arrhenius plots for HCOOH and DCOOH in various rare-gas solids including representative examples of different sites (indicated by solid and open symbols) are presented in Fig. 3. The isomerization rate for HCOOD was also measured in Ar and it was at least three orders of magnitude smaller at 8 K than for HCOOH.

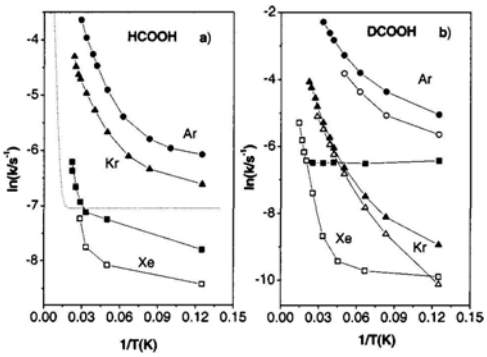

FIG. 3. Arrhenius plots for tunneling of (a) HCOOH and (b) DCOOH in various matrices. Data for two representative sites for each host are shown as solid and open symbols. The data for two sites shown in plot (a) for Xe as solid and open squares correspond to labels A and B in Fig. 2, respectively. For comparison, a simulated temperature dependence for tunneling from two lowest intramolecular vibrational states is shown as a dotted line.

The major conclusion drawn from Fig. 3 is that the tunneling rate depends crucially on the solid host and in most cases also on the local matrix morphology (matrix-site effect). The temperature dependencies are also in definite contrast with the behavior that tunneling from the thermally excited intramolecular vibrational levels would show. To make this clear we show in Fig. 3 (a) by a dotted line the simulated temperature dependence assuming tunneling from the two lowest torsional levels and four orders of magnitude higher tunneling probability from the first excited level than from the ground state. Clearly, comparing this result with the experiments suggests that the experimental temperature dependencies originate from the interaction of FA with the environment. For HCOOH, the tunneling rate decreases from Ar to Xe by one order of magnitude at 8 K. The rates for the two representative sites in solid Xe differ by a factor of ~ 2 at 8 K (see also Fig. 2). In Ar and Kr matrices the molecules in various sites have the same rates within the experimental error. For DCOOH, the different sites show different tunneling rates

in all the hosts. The tunneling rate for DCOOH in Ar is more than two orders of magnitude higher than in Kr at 8 K. The rates for molecules in different sites in Xe differ by a factor of ~ 30 at 8 K. It is also interesting to compare the tunneling rates of HCOOH and DCOOH in the same host. It is seen that the tunneling rates change considerably despite the deuteration of the carbon bound hydrogen shifts down the torsional frequency less than 2%. In solid Ar at 8 K. DCOOH tunnels three times faster than HCOOH. In Kr matrices, the trend is opposite: HCOOH tunnels ~ 30 times faster than DCOOH. In Xe host, the difference in rate constants depends strongly on which sites are compared.

These observations demonstrate that both changing the solid host, and changing the local environment within the same host can influence strongly the tunneling rates, the differences in the rate constants exceeding two orders of magnitude at 8 K. Related phenomena have been reported for reorientation of NH_3D^+ ions in Tutton salts.[12] In those experiments, however, the tunneling system was defined by the environment (rotation of NH_3D^+ between the inequivalent sites). In the present case, the tunneling system (internal rotation of formic acid) is well defined without the environment and therefore the effect of environment on the tunneling reaction is probed.

Next, we try to qualitatively understand different factors influencing the tunneling rate. Due to the large asymmetry of the torsion potential (see Fig. 1) the tunneling process involves excited vibra-tional states of *trans*-FA. In this respect, the energy difference between the *cis* and *trans* isomers and the vibrational level structure of *trans* are important to consider. It should be noticed that the two isomers have markedly different dipole moments (3.79 D for *cis*; 1.42 D for *trans*)[7] and hence their solvation energies are different. We estimated the solvation energies of *trans* and *cis*-FA in various hosts within the frame of the polarized continuum (PCM) model in

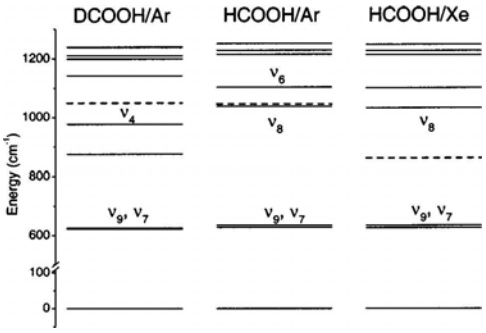

FIG. 4. Vibrational level structure of *trans*-HCOOH and *trans*-DCOOH as determined from their infrared spectra. The energy of the ground state of *cis*-FA estimated by using the gas-phase energetics (Ref. 7) and *ab initio* calculated solvation energies for the two conformers is shown with a dashed line. The labels for selected vibrational states correspond to torsion (ν_9), OCO scissor (ν_7), C-H out-of-plane wag (ν_8), C-D rocking (ν_4), and COH-CO deformation (ν_6) modes (Ref. 9).

GAUSSIAN 98 (Ref. 11) at the MP2/aug cc-pvTZ level using the calculated gas phase structures and the dielectric constants of the rare gases [1.63 (Ar); 1.88 (Kr); 2.19 (Xe)].[13] The differences for solvation energies of the *cis* and *trans* forms are 319 cm^{-1} (Ar), 412 cm^{-1} (Kr), and 508 cm^{-1} (Xe) indicating that solvation in a dielectric medium has a significant effect on the energetics. According to similar calculations performed on the transition state, the *cis*→*trans* barrier increases from Ar to Kr by 43 cm^{-1} and from Kr to Xe by 44 cm^{-1}. The vibrational energy level structure of *trans*-FA relative to the ground state of *cis*-FA is shown in Fig. 4 for HCOOH/Ar, DCOOH/Ar and HCOOH/ Xe. The position of the ground state of *cis*-FA estimated by the solvation calculations is shown with a dashed line in Fig. 4. Due to the limited accuracy of the solvation model the position of the ground state of *cis*-FA should be considered qualitative. Therefore, the discussion below is mostly hypothetical with respect to the exact energetics. In solid Ar, the smallest energy gap for the relaxation from the ground state of *cis*-HCOOH is connected with the first excited

state of the ν_8 mode (C-H out of plane wag) of the *trans* form. In contrast, in solid Xe, solvation lowers the energy of *cis*-FA and the most energetically favorable relaxation channel occurs to the first excited states of ν_7 (OCO scissors) and ν_9 (torsion) modes. In solid Ar, one-phonon emission is sufficient to dissipate the excess energy (Debye frequency of Ar = 93 cm^{-1}) while in Xe, a higher-order multiphonon process is required (Debye frequency of Xe = 64 cm^{-1}).[14] We can conclude from these examples that at least three factors contribute to the observed differences in the tunneling rates: (1) Change in the barrier height due to solvation which, according to the calculations, is relatively small in this case. (2) Due to differences in solvation energies, in different environments phonon-assisted tunneling may occur between different levels. The coupling between vibrational levels can vary strongly and therefore the effect on the tunneling rate can be large. (3) Change of the magnitude of the energy gap between the tunneling levels changes the order of the phonon process providing the energy dissipation. The differences of the rates between HCOOH and DCOOH should mainly originate from the change of the intrinsic level structure upon deuteration (see Fig. 4). The site effect can be explained on the same basis: It is plausible to assume that molecules in various sites have different solvation energies because the cavity size and geometry are key factors in the solvation. Additionally, coupling with phonons can be different for various sites.

The temperature dependencies of the rate constants are roughly described as $k(T) \propto T^3$ or T^4. Previously, roughly T^4 dependence was observed for translational tunneling of the acidic protons in benzoic acid dimers.[15] Theoretically, it was shown that T^2 or T^3 dependencies may arise from two-phonon emission/absorption and Raman processes.[16,17] Recently, a much stronger temperature dependence was reported for the $D + HD \rightarrow D_2 + H$ reaction in solid HD (Ref. 18) and the origin of the effect was considered theoretically.[3,19] The present observations should be valuable in testing theories for the temperature dependence of dissipative tunneling. In addition to the fundamental value the observed phenomenon can be used for solid-phase stabilization of desired species affected by tunneling decay by choosing a suitable environment.[20] It is interesting to note that indirect evidence of the influence of environment on a *cis-trans* isomerization tunneling reaction of hydroquinone in Ar and Xe matrices has been recently reported.[21]

In summary, it has been shown here that despite the relatively high energy barrier (~2800 cm^{-1}) *cis*-FA converts to *trans*-FA in timescale of minutes even at 8 K via pure tunneling mechanism. The tunneling rate depends strongly on the solid host and even on the local environment within a particular host, the differences in the tunneling rate constants exceeding two orders of magnitude at 8 K.

This work was supported by the Academy of Finland. One of the authors (E.M.S.M.) acknowledges a Ph.D. student grant of the Portuguese Foundation for Science and Technology.

[1] R. P. Bell, in *The Tunnel Effect in Chemistry* (Chapman and Hall, London, 1980).
[2] V. A. Benderskii, D. E. Makarov, and C. A. Wight, in *Chemical Dynamics at Low Temperatures* (Wiley, New York, 1994).
[3] G. K. Ivanov, M. A. Kozhusner, and L. I. J. Trakhtenberg, Chem. Phys. **113,** 1992 (2000).
[4] W. Al-Soufi, K. H. Grellmann, and B. Nickel, J. Phys. Chem. **95,** 10503 (1991).
[5] J. Hennig and H.-H. Limbach, J. Chem. Soc, Faraday Trans. 2 **75**, 752 (1979).
[6] G. Brunton, J. A. Gray, D. Griller, L. R. C. Barclay, and K. U. Ingold, J. Am. Chem. Soc. **100,** 4197 (1978).
[7] W. H. Z. Hocking, Z. Naturforsch. A **31A**, 1113 (1976).
[8] J. D. Goddard, Y. Yamaguchi, and H. F. Schaefer III, J. Chem. Phys. **96,** 1158 (1992).
[9] M. Pettersson, J. Lundell, L. Khriachtchev, and M. Räsänen, J. Am. Chem. Soc. **119,** 11715 (1997).
[10] L. Khriachtchev, J. Lundell, E. Isoniemi, and M. Räsänen, J. Chem. Phys. **113,** 4265 (2000).

[11] M. J. Frisch, G. W. Trucks, H. B. Schlegel *et at*, GAUSSIAN 98, Revision A.9, Gaussian, Inc., Pittsburgh, PA, 1998.
[12] H. L. Strauss, Ace. Chem. Res. **30,** 37 (1997).
[13] H. E. Hallam and G. F. Scrimshaw, in *Vibrational Spectroscopy of Trapped Species*, edited by H. E. Hallam (Wiley, London, 1973).
[14] H. J. Jodl, in *Chemistry and Physics of Matrix-Isolated Species*, edited by L. Andrews and M. Moskovits (North-Holland, Amsterdam, 1989).
[15] C. Rambaud, A. Oppenländer, M. Pierre, H.-P. Tromsdorff, and J.-C. Vial, Chem. Phys. **136,** 335 (1989).
[16] R. Silbey and H.-P. Trommsdorff, Chem. Phys. Lett. **165,** 540 (1990).
[17] A. Suárez and R. J. Silbey, J. Chem. Phys. **94,** 4809 (1991).
[18] T. Kumada, K. Komaguchi, Y. Aratono, and T. Miyazaki, Chem. Phys. Lett. **261,** 463 (1996).
[19] M. V. Basilevsky and G. V. Davidovitch, J. Chem. Phys. **115,** 6083 (2001).
[20] L. Khriachtchev, E. Maçôas, M. Pettersson, and M. Räsänen, J. Am. Chem. Soc. **124,** 10994 (2002).
[21] A. Nobuyuki, S. Kudoh, M. Takayanagi, and M. Nakata, Chem. Phys. Lett. **356,** 133 (2002).

Appendix IV

Infrared-induced conformational interconversion in carboxylic acids isolated in low-temperature rare-gas matrices.

Ermelinda M. S. Maçôas, Leonid Khriachtchev, Mika Pettersson, Jan Lundell, Rui Fausto and Markku Räsänen

Vib. Spectrosc. **2004**, *34*, 73-84.

Infrared-induced conformational interconversion in carboxylic acids isolated in low-temperature rare-gas matrices

Ermelinda M.S. Maçôas[a,b,*], Leonid Khriachtchev[a], Mika Pettersson[a], Jan Lundell[a], Rui Fausto[b], Markku Räsänen[a]

[a]*Department of Chemistry, University of Helsinki, P.O. Box 55 (A.I. Virtasen aukio 1), Helsinki FIN-00014, Finland*

[b]*Department of Chemistry (CQC), University of Coimbra, Coimbra P-3004-535, Portugal*

Received 17 March 2003; received in revised form 10 July 2003; accepted 11 July 2003

Abstract

An overview of our recent studies dealing with infrared-induced conformational interconversion of carboxylic acids isolated in rare-gas matrices is presented. Extensive rotational photoisomerization studies have been performed on formic acid, which is the simplest organic acid enabling this kind of processes. Formic acid has two conformers and interconversion between them can be induced by vibrational excitation. As such, it is an ideal model system to study the conformational dynamics of the carboxylic group. Formic acid molecules were found to be isolated in different local environments within the rare-gas matrices, as shown by the site splitting of the vibrational bands. Narrowband tunable infrared (IR) radiation was used to induce site-selective isomerization processes. The induced changes in the IR absorption spectra allowed for a detailed analysis of the vibrational properties of both conformers of formic acid isolated in solid argon. In particular, derived from the intermode coupling constants the local environment was shown to affects the intramolecular potential energy surface. Tunneling is involved in the rotamerization of formic acid, with the tunneling rate being affected by the local environment. Additionally, formic acid exhibits isomer-selective photodissociation where narrowband IR excitation can control the conformer-dependent photodissociation channels. Tunable IR radiation was also used to promote rotamerization in a series of matrix-isolated dicarboxylic acids (ethanedioic, propanedioic, and 2-butenedioic acids) by exciting the first overtone of the O-H stretching mode or a suitable combination mode at similar energies. Efficient isomerization involving rotation around the C-O bond was observed in most cases whereas the internal rotation around the C-C bond was found to be constrained for ethanedioic and (Z)-2-butenedioic acids.

Keywords: Vibrational excitation; Energy relaxation; Conformational interconversion; Matrix-isolation

1. Introduction

The low-temperature matrix-isolation technique combined with various spectroscopic methods (in particular, IR spectroscopy) is a powerful approach to the characterization of conformational proper-ties of molecules. In a matrix-isolation experiment the low temperature of the sample suppresses thermal reactions with significant activation energy, hence enabling stabilization of higher energy conformers. Very often the conformational distribution of the gaseous sample (prior to deposition) is trapped in the matrix upon freezing the sample [1]. If the energy barriers are sufficiently low, the annealing of the matrix may induce conformational conversion of the higher energy species into the lower energy ones. However, investigation of thermally induced isomerization reactions is possible only within a very limited range of energy barriers due to matrix-temperature limitations [1]. In contrast, photoinduced rotational isomerization is only limited by the photon energy.

* Corresponding author.

E-mail address: emacoas@qui.uc.pt

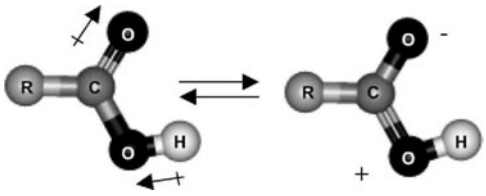

Fig. 1. The O=C-O-H dihedral angle of 0º is stabilized by a higher efficiency of the mesomerism within the carboxylic group [O=C-O-H ↔ O^--C=O^+-H] and by an attractive interaction between the C=O and O-H dipoles when compared with the 180º dihedral angle. Arrows indicate the direction of the dipoles.

A considerable number of studies have been dedicated to IR-induced rotamerization in low-temperature matrices [1-9]. Most of the earlier studies used broadband excitation, which can only be selective to some extent. However, a few examples are known in which narrowband irradiation was involved [10-16]. The limited number of systematic studies performed using narrowband selective vibrational excitation might be partially attributed to the lack of available tunable IR sources. The use of narrowband IR irradiation allows to excite selectively a specific vibrational mode of a desired conformer. This approach can be used to probe mode-selectivity of vibrational energy relaxation pathways.

Splitting of IR absorption bands of matrix-isolated species is a well-known phenomenon usually called a matrix-site effect. This splitting is caused by different local environments of the trapped species and potentially provides a way to study local matrix morphology and its effects on the molecular properties. Narrowband radiation can be used to pump selectively molecules [e.g. HONO and $(FCO)_2$] isolated in various matrix sites [15,16].

In the present work, we focus on the photoinduced rotamerization of matrix-isolated carboxylic acids. An isolated carboxylic group adopts preferentially a planar geometry. When compared with the 180º arrangement of the O=C-O-H dihedral angle, the 0º arrangement is stabilized by a higher efficiency of the mesomerism within the carboxylic group [O=C-O-H ↔ O^--C=O^+-H], an attractive interaction between the C=O and O-H bond-dipoles, and the absence of oxygen lone electron pair repulsion [17] (see Fig. 1). The interconversion between the two stable planar forms of the carboxylic group occurs via rotation of the O-H bond around the C-O axis. Since the reaction coordinate is mainly described by the motion of the hydrogen atom, tunneling can be important for the conversion mechanism. In fact, tunneling from the higher energy *cis* conformer of formic acid to the lower energy *trans* form was observed when the *cis* conformer was prepared in an Ar matrix by IR pumping [18]. The recently published studies on formic acid have further emphasized the importance of tunneling in the isomerization reactions [19,20]. Additionally, isomerization studies performed on hydroquinone and on a halogenated derivative of dihydroxybenzoquinone isolated in argon matrices [21,22] seem to indicate that the participation of tunneling in isomerization processes involving mainly motion of hydrogen atoms is quite general. Solid-state medium is expected to influence the tunneling rate [23-25], which depends also on the temperature due to the participation of the lattice phonons in a dissipative tunneling mechanism [26-28].

Isomer-selective photochemistry has motivated many works on IR-induced rotamerization. In addition to its fundamental value, isomer-selective photochemistry is a potential way to optically control chemical reactions. This is possible if the reaction occurs before the excitation energy is transferred to the coordinate that leads to rotamerization. For instance, geometrical considerations were suggested to explain the high CO/CO_2 yield ratio for the photodissociation of *trans*-formic acid in the gas phase [29], indicating that the dissociation is faster than conformational randomization. Experimental evidence of isomer-dependent photodissociation channels has also been recently reported for 1-$C_3H_7I^+$ in the gas

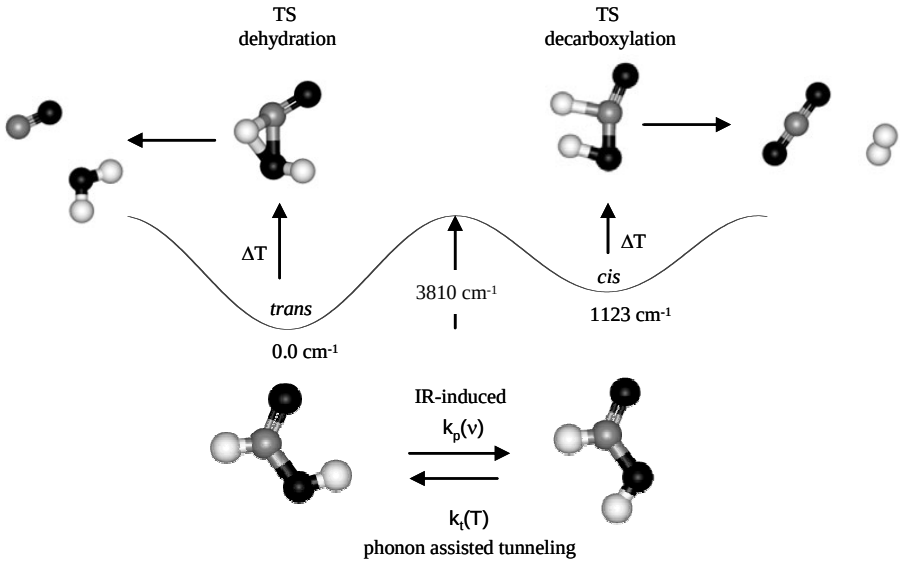

Fig. 2. Formic acid conformers. Energy difference and energy barrier estimated for the molecule isolated in solid Ar are shown as estimated at the CCSD(T)/aug-cc-pVTZ//MP2/aug-cc-pVTZ level for the molecule in vacuum and corrected by the PCM solvation model [19]. The transition state geometry for thermal (ΔT) dehydration and decarboxylation reaction are shown in connection with the *trans* and *cis* conformer, respectively. The predicted energy barrier for these reactions starting form the corresponding conformers is 280 kJ mol [38].

phase, where the products resulting from dissociation of the *gauche* and *anti* isomers correspond to different $C_3H_7^+$ isomeric forms [30,31].

The aim of this paper is to describe our studies on conformational isomerization reactions induced on carboxylic acids by selective vibrational excitation. Formic acid was used as model system for investigation of the conformational dynamics of the carboxylic group. First, we will discuss the use of vibrational spectroscopy coupled to narrowband tunable excitation for conformational identification. This photoreactive spectroscopic method is useful to study the vibrational properties of matrix-isolated formic acid conformers, in particular, the local environmental effects on mode coupling [32]. Next, the *trans* → *cis* isomerization induced by mode selective excitation in formic acid is addressed [20]. Our discussion is focused here on the high quantum yields observed for excitation energies below the torsional energy barrier. This is followed by the analysis of the influence of the medium on the tunneling mechanism that leads to the dark *cis* → *trans* formic acid conversion [19]. Additionally, isomer-selective UV-photo-dissociation of formic acid is described [33]. Finally, the conclusions drawn from photoinduced rotamerization studies on dicarboxylic acids [34-36] are presented.

2. Site-selective vibrational spectroscopy

Formic acid monomer exhibits two stable planar structures, the *cis* and the *trans* conformers shown in Fig. 2. *Trans*-formic acid has the hydrogen atoms on opposite sides of the C-O bond (H-C-O-H dihedral

angle of 180º), while in the *cis* conformer the hydrogen atoms are located on the same side of the C-O bond. The *trans* form is the most stable and hence predominant in the gas phase and in the as-deposited matrix samples. Excitation of the first overtone of the OH stretching mode (2νOH) of *trans*-formic acid isolated in Ar was earlier shown to promote *trans* → *cis* rotamerization [18]. On the other hand, the *cis* → *trans* conversion was shown to take place in the dark at low temperatures via a tunneling mechanism [18]. In the absence of optical pumping, this back-reaction limits the detectability of *cis*-formic acid after its preparation, even at the low working temperatures (4-60 K) used in rare-gas matrix studies.

Recently, other vibrational modes were excited to induce the *trans* → *cis* isomerization [20]. Formic acid molecules are isolated in different local environments of the rare-gas matrices, as shown by the site splitting of the IR absorption bands [32]. Pulsed IR radiation with a spectral linewidth of ≈ 0.1 cm^{-1}, provided by an optical parametric oscillator (Continuum), was used to promote the site-selective *trans* → *cis* rotamerization [19,32]. In order to maintain a sufficiently high concentration of the less stable *cis* conformer in the matrix, the IR absorption spectra were recorded under IR pumping of the *trans* form [32]. Without pumping, the concentration of the *cis* conformer produced by IR-irradiation decreases by a factor of three due to the *cis* → *trans* tunneling during the time needed to record a spectrum at 0.25 cm^{-1} resolution with a reasonable signal/noise ratio. Such a spectral resolution is needed to fully resolve the site-structure of the observed bands [32].

By comparing the IR absorption spectra recorded under pumping and the spectra of the as-deposited (non-irradiated) sample, we can identify bands belonging to each conformer isolated in a particular site, as illustrated in Fig. 3. As seen in this figure, the OH and C=O stretching vibrations of *cis* formic acid are shifted to higher wavenumbers from their *trans* values and the site splitting of the bands is resolved.

Table 1
Observed anharmonicities and coupling constants[a] for *trans*-formic acid.

trans-HCOOH

	Site 1	Site 2	Gas phase[b]
Combinations	Coupling constants (x_{ij}, cm^{-1})		
νOH + νC=O	-0.7	-0.5	-1.2
νOH + γCH	-3.9	-5.4	-3.6
νOH + COH-CO def.	-2.5	-2.3	-1.8
νOH + ωCH			-1.0
νOH + τCOH	(0)	(-0.7)	(-2.2)
νOH + δOCO	(-15.5)		(-4.7)
νCH + νC=O	-18.0	-14.3	-5.4
νCH + γCH	-23.5	-17.1	-22.1
νCH + COH-CO def.	-0.3	-1.0	-1.8
νCH + ωCH			-5.7
νC=O + COH-CO def.		-4.8	-2.6
νC=O + τCOH	(-6.4)	(-5.5)	
Overtones	Anharmonicity constants (x_{ii},cm^{-1})		
2νOH	-83.1	-83.1	-91.2
2νCH	-53.1		-52.4
2νC=O	-9.4	-9.4	-9.3
2COH-CO def.	-5.9	-5.7	-6.6

[a] $x_{ij} = \nu_{i+j} - \nu_i - \nu_j$; $x_{ii} = (2\nu_i - 2\times\nu_i/2$.
[b] Gas phase data was taken from [36]. Values in parentheses were calculated based on a tentative assignment. Values centred between site 1 and site 2 columns are average estimates for the two sites.

Detailed vibrational analysis of the near-IR region allowed for the identification of various overtone and combination bands [32]. Based on this assignment we have calculated site-selective anharmonicities and coupling constants for several modes of both conformers. The determined values for the *trans* conformer are presented in Table 1. By comparing the coupling constants obtained for this conformer in solid argon with the gas phase data [37], it was concluded that the cage potential affects the guest intermode couplings. The changes in the coupling constants are in many cases of similar magnitude as the constants themselves.

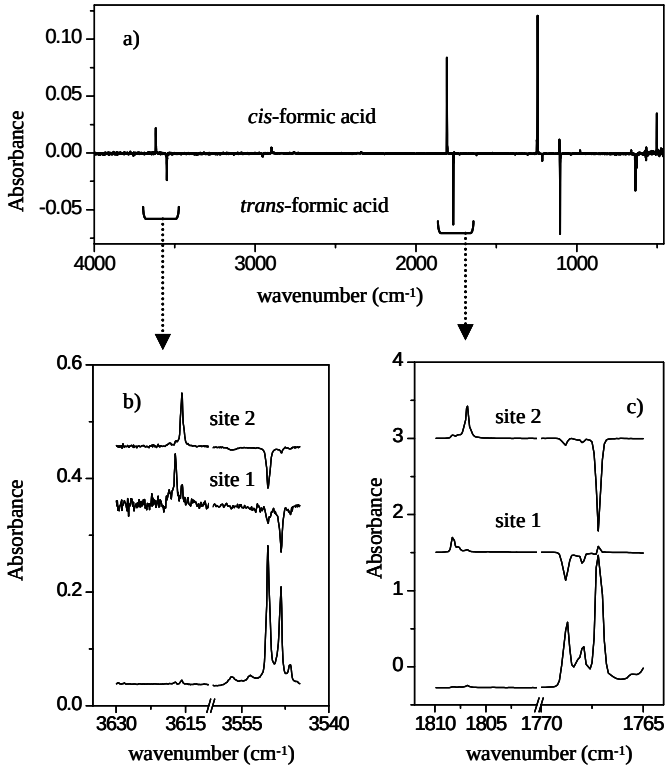

Fig. 3. IR absorption spectra of formic acid isolated in an Ar matrix. (a) Difference spectrum showing the result of pumping the overtone of the OH stretching of *trans*-formic acid, i.e. the increase of bands of the *cis* conformer and the decrease of the bands of the *trans* conformer. In (b) and (c) the site-selectivity of the IR-pumping is shown for the OH and C=O stretching regions. The lower spectrum show the bands of *trans*-formic acid present in the as-deposited sample. The difference spectra [the two upper traces of (b) and (c)] show the result of the excitation of different sites of formic acid, where the bands of the *cis* conformer isolated in the pumped site increase while the ones of the *trans* conformer decrease. (a)-(c) were obtained in experiments performed with different samples.

Moreover, the anharmonicity changes between molecules isolated in different sites (see, for example, the constants of νCH + νC=O or νCH + γCH modes in Table 1). Thus, one can expect the local environment to affect the vibrational energy relaxation pathways in condensed phase, which depend on mode couplings [38].

3. Rotamerization quantum yield as a function of the excitation energy

The quantum yields for the *trans* → *cis* reaction in formic acid were measured upon excitation of several vibrational modes of the *trans* conformer in the 2900-4700 cm^{-1} spectral range [20]. In the calculations, the *cis* → *trans* back reaction was taken into account (see Fig. 2). The quantum yield for the rotamerization process is determined from the *trans* → *cis* pumping efficiency, the absorption cross-section of the excited mode of the *trans* conformer and the intensity of the excitation radiation. The last two values are measured experimentally while the pumping

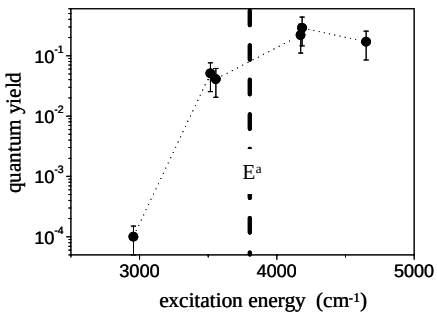

Fig. 4. Quantum yield for the *trans* → *cis* isomerization process of formic acid isolated in solid Ar as a function of the excitation energy. The points correspond to the following vibrational modes: 4651 cm^{-1}: νOH + COH-CO def.; 4184 cm^{-1}: νOH + τCOH; 4174 cm^{-1}: νCH + CO-COH def.; 3552 cm^{-1}: νOH; 3516 cm^{-1}: 2νC=O; 2955 cm^{-1}: νCH. The ab initio estimation for the energy barrier of the solvated molecule is indicated as a vertical dashed line at $E^a \approx 3810$ cm^{-1} [19]. The line connecting the points is for guiding the eyes.

efficiency is calculated on the basis of the tunneling rate coefficient and the photo-equilibrium concentration ratio of the two conformers under mode-selective pumping.

The quantum yield as a function of the excitation energy is shown in Fig. 4. Interestingly, all excited modes led to an efficient energy relaxation into the reaction coordinate (torsion around the C-O bond), resulting in rotational isomerization. The estimated energy barrier for the *trans* → *cis* rotamerization in formic acid isolated in solid Ar is 3810 cm^{-1} [20]. For excitation energies above this barrier, the average isomerization quantum yield is ≈ 20%, without remarkable changes associated with the nature of the excited modes.

In addition to the importance of the tunneling mechanism in the *cis* → *trans* process, its role on the *trans* → *cis* photo-induced rotamerization is evident from experiments with pumping below the energy barrier. Despite that excitation of the O-H stretching mode (νOH at 3549 cm^{-1}) or the first overtone of the C=O stretching mode (2νC=O at 3516 cm^{-1}) is energetically below the torsional barrier [20], the quantum yield decreases only by a factor of 4 when compared with the values for the higher energy modes. This high quantum yield was suggested to be due to the strong delo-calization of the torsional wavefunction between the two potential wells at these energies [20]. The extent of delocalization decreases rapidly with the distance from the top of the energy barrier. In agreement with this, the measured rotamerization quantum yield upon excitation of the C-H stretching mode (νCH at 2955 cm^{-1}) is about three orders of magnitude smaller than those at energies above the torsional barrier but still very reliably measure.

4. Environment and temperature effects on phonon-assisted tunneling

Even in a low-temperature matrix the *cis* conformer of formic acid decays spontaneously to the most stable *trans* conformer by phonon-assisted tunneling [18,19]. In this section, the effect of the matrix environment on the rate of the *cis* → *trans* tunneling is described [19]. The temperature-dependent tunneling rates for formic acid were measured in solid Ar, Kr and Xe. This was done by generating *cis*-formic acid via optical pumping and then following the decay kinetics by IR absorption spectroscopy [19]. The site selectivity of the process was also investigated. The Arrhenius plots for the *cis* → *trans* reaction rate of formic acid isolated in various rare-gas matrices are shown in Fig. 5.

The temperature effect on the *cis* → *trans* tunneling rate is essentially due to thermal excitation of the phonon modes that are coupled to the tunneling process. The lattice phonons compensate the energy mismatch between the torsional ground state of the *cis* conformer (that is the starting level for the tunneling) and the particular excited level of the *trans* conformer involved in the process. The specific temperature dependence of the rate constant originates from the type of phonon processes involved in the dissipative tunneling mechanism (e.g. emission, absorp-

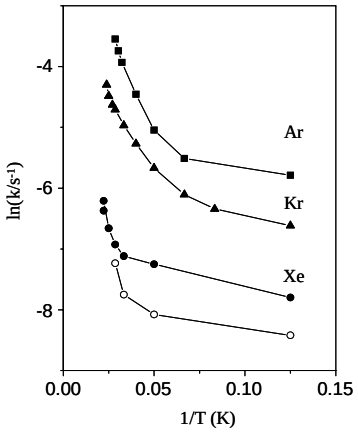

Fig. 5. Arrhenius plots for the *cis* → *trans* reaction rates of formic acid in rare-gas matrices ((■) Ar; (▲) Kr and (●), (○) Xe). Solid and open symbols are used for the two predominant sites of the formic acid isolated in Xe. Molecules isolated in the different sites observed in Ar and Kr matrices exhibit no difference in the temperature dependence of the tunneling rate.

tion or Raman processes [26,27]).

In order to understand the effect of the environment on the tunneling rate, it is important to know the position of the *cis* torsional ground state with respect to the energy level manifold of the *trans* conformer. This energy diagram determines the most probable states of the product participating in the tunneling. The energy gaps and the nature of the excited modes of the *trans* conformer involved in the process are factors affecting the *cis* → *trans* tunneling rate. The environment affects the potential energy surface of the guest molecules and, consequently, it can influence both factors. For example, the different solvation energy of the two formic acid conformers is expected to decrease their conformational energy difference in Xe when compared to Ar and Kr [19]. On the other hand, the *cis* → *trans* energy barrier was estimated to be higher in Xe than in Ar or Kr [19]. The different tunneling rates observed for the three studied hosts could be interpreted qualitatively on the basis of the estimated relative position of the *cis* torsional ground state with respect to the level manifold of the *trans* form [19].

Additionally, different local environments within the same host may have different solvation energies due to changes in the cavity size and geometry. Indeed, as shown in Fig. 5, the tunneling rate depends strongly on the host material and on the local morphology in solid Xe. Within our experimental error, the tunneling rates are site-independent when isolated in Ar and Kr matrices (see Fig. 5).

5. Isomer-selective photodissociation

The thermal unimolecular dissociation of formic acid can take place through decarboxylation and dehydration reactions [39] to produce, respectively, molecular hydrogen and carbon monoxide and carbon monoxide and water. As shown in Fig. 2, the transition states for these two reaction channels are geometrically connected either with *cis*-formic acid (decarboxylation) or *trans*-formic acid (dehydration) [39].

The theoretically predicted energy barriers for the dehydration and decarboxylation reactions on the S_o potential energy surface of formic acid are similar (~ 23,500 cm^{-1} [29]) whereas the energy barrier for the isomerization reaction is much smaller (<4000 cm^{-1}) [20]. In spite of that, a high CO/CO_2 photolysis branching ratio was observed after the 193 nm irradiation of *trans*-formic acid isolated in Ar and Kr (CO/CO_2 ~ 5 and 4 in Ar and Kr, respectively) [40]. An even higher branching ratio was observed for the gas-phase photodissociation after 193 and 248 nm irradiation [29]. The expected branching ratio based on the similarity of the energy barriers would be ~1, which differs from the experimental data. This difference can be explained assuming that photodissociation takes place on the S_o surface (after S_1 → S_o internal conversion [29]) via a transition state geometrically connected with the *trans* conformer; and the transition state is

formed before the vibrationally excited molecule statistically redistributes its vibrational energy [29]. Recently, we have shown that the photolysis of formic acid can be considered a clear case of isomer-selective reactions [33]. *Cis*-Formic acid was prepared in an Ar matrix by excitation of the 2νOH mode of *trans*-formic acid and the branching ratio was determined via simultaneous IR pumping (≈ 6930 cm^{-1}) and UV photolysis (193 nm) (see Fig. 6). In this situation, both conformers are present in the matrix during the UV irradiation and the production of CO_2 increases by a factor of 4 when compared to the 193 nm photolysis of *trans*-formic acid alone. A simple spectral subtraction procedure allowed to extract the CO/CO_2 ratio for the photolysis of *cis*-formic acid [33] (see Fig. 6). The proportion of the CO_2 product is as high as 72% for the UV photolysis of the *cis* conformer, which corresponds to a branching ratio of ≈ 0.4. This represents a change by more than one order of magnitude between the photolysis branching ratios of the two conformers.

The difference in the photodissociation process of the formic acid conformers is further supported by the band shapes of the CO_2 products. While the isolated CO_2 resulting from the photolysis of *trans*-formic acid exhibits two sharp bands, a broad CO_2 band is obtained from the *cis* form. The product of *trans*-formic acid photolysis seems to be essentially monomeric CO_2 isolated in a double-substitutional site [33]. On the other hand, the broadening of the CO_2 band obtained from the *cis* conformer might result from CO_2 complexed with H_2 [33]. This difference can be understood by assuming that the H_2 molecules produced from the *cis* photolysis do not have enough kinetic energy to leave the matrix cage. On the other hand, kinetically hot H_2 molecules are suggested to be produced in the photolysis of the *trans* conformer leading to the cage exit of H_2, thus preventing its complexation with CO_2.

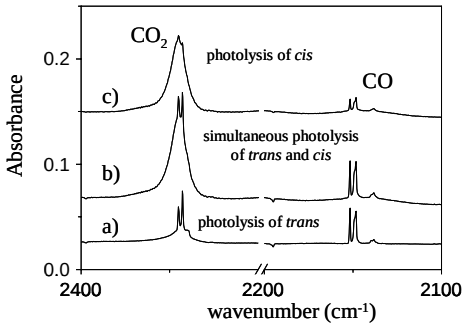

Fig. 6. Photolysis products (CO_2 and CO) of formic acid isolated in Ar at 8 K: (a) resulting from the 193 nm irradiation of *trans-formic* acid; (b) resulting from the simultaneous 193 nm and 6930 cm^{-1} irradiation of formic acid isolated in Ar (the *trans* → *cis* isomerization is induced under IR irradiation) and (c) resulting from the 193 nm irradiation of the *cis* conformer, obtained by subtraction of (a) from (b).

6. Photoinduced rotamerization in dicarboxylic acids

Excitation of the 2νOH vibration or a combination mode at similar energies was used to study rotamerization processes in dicarboxylic acids [34-36]. The four dicarboxylic acids studied are: ethanedioic, propanedioic, and (E)- and (Z)-2-butenedioic acid (see Fig. 7). In dicarboxylic acids, an intramolecular hydrogen bond involving the hydroxyl moiety of one of the carboxylic groups and the carbonyl oxygen of the other group can be formed. This intramolecular hydrogen bond leads to stabilization of the 180º O=C-O-H dihedral angle. In general, the loss of electron density in the O-H bond due to the intramolecular hydrogen bonding leads to a decrease in the corresponding force constant, and consequently to a redshift of the associated O-H stretching mode.

Ethanedioic acid (also known as oxalic acid) is the smallest of the studied dicarboxylic acids. According to quantum chemical calculations [41-43] oxalic acid

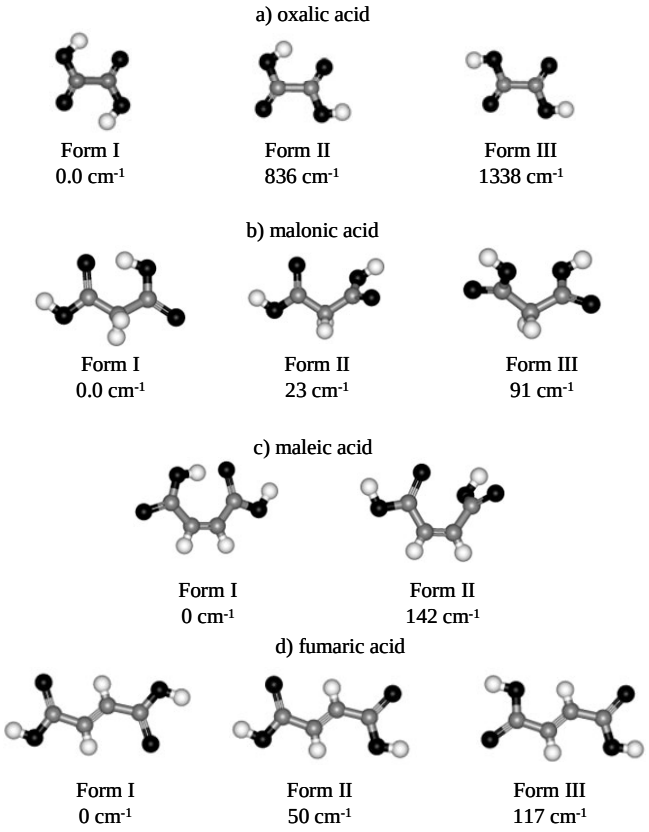

Fig. 7. Dicarboxylic acid conformers detected in the argon matrices and the corresponding estimated energy differences (in cm^{-1}). For all but malonic acid the energy differences presented were calculated on the basis of the observed relative population in the as-deposited matrices [33,35]. For malonic acid the computationally predicted value is given [34].

can have at least five conformers. The two lowest energy forms were earlier identified and isomerization between them was successfully promoted by both broadband-IR and UV irradiation [41], although these processes were not very efficient. In our studies, the three lowest energy conformers of oxalic acid were detected in the as-deposited Ar matrix with estimated energy differences (ΔE_{I}:ΔE_{II}:ΔE_{III}) of (0:836:1338 cm^{-1}) [34], see Fig. 7. The photoinduced rotamerization experiments allowed a detailed characterization of the mid-IR spectra of the previously observed forms I and II [34], as well as that of form III, which was detected for the first time in our work [34].

The relative energies of the three observed oxalic acid conformers can be understood on the basis of intramolecular hydrogen bonding and electrostatic repulsion between the negative charge densities localized at the oxygen atoms. Conformers I and II, bearing the relatively strong C=O... H-O hydrogen bonds are more stable than conformer III. On the other hand, both the stronger type of intramolecular hydrogen bonds [C=O ... H-O stronger than C-O(H)... H-O] and the less

important electrostatic effects between the lone electron pairs of the oxygen atoms (=O... OH weaker repulsive interaction comparing to HO ... OH and =O ... O=) lead to a lower energy for the *trans* arrangement around the C-C bond. This is the arrangement found in all of the three lowest energy conformers of oxalic acid.

Irradiation at 6712 cm^{-1} converts the most stable conformer into forms II and III. A further irradiation at 6755 cm^{-1} induces the II → I and II → III processes [34]. Identification of the conformers based on their IR absorption spectra was straightforward due to the high efficiency of the photo-induced processes [34]. This is illustrated in Fig. 8, where the OH and C=O stretching bands in the relevant difference spectra are presented. The lower trace shows the spectrum of the as-deposited oxalic acid in an Ar matrix, where only the bands of the conformational ground state (form I) are clearly visible. The middle difference spectrum shows the result of excitation of form I at 6712 cm^{-1}. The top trace of Fig. 8 presents the net result of irradiation of form I for about 1 h followed by pumping periodically forms I and II (at 6755 cm^{-1}) during *ca.* 30 min. In this case, the difference spectrum shows the growth of the absorption bands of conformer III while those belonging to conformers I and II decrease.

No evidence was found of photoinduced rotamerization involving rotation around the C-C bond, despite its theoretically predicted lower barrier for conformer II than that estimated for the observed II → III rotamerization [34]. This result can be understood if the energy barrier to internal rotation around the C-C bond for the free molecule differs strongly from that for the molecule isolated in the matrices. Indeed, rotation around the C-C bond involves extensive motion of heavy atoms and this should require reorganization of the matrix atoms around the guest molecule. This can lead to a considerable increase of the energy required for the isomerization. Another possibility is an inefficient relaxation mechanism to transfer the energy deposited into the 2νOH mode to the C-C torsion. However, the latter hypothesis is not supported either by the results obtained for formic acid, already described in this paper, or the results obtained for two of the studied carboxylic acids (where C-C rotation was observed after 2νOH excitation).

The propanedioic acid (malonic acid) molecule was detected in three different forms, shown in Fig. 7, in an as-deposited Ar matrix [35]. Near-IR irradiation of the matrix produced a significant rearrangement of the conformational distribution, which enabled the assignment of the bands to the three lowest energy conformers predicted theoretically. In analogy with oxalic acid, the most stable conformer of malonic acid is stabilized by intramolecular hydrogen bonding. The redshift induced by the intramolecular hydrogen bond of malonic acid is about four times larger (295 cm^{-1}) than that of oxalic acid (70 cm^{-1}).

The observed interconversion processes involved rotation around the C-O bond as well as around the C-C bond. This means that the restrictions imposed by the matrix to the rotation around the C-C bond are less severe in malonic acid than in oxalic acid. This difference could be associated with the fact that malonic acid is a bigger molecule with all relevant conformers being non-planar. Hence a less compact arrangement of the lattice atoms around the malonic acid molecules can be expected to allow the heavy atoms to move, contrary to the case of the small planar oxalic acid.

The IR absorption spectrum of (Z)-2-butenedioic acid (fumaric acid) isolated in Ar was also interpreted in terms of the three lowest energy conformers predicted theoretically [36] and shown in Fig. 7. As expected on the basis of the previous studies on α,β-unsaturated molecules [44], the relative conformational energy in fumaric acid increases with the number of *trans* arrangements around the C_α-C bonds. On the other hand, in the case of maleic acid [(E)-2-butenedioic acid] the *cis* arrangement around both C_α-C bonds is not favored due to the strong repulsive

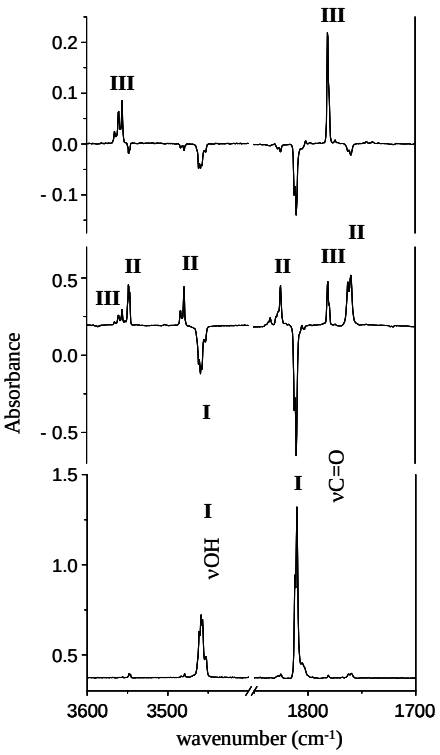

Fig. 8. IR absorption spectra (3600-3400 cm^{-1} and 1850-1700 cm^{-1}) showing the result of near-IR irradiation of oxalic acid isolated in solid argon at 7.5 K. The lower plot shows the spectrum of the as-deposited sample where the main bands correspond to the OH and C=O stretching absorptions of the conformational ground state (form I). The middle plot is a difference spectrum where the bands belonging to form I point downwards and the bands of forms II and III are pointing upwards. The upper plot is a difference spectrum showing the bands of forms I and II pointing downwards and the bands of form III pointing upwards. See text for the pumping details.

interaction between the lone pairs of the carbonylic oxygen atoms (see Fig. 7). Hence, for this molecule the most stable conformer has one *cis* and one *trans* conformation along the C_α-C axis and it is stabilized by a very strong OH ... O= intramolecular hydrogen bond (the observed redshift of the ν*OH* vibration frequency associated with the intramolecularly bonded hydroxyl group is as large as 440 cm^{-1} [36]). The second lowest energy conformer of maleic acid possesses a non-planar geometry with two nearly perpen-dicular carboxylic groups, which minimizes the electrostatic and steric repulsions between these groups.

Interconversion between the two lowest energy conformers of maleic acid was induced by IR excitation and also by annealing the matrix at 35 K [36]. As expected, annealing of the matrix resulted in conversion from the less stable form II to the conformational ground state (form I) [36]. Tuning the IR radiation over the 6940-6835 cm^{-1} region allowed us to find only one mode, at 6901 cm^{-1}, which was active to promote rotamerization. This mode corresponds to the 2ν*OH* vibration of form II and it promotes the II → I rotamerization. This isomerization process in maleic acid involves rotation around both the C-O and C_α-C bonds. It should be stressed that we were able to induce rotamerization starting from the non-planar conformer (form II) but we did not succeed to induce any isomerization processes from the planar conformer (form I). If the anharmonicity of the 2ν*OH* mode in form I is similar to that of the same vibration in conformer II, then form I absorbs within the probed spectral region. Hence, this observation further supports the results previously discussed for both oxalic and malonic acids that, for the planar conformers, the energy barrier to rotation around the C-C bond seems to increase considerably in matrices as compared with the gas phase. This observation is also consistent with the idea that the reaction barrier for conformational isomerization processes may be considera-bly different depending on the nature of the cage occupied by the trapped molecule. A more compact trapping site for the planar conformers would imply a higher energy barrier for the rotamerization while the non-planar conformers isolated in bigger cages would have a lower rotamerization barrier.

In the case of fumaric acid, no rota-merization was found while IR irradiation

was scanned through the 7018-6873 cm^{-1} spectral region. From the IR-pumping experiments performed on the other di-carboxylic acids studied, we were expecting to find at least two active 2νOH modes in this region belonging to form II (in forms I and III this mode is infrared inactive due to symmetry restrictions). The annealing experiments were equally inefficient in inducing rotational isomerization processes in fumaric acid. Since conformational interconversion between the three observed conformers of fumaric acid should occur through internal rotation around the C_α-C bonds, as for the previous molecules, this negative observation is also consistent with an increased barrier to rotation around the C_α-C bond for the planar conformers in matrices. On the other hand, internal rotation around the C-O bonds of fumaric acid would lead to high energy conformers, with energies higher than the ground conformational state by 2100 cm^{-1}. This situation contrasts with that for the other molecules studied where conformers differing by internal rotation around the C-O bonds are relatively close in energy. Though these high energy species could eventually be formed, they could convert back by tunneling to the more stable forms fast enough to prevent their detection under our experimental conditions [19,36].

7. Concluding remarks

In this work, an overview of our recent studies dealing with infrared-induced conformational interconversion of carboxylic acids isolated in rare-gas matrices was presented. Photoreactive spectroscopy (narrowband IR pumping coupled with vibrational spectroscopy) is a powerful method to investigate conformational properties of matrix-isolated molecules. This method allowed us to probe the local morphology effects on several intermode couplings and anharmonicity constants by investigating the site-resolved vibrational spectroscopy of formic acid isolated in solid Ar.

The *trans* → *cis* isomerization reaction induced by mode-selective irradiation of *trans*-formic acid was studied. The excitation energy was quite efficiently relaxed into the reaction coordinate (C-O torsion) from all vibrationally excited levels used here. Tunneling was found to play an important role in the *trans* → *cis* photoinduced reaction mechanism. On the other hand, phonon-assisted tunneling mechanism was demonstrated on the reverse *cis* → *trans* process as well. In this case, a strong dependence of the reaction rate on both temperature and solid host was found. The local morphology within the same host was also shown to influence the tunneling rate. From these studies it is possible to conclude that the tunneling mechanism can contribute in similar isomerization reactions for various molecules bearing a hydroxyl group. Photodissociation of formic acid was shown to be an isomer-selective reaction, where the time scale for rotamerization is longer than for dissociation. Narrowband IR irradiation was shown to be an effective switch between the two main reaction channels of formic acid UV-photolysis (decarboxylation and dehydration) by changing the *cis/trans* ratio in the irradiated matrix.

Using near-IR irradiation we were able to promote conformational interconversion in a series of dicarboxylic acids. Excitation of the first O-H stretching overtone leads to internal rotation around the C-O bond in oxalic, malonic and maleic acid but does not isomerize fumaric acid. Rotamerization around the C-C bond was observed only when the precursors for IR-pumping were non-planar, possibly due to the effect of a more restrictive packing of the lattice atoms around the planar conformers that hinders the internal rotation when it involves an extensive motion of heavy atoms.

Acknowledgements

The Academy of Finland and the Portuguese Foundation for Science and Technology are thanked for financial support.

References

[1] A.J. Barnes, J. Mol. Struct. 113 (1984) 161.
[2] M. Räsänen, H. Kunttu, J. Murto, Laser Chem. 9 (1988) 123.
[3] T. Lotta, J. Murto, M. Räsänen, A. Aspiala, J. Mol. Struct. 114 (1984) 333.
[4] H.H. Günthard, J. Mol. Struct. 113 (1984) 141.
[5] R.N. Perutz, Chem. Rev. 85 (1985) 97.
[6] H. Frei, G.C. Pimentel, Chemistry and Physics of Matrix-Isolated Species, in: L. Andrews, M. Moskovits (Eds.), Elsevier B.V., Amsterdam, 1989, p. 139.
[7] M. Poliakoff, J.J. Turner, Chemical and Biochemical Applications of Lasers, in: C.B. Moore (Ed.), vol. 5, 1980, p. 175.
[8] H. Frei, G.C. Pimentel, Annu. Rev. Phys. Chem. 36 (1985) 491.
[9] S. Kudoh, M. Takayanagi, M. Nakata, T. Ishibashi, M. Tasumi, J. Mol. Struct. 479 (1999) 41.
[10] A.K. Knudsen, G.C. Pimentel, J. Phys. Chem. 95 (1991) 2823.
[11] J. Pourcin, G. Davidovics, H. Bodot, L. Abouaf-Marguin, B. Gauthier-Roy, Chem. Phys. Lett. 74 (1980) 147.
[12] W.F. Hoffman III, J.S. Shirk, Chem. Phys. 78 (1983) 331.
[13] P. Roubin, S. Varin, P. Verlaque, S. Coussan, J.-M. Berset, J.-M. Ortega, A. Peremans, W.-Q. Zheng, J. Chem. Phys. 107 (1997) 7800.
[14] S. Coussan, Y. Bouteiller, J.P. Perchard, W.Q. Zheng, J. Phys. Chem. A 102 (1998) 5789.
[15] S. Sander, H. Willner, L. Khriachtchev, M. Pettersson, M. Räsänen, E.L. Varetti, J. Mol. Spectrosc. 203 (2000) 145.
[16] L. Khriachtchev, J. Lundell, E. Isoniemi, M. Räsänen, J. Chem. Phys. 113 (2000) 4265.
[17] K.B. Wiberg, K.E. Laidig, J. Am. Chem. Soc. 109 (1987) 5935.
[18] M. Pettersson, J. Lundell, L. Khriachtchev, M. Räsänen, J. Am. Chem. Soc. 119 (1997) 11715.
[19] M. Pettersson, E.M.S. Maçôas, L. Khriachtchev, J. Lundell, R. Fausto, M. Räsänen, J. Chem. Phys. 117 (2002) 9095.
[20] M. Pettersson, E.M.S. Maçôas, L. Khriachtchev, R. Fausto, M. Räsänen, J. Am. Chem. Soc. 125 (2003) 4058.
[21] N. Akai, S. Kudoh, M. Takayanagi, M. Nakata, Chem. Phys. Lett. 356 (2002) 133.
[22] N. Akai, S. Kudoh, M. Takayanagi, M. Nakata, J. Phys. Chem. 106 (2002) 11029.
[23] V.A. Benderskii, D.E. Makarov, C.A. Wight, in: Chemical Dynamics at Low Temperature, Wiley, New York, 1994.
[24] G.K. Ivanov, M.A. Kozhushner, L.I. Trakhtenberg, J. Chem. Phys. 113 (2000) 1992.
[25] M.V. Basilevsky, G.V. Davidovitch, J. Chem. Phys. 115 (2001) 6072.
[26] R. Silbey, H.-P. Trommsdorff, Chem. Phys. Lett. 165 (1990) 540.
[27] A. Suarez, R.J. Silbey, Chem. Phys. 94 (1991) 4809.
[28] T. Kumada, K. Komaguchi, Y. Aratono, T. Miyazaki, Chem. Phys. Lett. 261 (1996) 463.
[29] H. Su, Y. He, F. Kong, W. Fang, R. Liu, J. Chem. Phys. 113 (2000) 1891.
[30] S.T. Park, S.K. Kim, M.S. Kim, Nature 415 (2002) 306.
[31] S.T. Park, M.S. Kim, J. Chem. Phys. 117 (2002) 124.
[32] E.M.S. Maçôas, J. Lundell, M. Pettersson, L. Khriachtchev, R. Fausto, M. Räsänen, J. Mol. Spectrosc. 219 (2003) 70.
[33] L. Khriachtchev, E. Macoas, M. Pettersson, M. Räsänen, J. Am. Chem. Soc. 124 (2002) 10994.
[34] E.M.S. Maçôas, R. Fausto, M. Pettersson, L. Khriachtchev, M. Räsänen, J. Phys. Chem. A 104 (2000) 6956.
[35] E.M.S. Maçôas, R. Fausto, J. Lundell, M. Pettersson, L. Khriachtchev, M. Räsänen, J. Phys. Chem. A 104 (2000) 11725.
[36] E.M.S. Maçôas, R. Fausto, J. Lundell, M. Pettersson, L. Khriachtchev, M. Räsänen, J. Phys. Chem. A 105 (2001) 3922.
[37] M. Freytes, D. Hurtmans, S. Kassi, J. Lievin, J. Vander Auwera, A. Campargue, M. Herman, Chem. Phys. 283 (2002) 47.
[38] V.E. Bondybey, Adv. Chem. Phys. 47 (1981) 521.
[39] J. Goddard, Y Yamaguchi, H.F. Schaefer III, J. Chem. Phys. 96 (1992) 1158.
[40] J. Lundell, M. Rasanen, J. Mol. Struct. 436-437 (1997) 349.
[41] J. Nieminen, M. Rasanen, J. Murto, J. Phys. Chem. 96 (1992) 5303.
[42] J. Higgins, X. Zhou, R. Liu, T.T.-S. Huang, J. Phys. Chem. A 101 (1997) 2702.
[43] P.D. Godfrey, M.J. Mirabella, R.D. Brown, J. Phys. Chem. A 104 (2000) 258.
[44] A. Kulbida, M.N. Ramos, M. Räsänen, J. Nieminen, O. Schrems, R. Fausto, J. Chem. Soc. Faraday Trans. 91 (1995) 1571.

Appendix V

Rotational isomerism in acetic acid: The first experimental observation of the high-energy conformer.

Ermelinda M. S. Maçôas, Leonid Khriachtchev, Mika Pettersson, Rui Fausto and Markku Räsänen

J. Am. Chem. Soc. **2003**, *125*, 16188-16189.

Rotational Isomerism in Acetic Acid: The First Experimental Observation of the High-Energy Conformer

Ermelinda M. S. Maçôas,[*,†,‡] Leonid Khriachtchev,[†] Mika Pettersson,[†,§] Rui Fausto,[‡] and Markku Räsänen[†]

Laboratory of Physical Chemistry, P. O. Box 55, FIN-00014 University of Helsinki, Finland and Department of Chemistry-CQC, University of Coimbra, P-3004-535, Coimbra, Portugal

Received date September 4, 2003; E-mail: emacoas@qui.uc.pt

Conformational studies of simple carboxylic acids and amines aid to understand the reactivity of biologically relevant molecular systems, where the conformational properties of these functional groups play an important role.[1-3] Recently, conformation-selective photochemistry has been recognized as a new approach to laser control of chemical reactions.[4] Different conformers can exhibit quite different photochemistry as it was shown, for example, in the case of UV photolysis of *cis*- and *trans*- formic acid (HCOOH).[5]

Acetic acid (CH_3COOH, AA) is a molecule of considerable interest from the point of view of conformation-selective photochemistry. This molecule can theoretically adopt two stable structures (see Figure 1). Both conformers belong to the C_s symmetry group and have the in-plane hydrogen of the methyl group eclipsed with the carbonyl bond. The lowest energy conformer is characterized by the *trans* arrangement around the C-O bond with respect to the relative orientation of the O-H and C-C bonds. The other conformer, which is predicted to be 1882.7 cm^{-1} higher in energy,[6] exhibits the *cis* arrangement of these two bonds around the C-O bond. Despite the reliable theoretical predictions, no experimental evidence of the existence of the *cis* conformer has been found so far.[6,7-11] In this work, we report the first experimental observation of *cis*-AA. We show that *cis*-AA can be produced in an Ar matrix by vibrational excitation of the conformational ground-state and that it decays back to *trans* in dark even at 8 K, via tunneling. The tunneling mechanism for the *cis* → *trans* dark reaction is supported by studies on the CH_3COOD isotopologue showing very strong effect of deuteration on the reaction rate.

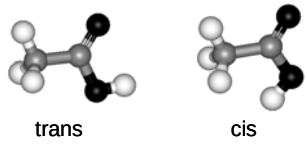

Figure 1. *Cis* and *trans* conformers of acetic acid (CH_3COOH).

In the experiments, acetic acid (Sigma-Aldrich, >99 %) was mixed with argon (AGA 99.9999%) in a bulb with the ratio AA/Ar=1/1000. The samples were deposited on a CsI window held at 15 K in a cryostat (APD DE 202 A). After deposition, the samples were cooled to 8 K. The IR pumping was carried out with pulsed (~5 ns) narrowband IR radiation of an optical parametric oscillator (Sunlite with an IR extension, Continuum, FWHM ~0.1 cm^{-1}, repetition rate= 10 Hz, and pulse energy density ~0.5 mJ/cm^2) as described elsewhere.[12-14] The IR absorption spectra were measured with a FTIR spectrometer (Nicolet 60 SX) with a resolution of 1 or 0.25 cm^{-1}. The experimental setup was arranged in such a way that IR absorption spectra could be recorded during irradiation. The Gaussian 98 program package was used

* Corresponding author. E-mail: emacoas@qui.uc.pt
†University of Helsinki.
‡University of Coimbra.
§ Present address: Department of Chemistry, University of Jyväskylä, P. O. Box 35, FIN-40014 University of Jyväskylä, Finland.

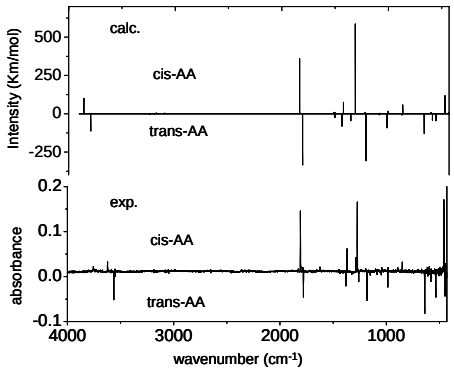

Figure 2. Theoretical and experimental vibrational spectra of *cis* and *trans* acetic acid. The lower trace is the experimental difference spectrum showing the result of vibrational excitation of the *trans* conformer in the Ar matrix at 8 K. In the upper trace the difference spectrum is simulated based on MP2/6-311G++(2d,2p) calculations. The bands of the *cis* conformer point upwards while the bands due to the *trans* conformer point downwards.

for the ab initio calculations.[15]

After deposition, the AA monomer is present in the matrix only in the *trans* geometry, and our IR absorption spectrum agrees well with the literature data.[10] To excite the *trans*-AA monomer at energies above the internal rotation barrier, we usedthe OH stretching overtone (2νOH at 6957.9 cm^{-1}). Resonant excitation of this mode induces considerable changes in the IR absorption spectrum (see Figure 2). According to our assignment (see Table 1), the bands pointing upwards in the presented difference spectrum correspond to previously unreported *cis*-AA, while the bands pointing downwards correspond to the known *trans* conformer. The observed blue shifts of the hydroxyl (59 cm^{-1}) and carbonyl (28 cm^{-1}) stretching modes (νOH and νC=O, respectively) in the product with respect to the *trans* conformer are very characteristic for various carboxylic acids.[14] The νC=O and the COH angular deformations (δCOH) are the most intense bands of *cis*-AA. These bands are observed at 1807 cm^{-1} (νC=O) and 1272 cm^{-1} (δCOH), in good agreement with the ab initio estimations (1833 and 1310 cm^{-1}, respectively). In general, the experimental difference spectrum showing bands of both conformers of AA agrees very well with the spectrum simulated by ab initio calculations with respect to band positions and relative intensities (see Figure 2), thus giving strong support to the identification of the product of IR irradiation. The detailed discussion of the spectra of *cis*-AA exceeds the scope of this Communication.

In the equilibrium established under resonant IR irradiation, about 10% of the initial concentration of the *trans* conformer in the matrix is converted into the *cis* form. Once the IR irradiation is stopped, *cis*-AA decays back to the *trans* form in a minute timescale. As measured in the dark in solid Ar at 8 K, the *cis*-AA concentration follows

Table 1. Observed frequencies of *cis*-AA and *trans*-AA isolated in an Ar matrix at 8K compared with the predicted values at the MP2/6-311++G(2d,2p) level.

	trans-AA		*cis*-AA	
assignment[a]	obs.	calc.	obs.	calc.
νOH	3563.8	3793.6	3622.6	3859.5
νHCH_2 s.	3051[b]	3236.9	-	3229.7
νHCH_2 a.	2996[b]	3196.0	-	3178.0
νCH_3	2944[b]	3115.3	-	3099.4
νC=O	1779.0	1805.2	1807.4	1832.6
δHCH_2 a.	1438.8	1506.3	1448.3	1514.3
δHCH_2 s.	1433.6	1501.0	1444.5	1501.2
δCH_3	1379.4	1434.5	1368.3	1421.5
νC-O	1259.4	1352.7	1192.9	1218.4
(?)			1285.4	
δCOH	1179.8	1210.4	1271.9	1309.5
γCH_3 a.	1047.2	1084.6	1042.4	1078.7
γCH_3 s.	985.5	1011.7	982.2	1002.9
νC-C	-	871.8	848.6	864.9
τC-O	637.8	663.4	458.0	468.2
δOCO	580.4	586.3	-	600.7
γC=O	534.2	553.1	-	605.2
δCC=O	428[b]	427.0	-	436.0
τCH_3	-	80.2	-	95.2

[a] The ab initio cartesian force constants and optimized geometries were used for the normal coordinate analysis. [b]Values taken from ref. 10. Symbols: ν- stretching; δ- bending; γ- rocking; τ- torsion.

a one exponential decay with rate constant $k_t(CH_3COOH)= 2.1x10^{-2}$ s^{-1}. According to the ab initio calculations, the barrier for the *cis*→ *trans* isomerization is ~2550 cm^{-1}, [6] which gives a negligible rate for the overbarrier reaction at 8 K (~10^{-186} s^{-1}, estimated using the Arrhenius formula with the torsional frequency of *cis*-AA for the preexponential factor). The overbarrier reaction may become significant only above 100 K. This shows that the *cis*→ *trans* isomerization occurs through the barrier.

The reaction coordinate for the rotational isomerization in AA is most probably described by the O=C-O-H dihedral angle, which is the internal coordinate for the O-H torsional motion. Similarly to formic acid,[16] the tunneling reaction in acetic acid presumably takes place mainly from the torsional ground state of the *cis* conformer, because the population of the excited torsional levels is very low at the matrix temperature. The observed *cis*→ *trans* reaction for AA isolated in an Ar matrix at 8 K is 1 order of magnitude faster than the corresponding process for formic acid under the same experimental conditions,[16] which definitely complicates its experimental observation. The relative values of the tunneling rates of formic and acetic acid can be simply explained by differences in the torsional potential of these molecules. The one-dimensional potential energy surfaces calculated for the rotational isomeri-zation of these molecules at the same MP2/6-311++G(2d,2p) level of theory, show that the *cis* to *trans* barrier height is 370 cm^{-1} lower for AA. The permeability of the reaction barrier from the torsional ground state of *cis*-AA, calculated using the ab initio potential and the WKB approximation,[17] is higher by a factor of ~30 as compared with formic acid.[16] This agrees quite well with our results on the *cis*→ *trans* tunneling rates of acetic and formic acid in solid Ar. However, it is understood that the real situation is not so simple, and many other parameters (in addition to the barrier permeability) should be considered.[16]

IR-induced isomerization of CH_3COOD isolated in solid Ar was also studied. The 2νOD mode at 5170 cm^{-1} was used to excite this molecule over the isomerization barrier, resulting in the *trans*→ *cis* conversion. As a result of deuteration, it was found that the *cis*→ *trans* back reaction slows down by a factor of ~$3x10^4$ as compared with CH_3COOH [$k_t(CH_3COOD)$ ~$7.3x10^{-7}$ s^{-1}]. This value agrees reasonably well with the estimated 7 orders of magnitude lower barrier permeability upon deuteration. This is our final proof of the conversion of *cis*-AA to *trans*-AA via tunneling.

In conclusion, the *cis* conformer of acetic acid was produced in solid Ar by exciting the OH (OD) stretching overtone modes of two isotopic forms of the *trans* conformer (CH_3COOH, CH_3COOD). The experimental evidence for the preparation of the *cis* form is supported by the theoretical vibrational analysis. It is shown that the *cis* to *trans* tunneling reaction occurs in the solid environment even at the lowest temperatures used (8 K). For CH_3COOH, the tunneling rate is ~$2x10^{-2}$ s^{-1}, which means that in several minutes the *cis* conformer produced by IR irradiation is fully converted back to *trans* in dark. Deuteration of the hydroxyl group increases the lifetime of the unstable conformer dramatically (by ~$3x10^4$).

Acknowledgment. The Academy of Finland is thanked for financial support. E.M.S.M. and R.F. acknowledge the Portuguese Foundation for Science and Technology (Ph.D. grant SFRH/ BD/4863/2001 and project POCTI/43366/QUI/ 2001).

References

(1) Cantor, C. R.; Schimmel, P. R.; *Biophysical Chemistry*; W. H. Freeman, Co.: New York, 1980.
(2) Huff, J. B.; Askew, B.; Duff, R. J.; Rebek, J *J. Am. Chem. Soc.* **1988**, *110*, 5908-5909.
(3) Tadayoni, B. M.; Parris, K.; Rebek J *J. Am. Chem. Soc.* **1989**, *111*, 4503-4505.
(4) Goez, M. *Angew. Chem. Int. Ed.* **2003**, *42*, 2336-2337.
(5) Khriachtchev, L.; Maçôas, E. M. S.; Pettersson, M.; Räsänen, M. *J. Am. Chem. Soc.* **2002**, *124*, 10994-10995.
(6) Senent, M. L. *Mol. Phys.* **2001**, *99*, 1311-1321.
(7) Weltner, W *J. Am. Chem. Soc.* **1955**, *77*, 3941-3950.
(8) van Eijck, B. P.; van Opheusden, J.; van Schaik, M. M. M.; van Zoeren, E. *J. Mol. Spectrosc.* **1981**,

86, 465-479.
(9) Burneau, A.; Génin, F.; Quilès, F. *Phys. Chem. Chem. Phys.* **2000**, *2*, 5020-5029
(10) Berney, C. V.; Redington, R. L.; Lin, K. C. *J. Chem. Phys.* **1970**, *53*, 1713-1721.
(11) Sato, H.; Hirata, F. *J. Mol. Struct (Theochem)* **1999**, *113*, 461-462
(12) Pettersson, M.; Lundell, J.; Khriachtchev, L.; Räsänen, M. *J. Am. Chem. Soc.* **1997**, *119*, 11715-11716.
(13) Khriachtchev, L; Lundell, J.; Isoniemi, E; Räsänen, M. *J. Chem. Phys.* **2000**, *113*, 4265-4273.
(14) Maçôas, E. M. S.; Lundell, J.; Pettersson, M.; Khriachtchev, L.; Fausto, R.; Räsänen, M. *J. Mol. Spectrosc.* **2003**, *219*, 70-80.
(15) M. J. Frisch, G. W. Trucks, H. B. Schlegel et al. GAUSSIAN 98, Revision A. 9, Gaussian, Inc., Pittsburgh, PA, 1998.
(16) M. Pettersson, E. M. S. Maçôas, L. Khriachtchev, J. Lundell, R. Fausto, and M. Räsänen, *J. Chem. Phys.* **2002**, *117*, 9095-9098.
(17) Bell, R. P.; In *The tunnel Effect in Chemistry*; Chapman and Hall Ltd: London, 1980.

Appendix VI

Photochemistry and vibrational spectroscopy of the trans and cis conformers of acetic acid in solid Ar.

Ermelinda M. S. Maçôas, Leonid Khriachtchev, Rui Fausto and Markku Räsänen

J. Phys. Chem. A **2004**, *108*, 3380-3389.

Photochemistry and Vibrational Spectroscopy of the Trans and Cis Conformers of Acetic Acid in Solid Ar

E. M. S. Maçôas,*[,†,‡] L. Khriachtchev,[†] R. Fausto,[‡] and M. Räsänen[†]

Department of Chemistry, University of Helsinki, P.O. Box 55, FIN-00014 Helsinki, Finland, and Department of Chemistry (CQC), University of Coimbra, P-3004-535 Coimbra, Portugal

Received: December 12, 2003; In Final Form: February 9, 2004

Acetic acid monomer has two stable geometries, the *cis* and *trans* conformers. The high-energy *cis* conformer has been recently detected experimentally for the first time [Maçôas et al. *J. Am. Chem. Soc.* 2003, *125*, 16188]. The *cis* conformer can be produced in low-temperature rare-gas matrixes upon vibrational excitation of the ground-state *trans* conformer. Fast tunneling from *cis*- to *trans*-acetic acid takes place even at the lowest working temperatures (8 K), limiting the time available to study the high-energy form. Deuteration of the hydroxyl group reduces the tunneling rate by approximately 4 orders of magnitude, increasing accordingly the lifetime of the unstable conformer and its available concentration. In this work, we present a detailed analysis of the vibrational spectra of the *cis* form of four acetic acid isotopologues (CH_3COOH, CH_3COOD, CD_3COOH and CD_3COOD). Photolysis (193 nm) of the *trans* and *cis* forms of the perdeuterated compound was performed to evaluate the possible conformational dependence of photodissociation of acetic acid. However, no evidence of conformer specific photodissociation was found. The UV photolysis of the matrix-isolated acetic acid reveals very different products from the gas phase. Methanol complexed with carbon monoxide is the major product of photolysis of acetic acid isolated in Ar matrixes whereas it has never been observed as a photolysis product in the gas phase.

Introduction

Acetic acid has two planar conformers, *trans* and *cis*, with a computationally predicted energy difference of about 1883 cm^{-1} in favor of the *trans* conformer and an energy barrier for the *trans* to *cis* isomerization of 4432 cm^{-1}.[1] The spectroscopic properties and reactivity of the *trans* conformer have been studied in detail.[2-5] Nevertheless, despite the fact that acetic acid has been the subject of many experimental and theoretical studies,[1-10] including studies of conformational equilibrium in the gas phase and aqueous solution, only recently was the *cis* conformer detected experimentally.[11] The IR absorption spectra of *cis*-CH_3COOH was measured in an Ar matrix after excitation of the O-H stretching overtone of *trans*-CH_3COOH.[11] The preparation of *cis* acetic acid followed the method of selective IR pumping as was earlier applied.[12-14] The produced *cis* conformer tunnels back to the *trans* form in a minute time scale, which greatly limits the time available to study the high-energy conformer.[11] In that study, to overcome the limitation due to the lifetime of the unstable conformer, the IR absorption spectrum was collected during IR irradiation of *trans*-CH_3COOH. Deuteration of the hydroxyl group slows down the tunneling rate, allowing a more accurate study of this species.

Small molecules with more than one

* To whom correspondence should be addressed. E-mail: emacoas@qui.uc.pt

[†] University of Helsinki

[‡] University of Coimbra

conformer may exhibit conformer-selective photochemistry, as shown in the case of UV photolysis of formic acid (HCOOH) in solid argon.[15] Photochemical excitation, as opposed to thermal excitation, may deposit energy selectively into a molecule, thus inducing specific reaction channels.[16] Decomposition dynamics of acetic acid has been extensively investtigated both theoretically and experimentally (see ref 17 for an overview on this subject and references therein). Theoretically, the ground-state decomposition channels of acetic acid were shown to depend on the initial conformational state,[18] the decarboxylation channel being associated with the *cis* conformer and the dehydration channel with the *trans* conformer. Experimentally, thermal decomposition in the gaseous phase occurs mainly via the decarboxylation and dehydration channels in a 1:2 proportion, yielding carbon dioxide with methane and ketene (CH_2=C=O) with water, respectively.[19-20] The gas-phase photodecomposition of acetic acid was shown to produce mainly acetyl and hydroxyl radicals.[21-24]

The present work has a 2-fold task. First, we study in detail the vibrational spectra of the *cis* conformer of acetic acid isolated in solid Ar, including three deuterated isotopologues (CH_3COOD, CD_3COOH, and CD_3COOD), with special emphasis on the perdeuterated form. A revised vibrational assignment for the *trans* conformers is also proposed. Second, we study the photolysis of acetic acid isolated in Ar. Perdeuterated acetic acid was used to evaluate the conformational specificity of the 193 nm photo-decomposition process. The lack of conformer dependent photodecomposition channels is discussed, as well as the influence of solid matrix on the photo-decomposition products of acetic acid.[25-29] The 1:1 complex of methanol with carbon monoxide that is the major product of photolysis in the Ar matrix is identified on the basis of ab initio calculations.

Experimental and Computational Details

The gaseous samples were prepared by mixing acetic acid (Sigma-Aldrich, >99%) or its isotopologues (CD_3COOD and CH_3COOD, 99.5%), degassed by several freeze-pump-thaw cycles, with high-purity argon (AGA, 99.9999%), typically in the 1:2000 or 1:1000 proportions. The CD_3COOH species was obtained from the fully deuterated species by exchange of deuterium atom of the hydroxyl group with H_2O adsorbed on the inner surface of the sample container and the deposition line. The CD_3COOH isotopologue was also present in the CD_3COOD samples as an impurity. The gaseous mixtures were deposited onto a CsI substrate at 15 K in a closed cycle helium cryostat (APD, DE 202A) and subsequently cooled to 8 K. The IR absorption spectra (7900-400 cm^{-1}) were measured with a Nicolet SX-60 FTIR spectrometer. A liquid nitrogen cooled MCT detector and a Ge/KBr beam splitter were used to record the mid-IR absorption spectra, with spectral resolutions from 0.25 to 1.0 cm^{-1}, and a liquid-nitrogen-cooled InSb detector and a quartz beam splitter were used for the near-IR absorption spectra, with a spectral resolution of 0.5 cm^{-1}. Typically, 100-500 interferograms were co-added.

Tunable pulsed IR radiation provided by an optical parametric oscillator (OPO Sunlite, Continuum, with IR extension) was used to produce *cis*-acetic acid via vibrational excitation of *trans*-acetic acid.[11] The pulse duration was ca. 5 ns, the spectral line width was ~0.1 cm^{-1}, and the repetition rate was 10 Hz. The pulse energy of the OPO in the 7000-5000 cm^{-1} spectral region is ~0.5 mJ. The Burleigh WA-4500 wavemeter was used to control the OPO radiation frequency, providing an absolute accuracy better than 1 cm^{-1}. Whenever necessary, the IR absorption spectra were collected during pumping to compensate for the *cis* to *trans* tunneling process. The pumping beam was quasi-collinear with

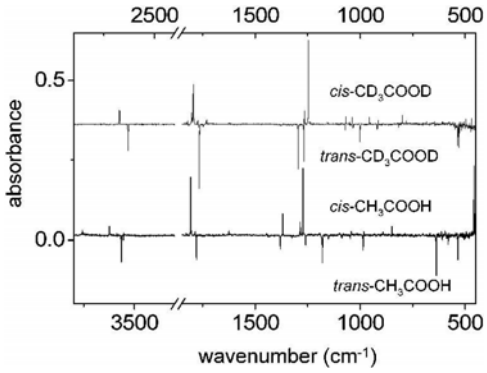

Figure 1. Difference IR absorption spectra showing the formation of *cis*-acetic acid (CH_3COOH and CD_3COOD) as a result of excitation of the 2νOH(D) modes of the *trans* conformer.

the spectrometer beam, and an interference filter transmitting in the 3300-1100 cm^{-1} region was attached to the detector to prevent its exposure to the pumping radiation. The photodissociation was induced with 193 nm radiation of an excimer laser (MPB, MSX-250) operating at 1-3 Hz with a typical pulse energy of 16 mJ. The UV irradiation of the *trans* conformer produces conversion to the *cis* conformer and vice versa. IR pumping of the UV-produced conformer was undertaken during UV irradiation to convert this conformer back into the conformer under study.

The ab initio calculations were performed using the GAUSSIAN98 package of programs.[30] The vibrational spectra of the *cis* and *trans* forms of various acetic acid isotopologues were calculated at the MP2/6-311++G(2d,2p) level. The ab initio Cartesian harmonic force constants obtained were later used in the normal coordinate analysis. The stable geometries, counterpoise-corrected interaction energies, and vibrational spectra of the complexes of methanol and carbon monoxide were evaluated at the same level of theory.[31]

Results and Discussion

Vibrational Assignment. For all studied isotopologues, acetic acid adopts exclusively the *trans* geometry in the as-deposited (nonirradiated) Ar matrix. To excite the acetic acid monomer at energies above the internal rotation barrier, we have used the overtone of the OH(D) stretching of the *trans*-conformer, observed at 6957.9, 6958.4, 5169.5, and 5167.8 cm^{-1} for CH_3COOH, CD_3COOH, CH_3COOD, and CD_3COOD, respectively. Excitation of this mode using a narrowband IR source promotes the conversion from the *trans* conformer to the *cis* form, as reported for a number of other carboxylic acids.[32] Figure 1 shows the spectrum obtained as a difference between the IR absorption spectra measured after and before the IR pumping of CH_3COOH and CD_3COOD. The bands pointing upward correspond to *cis*-acetic acid and the bands pointing downward correspond to the *trans* conformer. The spectral assignments here presented are based on the calculated ab initio harmonic vibrational frequencies and normal coordinate analysis of acetic acid monomer. The experimental and calculated frequencies and normalized intensities as well as the potential energy distribution for the *cis* and *trans* conformers of CH_3COOH and CD_3COOD are presented in Tables 1 and 2. The data for CH_3COOD and CD_3COOH can be found in the Supporting Information (Tables S1 and S2).

Assignment for the Trans Conformer. In general, the PEDs calculated for the *trans* conformers agree with those reported earlier.[6] Several studies have been previously dedicated to the analysis of the IR absorption spectra of the *trans*-acetic acid in the gas phase and isolated in Ar matrixes.[2-5] In our work, we could not observe the $CH(D)_3$ stretching modes for any of the isotopologues studied, which agrees with their very low calculated intensity (see Tables 1 and 2). For the absorptions from 3600 to 1250 cm^{-1} (OH(D), $CH(D)_3$, C=O, and C-O stretches) our analysis supports the previous

TABLE 1: Observed Frequencies and Relative Intensities[a] of *cis*- and *trans*-CH_3COOH Isolated in an Ar Matrix at 8 K Compared with the Values Predicted at the MP2/6-311++G(2d,2p) Level[a]

assignment (PED)		ν^{trans}_{calc}	ν^{trans}_{obs}	assignment (PED)	ν^{cis}_{calc}	ν^{cis}_{obs}	$\Delta\upsilon^{cis-trans}_{calc}$	$\Delta\upsilon^{cis-trans}_{obs}$
ν(OH) (98)	a'	3793.6 (20.9)	3563.8 (42.4)	ν(OH) (99)	3859.5 (17.1)	3622.6 (8.4)	+65.9	+58.8
$\nu(HCH_2)$ s. (100)	a'	3236.9 (0.6)	3051 [b]	$\nu(HCH_2)$ s. (97)	3229.7 (0.5)		-7.2	
$\nu(HCH_2)$ as. (100)	a''	3196.0 (0.5)	2996 [b]	$\nu(HCH_2)$ as. (100)	3178.0 (0.9)		-18.0	
$\nu(CH_3)$ (98)	a'	3115.3 (0.3)	2944 [b]	$\nu(CH_3)$ (96)	3099.4 (0.9)		-15.9	
				$\delta(CH_3) + \tau$(C-O) [c]		1828.2 (3.8)		
ν(C=O) (80)	a'	1805.2 (77.8)	1779.0 (91.0)	ν(C=O) (82)	1832.6 (66.3)	1807.4 (94.3)	+27.4	+28.4
						1784.8 (5.7)		
$\delta(HCH_2)$ as. (89)	a''	1506.3 (2.3)	1438.8 (1.8)	$\delta(HCH_2)$ as. (91)	1514.3 (2.1)	1448.3 (1.3)	+8.0	+9.5
$\delta(HCH_2)$ s. (90)	a'	1501.0 (4.3)	1433.6 (4.1)	$\delta(HCH_2)$ s. (92)	1501.2 (2.0)	1444.5 (2.7)	+0.2	+10.9
δ(CH3) (82)	a'	1434.5 (14.1)	1379.4 (23.3)	$\delta(CH_3)$ (96)	1421.5 (12.8)	1368.3 (29.0)	-13.0	-11.1
			1324.4 (3.2)					
				ν(C-C) + τ(C-O) [c]		FR 1285.4 (21.2)		
ν(C-O) (25) + δ(COH) (29) + $\delta(CH_3)$ (19)	a'	1352.7 (10.4)	1259.4 (20.8)	ν(C-O) (24) + δ(COH) (32) + $\gamma(CH_3)$ s. (18)	1218.4 (1.5)	1192.9 (3.0)	-134.3	-66.5
δ(COH) (47) + $\gamma(CH_3)$ s. (16) + ν(C-O) (12)	a'	1210.4 (56.7)	1179.8 (82.0)	δ(COH) (55) + ν(C-O) (14) + ν(C-C) (12)	1309.5 (100.0)	FR 1271.9 (100.0)	+99.1	+92.1
τ(C-O) + γ(C=O)[b]			1150.4 (7.6)					
$\gamma(CH_3)$ a. (70)+ γ(C=O) (21)	a'	1084.6 (1.4)	1047.2 (5.5)	$\gamma(CH_3)$ a. (70) + γ(C=O) (20)	1078.7 (0.9)	1042.4 (6.5)	-5.9	-4.8
$\gamma(CH_3)$ s. (61) + ν(C-O) (20)	a''	1011.7 (21.4)	985.5 (24.7)	$\gamma(CH_3)$ s. (61) + ν(C-O) (20)	1002.9 (2.9)	982.2 (5.3)	-8.8	-3.3
				2(τC-O) [c]		890.5 (4.1)		
ν(C-C) (58) + ν(C-O) (37)	a'	871.8 (2.1)		ν(C-C) (53) + ν(C-O) (38)	864.9 (10.8)	848.6 (8.0)		
τ(C-O) (77) + γ(C=O) (15)	a''	663.4 (23.9)	637.8 (74.7)	τ(C-O) (79) + γ(C=O) (20)	468.2 (27.2)	458.0 (95.9)	-195.2	-179.8
δ(OCO) (85)	a'	586.3 (9.7)	580.4 (16.0)	δ(OCO) (86) + ν(C-C) (11)	600.7 (2.0)		+14.4	
γ(C=O) (69) + τ(C-O) (23) + $\gamma(CH_3)$ a. (15)	a''	553.1 (8.5)	534.2 (38.5)	γ(C=O) (63) + τ(C-O) (19) + $\gamma(CH_3)$ a. (18)	605.2 (0.4)		+52.1	
δ(CC=O) (86)	a'	427.0 (1.1)	428 [b]	δ(CC=O) (84) + $\gamma(CH_3)$ s. (10)	436.0 (1.0)		+9.0	
$\tau(CH_3)$ (97)	a''	80.2 (0.06)		$\tau(CH_3)$ (98)	95.2 (0.3)		+15	

[a] The observed and calculated intensities were normalized by the intensity of the strongest band of both *cis* and *trans* conformers. The normalized values are shown in parentheses. The calculated potential energy distributions on the basis of the ab initio harmonic force constant are also shown. [b] From ref 5. [c] Tentative assignment. Symbols: *ν*- stretching; *δ*- bending; *γ*- rocking; τ-torsion; FR— involved in Fermi resonance.

assignments. The discrepancy concerns the assignment of the COH bending mode (δ(COH)) made previously.[5] In that paper, an increase of the δ(COH) frequency upon deuteration was claimed. The (δ(COH) modes of *trans*-CH_3COOH and *trans*-CD_3COOH were assigned to the bands at 1181 and 1208 cm^{-1}, respectively, whereas the δ(COD) modes for *trans*-CH_3COOD and *trans*-CD_3COOD were assigned to the bands at 1267 and 1268 cm^{-1}, respectively. We suggest a different assignment of the δ(COD) modes. On the basis of our calculations, the δ(COH) modes are close to 1200 cm^{-1} for *trans*-CH_3COOH and *trans*-CD_3COOH (assigned to the observed bands at 1179.8 and 1207.2 cm^{-1}, respectively), and for *trans*-CH_3COOD and *trans*-CD_3COOD the δ(COD) modes should be red shifted by more than 200 cm^{-1} from the δ(COH) bands. This is a normal red shift for the δ(COH(D)) mode, expected upon deuteration of the hydroxyl group. Therefore, in agreement with the theoretical predictions, we assign the bands observed at 955.4 and 1000.9 cm^{-1} to this vibration for *trans*-CH_3COOD and *trans*-CD_3COOD, respectively. These bands had been previously assigned to different $CH(D)_3$ deformation modes.[5] The comparison between observed and calculated intensities gives further support to

the present revised assignment. For *trans*-CD_3COOD, the δ(COD) mode is expected to be located between the CD_3 bending modes (δ(CD_3)) and the CD_3 rocking modes (γ(CD_3)) and to have an intensity higher than all those vibrations (see Table 2). Accordingly, the band at 1000.9 cm^{-1} is located between the CD_3 angular deformation modes, being the highest intensity band in the 1100 to 800 cm^{-1} region. For *trans*-CH_3COOD, the δ(COD) had been assigned to a band at 1267 cm^{-1},[5] which we reassign now to the ν(C-O) vibration. The ν(C-O) mode was previously assigned to a band at 1271 cm^{-1} that is very weak in our spectra and it is most probably due to matrix site effects.[5] On the other hand, for *trans*-CD_3COOD, the ν(C-O) and δ(COD) modes were previously assigned to the bands at 1296 and 1268 cm^{-1},[5] and they are observed in our spectra at 1294.5 and 1267.5 cm^{-1}, respectively. Those are strong bands probably caused by coupling of ν(C-O) with a non fundamental mode (see Table 2).

Another discrepancy with the assignments made in ref 5 concerns the COH torsion (τ(C-O)) and C=O rocking modes (γ(C=O) in this work and simply *γ* in ref 5) of *trans*-CH_3COOH and -CD_3COOH. These two a" modes are expected in the 700-500 cm^{-1} region. In the present work, the τ(C-O) modes are assigned to the higher frequency and stronger bands observed in this region (637.8 and 609.0 cm^{-1} for CH_3COOH and CD_3COOH, respectively) (see Table 1). This mode is also observed above 600 cm^{-1} (at 635.4 cm^{-1}) for *trans*-formic acid in solid Ar.[13,14] The γ(C=O) mode of CH_3COOH is here assigned to the band observed at lower frequencies (534.2 cm^{-1}). For CD_3COOH, this mode was not observed due to its low intensity but we believe it should be assigned to the band at 479 cm^{-1} reported previously.[5] Our assignment for the τ(C-O) and γ(C=O) modes is in the reverse order with respect to the literature data.[1,2,5] The present assignment is based on our ab initio calculations, and it respects the predicted relative position and intensities of the bands originated by the 3 modes absorbing in the 700-500 cm^{-1} region (see Table 1), and it is also supported by previously reported results on normal coordinate analysis.[6]

Assignment for the Cis Conformer. The spectral assignment for the *cis* conformers is quite straightforward based on the ab initio spectra. The ν(OH(D)) mode of *cis*-acetic acid is blue shifted by 40-60 cm^{-1} from the corresponding mode of the *trans* conformers, in good agreement with the ab initio predictions for acetic acid and also with the observed analogous shift of formic acid (~60 cm^{-1}).[13,14] The ν(C=O) mode appears also 20-30 cm^{-1} shifted to higher wavenumbers in the *cis* conformers as compared with the *trans* conformers (see Tables 1 and 2). The methyl stretching modes, predicted with very low intensities in the 3300-3000 cm^{-1} and 2400-2200 cm^{-1} spectral regions for CH_3COOH and CD_3COOD, respectively, were not observed experimentally.

For CH_3COOH, the ν(C-O) and δ(COH) vibrations are strongly coupled and perhaps they can be better defined as the COH-CO deformation modes, similarly to formic acid.[13,14] According to the calculations, the mode with the highest contribution from the δ(COH) coordinate of *cis*-CH_3COOH (1309.5 cm^{-1}) is blue shifted by almost 100 cm^{-1} from the corresponding mode of the *trans* conformer (1210.4 cm^{-1}). In contrast, for *cis*-CH_3COOH a mode with nearly the same contribution from the ν(C-O) and δ(COH) coordinates (1218.4 cm^{-1}) is predicted to be red shifted by more than 100 cm^{-1} from the corresponding mode of *trans* (1352.7 cm^{-1}). For both conformers, the δ(COH) mode is predicted to be the most intense vibration in the 1400-1200 cm^{-1} region. For *cis*-CD_3COOD, the ν(C-O) and δ(COD) modes are not coupled significantly and the assignments presented in Table 2 agree with both the computational band positions and intensities.

The C-C stretching modes (ν(C-C)) are

TABLE 2: Observed Frequencies and Relative Intensities[a] of *cis*- and *trans*-CD_3COOD Isolated in an Ar Matrix at 8 K Compared with the Values Predicted at the MP2/6-311++G(2d,2p) Level.

assignment (PED)		ν^{trans}_{calc}	ν^{trans}_{obs}	assignment (PED)	ν^{cis}_{calc}	ν^{cis}_{obs}	$\Delta\upsilon^{cis-trans}_{calc}$	$\Delta\upsilon^{cis-trans}_{calc}$
						2675.5$^{(9.4)}$		
ν(OD) (99)	a'	2759.3$^{(16.1)}$	2630.4$^{(27.7)}$ 2629$^{(26.5)}$	ν(OD) (99)	2809.9$^{(13.4)}$	2672.9$^{(21.2)}$	+50.6	+42.5
$\nu(DCD_2)$ s. (99)	a'	2401.2$^{(0.4)}$	2275[b]	$\nu(DCD_2)$ s. (98)	2394.1$^{(0.2)}$		-7.1	-
$\nu(DCD_2)$ as. (100)	a''	2365.2$^{(0.3)}$	2240[b]	$\nu(DCD_2)$ as. (100)	2352.5$^{(0.6)}$		-12.7	-
$\nu(CD_3)$ (98)	a'	2239.2$^{(<0.1)}$	2116[b]	$\nu(CD_3)$ (98)	2228.4$^{(0.3)}$		-10.8	
						1863.8$^{(3.2)}$		
			1769.8$^{(6.4)}$			1801$^{(31.9)}$		
ν(C=O) (85)	a'	1792.1$^{(94.0)}$	1765.0$^{(80.7)}$	ν(C=O) (86)	1821.6$^{(89.4)}$	1794.4$^{(96.4)}$	+29.5	+29.4
			1746.8$^{(4.5)}$			1730.3$^{(6.1)}$		
			1743.7$^{(3.5)}$					
			1376.4$^{(2.4)}$			1367.7$^{(1.9)}$		
						FR 1264.6$^{(15.6)}$		
ν(C-O) (43) + ν(C-C) (31)	a'	1319.2$^{(75.9)}$	FR 1294.5$^{(54.4)}$	ν(C-O) (39) + ν(C-C) (30) + $\delta(CD_3)$ (10)	1280.5$^{(100.0)}$	FR 1246.2$^{(100.0)}$	-38.7	-34.8
			FR 1267.5$^{(49.2)}$			1238.1$^{(5.7)}$		
$\delta(CD_3)$ (63) + $\delta(DCD_2)$ s. (16) + ν(C-O) (14)	a'	1106.1$^{(4.4)}$	1071.3$^{(8.2)}$	$\delta(CD_3)$ (61) + $\delta(DCD_2)$ s. (20) + ν(C-O) (11)	1100.6$^{(8.1)}$	1066.9$^{(8.5)}$	-5.5	-4.4
$\delta(DCD_2)$ a. (91)	a''	1084.9$^{(1.1)}$	1044.8$^{(1.8)}$	$\delta(DCD_2)$ a. (94)	1090.2$^{(1.1)}$	1050.5$^{(2.3)}$	+5.3	+5.7
$\delta(DCD_2)$ s. (81) + $\delta(CD_3)$ (15)	a'	1072.4$^{(6.3)}$	1033.2$^{(4.9)}$	$\delta(DCD_2)$ s. (78) + $\delta(CD_3)$ (18)	1073.4$^{(8.8)}$	1036.5$^{(9.7)}$	+1.0	+3.3
δ(COD) (62) + δ(OCO) (12)	a'	1019.1$^{(22.7)}$	1000.9$^{(22.1)}$	δ(COD) (58) + $\gamma(CD_3)$ s. (14)	973.5$^{(5.9)}$	954.6$^{(5.7)}$	-45.6	-56.3
$\gamma(CD_3)$ a. (51) + γ(C=O) (42)	a''	940.7$^{(2.2)}$	917.9$^{(8.6)}$	$\gamma(CD_3)$ a. (52) + γ(C=O) (40)	933.3$^{(1.4)}$	913.1$^{(4.4)}$	-7.4	-4.8
$\gamma(CD_3)$ s. (65) + ν(C-O) (22)	a'	832.8$^{(8.4)}$	815.7$^{(6.4)}$	$\gamma(CD_3)$ s. (40) + δ(COD) (23) + ν(C-C) (23)	795.2$^{(1.7)}$		-37.6	
ν(C-C) (54) + δ(COD) (18) + ν(C-O) (14) + $\delta(CD_3)$ (11)	a'	768.5$^{(0.9)}$		ν(C-C) (27) + ν(C-O) (40) + $\gamma(CD_3)$ s. (17)	813.8$^{(9.1)}$	799.3$^{(9.4)}$	-19.0	
γ(C=O) (28) + $\gamma(CD_3)$ a. (32) + τ(C-O) (41)	a''	550.6$^{(9.7)}$	534.7$^{(27.0)}$	γ(C=O) (55) + $\gamma(CD_3)$ a. (39)	516.4$^{(2.1)}$		-34.2	
δ(OCO) (75) + δ(COD) (13)	a'	536.4$^{(12.4)}$	530.3$^{(24.5)}$	δ(OCO) (76) + ν(C-C) (14)	565.3$^{(0.2)}$		+28.2	
τ(C-O) (58) + γ(C=O) (34)	a''	421.7$^{(12.1)}$		τ(C-O) (89) + γ(C=O) (10)	352.0$^{(1.5)}$		-69.7	
δ(CC=O) (76) + $\gamma(CD_3)$ s. (18)	a'	375.5$^{(1.0)}$		δ(CC=O) (75) + $\gamma(CD_3)$ s. (18)	377.7$^{(17.3)}$	382.3$^{(50.6)}$	+2.2	
$\tau(CD_3)$ (97)	a''	58.9$^{(<0.1)}$		$\tau(CD_3)$ (98)	69.2$^{(0.5)}$		+10.3	

[a] The observed and calculated intensities were normalized by the intensity of the strongest band of both cis and trans conformers. The normalized values are shown in parentheses. The calculated potential energy distributions on the basis of the ab initio harmonic force constant are also shown. [b] From ref 5. Symbols: *ν*, stretching; *δ*, bending; *γ*, rocking; τ, torsion; FR, involved in Fermi resonance.

observed for the *cis* conformers in the 850-800 cm^{-1} region. These modes are predicted to be much more intense in the *cis* form than in the *trans* conformer. Below 800 cm^{-1} our analysis is limited by the relatively low concentration of the *cis* form. Therefore, we could only detect strong modes for *cis*-CH_3COOH like the τ(C-O) fundamental. This mode absorbs at 458.0 cm^{-1}, red shifted by 180 cm^{-1} from the corresponding band of *trans*-CH_3COOH, which agrees with the 195 cm^{-1} shift predicted by the ab initio calculations. A band observed at 890.5 cm^{-1} is tentatively assigned to the C-O torsion overtone of *cis*-CH_3COOH. In this case, the anharmonicity of the τ(C-O) mode in *cis*-CH_3COOH is similar to that of the analogous mode of *cis*-HCOOH (≈13 cm^{-1}).[13]

Several low-intensity bands are unassigned in Tables 1 and 2 or assigned tentatively to overtones or combination modes. Some of them can also be due to matrix-site effects. It is not our purpose to discuss the assignment of those bands. It should be mentioned only that the spectrum of *cis*-CH_3COOH shows a relatively intense band at 1285.4 cm^{-1} that probably originates from a nonfundamental mode with enhanced intensity due to coupling with the very intense δ(COH) mode (at 1271.9 cm^{-1}). It is assigned tentatively to the ν(C-C) + τ(C-O) combination mode. In the case of

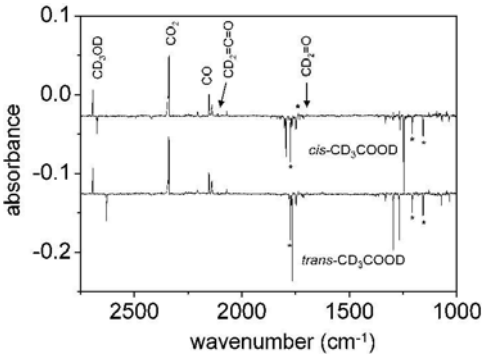

Figure 2. Difference IR absorption spectra showing the result of 193 nm photolysis of the *cis* and *trans* conformers of perdeuterated acetic acid in solid Ar at 8 K. Bands marked with an asterisk are from CD_3COOH present as an impurity in the sample.

CD_3COOD, both conformers exhibit a doublet in the region of the ν(C-O) mode separated by 18 and 27 cm^{-1} for *cis* and *trans*, respectively. We believe that this is due to the coupling of the ν(C-O) mode with a nonfundamental mode rather than due to matrix site effects.

193 nm Photolysis. One of the motivations of this work was to investigate the possible conformational selectivity of UV photolysis of acetic acid. In an Ar matrix, conversion of *cis*-CH_3COOH and *cis*-CD_3COOH to the corresponding *trans* forms by tunneling is very fast, which limits the concentration of the *cis* conformer. Therefore, the influence of the molecular conformation on the photolysis of acetic acid is better studied for the CD_3COOD isotopologue, due to its relatively slow *cis*-to-*trans* tunneling. Indeed, for this deuterated molecule, the half-life of the *cis* conformer is approximately 5 days, whereas for *cis*-CH_3COOH it is 16 s.[11] As already mentioned, the *cis* conformer appears as one of the products of UV photolysis off *trans*-CD_3COOD, and vice versa. Thus, to minimize the effect of UV-induced rotamerization, UV photolysis of one conformer (*trans* or *cis*) was undertaken while the other conformer was pumped with resonant IR radiation. Excitation of the OD stretching overtone of the conformer produced by UV radiation converts it back to the starting conformer. The ν(OD) overtone is observed at 5167.8 and 5257.4 cm^{-1} for *trans*- and cis-CD_3COOD isolated in solid Ar.

The main photolysis products are molecular complexes involving CO_2 or CO, namely CO complexed with methanol (see later). No conformational dependence was found upon photolysis of CD_3COOD, as seen in Figure 2. We can suggest a number of possible reasons why the acetic acid photolysis is conformationally independent, in contrast to the photolysis of formic acid. If vibrational relaxation in the excited electronic state of acetic acid is faster than dissociation, as was suggested for excitation at 218 and 200 nm,[22,23] then photodecomposition is expected to be a conformationally independent process. In formic acid, torsional randomization was assumed to be a slower process as compared to formation of the transition state for decomposition.[15] In fact, it has been estimated recently that in the S_1 surface isomerization of formic acid occurs on a picosecond time scale, whereas decomposition takes place in a femtosecond time scale.[33] In matrix-isolated formic acid, the S_1 Franck—Condon geometry relaxes to a vibrationally excited ground state and decomposition results mainly in formation of molecular products.[15] The same process was used to explain molecular elimination upon photolysis of formic acid in the gas phase.[34] In contrast, it is known that the primary gas-phase photolysis products of acetic acid are mainly radicals (CH_3CO, OH, CH_3, COOH,),[22-24,35] even though molecular elimination products upon UV broadband photolysis were reported in earlier works.[36] This indicates that the decomposition takes place mainly on the excited-state surfaces rather than in the vibrationally excited ground state. The molecular products of solid-state photolysis of acetic acid, formed upon cage-induced recombination of the primary radicals, indicate that the branching ratio

for radical formation is conformationally independent. The photodecomposition dynamics in acetic acid has been studied theoretically using the MP2 and CASSCF methods.[17] In that study, it has been shown that the transition state for C-C cleavage on the T_1 surface has a geometry very similar to that of *cis*-acetic acid, whereas the transition state for C-O cleavage on the T_1 surface and for both C-C and C-O cleavages on the S_1 surface are connected geometrically to *trans*-acetic acid.[17] This means that the branching ratio between radicals could in principle be affected by the molecular conformation. In practice, because $T_1 \leftarrow S_0$ is a forbidden transition and at the S_1/T_1 crossing point the T_1 Franck-Condon geometry is already relaxed to a geometry bearing no memory of the initially excited conformer, decomposition to radicals on the T_1 surface seems to be conformationally independent. On the S_1 surface, the C-O cleavage is the only energetically accessible process. Finally the UV-induced isomerization competes with photodecomposition upon 193 nm irradiation of acetic acid, as seen from the production of *cis*-CD_3COOD upon irradiation of *trans*-CD_3COOD, and vice versa. This might be another reason for photodecomposition to be a conformationally independent process in acetic acid as opposed to formic acid, where isomerization does not compete appreciably with decomposition.

The easily identified photodecomposition products of CD_3COOD are methanol,[37] carbon monoxide, and carbon dioxide.[38-40] In addition, we could detect also weaker bands from formaldehyde and ketene.[41,42] These species are isolated as complexes with the corresponding photo-lysis product, as will be later discussed. The same products are observed upon photolysis of CH_3COOH, with some small differences in the branching ratios as compared with the deuterated isotopologue. Figure 3 is a difference spectrum showing the result of photolysis of CH_3COOH in solid Ar. In Table 3 the

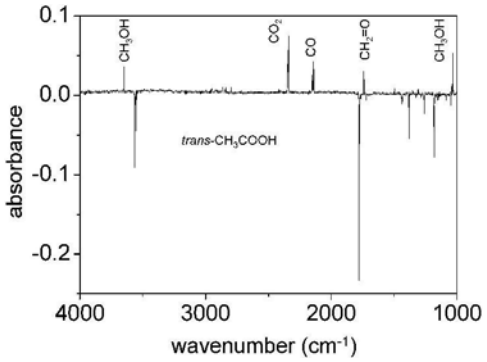

Figure 3. Difference IR absorption spectrum showing the result of 193 nm photolysis of *trans*-CH_3COOH isolated in solid Ar at 8 K.

emerging bands upon photolysis of CD_3COOD and CH_3COOH are listed together with previously reported data on the relevant monomeric species isolated in Ar

Most interestingly, this is the first time that methanol and carbon monoxide are among the products of molecular elimination channels upon photolysis of monomeric acetic acid. These products might be the result of recombination of acetyl and hydroxyl radicals formed on the S_1 or T_1 surfaces,[17] which remain in close contact within the same matrix cage after decomposition of acetic acid. Methanol and carbon monoxide could also be formed upon further photolysis of primary acetic acid decomposition products, for instance, photolysis of ketene in the presence of water.[43] Figure 4 illustrates a possible photodecomposition scheme. According to this scheme, the final products are dictated by the recombination of radicals, which is caused by the matrix-cage effect.[29] The matrix cage is known to affect substantially the decomposition dynamics of the isolated molecule due to the fact that, even for the light fragments, cage exit is a rather improbable phenomenon. Furthermore,

TABLE 3: Comparison between the Observed IR Frequencies (cm^{-1}) for the 193 nm Photolysis Products of CD_3COOD and CH_3COOH with Reported Data on Monomeric CD_3OD/CH_3OH, CD_4/CH_4, CO_2, CO, $CD_2=O/CH_2=O$, and $CH_2=C=O$ Isolated in Solid Ar[a]

CD_3COOD products		Literature data [a]		mode	Literature data [a]		CH_3COOH products	
		CD_3OD			CH_3OH			
2693.6	m	2706.1	m	νOH	3667.3	s	3649.6	m
2205.9	w	2219.1	w	νCH_3	3005.3	m	2996.8	vw
2258	vw	2254.3	m	νCH_3	2961.9	s	2949.2	vw
2246	vw							
2070	w	2078.3	m	νCH_3	2847.9	s	2839.5	vw
		1031.3	m	δCH_3	1474.1	vw		
		1068.1	vw	δCH_3	1465.8	vw		
1129	w	1132.7	m	δCH_3	1451.4	vw		
782.4	w	775.4	m	δCOH	1335	m	1351	vw
858.1	vw	860.4	vw	ρCH_3	1157	vw		
		1055.2	vw	ρCH_3	1076.7	vw		
978.8	w	983.4	m	νCO	1034.0	vs	1034	s
				τCO	240	vs		
		CD_4 [b]			CH_4			
		2260.3	s	νCH_3	3037.0	s		
		993.4	s	δCH_3	1307.7	s	1308.3	w
		CO_2 [c]						
2347.5	br	2345.2	vs	νCO_2			2345.6	br
2344.5	br						2344.4	br
2341.6	br						2340.2	s
2339.2	vs	2339.0	vs	νCO_2			2338.9	vs
663.9	m	663.3	m	δCO_2			663.9	m
662.3	m	661.8	m	δCO_2			662.3	m
		CO [d]						
2152.5	m						2152.0	m
2151.9	m						2151.6	m
2151.5	sh						2151.0	sh
2150.3	m						2149.9	m
							2141.1	sh
2140.0	m	2140.1	sh	$\nu C{\equiv}O^D$			2140.2	m
2139.3	m	2138.5	s	$\nu C{\equiv}O^M$			2140.0	m
		2136.7	sh	$\nu C{\equiv}O^M$			2139.4	sh
2138	br						2138.3	m
		$CD_2=O$			$CH_2=O$			
		2176.8	s	νCH_2	2863.0	s	2863	vw
		2069.1	s	νCH_2	2797.1	s	2794.2	w
1696.1	vw	1697.8	s	νC=O	1742.0	s	1739.9	m
		1099.1	vw	δCH_2	1498.8	m	1496.7	w
		987.1	w	ρCH_2	1244.8	w		
		938.3	vw	ωCH_2	1168.0	w		
					$CH_2=C=O$			
				νCH_2	3062	m		
2112.1	w			νC=O	2140	vs	2140 [e]	m
				δCH_2	974	m		
				ρC=O	579	m		
				ρC=O	525	s		

[a] Symbols: vs, very strong; s, strong; m, medium; w, weak; vw, very weak; br, broad; sh, shoulder; *ν*, stretching; *δ*, bending; γ, rocking; ω, wagging and τ, torsion. [b] Data were taken from refs 37-42 and 52. [c] Data of CD_4 isolated in Kr matrixes taken from ref 52. [d] The splitting of the CO_2 bands was assigned to molecules isolated in different sites in ref 40. [e] The letters M and D stand for monomer and dimer, respectively.[38,39] [f] Band overlapping with the envelope of bands from CO, see text for a detailed explanation.

because the molecular species formed as a result of permanent dissociation remain in the same cage, they might form stable complexes. In fact, photolysis of matrix isolated species has been used to prepare various 1:1 molecular complexes.[44-49]

Another product of photolysis of acetic acid is CO_2. On the basis of the frequently used ratio of ~10 between CO_2 and CO absorption cross sections,[50,51] the CO/CO_2 product ratio upon photolysis is ~5. Methane is expected to be formed together with CO_2, from recombination of the $CH(D)_3$ and OCOH(D) radicals formed after C-C bond cleavage on the T_1 surface.[17] Nevertheless, the bands of methane are not readily identified after photolysis of CD_3COOD (Table 3), which is most probably due to the much smaller IR absorption cross section of methane modes as compared with CO_2. In the photolysis of CH_3COOH we assigned one band emerging at 1308.3 cm^{-1} to methane reported previously at 1307.7 cm^{-1}.[52] The C-H stretching mode of the methane monomer is known to be a broad band in rare-gas matrixes.[52] This can explain why this mode is not observed upon photo-dissociation of CH_3COOH despite having a higher intrinsic intensity than the bending mode.[53]

A band at 2112.1 cm^{-1}, rising upon photolysis of CD_3COOD, is assigned to the ν(C=O) mode of deuterated ketene (CD_2= C=O). In agreement, this mode is observed for CH_2=C=O in the 2134-2144 cm^{-1} region and it is predicted by ab initio calculations to shift toward lower frequencies by 21.6 cm^{-1} for CD_2=C=O.[42] It is the strongest mode of ketene,[42] with an absorption cross section much larger than any other vibration of this species (~555 and 440 km/mol, calculated for CH_2= C=O and CD_2=C=O, respectively). The 2112.1 cm^{-1} band increases quickly in the earlier stages of photolysis and decreases upon long photolysis. This behavior is in agreement with the fact that ketene can also be photolyzed with 193-nm radiation.[43] The estimated $CO:CD_2$=C=O ratio is ~20:1, even in the earlier stages of photolysis. This means that the photolysis channel leading to production of ketene is minor or its formation rate is comparable with its decomposition in the present experimental conditions. Ketene is not readily identified as a product of photolysis of CH_3COOH because the ν(C=O) band of CH_2=C=O overlaps with the absorption of carbon monoxide. Nevertheless, it can be seen in Figure 5 that the band shape of the carbon monoxide absorption near 2140 cm^{-1} changes significantly during photolysis, and the overlapping ketene band can cause this modification. Furthermore, after 600 pulses there is a band at 1593.9 cm^{-1} that can be due to formation of complexed water, which is the other molecular species produced together with ketene.[15] This band disappears after 3300 pulses, which probably indicates that water reacts with the photolysis products of ketene. The major products of 193 nm photolysis of ketene are CH_2 + CO and HC=CO + H in a 1:3 proportion.[15] Because these radicals will be in close contact with water inside the matrix cage, they can react with water, forming various radicals, which react further producing at some point stable molecular species (formaldehyde, carbon monoxide, and molecular hydrogen; see Figure 4). Notice that formaldehyde (CH_2=O) might also be generated from photolysis of the methanol molecules formed directly from recombination of the acetyl and hydroxyl radicals (Figure 4).[54] The formation of formaldehyde from photolysis of CH_3COOH is evident because we have detected the four strongest vibrations of this molecule (see Table 3). However, only the νC=O band of deuterated formaldehyde was observed (1696.1 cm^{-1}) upon photolysis of CD_3-COOD. This emerging band is very weak, indicating that formaldehyde is a minor product of photolysis of CD_3COOD.

Complex between Carbon Monoxide and Methanol. Methanol formed upon 193 nm photolysis of acetic acid in solid Ar is produced together with carbon monoxide in the same matrix cage. It is known that when methanol is isolated in an Ar matrix doped with 2% of carbon monoxide a 1:1 complex is formed between the two molecules.[55] On one hand, the bands of methanol are consistent with the forma-tion of one specific type of complex (see discussion later). On the other hand, carbon monoxide can be produced upon solid-state photolysis of acetic acid via various mechanisms, such as photolysis of ketene in the presence of water, photolysis of methanol, and direct recombination of acetyl and hydroxyl radical. From the possible decomposition pathways shown in Figure 4, carbon monoxide could be sharing the matrix cage with methanol, formaldehyde, and molecular hydrogen or with another carbon monoxide molecule and hydrogen. In fact, the produced carbon monoxide upon UV irradiation of acetic acid exhibits two sets of bands separated by ~10 cm^{-1}, indicating that at least two different types of complexes with CO are produced.

Previously, a red shift (18 cm^{-1}) was observed for the ν(OH) mode of CH_3OH isolated in an Ar matrix containing 2% of CO.[55] This shift agrees with our data on ν(OH) of CH_3OH formed upon photolysis of CH_3COOH (Table 3). A proportional shift was observed in the ν(OD) mode of CD_3OD complexed with CO (13 cm^{-1}) as compared with the monomer isolated in solid Ar.[37] The red shift of the ν(OH) frequency of methanol upon complexation with CO disagrees with the earlier compu-tationally predicted blue shift for all stable geometries of this complex.[56] In view of this disagreement, we performed geometry optimizations and energy calculations based on those geometries with a more complete basis set. In Figure 6 the four stable geometries of the complex formed between CH_3OH and CO are shown. The energetics of these structures and the expected frequency shifts for the complexed units with respect to the free monomers appear in Table4.

From the four optimized geometries of the complex, two have a linear arrangement of the CO molecule with respect with the OH bond (I and II) and two have an L-shape arrangement (III and IV). Structure

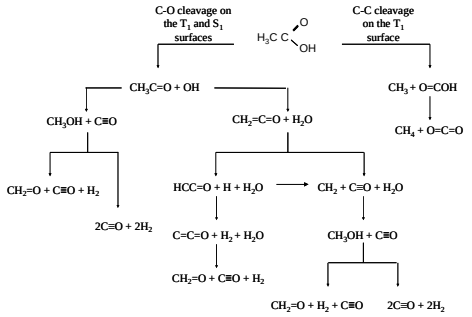

Figure 4. Photodecompositiom channels of acetic acid. In addition to the presented decomposition channels, there is also a possibility of recombination of the primary radicals back to acetic acid in the vibrationally excited ground state that can dissociate directly into the observed molecular products of thermal decomposition ($CH_2=C=O + H_2O$ and $CH_4 + CO_2$).

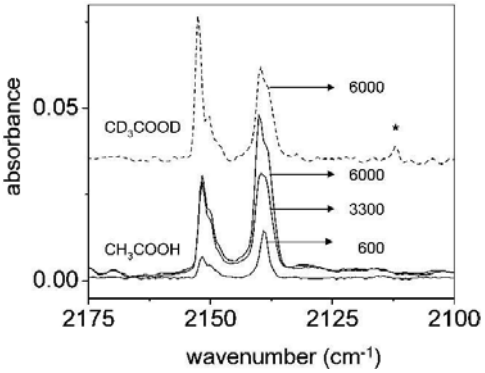

Figure 5. IR absorption bands emerging in the 2175-2100 cm^{-1} region upon 193 nm photolysis of CH_3COOH with 600, 3300, and 6000 pulses. The same region is shown for photolysis of CD_3COOD (---) after 6000 pulses of 193 nm radiation for comparison. The band marked with an asterisk was assigned to deuterated ketene ($CD_2=C=O$).

I has the OH···CO interaction whereas structure II has an interaction of the OH···OC type. Both of them are predicted to have the OH···O/C distances and O-H···O/C angles characteristic of interact-tions via hydrogen bonds (2.3 Å and 180°), as shown in Figure 6. In structure III the oxygen atom of CO is closer to the hydrogen atom of the hydroxyl group in methanol, whereas in structure IV it is the carbon atom of CO that is closer to the hydroxylic hydrogen. For III and IV, the OH···O and OH···C calculated distances are 2.9 and 2.8 A, respectively, and the O-H···O/C angles deviate from the characteristic values of hydrogen bonded systems. The energies of the stable geometries of the 1:1 complex between methanol and CO are in qualitative agreement with the previously reported data.[56] The only difference is the somewhat increased stability of structure IV with respect to the other structures. Our calculations predict a complexation-induced red shift in the ν(OH) mode of methanol for structures I, III, and IV and a blue shift for complex II.

The formation of complex II in the matrix can be ruled out because the predicted complexation shift of the ν(OH) is positive (blue) whereas the observed shift is negative (red). Among the three structures exhibiting a complexation-induced red shift in the ν(OH) mode, complex I exhibits vibrations in good agreement with the experiment, and it has the highest interaction energy. This is particularly evident for ν(OH), the three ν(CH), and the δ(COH) modes (observed shifts of -26.8, -7.5, -11.0, -8.1, and +31.8 and the corresponding predicted values -17.7, -8.5, -12.7, -8.4, and +16.3). For the most stable complex structure, the calcuations predict a blue shift of 12.5 cm^{-1} on the νC≡O vibration, in good agreement with the observed shift of about +12 cm^{-1} for the high-frequency set of bands of CO. Thus, according to the calculations, the high-frequency set of bands of CO (~2150 cm^{-1}) should be assigned to complex I. The identification of complex I

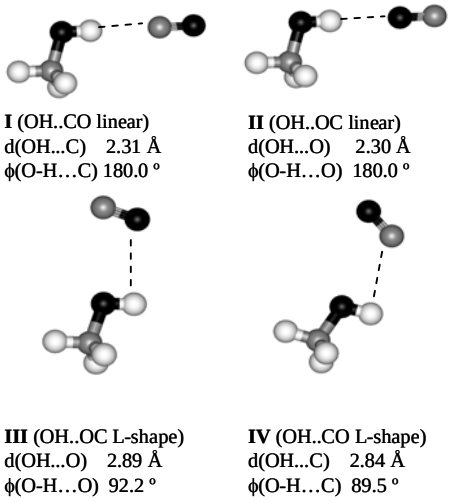

Figure 6. Optimized geometries for the 1:1 complex between methanol and carbon monoxide. Relevant geometrical parameters of complexes are shown.

TABLE 4: Comparison between Predicted [MP2/ 6-311++(2d,2p)] Frequency Shifts for the Four Stable Structures of the Complex between Methanol and Carbon Monoxide with Respect to the Free Monomers and the Observed Shifts for the Complex Isolated in Solid Ar.

free monomer (cm^{-1})	I OH···CO linear	II OH···OC linear	III OH···OC L-shape	IV OH···CO L-shape	obsd[a]
3902.9	-26.8	+12.0	-7.4	-9.1	-17.7
3205.0	-7.5	-2.2	+1.1	-0.7	-8.5
3144.2	-11.0	-4.4	+1.8	+1.5	-12.7
3075.1	-8.1	-3.4	+1.0	+0.7	-8.4
2120.1	+12.5	-3.3	-1.6	+4.3	+12
1544.8	+0.3	+0.2	-0.1	-0.2	
1532.1	+0.2	+0.2	-0.5	-0.7	
1508.1	-0.9	-0.3	-0.4	-0.7	
1387.3	+31.8	+12.2	-0.4	-1.4	+16.3
1191.2	+0.2	0.0	+0.3	-0.2	
1095.4	+19.0	+7.3	0.0	+5.1	
1053.9	+9.8	+3.5	-0.1	+0.2	-0.3
288.3	+195.1	+76.9	+9.8	+29.3	
E_{int}[b]	-1.66	-0.60	-0.72	-1.06	
	(-1.24)	(-0.48)	(-0.53)	(-0.56)	

[a] Observed shifts with respect to the bands of the free monomers isolated in an Ar matrix.[37] [b] BSSE corrected interaction energy (kJ mol^{-1}) calculated at the at the MP2/6-311++(2d,2p) level and values taken form ref 56 in parentheses.

is further supported by the fact that the predicted effect of deuteration on the complexation induced shift (a 7 cm^{-1} smaller red shift for νOD) agrees with the observed isotopic effect (smaller red shift by 5 cm^{-1}). The predicted effect of deuteration on the shift of the ν(C≡O) band is very small (0.3 cm^{-1}) so that it gives no indication about the complex geometry. We did not find strong experimental indications in the ν(OH) region of complexes III and IV. In the ν(C≡O) region, the bands observed at ~2140 cm^{-1} may originate from the CO dimer isolated in solid Ar.[38,39] In the present experiments, the CO dimers can be formed upon photolysis of either methanol or ketene (see Figure 4). The possibility of ternary complexes involving CO, formaldehyde, and molecular hydrogen producing bands near the free monomer band cannot be excluded.

Upon annealing the matrix at 25 K after photolysis of CH_3COOH, the ν(OH) band (3649.6 cm^{-1}) practically disappears and three new bands appear at 3647.4, 3646.5, and 3645.3 cm^{-1}. A similar intensity reorganization takes place for the ν(C=O) bands assigned to complex I: the envelope of bands at higher frequency decreases and a new set of bands appear shifted by ~4 cm^{-1} from the decreasing bands (see Figure 7). The observed intensity reorganization is not consistent with conversion to a different complex geometry. In the present case, where only the most stable complex structure is observed upon photolysis, annealing the matrix at 25 K is not expected to decrease its concentration. When photolysis produces a distribution of conformers that is not in thermal equilibrium,[47] annealing the matrix should lead to conversion of the less stable complexes into the lower energy forms. Instead we observed the decrease of bands assigned to the most stable complex. This makes us suggest that the observed modifications are caused by thermal relaxation of the matrix local surrounding, allowing a more suitable orientation of the complex within the cage, in other words, conversion of the matrix sites. The intensity ratio of the increasing and decreasing bands upon annealing is ~1, which supports the fact that the same complex structures produces both sets of bands by taking into account that the ν(OH) absolute intensity is very sensitive to the complex geometry. In fact, the calculated ν(OH) intensities have a ratio of 5:3:1:1 between complexes I:II:III:IV.

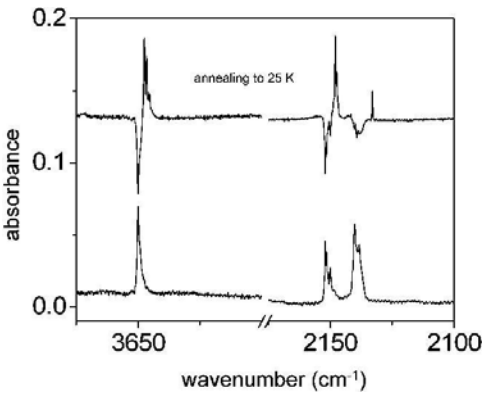

Figure 7. Thermally induced changes on the methanol (ν(OH) mode) and CO bands upon annealing at 25 K. The lower trace shows the spectrum collected after photolysis of acetic acid in solid Ar at 8 K. The upper trace is the difference spectra showing the effect of annealing at 25 K.

There is also a broad feature centered at ~2140 cm^{-1} whose intensity decreases upon annealing to 25 K whereas a new band appears at 2133 cm^{-1}. It is not clear if these bands are related to each other, and the origin of the new narrow band remains unknown. In fact, interpretation of the spectral changes upon annealing are complicated by the fact that there is a small amount of hydrogen atoms that escape the cage during photolysis and can be thermally mobilized. This is a known phenomenon occurring during annealing of a matrix where a molecular species containing hydrogen was photolyzed.[29,57,58] A strong support for mobility of thermally

activated hydrogen atoms is the appearance of the band at 1862.4 cm^{-1}, which is in good agreement with the very strong band observed for the free HCO radical in Ar matrixes (1863 cm^{-1}).[59] In the present experimental conditions, the H atom mobility is most probably a local process rather than a global process.

Photolysis Branching Ratios. After identification of the acetic acid photolysis products we can estimate the branching ratios for the proposed photolysis channels. The lack of information on the formation yield of the transient radicals prevents us from clarifying the source of the CO complexes giving bands at ~2140 cm^{-1}. Nevertheless, using the formaldehyde bands we can estimate the percentage of CO molecules involved in ternary complexes with formaldehyde and molecular hydrogen. The ν(C=O) mode of ketene absorbs at 2140 cm^{-1} in solid Ar, but the relative amount of ketene formed is very small and we neglected its contribution to the envelope of bands around 2140 cm^{-1}. The integrated intensities of the photolysis products, normalized by their intrinsic intensity (calculated or experimental), were used to estimate the proportion of the photolysis channels. The bands at 2150 cm^{-1} were used for complex I between methanol and CO. We chose the CO band (instead of νOH of methanol) because computationally its intrinsic intensity is practically unchanged upon complexation with methanol. The carbon dioxide bands at ~2340 cm^{-1} were used to estimate the importance of the C-C cleavage channel.

As a result, 29% of the acetic acid molecules yield methanol plus carbon monoxide complexes, 15% yield carbon monoxide complexed with formaldehyde and molecular hydrogen, 39% yield quarternary complexes of two carbon monoxide molecules and two hydrogen molecules and, finally, 17% dissociate to carbon dioxide and methane. Even if we assumed that the absorption of ketene contributes to a half of the intensity of the envelope of bands at 2140 cm^{-1} (which is definitely an overestimate), the percentage of ketene formed upon 193 nm irradiation of acetic acid would be small (~5%). In this case we would obtain 37%, 17%, 20%, and 21% for the channels connected with CO + CH_3OH (complex I), CO + CH_2=O + H_2 (ternary complex), 2CO + $2H_2$ (quaternary complex), and CO_2 + CH_4 complexes, respectively.

The distribution of photodecomposition products is in agreement with the fact that the C-C cleavage, generating carbon dioxide and methane, occurs only on the T_1 surface due to energetic restrictions.[17] On the other hand, C-O cleavage occurs both on the S_1 and T_1 surfaces, meaning that it has a higher probability than the C-C cleavage. Although the intersystem crossing from S_1 to T_1 is a spin forbidden process, it was concluded that structural similarities between the crossing point of these two surfaces and the S_1 minimum indicate that this process can happen to a noticeable extent.[17]

Photolysis of perdeuterated acetic acid shows somewhat different branching ratios when compared with CH_3COOH. In the case of CD_3COOD, we can evaluate directly the amount of ketene formed from its ν(C=O) band at 2112 cm^{-1}. The estimated percentage of the different products are 45:5:33:16:1 for channels connected with CO + CH_3OH : CO + CH_2=O + H_2 : 2CO + $2H_2$: CO_2 + CH_4 : CD_2=C=O + H_2O. Compared with the photodissociation of CH_3COOH, these numbers indicate a considerable difference in the efficiency of the channels leading to formation of CO, formaldehyde, and molecular hydrogen. This is evidenced by the difference in the relative intensity of the CO bands at 2140 and 2150 cm^{-1} upon photolysis of both isotopologues (Figure 5). The deuteration-induced changes in the branching ratios can be caused by isotopic effects on the processes in the scheme presented in Figure 4; however, it is difficult to specify them. For instance,

these can include isotope effects of the absorption cross-section of ketene, formaldehyde, methane, methanol, and water at 193 nm.

Conclusions

The results of this work can be separated into four parts:

1. We have analyzed the vibrational spectroscopy of *cis*-acetic acid isolated in solid Ar, which was produced using vibrational excitation of the *trans* form. The vibrational assignment for various isotopologues was given for the *cis* form, and some bands were reassigned for the *trans* form (see Tables 1 and 2).

2. The perdeuterated isotopologue was used to test the conformational selectivity of the solid-state photolysis (193 nm) of acetic acid. No conformational dependence of the acetic acid photodissociation was found. This was explained in terms of decomposition on the excited-state surfaces leading primarily to unselective radical formation.

3. Upon 193 nm irradiation, acetic acid isolated in an Ar matrix decomposes permanently into a number of molecular complexes (see Figure 4 and Table 3). The photodecomposition dynamics for the isolated molecule is complicated, and not all channels are fully understood at the moment. It involves reaction of the radicals formed as primary products and further photodissociation of those secondary products. The major photolysis products are methanol complexed with carbon monoxide, the quaternary complex involving two carbon monoxide molecules and two hydrogen molecules, ternary complexes between carbon monoxide, formaldehyde, and probably molecular hydrogen, and carbon monoxide complexed with methane. Ketene, which is the main product of thermal decomposition of acetic acid, was detected only in small amounts (<5%) upon solid-state photolysis of acetic acid, and it is further photolyzed by 193 nm radiation, which makes estimation of its production conditional. In fact, apart from methane and carbon dioxide, all the molecular products observed could be explained in terms of photochemistry of the ketene-water complex.

4. The 1:1 complex between methanol and carbon monoxide was studied on the basis of ab initio calculations. We observed the most stable form of the complex, described by a planar structure with the $OH^{\cdots}CO$ hydrogen bond. Upon annealing at 25 K, the complex structure undergoes small modifications, which are explained in terms of thermal reorganization of the local matrix morphology.

Acknowledgment. The Academy of Finland is thanked for financial support. E.M. and R. F. acknowledge the Portuguese Foundation for Science and Technology (Ph.D. grant SFRH/BD/4863/2001 and POCTI/QUI/43366/2001). Dr. Mika Pettersson is thanked for valuable discussions.

Supporting Information Available: Frequencies and intensities for CH_3COOD and CD_3COOH. This material is available free of charge via the Internet at http://pubs.acs.org.

References and Notes

(1) Senent, M. L. *Mol. Phys.* **2001,** *99*, 1311.
(2) Haurie, M.; Novak, A. *J. Chim. Phys.* **1965,** *62*, 137.
(3) Wilmshurst, J. K. *J. Chem. Phys.* **1956,** *6*, 1171.
(4) Weltner, W. *J. Am. Chem. Soc.* **1955,** *77*, 3941.
(5) Berney, C. V.; Redington, R. L.; Lin, K. C. *J. Chem. Phys.* **1970,** *53*, 1713.
(6) Burneau, A.; Genin, F.; Quiles, F. *Phys. Chem. Chem. Phys.* **2000,** 2, 5020.
(7) Nielsen, O. F.; Lund, P.-A. *J. Chem. Phys.* **1983,** *78*, 652.
(8) Johnson, M. R.; Neumann, M.; Nicolai, B.; Smith, P.; Kearly, G. J. *Chem. Phys.* **1997,** 275, 343.
(9) Kosugi, K.; Makabayashy, T.; Nishi, N. *Chem. Phys. Lett.* **1998,** 297, 25.
(10) Grenie, Y.; Cornut, J.-C; Lassegues, J.-C. *J. Chem. Phys.* **1971,** 55, 5844.
(11) Maçôas, E. M. S.; Khriachtchev, L.; Pettersson, M.; Fausto, R.; Räsänen, M. *J. Am. Chem. Soc.* **2003,** 725, 16188.
(12) Khriachtchev, L.; Lundell, J.; Isoniemi, E.;

Räsänen, M. *J. Chem. Phys*. **2000,** *113*, 4265.
(13) Maçôas, E. M. S.; Lundell, J.; Pettersson, M.; Khriachtchev, L.; Fausto, R.; Räsänen, M. *J. Mol. Spectrosc.* **2003,** 279, 70.
(14) Pettersson, M.; Lundell, J.; Khriachtchev, L.; Räsänen, M. *J. Am. Chem. Soc.* **1997,** 779, 11715.
(15) Khriachtchev, L.; Maçôas, E. M. S.; Pettersson, M.; Räsänen, M. *J. Am. Chem. Soc.* **2002,** *124*, 10994.
(16) Goez, M. *Angew. Chem., Int. Ed*. **2003,** *42*, 2336.
(17) Fang, W.-H.; Liu, R.-Z.; Zheng, X.; Phillips, D. L. *J. Org. Chem.* **2002,** *67*, 8407.
(18) Moreira, I. P. R. *J. Mol. Struct.(THEOCHEM)* **1999,** *466*, 119.
(19) Butkovskaya, N. I.; Manke, G. II; Setser, D. W. *J. Phys. Chem.* **1995,** *99*, 11115.
(20) Longfellow, C. A.; Lee, Y. T. *J. Phys. Chem.* **1995,** *99*, 15532.
(21) Owrutsky, J. C; Baronavski, A. P. *J. Chem. Phys.* **1999,** 777, 7329.
(22) Hunnicutt, S. S.; Waits, L. D.; Guest, J. A. *J. Phys. Chem.* **1991,** *95*, 562.
(23) Hunnicutt, S. S.; Waits, L. D.; Guest, J. A. *J. Phys. Chem.* **1989,** *93*, 5188.
(24) Peterman, D. R.; Daniel, R. G.; Horwitz, R. J.; Guest, J. A. *Chem. Phys. Lett.* **1995,** *236*, 564.
(25) Pettersson, M.; Khriachtchev, L.; Jolkkonen, S.; Räsänen, M. *J. Phys. Chem.* A **1999,** *103*, 9154.
(26) Bondybey, V. E.; Brus, L. E. *J. Chem. Phys.* **1975,** *62*, 620.
(27) Schriever, R.; Chergui, M.; Schwentner, N. *J. Phys. Chem.* **1991,** 97, 6124.
(28) Gödderz, K. H.; Schwentner, N.; Chergui, M. *J. Chem. Phys.* **1996,** 705, 451.
(29) Bondybey, V. E.; Räsänen, M.; Lammers, A. *Annu. Rep. Prog. Chem. C* **1999,** *95*, 331.
(30) Frisch, M. I; Tracks, G. W.; Schlegel, H. B.; Scuseria, G. E.; Robb, M. A.; Cheeseman, J. R.; Zakrzewski, V. G.; Montgomery, J. A.; Stratmann, R. E.; Burant, J. C; Dapprich, S.; Millam, J. M.; Daniels, A. D.; Kudin, K. N.; Strain, M. C; Farkas, O.; Tomasi, J.; Barone, V.; Cossi, M.; Cammi, M.; Mennucci, B.; Pomelli, C; Adamo, C; Clifford, S.; Ochterski, J.; Petersson, G. A.; Ayala, P. Y.; Cui, Q.; Morokuma, K.; Malick, D. K.; Rabuck, A. D.; Raghavachari, K.; Foresman, J. B.; Cioslowski, J.; Ortiz, J. V.; Baboul, A. G.; Stefanov, B. B.; Liu, G.; Liashenko, A.; Piskorz, P.; Komaromi, I.; Gomperts, R.; Martin, R. L.; Fox, D. J.; Keith, T.; Al-Laham, M. A.; Peng, C. Y.; Nanayakkara, A.; Gonzalez, C; Challacombe, M.; Gill, P. M. W.; Johnson, B. G.; Chen, W.; Wong, M. W.; Andres, J. L.; Head-Gordon, M.; Replogle, E. S.; Pople, J. A. *Gaussian 98*, revision A.9; Gaussian, Inc.: Pittsburgh, PA, 1998.
(31) van Duijneveldt, F. B.; van Duijneveldt-van de Rijdt, J. G. C. M.: van Lenthe, J. H. *Chem. Rev*. **1994,** *94*, 1873.
(32) Maçôas, E. M. S.; Khriachtchev, L.; Pettersson, M.; Lundell, J.; Fausto, R.; Rasanen, M. *Vibr. Spectrosc.* **2004,** *34*, 73.
(33) He, H.-Y.; Fang, W.-H. *J. Am. Chem. Soc.* **2003,** 725, 16139.
(34) Su, H.; He, Y.; Kong, F. *J. Chem. Phys.* **2000,** *113*, 1891.
(35) Naik, P. D.; Upadhyaya, H. P.; Kumar, A.; Sapre, A. V.; Mittal, J. P. *Chem. Phys. Lett.* **2001,** *340*, **1**16.
(36) Ausloos, P.; Steacie, E. W. R. *Can. J. Chem.* **1955,** *33*, 1530.
(37) Barnes, A. J.; Hallam, H. E. *Trans. Faraday Soc.* **1970,** *66*, 1920.
(38) Dubost, H. *Chem. Phys.* **1976,** *12*, 139.
(39) Abe, H.; Takeo, H.; Yamada, K. M. T. *Chem. Phys. Lett.* **1999,** *311*, 153.
(40) Irvine, M. J.; Mathieson, J. G.; Pullin, A. D. E. *Aust. J. Chem* **1982,** *35*, 1971.
(41) Khoshkhoo, H.; Nixon, E. *Spectrochim. Acta A* **1973,** *29*, 603.
(42) Romano, R. M.; Vedova, C. O. D.; Downs, A. J. *J. Phys. Chem. A* **2002,** *106*, 7235.
(43) Glass, G. P.; Kumaran, S. S.; Michael, J. V. *J. Phys. Chem.* **2000,** *104*, 8360.
(44) Schatte, G.; Willner, H.; Hoge, D.; Knozinger, E.; Schrems, O. *J. Phys. Chem.* **1989,** *93*, 6025.
(45) Lundell, J.; Räsänen, M. *J. Phys. Chem.* **1993,** *97*, 9657.
(46) Lundell, J.; Räsänen, M. *J. Phys. Chem.* **1995,** *99*, 14301.
(47) Heikkila, A.; Pettersson, M.; Lundell, J.; Khriachtchev, L.; Räsänen, M. *J. Phys. Chem. A* **1999,** *103*, 2945.
(48) Khriachtchev, L.; Pettersson, M.; Tuominen, S.; Räsänen, M. *J. Chem. Phys.* **1997,** 707, 7252.
(49) Breda, S.; Lapinski, L.; Reva, I.; Fausto, R. *J. Photochem Photobiol. A.; Chem.* **2004,** *162*, 39.
(50) Jiang, G. J.; Person, W. B.; Brown, K. G. *J. Chem. Phys.* **1975,** *62*, 1201.
(51) Stanton, J. F.; Watts, J. D.; Bartlett, R. J. *J. Chem. Phys.* **1991,** *94*, 404.
(52) Cabana, A.; Savitsky, G. B.; Hornig, D. F. *J. Chem. Phys.* **1963,** *39*, 2942.
(53) Galabov, B.; Yamaguchi, Y.; Remington, R. B.; Shaefer, H. F. III. *J. Phys. Chem. A* **2002,** 706, 819.
(54) Wen, Y.; Segall, J.; Dulligan, M.; Witting, C. *J. Chem. Phys.* **1994,** 707, 5665.
(55) Murto, J.; Ovaska, M. *Spectrochim. Acta A* **1983,** *39*, 149.
(56) Latajka, Z.; Ratajczak, H.; Murto, J.; Orville-Thomas, W. J. *J. Mol. Struct.* **1989,** *194*, 45.
(57) Apkarian, V. A.; Schwentner, N. *Chem. Rev.* **1999,** *99*, 1481.
(58) Khriachtchev, L.; Pettersson, M.; Runeberg, N.; Lundell, J.; Räsänen, M. *Nature* **2000,** *406*, 874.
(59) Milligan, D. E.; Jacox, M. E. *J. Chem. Phys.* **1969,** 57, 277.

TABLE S1 – Observed frequencies and relative intensity [a] of *cis*- and *trans*-CH_3COOD isolated in an Ar matrix at 8 K compared with the values predicted at the MP2/6-311++G(2d,2p) level. The calculated potential energy distribution on the basis of the ab initio harmonic force constant is also shown.

assignment (PED)		ν^{tran}		assignment (PED)	ν^{cis}		$\nu^{cis-trans}$	
		calc	obs		calc	obs	calc	obs
νHCH_2 s. (100)	a'	$3236.7^{(0.8)}$	3039 [b]	νHCH_2 s. (97)	$3229.6^{(0.6)}$		-7.1	
νHCH_2 a. (100)	a''	$3196.0^{(0.6)}$	2997 [b]	νHCH_2 as. (100)	$3178.0^{(1.3)}$		-18.0	
νCH_3 (98)	a'	$3115.3^{(0.4)}$	2952 [b]	νCH_3 (96)	$3099.4^{(1.3)}$		-15.9	
νOD (99)	a'	$2759.3^{(17.6)}$	$2629.0^{(38.4)}$	νOD (99)	$2809.9^{(14.7)}$	$2673.7^{(21.1)}$	+50.6	+44.7
νC=O (83)	a'	$1796.5^{(100.0)}$	$1769.8^{(88.7)}$ $1753.3^{(6.0)}$	νC=O (84)	$1825.3^{(96.0)}$	$1820.2^{(19.4)}$ $1799.8^{(73.6)}$ $1760.1^{(7.4)}$	+28.8	+30.0
δHCH_2 as. (89)	a''	$1506.3^{(3.0)}$	$1437.1^{(2.1)}$	δHCH_2 a. (91)	$1514.2^{(3.0)}$	$1428.7^{(2.0)}$	+7.9	-8.4
δHCH_2 s. (91)	a'	$1500.7^{(6.0)}$	$1434.4^{(3.1)}$ $1381.3^{(4.0)}$	δHCH_2 s. (93)	$1500.7^{(3.4)}$	$1421.4^{(1.4)}$	0.0	-13.0
δCH_3 (91)	a'	$1430.2^{(18.9)}$	$1376.6^{(32.0)}$ $1270.5^{(4.0)}$	δCH_3 (96)	$1421.3^{(15.1)}$	$1367.5^{(23.2)}$ $1241.3^{(4.0)}$	-8.9	-9.1
νC-O (41) + νC-C (23) + δCH_3 (10)	a'	$1303.1^{(68.7)}$	$1266.9^{(73.2)}$	νC-O (39) + νC-C (23) + γCH_3 s. (11)	$1270.3^{(98.9)}$	$1237.9^{(100.0)}$	-32.8	-29.0
γCH_3 a. (71) + γC=O (21)	a'	$1084.6^{(1.9)}$		γCH_3 a. (70) + γC=O (20)	$1078.5^{(1.5)}$	$1043.3^{(3.7)}$	-6.1	
γCH_3 s. (43) + δCOD (27) + νC=O (12)	a'	$1069.1^{(2.0)}$	$1050.2^{(5.3)}$	γCH_3 s. (53) + δCOD (23)	$1059.9^{(16.7)}$	$1035.7^{(1.6)}$	-9.2	-14.5
δCOD (33) + νC-O (35) + γCH_3 s. (27)	a''	$973.7^{(39.7)}$	$955.4^{(31.7)}$	δCOD (45) + νC-O (32) + γCH_3 s. (18)	$903.4^{(0.1)}$		-70.3	
νC-C (60) + νC-O (21) + δCOD (18)	a'	$827.6^{(0.2)}$	835 [b]	νC-C (59) + νC-O (23) + δCOD (15)	$857.8^{(16.3)}$	$839.4^{(12.3)}$	+30.2	+4.4
γC=O (59) + τC-O (23) + γCH_3 a. (18)	a''	$618.1^{(6.9)}$	$603.6^{(9.1)}$	γC=O (77) + γCH_3 a. (20)	$594.5^{(0.7)}$		-23.6	
δOCO (74) + δCOD(14)	a'	$550.4^{(13.4)}$	$544.5^{(23.3)}$	δOCO (81)	$587.9^{(2.7)}$		+37.5	
τC-O (76) + γC=O (23)	a''	$437.4^{(17.7)}$	$421.7^{(15.5)}$	τC-O (92)	$354.2^{(18.4)}$		-83.2	
δCC=O (82)	a'	$420.0^{(2.1)}$	418 [b]	δCC=O (81)	$422.0^{(1.4)}$		+2.0	
τCH_3 (98)	a''	$80.2^{(0.1)}$		τCH_3 (98)	$94.5^{(0.4)}$		+14.3	

[a] The observed and calculated intensities were normalized by the intensity of the strongest band of both *cis* and *trans* conformers. The normalized values are shown in parenthesis.
[b] From ref. 5. Symbols: ν- stretching; δ- bending; γ- rocking; τ-torsion.

TABLE S2 – Observed frequencies (3300-700 cm^{-1}) and relative intensity[a] of *cis*- and *trans*-CD_3COOH isolated in an Ar matrix at 8 K compared with the values predicted at the MP2/6-311++G(2d,2p) level. The calculated potential energy distribution on the basis of the ab initio harmonic force constant is also shown.

assignment (PED)		ν^{trans}		assignment (PED)	ν^{cis}		$\nu^{cis-trans}$	
		calc	obs		calc	obs	calc	obs
νOH (98)	a'	3793.6$^{(19.5)}$	3563.8$^{(36.0)}$	νOH (99)	3859.5$^{(16.0)}$		+65.9	
νDCD_2 s. (99)	a'	2401.2$^{(0.3)}$	2285 [b]	νDCD_2 s. (98)	2394.1$^{(0.2)}$		-7.1	
νDCD_2 as. (100)	a''	2365.2$^{(0.2)}$	2230 [b]	νDCD_2 as. (100)	2352.5$^{(0.5)}$		-12.7	
νCD_3 (98)	a'	2239.2$^{(<0.1)}$	2118 [b]	νCD_3 (98)	2228.4$^{(0.2)}$		-10.8	
						1807$^{(12.6)}$		
			1779.0$^{(13.5)}$			1800.2$^{(4.9)}$		
νC=O (82)	a'	1800.9$^{(74.6)}$	1773.7$^{(38.7)}$	νC=O (83)	1829.0$^{(63.1)}$	1797.8$^{(35.8)}$	+28.1	+24.1
			1379.3$^{(3.8)}$					
			1363.9$^{(4.9)}$					
νC-O (32) + δCOH (29) + νC-C (18)	a'	1371.4$^{(19.7)}$	1331.5$^{(14.4)}$	νC-O (22) + δCOH (40) + νC-C (14) + δCH_3 (13)	1214.4$^{(2.0)}$	1278.0$^{(100.0)}$		-53.5
						1271.5$^{(17.7)}$		
						1246.3$^{(5.0)}$		
δCOH (53) + δCD_3 (12) + νC-C (12) + νC-O (10)	a'	1204.1$^{(56.9)}$	1207.2$^{(29.6)}$	δCOH (50) + νC-O (17) + νC-C (17)	1317.9$^{(100.0)}$	1368.3$^{(6.0)}$	+113.8	+161.1
			1179.7$^{(7.4)}$					
δCD_3 (55) + δDCD_2 s. (17) + νC-O (17)	a'	1104.5$^{(8.1)}$	1156.6$^{(23.9)}$	δCD_3 (51) + δDCD_2 s. (24) + νC-O (16)	1096.1$^{(2.8)}$		-8.4	
δDCD_2 a. (91)	a''	1084.9$^{(0.9)}$	1069.8$^{(6.8)}$	δDCD_2 a. (94)	1090.3$^{(0.8)}$		+5.4	
δDCD_2 s. (80) + δCD_3 (15)	a'	1072.2$^{(6.7)}$	1046.3$^{(1.8)}$	δDCD_2 s. (74) + δCD_3 (20)	1073.0$^{(6.2)}$		+0.8	
			1034.2$^{(2.4)}$					
γCD_3 a. (50) + γC=O(42)	a''	940.9$^{(1.9)}$	985.4$^{(1.5)}$	γCD_3 a. (52) + γC=O(40)	934.0$^{(0.7)}$		-6.9	
			919.3$^{(4.2)}$					
γCD_3 s. (68) + νC-O (14) + δCC=O (10)	a'	834.9$^{(6.3)}$	816.7$^{(7.2)}$	γCD_3 a. (50) + νC-C (21)	829.5$^{(0.4)}$		-5.4	
νC-C (49) + νC-O (26) + δCD_3 (13)	a'	816.0$^{(0.8)}$		νC-C (26) + νC-O (39) + γCD_3 s. (17)	815.3$^{(7.1)}$	800.1$^{(7.2)}$	-0.7	
τC-O (94)	a''	640.2$^{(27.4)}$	609.0$^{(45.8)}$	τC-O (42) + + γC=O (29) + γCH_3 a. (29)	538.4 $^{(4.0)}$		-101.8	
δOCO (81) + νC-C (12)	a'	567.2$^{(8.7)}$	563.1$^{(16.1)}$	δOCO (79) + νC-C (17)	577.7$^{(1.6)}$		+10.5	
γC=O (65) + γCD_3 a.(33)	a''	493.4$^{(2.2)}$	479 [b]	γC=O (35) + τC-O (56) + γCH_3 a. (11)	454.5$^{(22.0)}$		-39.0	
δCC=O (78) + γCD_3 s. (19)	a'	380.9$^{(0.6)}$	408 [b]	δCC=O (76) + γCD_3 s. (20)	388.7$^{(1.2)}$		+7.8	
τCD_3 (97)	a''	58.9 $^{(<0.1)}$		τCD_3 (99)	69.8$^{(0.4)}$		+10.9	

[a] The observed and calculated intensities were normalized by the intensity of the strongest band of both *cis* and *trans* conformers. The normalized values are shown in parenthesis. The observed range of the spectra of the *cis* conformer was limited by an interference filter. [b] From ref. 5. Symbols: ν- stretching; δ- bending; γ- rocking; τ-torsion.

Appendix VII

Rotational isomerism of acetic acid isolated in rare-gas matrices: Effect of medium and isotopic substitution on IR-induced isomerization quantum yield and cis → trans tunneling rate.

Ermelinda M. S. Maçôas, Leonid Khriachtchev, Mika Pettersson, Rui Fausto and Markku Räsänen

J. Chem. Phys. **2004**, *121*, 1331-1338

Rotational isomerism of acetic acid isolated in rare-gas matrices: Effect of medium and isotopic substitution on IR-induced isomerization quantum yield and *cis* → *trans* tunneling rate

E. M. S. Maçôas[a)]
Department of Chemistry, University of Helsinki, P.O. Box 55, FIN-00014 Helsinki, Finland and Department of Chemistry (CQC), University of Coimbra, P-3004-535 Coimbra, Portugal

L. Khriachtchev
Department of Chemistry, University of Helsinki, P.O. Box 55, FIN-00014 Helsinki, Finland

M. Pettersson[b)]
Department of Chemistry, University of Helsinki, P.O. Box 55, FIN-00014 Helsinki, Finland

R. Fausto
Department of Chemistry (CQC), University of Coimbra, P-3004-535 Coimbra, Portugal

M. Räsänen
Department of Chemistry, University of Helsinki, P.O. Box 55, FIN-00014 Helsinki, Finland

(Received 5 April 2004; accepted 21 April 2004)

Rotational isomerization of acetic acid (CH_3COOH) is studied in Ar, Kr, and Xe matrices. The light-induced *trans*→*cis* reaction is promoted using resonant excitation of a number of modes in the 3500-7000 cm^{-1} region, and the quantum yields for this process are measured for various acetic acid isotopologues and matrix materials. For excitation of acetic acid at energies *above* the predicted isomerization energy barrier ($\geq$ 4400 cm^{-1}), the measured quantum yields are in average 2%-3%, and this is one order of magnitude smaller than the corresponding values known for formic acid (HCOOH). This difference is interpreted in terms of the presence of the methyl group in acetic acid, which enhances energy relaxation channels competing with the rotational isomerization. This picture is supported by the observed large effect of deuteration of the methyl group on the photoisomerization quantum yield. The *trans*→*cis* reaction quantum yields are found to be similar for Ar, Kr, and Xe matrices, suggesting similar energy relaxation processes for this molecule in the various matrices. The IR-induced *cis*→*trans* process, studied for acetic acid deuterated in the hydroxyl group, shows reliably larger quantum yields as compared with the *trans*→*cis* process. For pumping of acetic acid at energies *below* the predicted isomerization barrier, the *trans*→*cis* reaction quantum yields decrease strongly when the photon energy decreases, and tunneling is the most probable mechanism for this process. For the *cis*→*trans* dark reaction, the observed temperature and medium effects indicate the participation of the lattice phonons in the tunneling-induced process. © *2004 American Institute of Physics.* [DOI: 10.1063/1.1760733]

I. INTRODUCTION

A large number of molecules have been found to undergo rotational isomerization upon vibrational excitation of the monomer isolated in low-temperature rare-gas matrices.[1-16] In general, it is required that the excitation energy is transferred from the initially excited vibrational mode to the reaction coordinate at energies higher than the reaction barrier.[3] However, it has been recently shown that isomerization of the carboxylic group can take place due to

[a)] Author to whom correspondence should be addressed. Email address: emacoa@qui.uc.pt
[b)] Present address: Department of Chemistry, University of Jyväskylä, P.O.Box 35, FIN-40014, Finland

tunneling even when the excess energy is transferred to the reaction coordinate (C-O torsion) below the reaction barrier.[7]

Isomerization is in competition with other possible energy relaxation channels. In low-temperature matrices, the guest-guest energy transfer is reduced due to the low concentration of the guest molecules. On the other hand, energy relaxation may involve the transfer of excitation energy to the vibrational modes of the lattice.[17] This process can be viewed as a phonon-assisted intramolecular vibrational energy relaxation (IVR), in which the lattice phonons act like a thermal bath that compensates the energy differences between the relevant intramolecular vibrational states. The relaxation rates are then expected to be dependent on the number of phonons involved and on the temperature of the phonon bath.[17] The IR-induced isomerization quantum yield depends on the proportion of energy relaxation channels depositing energy into the reaction coordinate and the lifetimes of the molecular states involved. In rare-gas matrices, those factors are affected by the excitation energy, the host, and the nature of the excited mode.[1,11-13,17,18]

Large quantum yields (20%-40%) were obtained for the IR-induced isomerization of formic acid (HCOOH) excited at various modes above the energy barrier in Ar matrices.[7,19] This high efficiency was connected with the relatively large energy gaps in the vibrational manifold of this molecule that delay energy relaxation within the potential well of the initially excited conformer, allowing isomerization to take place.[19] Similarly, high quantum yields for isomerization were estimated for the HONO molecule excited at the OH stretching mode (νOH) in Kr matrices.[1] In contrast, very low values were reported for $CH_2FC(F)=CH_2$ isolated in solid Ar(10^{-5}%-10^{-2}%).[11]

Acetic acid (CH_3COOH) has two stable structures that are interconverted by rotation around the C-O bond, the *cis* and *trans* conformers shown in Fig. 1. Only recently, the higher energy *cis* conformer was detected experimentally, using excitation of the OH stretching overtone of the *trans* conformer isolated in an Ar matrix.[20] In that work, *cis*-acetic acid was found to tunnel back to the ground conformational state in dark even at temperatures as low as 8 K. According to the *ab initio* calculations, the *trans* → *cis* energy barrier is about 4400 cm^{-1} and the *cis* form is higher in energy than the *trans* form by about 1880 cm^{-1}.[21] For formic acid the corresponding calculated values are ~ 4200 cm^{-1} and ~ 1400 cm^{-1} for the *trans* → *cis* energy barrier and the relative energy of *cis*-formic acid, respectively.[22] Importantly, acetic acid differs from formic acid by the presence of a methyl rotor, which has a low barrier for internal rotation (~ 170 cm^{-1} for the *trans* conformer).[21] In the gas phase, the presence of low barrier internal rotations have been postulated to be responsible for the decrease of the lifetime of excited states associated with vibrations close to the center of flexibility, due to the enhancement of the coupling of vibrational and internal rotational states.[23-27] In the solid phase, the methyl rotor may also enhance couplings between the intramolecular vibrational states and the phonon bath. Thus, the comparison between the isomerization quantum yields for formic and acetic acids in similar experimental conditions aids to evaluate the role of the methyl rotor in the dynamics of vibrational energy relaxation.

In acetic and formic acids, the fast *cis* → *trans* conversion by tunneling poses limitations to the detection of the high energy conformers.[6,28,20] The tunneling rate of matrix isolated *cis*-formic acid was shown to depend on the temperature, the rare-gas host, and even the local environment within the same host (matrix site).[28] In that work, a qualitative interpretation of the experimental results was attempted on the basis of the relative position of the initial and final states of tunneling. At least three solvation effects were pointed out as influencing the tunneling dynamics, namely, the changes in barrier height, nature of the states involved, and energy gaps between the tunneling states. For the moment, the relative impor-

tance of those factors affecting tunneling is still not well understood. Computational simulations and systematic experimental studies of tunneling in different conformational systems, like acetic acid, are two approaches that are likely to give valuable information on the subject.

In the present work, we study the rotational isomerization of matrix-isolated acetic acid under resonant excitation in the 3500-7000 cm^{-1} range and the *cis* → *trans* dark reaction. The dependence of the *trans* → *cis* isomerization quantum yield on the excited vibration, excitation energy, and rare-gas host is evaluated. In addition, the effect of isotopic substitution on the isomerization efficiency is investigated. For the hydroxyl deuterated isotopologues, the isomerization quantum yields are obtained for both the *trans* → *cis* and *cis* → *trans* processes. Finally, the medium and temperature effects on the tunneling rates for the *cis* → *trans* dark reaction are investigated and compared with the available data on formic acid.

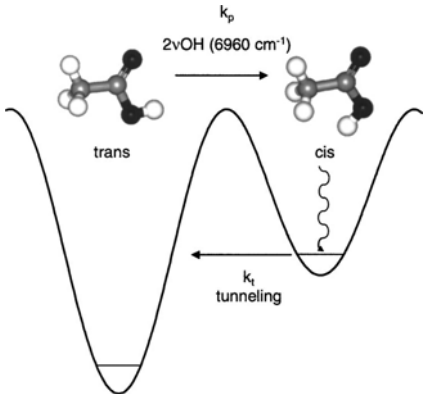

FIG. 1. Isomerization reaction of acetic acid. The *trans* → *cis* isomerization can be induced by excitation of the 2νOH mode of the *trans* conformer isolated in rare-gas matrices, while the *cis* → *trans* process occurs in dark via tunneling. The *trans* → *cis* isomerization barrier of 4432 cm^{-1} and the relative energy for the *cis* conformer of 1882.7 cm^{-1} are calculated by *ab initio* methods (Ref. 21).

II. EXPERIMENTAL DETAILS

The gaseous samples were prepared by mixing acetic acid (Sigma-Aldrich, >99%) or its isotopologues (CD_3COOD and CH_3COOD, Sigma-Aldrich, 99.5%), degassed by several freeze-pump-thaw cycles, with high purity Ar, Kr, and Xe (AGA, >99.99) typically in the 1:2000 or 1:1000 proportions. The CD_3COOH form was obtained from the fully deuterated form by exchange of deuterium with H_2O adsorbed on the inner surface of the sample container and the deposition line. The gaseous mixtures were deposited onto a CsI substrate at 15-35 K (depending on the matrix material) in a closed cycle helium cryostat (APD, DE 202A) and subsequently cooled down to 8 K. The IR absorption spectra (7900-400 cm^{-1}) were measured with a Nicolet SX-60 Fourier transform infrared (FTIR) spectrometer. A liquid-nitrogen-cooled MCT detector and a Ge/KBr beam splitter were used to record the mid-IR absorption spectra (0.25-1.0 cm^{-1} resolution), and a liquid nitrogen cooled InSb detector and a quartz beam splitter were used to record the near-IR absorption spectra (0.5 cm^{-1} resolution). Typically 100-500 interferograms were coadded.

Tunable pulsed IR radiation, provided by an optical parametric oscillator (OPO Sunlite, Continuum, with IR extension) was used to produce *cis*-acetic acid *via* vibrational excitation of *trans*-acetic acid. The pulse duration was ca. 5 ns, the spectral linewidth ~0.1 cm^{-1}, and the repetition rate 10 Hz. The Burleigh WA-4500 wavemeter was used to control the OPO radiation frequency, providing an absolute accuracy better than 1 cm^{-1}. The pumping beam was quasicollinear with the spectrometer beam allowing simultaneous irradiation and recording of IR absorption spectra, and an interference filter transmitting in the 3300-1100 cm^{-1} range was attached to the detector

TABLE I. Vibrational frequencies of *trans-acetic* acid in the 3500-7000 cm^{-1} region for acetic acid isolated in solid Ar. The vibrational assignment is based on the observed fundamental modes for the molecule isolated in solid Ar reported in Ref. 29. Symbols; ν, stretching; δ, bending; τ torsion; and γ, rocking.

CH_3COOH		CH_3COOD		CD_3COOH		CD_3COOD	
assignment	cm^{-1}	assignment	cm^{-1}	assignment	cm^{-1}	assignment	cm^{-1}
νOH	3564	νOD	2629	νOD	3564		
νOH + γC=O	4096	νCH_3 + νCO	4215	νOH + δCC=O	3941		
νOH + τCO	4201	νHCH_2 + νCO	4264		3946		
$\nu HCH_2 + \delta CH_3$	4411	$\nu HCH_2 + \delta CH_3$	4410	νOH + γC=O	4041		
νOH + δCOH	4708	νOD + νC=O	4396	νOH + τCOH	4173	νOD + νC=O	4392
$\nu OH + \delta CH_3$	4876	$\nu HCH_2 + \delta HCH_2$	4464	$\nu OH + \delta CH_3$	4710		
		2νOD	5170	νOH + νC-O	4881	2νOD	5168
νOH + νC=O	5351		5148	νOH + νC=O	5335		
2νOH	6957			2νOH	6958		

to prevent its exposure to the pumping radiation.

For the CH_3COOH and CD_3COOH isotopologues, a photoequilibrium of the *trans* and *cis* forms is established under IR pumping of the *trans* conformers, as a result of the interplay between *cis*-acetic acid photogeneration and its depletion due to tunneling. At the equilibrium, the pumping and tunneling rates are equal:

$$k_p(\nu)[trans\text{-}CH_3COOH]_{eq}=k_t(T)[cis\text{-}CH_3COOH]_{eq}. \quad (1)$$

It follows that the averaged pumping rate $k_p(\nu)$ can be determined from the tunneling rate $k_t(T)$, and the ratio of the *cis* and *trans* photoequilibrium concentrations, as described elsewhere.[19] For these calculations, the bands corresponding to the CH_3 bending of *trans*-CH_3COOH, the C=O stretching of *cis*-CH_3COOH, the COH bending of *trans*-CD_3COOH and the C-O stretching mode of *cis*-CD_3COOH were used.[29] Since deuteration of the hydroxyl group decreases the tunneling rate by orders of magnitude, for the CH_3COOD and CD_3COOD species the pumping rate coefficients were determined directly from the pumping-induced changes in concentration of one of the conformers.[20] For these two isotopologues, the concentrations were obtained from the integrated absorption of the bands corresponding to the C-O stretches of the *trans* and *cis* forms.[29] To avoid the influence of tunneling on the determination of the pumping rates, only the points obtained in the first 10 min of irradiation were considered for the OD-substituted species. Once the pumping rates are known, the quantum yields of the rotamerization processes $\phi(i)$ can be extracted from the following equation:

$$k_p(\nu) = \phi(i)\sigma^i_T(\nu)I(\nu), \quad (2)$$

where $\sigma^i_T(\nu)$ (in cm^2) is the absorption cross section of the excited mode, I (in s^{-1} cm^{-2}) is the photon intensity of the pumping beam and i refers to the excited vibrational mode. The absorption cross section is obtained using the measured IR absorption at the excitation frequency, the known acetic acid concentration, and the matrix thickness. We estimated that the experimental error associated with the quantum yield values is roughly 50%.

III. EXPERIMENTAL RESULTS

After deposition, the matrix-isolated acetic acid is found in the most stable *trans* geometry. The vibrational modes of *trans*-

acetic acid observed in the 3500-7000 cm^{-1} spectral region for the monomer isolated in solid Ar are listed in Table I, and the absorption wavenumbers in the mid-IR region can be found elsewhere.[20,29,30] The vibrational assignments for the overtone and combination modes presented in this table were based on the reported values for the fundamental modes and on the expected isotopic shifts.[20,29] For the molecule isolated in Kr and Xe matrices, the observed modes in the 3500-7000 cm^{-1} range appear shifted to lower frequencies as compared with the values found in an Ar matrix, as a consequence of the known matrix effect caused by guest-host interactions. This effect is illustrated in Table II where the bands observed in the Ar, Kr, and Xe matrices are listed for the CH_3COOH isotopologue.

The *trans* → *cis* isomerization was induced by irradiating the sample at frequencies corresponding to some of the most intense bands in the 3500-7000 cm^{-1} spectral region. In Fig. 2, the spectral changes induced in the regions of the OH and C=O stretches by pumping at the νOH overtone (2νOH) of CH_3COOH are shown. The isomerization quantum yields estimated for several excited modes in various matrices are listed in Table III and plotted in Fig. 3. For the CH_3COOH isotopologue, the quantum yield is essentially independent of the excited mode, when the excitation energy is *above* the calculated isomerization barrier (~ 4400 cm^{-1}). The obtained quantum yields are about one order of magnitude smaller than the values measured for formic acid under similar experimental conditions (see Fig. 3).[7,19,31] At energies *below* ~ 4400 cm^{-1}, the quantum yield depends strongly on the excitation energy.

For CD_3COOD, the quantum yields obtained by excitation of the 2νOD and the νOD + τC=O combination mode were found to be 0.011 and 0.016, being similar to the values for CH_3COOH (averaged value for pumping above the calculated isomerization barrier ~ 0.025). On the other hand, the quantum yields obtained for CD_3COOH (0.15 for 2νOH, and 0.085 for νOH + νC=O) and CH_3COOD (0.0036 for 2νOD) differ from each other and from the averaged values for CH_3COOH (~ 0.025, see Fig. 3).

The concentration of the *cis* conformer is limited by the low *trans* → *cis* isomerization quantum yield and by the *cis* → *trans* tunneling (Fig. 4).[20] Therefore, the data concerning the photoinduced *cis* → *trans* process is much more limited. For the OH-isotopologues, the *cis* → *trans* tunneling rate is fast (see Fig. 4),[20] which practically prevents measurement of the quantum yield for the *cis* → *trans* isomerization process. However, in the case of the OD-isotopologues the tunneling is much slower,[20] and we could follow the pumping kinetics while exciting the 2νOD band of

TABLE II. Vibrational frequencies of *trans*-CH_3COOH in the 3500-7000 cm^{-1} region in solid Ar, Kr, and Xe. The vibrational assignment is based on the observed fundamental modes for the molecule isolated in solid Ar reported in Ref. 29. The splitting of bands observed for Kr and Xe are due to site effects. Symbols; ν, stretching; δ, bending; τ torsion; and γ, rocking.

Assignment	Ar	Kr	Xe
νOH	3564	3552	3546
		3551	3538
		3549	3532
			3528
νOH + γC=O	4096	4082	4066
		4079	
νOH + τCO	4201	4190	4171
$\nu HCH_2 + \delta CH_3$	4411	4400	4403
νOH + δCOH	4708	4694	4678
$\nu OH + \delta CH_3$	4876	4866	4846
νOH + νC=O	5341	5326	5306
			5303
2νOH	6957	6932	6887
			6881

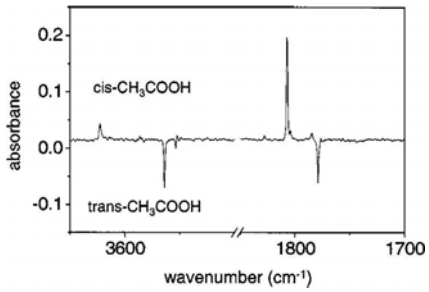

FIG. 2. Difference IR absorption spectrum obtained by excitation of the 2νOH mode of the *trans* form. The bands at 3564 and 1779 cm^1 belong to the *trans* form of acetic acid, and the bands at 3623 and 1807 cm^{-1} belong to the *cis* form.

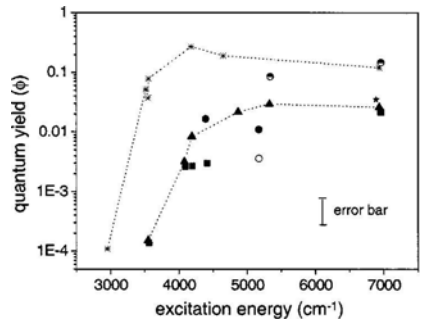

FIG. 3. Quantum yield for the IR-induced *trans* → *cis* isomerization of acetic acid [CH_3COOH in solid Ar (■), Kr (▲); and Xe ★); and CD_3COOH (◓), CH_3COOD (o), and CD_3COOD (●) in solid Ar]. The results for the *trans* → *cis* isomerization of formic acid in solid Ar are shown for comparison (*).The *trans* → *cis* isomerization barriers calculated for acetic and formic acid are ~ 4400 and 4200 cm^{-1}, respectively (Refs. 21, 22).

the *cis* form at ≈ 5258 cm^{-1}, i.e., well above the predicted *cis* → *trans* isomerization barrier. This enables estimation of the quantum yields for the *cis* → *trans* isomerization in CD_3COOD and CH_3COOD. In both cases, the quantum yield was found to be reliably higher than that for the corresponding *trans* → *cis* isomerization (by a factor of 40 for CD_3COOD and by a factor of 3 for CH_3COOD).

TABLE III. Quantum yields for the IR-induced *trans*→ *cis* isomerization of acetic acid isolated in rare-gas matrices. The relative error has been estimated as 50% of the quantum yield value.

Excited mode/ Energy (cm^{-1})		Ar	Kr
CH_3COOH[a]			
νOH	[b]3554	1.4×10^{-4}	1.5×10^{-4}
νOH + γC=O	[b]4090	2.6×10^{-3}	3.2×10^{-3}
νOH + τCO	[b]4195	2.7×10^{-3}	8.4×10^{-3}
$\nu HCH_2 + \delta CH_3$	[b]4406	3.0×10^{-3}	...
$\nu OH + \delta CH_3$	4866	...	2.2×10^{-2}
νOH + νC=O	5326	...	2.9×10^{-2}
2νOH	[b]6944	2.2×10^{-2}	2.6×10^{-2}
CH_3COOD			
2νOD	5170	3.6×10^{-3}	...
CD_3COOH			
νOH + νC=O	5335	8.5×10^{-2}	...
2νOH	6958	1.5×10^{-1}	...
CD_3COOD			
νOD + νC=O	4392	1.6×10^{-2}	...
2νOD	5168	1.1×10^{-2}	...

[a]The quantum yield determined for pumping at the 2νOH mode of the molecule isolated in solid Xe is 3.5×10^{-2}. [b]Average value used for pumping acetic acid in the Ar and Kr matrices. Symbols; ν, stretching; δ, bending; τ torsion; and γ, rocking.

The effects oftemperature and medium on the dark *cis* →*trans* reaction of acetic acid were evaluated by following the tunneling kinetics at various temperatures and in different rare-gas matrices. The Arrhenius plots are shown in Fig. 4. The tunneling rate is found to be similar in Ar and Kr matrices, and it is enhanced by a factor of ~ 5 in a Xe matrix. The tunneling rate increases at higher temperatures. The data for the temperature dependence in a Xe matrix is less accurate because of the large tunneling rates. Deuteration of the methyl group increases the tunneling rate. This is shown by comparing the values measured for CD_3COOH and CD_3COOD (7.1×10^{-2} s^{-1} and 1.1×10^{-6} s^{-1}, respectively) with those obtained for CH_3COOH and CH_3COOD (2.1×10^{-2} s^{-1} and 7.3×10^{-7} s^{-1}, respectively), as measured in solid Ar at 8 K.

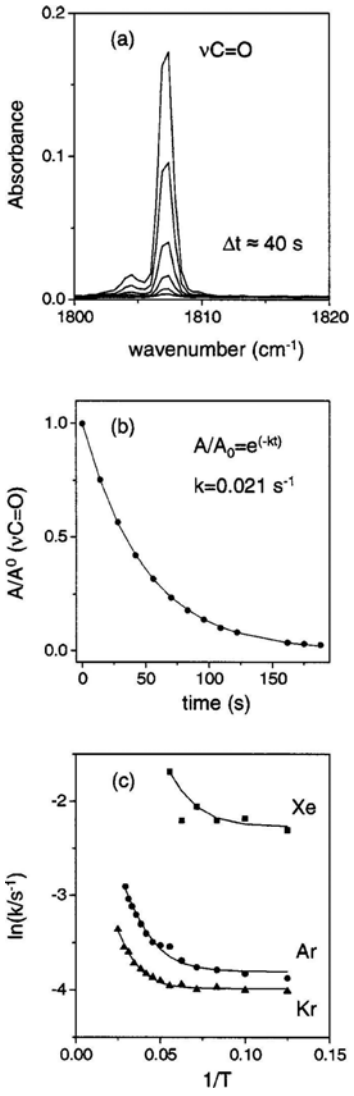

FIG. 4 . Tunneling kinetics for the *cis* → *trans* isomerization of acetic acid in rare-gas matrices: (a) time decay of the νC=O band of *cis*-CH_3COOH in solid Ar at 8 K, (b) exponential fit of the integrated intensity of this band, and (c) Arrhenius plots for the *cis* → *trans* tunneling rate. In plot (c), the experimental data are fitted using an expression for a temperature dependent rate constant [$k(T)= k_0 + k_1 exp(-E_a/RT)$], where k_0, k_1 and E_a are the parameters. The extracted activation energies (E_a) are (57 ± 4), (72 ± 4), and (53 ± 12) cm^{-1}, the k_0 values are (0.0223 ± 0.0007), (0.0186 ± 0.0002), and (0.104 ± 0.005) s^{-1}, and the k_1 values are (0.40 ± 0.07), (0.24 ± 0.03) and (6 ± 6) s^{-1} for Ar, Kr and Xe, respectively.

IV. DISCUSSION

A. Quantum yield for the IR-induced isomerizations

For the 2νOH mode (~ 7000 cm^{-1}) of the CH_3COOH isotopologue, the quantum yield estimated for the three matrix materials (2.2%, 2.6%, and 3.5%, in Ar, Kr, and Xe, respectively) increases slightly with the polarizability of the rare gas as found previously for other compounds.[3,4] However, the values here reported for the three matrices are still within a possible experimental error. Therefore, the quantum yield for acetic acid *trans* → *cis* isomerization is not strongly affected by the rare-gas host; in particular, the activated relaxation channels and their efficiency seem to be similar in various matrices.

At excitation energies above the calculated isomerization barrier (>4400 cm^{-1}), the quantum yields for the *trans* → *cis* process in Ar and Kr matrices at 8 K show no difference for various modes (within the experimental error), the obtained values being around 2%-3%. The energy above which the quantum yield reaches a relatively stable value (4500 cm^{-1}) agrees with the computational barrier height, which supports the theoretical estimation. The lack of evident mode specific effects on the quantum yield was also reported for formic acid in solid Ar[7,19,31] For both molecules, the range of excitation energies probed corresponds to the discrete region of vibrational states and, thus, mode specific effects are generally possible. We can speculate that the observed lack of mode specificity in the isomerization quantum yield is connected with a slow isomerization rate, allowing effective randomization of the excitation energy between various modes. The coupling of the intramolecular vibrational states with the lattice possibly plays an important role in this randomization process. It should be remembered that the experiment probes the probability of becoming trapped in either well, and after excitation the molecule may undergo isomerization back and forth between the *trans* and *cis* forms before

cooling sufficiently to be trapped in either well. The time between initial excitation and trapping may indeed be long enough to allow extensive randomization of energy irrespective of the initially excited mode. Another possibility is that all excited states decay essentially to a few common low energy states with a dominant contribution to the energy relaxation dynamics. The excitation energy introduced into the molecule is still in the low density of states where such bottleneck states could be found.

Deuteration of the methyl group increases the quantum yield for the *trans* → *cis* isomerization from 2%-3% to 8%-15%, as seen from comparison of the values obtained for CH_3COOH and CD_3COOH. This difference shows that the methyl group plays an important role in the isomerization dynamics. It may be that CH_3 yields faster energy relaxation process than CD_3 because its higher energy modes can participate in lower-order couplings leading to a more efficient nonreactive deactivation of the excited states.

Deuteration of the hydroxyl group decreases the quantum yield by almost one order of magnitude (from 2%-3% to 0.4%). This information is provided by the values obtained for the almost isoenergetic vibrations of CH_3COOH and CH_3COOD at ~5250 cm^{-1}. In the case of deuteration of the hydroxyl group, the reaction coordinate is directly affected by the isotopic substitution, which decreases the frequency of the τC-O mode. Therefore, at similar energies, the τC-O coordinate should be in a higher excited state in CH_3COOD than in CH_3COOH. Thus, in CH_3COOH the couplings between the τC-O and the excited states are expected to be of lower order than those in CH_3COOD, which relatively increases the isomerization efficiency in CH_3COOH.

Remarkably, no significant difference is observed between the isomerization quantum yields for CH_3COOH and CD_3COOD. This observation is in agreement with the previous discussion. Indeed, in the perdeuterated isotopologue, two opposite effects due to isotopic substitution in the methyl group (increase in the quantum yield) and in the hydroxyl group (decrease in the quantum yield) seem to compensate each other, leading to a minor net effect.

Several modes with energies below the computed isomerization barrier (e.g., pumping at ~ 4200, 4100, and 3560 cm^{-1}) were also found to be active in promoting the *trans* → *cis* process in acetic acid. In this case, a tunneling mechanism is presumably involved. As shown in Fig. 3, for these excitations, the quantum yield increases strongly with the energy. A similar dependence of the quantum yield on the excitation energy is observed for formic acid in solid Ar. The effect was previously explained based on the delocalization of the torsional wave functions between the *cis* and *trans* potential wells.[7]

As seen in Fig. 3, the isomerization quantum yield is about one order of magnitude higher for formic acid than for acetic acid. As already mentioned, the presence of the methyl group in acetic acid can enhance the coupling of intramolecular vibrational states with each other and with lattice motion. Additionally, the low-frequency modes originated by the methyl group are capable of participating in the energy relaxation similar to the lattice phonon. Possibly these two effects lead to an increase of the rate for intramolecular energy transfer and/or to an increase in the number of relaxation channels competing with isomerization.[25] On the other hand, large-amplitude vibrations such as τC-O and τC-C are thought to be considerably anharmonic and, thus, strong coupling between the two internal rotors of acetic acid may also be operating. This is particularly important, since the methyl motion has a lower frequency than τC-O and part of the energy deposited into the reaction coordinate may also be dissipated through the methyl motion without isomerization. Another interesting observation is that the isomerization quantum yield starts decreasing at energies lower by ~ 500 cm^{-1} for formic acid than for

acetic acid, in qualitative agreement with the predicted lower isomerization barrier for formic acid. The difference between the energy barriers is also experimentally supported by the large gap (roughly two orders of magnitude) between isomerization yields for pumping of formic and acetic acids at the OH-stretching modes.

The reverse, *cis* → *trans* photoinduced isomerization of acetic acid was also investigated. In this case, excitation of the 2νOD mode of *cis*-CD_3COOD and *cis*-CH_3COOD was found to be more efficient in promoting the isomerization than the excitation of the same mode of the corresponding *trans* conformers to promote the *trans* → *cis* conversion. The energy barrier for the *cis* → *trans* process was estimated to be ≈1880 cm^{-1} lower than for the *trans* → *cis* conversion.[21] Hence, this factor may partially contribute to the observed difference in the isomerization quantum yields. However, this explanation is not supported by the fact that the *trans* → *cis* quantum yields here reported are practically insensitive to the excitation energy, as long as it is above the calculated isomerization barrier. Furthermore, the barrier height is the same for CD_3COOD and CH_3COOD, but the relative changes in quantum yield are quite different ($\phi_{c/t} \approx 44$ for CD_3COOD and $\phi_{c/t} \approx 3$ for CH_3COOD, where $\phi_{c/t}$ denotes the ratio of the *cis* → *trans* and *trans* → *cis* quantum yields). Accordingly, this factor does not seem to be the dominant one in the studied system. A similar behavior was also observed for HONO isolated in solid Kr ($\phi_{c/t} \approx 7$), where the isomerization barriers (E_i) for the direct and reverse processes are nearly identical (ΔE_i = 130 cm^{-1}).[1] For the case of HONO, it has been suggested that kinetic or potential couplings between the excited vibrations and nearly resonant vibrational states could be responsible for the more efficient energy transfer from the excited states to the reaction coordinate upon excitation of the *cis* isomer.[32,33] These factors may also be relevant for acetic acid.

B. Tunneling rate for the *cis* → *trans* dark reaction

As mentioned earlier, the *cis* → *trans* isomerization of acetic acid is observed in dark. As it was discussed for the analogous case of formic acid,[28] the initial state in this dark process is essentially the ground state of the *cis* conformer and the final state is some excited vibrational level of the *trans* conformer.[20] From this excited state the energy relaxes via a cascading process controlled by the energy gaps between intramolecular states and mode couplings. The observed temperature dependence of the tunneling rate for the *cis* → *trans* isomerization of acetic acid (see Fig. 4) indicates participation of low energy quanta in the tunneling process, which compensates the energy mismatch between the intramolecular levels involved in the process.[17,18] The fitting of the tunneling kinetics measured in the three studied matrices with a temperature dependent rate of the type $k(T) = k_0 + k_1 \exp(-E_a/RT)$ yields activation energies of 50-80 cm^{-1} (see Fig. 4). These activation energy values are consistent with the participation of lattice phonon modes in the tunneling process in the various hosts, where the Debye frequencies range from 40 to 70 cm^{-1}.[34] In addition, it should be remembered that the methyl torsion (estimated below 100 cm^{-1} in the *cis* conformer) (Ref. 21) might also be involved in the mechanism.

For acetic acid, the *cis* → *trans* tunneling rate is larger by at least one order of magnitude (for all hosts at 8 K) than the tunneling rate observed for formic acid.[28] The faster tunneling in acetic acid can be primarily connected to its predicted lower barrier for the *cis* → *trans* conversion as compared with formic acid, the computed difference being ~ 300 cm^{-1}.[21,22] Note that the increase in the *cis* → *trans* tunneling rate is quantitatively similar to the decrease in the *trans* → *cis* isomerization quantum yield, discussed earlier. It follows that the faster tunneling rate for acetic acid can also be a consequence of an efficient deac-

tivation of the excited state of the *trans* form by the low-energy states of the methyl group.

For acetic acid, the tunneling rate in solid Ar is somewhat higher than in solid Kr, while in solid Xe the rate is faster than in those two matrices by a factor of ~5. A significantly different matrix effect was observed for formic acid, where the tunneling rates increase in the order $k_{Ar} > k_{Kr} > k_{Xe}$.[28] This difference indicates a very specific dependence of the tunneling rate on the solute-solvent interactions in the studied systems. For formic acid, the dependence of the tunneling rate with the matrix host was interpreted as resulting from the interplay of three factors determined by solvation effects.[28] It was shown that the tunneling rate can also be affected by the local environment within the same host.[28] Practically, this means that any detailed interpretation of the observed matrix effect is not realistic at the moment due to the high complexity of the system. Particularly in acetic acid, the lower energy vibrational modes of the methyl group may participate in the tunneling mechanism, in addition to the phonon modes.

Some general ideas can be extracted from the comparison of the tunneling rates for different isotopologues in a given matrix. As expected, the tunneling rate was found to decrease by ca. four orders of magnitude upon substitution of the tunneling particle (OH → OD) both for CH_3 and CD_3 containing isotopologues in Ar matrices.[20] On the other hand, for the CD_3COOH isotopologue, the tunneling rate in solid Ar at 8 K (7.1×10^{-2} s^{-1}), is about three times faster than that observed for CH_3COOH in the same experimental conditions (2.1×10^{-2} s^{-1}). Similarly, the tunneling rate for the fully deuterated species (1.1×10^{-6} s^{-1}) is almost twice faster than for CH_3COOD ($7.3\times10^{-7}s^{-1}$). These relative values of tunneling rates can be correlated with an increased efficiency in the energy dissipation within the *trans* well in the acetic acid isotopologues bearing a deuterated methyl group. The smaller energy quanta of the deuterated methyl group can provide a better match with the small energy gap to be overcome in the tunneling process. However, this interpretation is certainly an oversimplification, since the change of the intramolecular vibrational structure occurring upon isotopic substitution may also change both the nature of the states and order of coupling with the phonons involved in the tunneling process.[28]

V. CONCLUSIONS

Narrowband tunable IR radiation was used to excite selectively various vibrational modes in the 3500-7000 cm^{-1} spectral region of monomeric acetic acid isolated in rare-gas matrices. The isomerization quantum yields for both *trans* → *cis* and *cis* → *trans* processes were estimated, and the influence of medium, isotopic substitution, and nature of the excited vibrational mode were investigated. The higher energy conformer (*cis*) of acetic acid tunnels back to the conformational ground state (*trans*) even at the lowest working temperature used (8 K). The effects of temperature and medium on the kinetics of the phonon-assisted tunneling process were also addressed.

The main conclusions to be drawn from this study are as follows:

(1) Above the calculated isomerizaton barrier (~ 4400 cm^{-1}), the quantum yield of the IR-induced *trans* → *cis* isomerization of acetic acid in solid rare gases is rather insensitive to the excited vibrational mode and the rare-gas host. The IR-induced *cis* → *trans* isomerization is more efficient than the *trans* → *cis* process. Below 4400 cm^{-1}, the quantum yield for the *trans* → *cis* isomerization depends strongly on the excitation energy, and this is probably due to the participation of tunneling in the IR-induced mechanism.

(2) Deuteration of the methyl group increases the *trans* → *cis* isomerization quantum yield, while deuteration of the hydroxyl group has the opposite effect. This behavior is probably connected with the different orders of couplings between the excited modes. In the CD_3-isotopologues as compared with the CH_3-isotopologues, the less efficient couplings between the excited

modes and the methyl torsion seem to decrease the rate of deactivation of the excited states, increasing the isomerization probability. In the OD-isotopologues as compared with the OH-isotopologues, less efficient couplings between the excited vibrational states and the τCO mode could be responsible for a lower efficiency of energy transfer to the reaction coordinate.

(3) On average, the *trans* → *cis* isomerization quantum yield is one order of magnitude smaller for acetic acid (CH_3COOH) than the values for formic acid (HCOOH).[7,19] The presence of the low-barrier methyl rotor increases the number of states coupled to the initially excited state, thus probably increasing the number of accessible energy relaxation channels that deactivate the excited mode without transferring energy to the reaction coordinate.

(4) For acetic acid, the *cis* → *trans* tunneling rates of the dark reaction follow the trend $k_{Xe}>>k_{Ar}>k_{Kr}$, which differs from the case of formic acid ($k_{Ar}>k_{Kr}>k_{Xe}$).[28] This result indicates that the tunneling kinetics depends on specific solvation effects. The *cis* → *trans* tunneling rate is larger for acetic acid than for formic acid by at least one order of magnitude (at 8 K). This difference is presumably connected with the lower isomerization barrier predicted for acetic acid. In addition, this behavior can also be connected with the low-frequency modes of the methyl group in acetic acid increasing the efficiency of the energy relaxation within the *trans* well.

ACKNOWLEDGMENTS

The Academy of Finland is thanked for financial support. E.M. and R.F. acknowledge the Portuguese Foundation for Science and Technology (Ph.D. Grant No. SFRH/BD/4863/2001 and POCTI/QUI/43366/2001).

[1] L. Khriachtchev, J. Lundell, E. Isoniemi, and M. Räsänen, J. Chem. Phys. **113,** 4265 (2000).
[2] A. J. Barnes, J. Mol. Struct. **113,** 161 (1984).
[3] M. Räsänen, H. Kunttu, and J. Murto, Laser Chem. 9, 123 (1988).
[4] T. Lotta, J. Murto, M. Räsänen, and A. Aspiala, J. Mol. Struct. **114,** 333 (1984).
[5] S. Sander, H. Willner, L. Khriachtchev, M. Pettersson, M. Räsänen, and E. L. Varetti, J. Mol. Spectrosc. **203,** 145 (2000).
[6] M. Pettersson, J. Lundell, L. Khriachtchev, and M. Räsänen, J. Am. Chem. Soc. **119,** 11715 (1997).
[7] M. Pettersson, E. M. S. Maçôas, L. Khriachtchev, R. Fausto, and M. Räsänen, J. Am. Chem. Soc. **125,** 4058 (2003).
[8] H. H. Gunthard, J. Mol. Struct. **113,** 141 (1984).
[9] R. N. Perutz, Chem. Rev. (Washington, D.C.) 85, 97 (1985).
[10] S. Kudoh, M. Takayanagi, M. Nakata, T. Ishibashi, and M. Tasumi, J. Mol. Struct. **479,** 41 (1999).
[11] A. K. Knudsen and G. C. Pimentel, J. Phys. Chem. **95,** 2823 (1991).
[12] W. F. Hoffman and J. S. Shirk, Chem. Phys. **78,** 331 (1983).
[13] P. Roubin, S. Varin, P. Verlaque, S. Coussan, J. M. Berset, J. M. Ortega, A. Peremans, and W. Q. Zheng, J. Chem. Phys. **107,** 7800 (1997).
[14] M. Poliakoff and J. J. Turner, in *Chemical and Biochemical Applications of Lasers,* edited by C. B. Moore (Academic, New York, 1980), Vol. 5.
[15] H. Frei and G. C. Pimentel, in *Chemistry and Physics of Matrix-Isolated Species,* edited by L. Andrews and M. Moskovits (Elsevier Science, Amsterdam, 1989).
[16] H. Frei and G. C. Pimentel, Annu. Rev. Phys. Chem. 36, 491 (1985).
[17] F. Legay, in *Chemical and Biochemical Applications of Lasers,* edited by C. B. Moore (Academic, New York, 1977), Vol. II.
[18] V E. Bondybey, M. Räsänen, and A. Lammers, Annu. Rev. Phys. Chem. **95,** 331 (1999).
[19] E. M. S. Maçôas, L. Khriachtchev, M. Pettersson, J. Juselius, R. Fausto, and M. Räsänen, J. Chem. Phys. **119,** 11765 (2003).
[20] E. M. S. Maçôas, L. Khriachtchev, M. Pettersson, R. Fausto, and M. Räsänen, J. Am. Chem. Soc. **125,** 16188 (2003).
[21] M. L. Senent, Mol. Phys. **99,** 1311 (2001).
[22] J. D. Goddard, Y. Yamaguchi, and H. F. Schaefer, J. Chem. Phys. 96, 1158 (1992).
[23] K. W. Holtzclaw and C. S. Parmenter, J. Chem. Phys. **82,** 5283 (1985).
[24] C. S. Parmenter and B. M. Stone, J. Chem. Phys. 84, 4710 (1986).
[25] A. McIlroy and D. I. Nesbitt, J. Chem. Phys. **101,** 3421 (1994).
[26] G. A. Bethardy, X. L. Wang, and D. S. Perry, Can. J. Chem. **72,** 652 (1994).
[27] D. S. Perry, G. A. Bethardy, and X. L. Wang, Ber. Bunsen-Ges. Phys. Chem. **99,** 530 (1995).
[28] M. Pettersson, E. M. S. Maçôas, L. Khriachtchev, J. Lundell, R. Fausto, and M. Räsänen, J. Chem. Phys. **117,** 9095 (2002).
[29] E. M. S. Maçôas, L. Khriachtchev, R. Fausto, and M. Räsänen, J. Phys. Chem. A **108,** 3380 (2004).
[30] C. V. Berney, R. L. Redington, and K. C. Lin, J. Chem. Phys. 53, 1713 (1970).
[31] E. M. S. Maçôas, L. Kriachtchev, M. Pettersson, J. Lundell, R. Fausto, and M. Räsänen, Vib. Spectrosc. 34, 73 (2004).
[32] Y Guan, G. C. Lynch, and D. L. Thompson, J. Chem. Phys. **87,** 6957 (1987).
[33] F. Richter, M. Hochlaf, P. Rosmus, F. Gatti, and H. D. Meyer, J. Chem. Phys. **120,** 1306 (2004).
[34] H. J. Jodl, in *Chemistry and Physics of Matrix-Isolated Species,* edited by L. Andrews and M. Moskovits (Elsevier Science, Amsterdam, 1989).

Appendix VIII

Internal rotation in propionic acid: Near-infrared induced isomerization in solid argon.

Ermelinda M. S. Maçôas, Leonid Khriachtchev, Mika Pettersson, Rui Fausto and Markku Räsänen,

J. Phys. Chem., **2005**, *109*, 3617-3624

Internal rotation in propionic acid: Near-infrared induced isomerization in solid argon

Ermelinda M. S. Maçôas, *,†,‡,§ Leonid Khriachtchev, † Mika Pettersson, †,‖ Rui Fausto, ‡ and Markku Räsänen†

Laboratory of Physical Chemistry, University of Helsinki, P.O.Box 55, FIN-00014 Helsinki, Finland, and Department of Chemistry (CQC), University of Coimbra, P-3004-535 Coimbra, Portugal.

Received: December 30, 2004; In Final Form: March 9, 2005

The conformational system of propionic acid (CH_3CH_2COOH) is studied in solid argon. It is predicted by the ab initio calculations that this molecule has four stable conformers. These four structures are denoted T_t, $T_g^{\pm}$, C_t and $C_g^{\pm}$, and they differ by the arrangement around the C-O and C_α-C bonds. The ground-state T_t conformer is the only form present at 8 K after deposition of an argon matrix containing propionic acid. For the CH_3CH_2COOH and CH_3CH_2COOD isotopologues, narrow-band excitation of the first hydroxyl stretching overtone of the conformational ground state promotes the C_α-C and C-O internal rotations producing the $T_g^{\pm}$ and C_t conformers, respectively. A subsequent vibrational excitation of the produced $T_g^{\pm}$ form induces its conversion into the $C_g^{\pm}$ conformer by rotation around the C-O bond. In dark, all the produced conformers decay to the conformational ground state with different rates. The decay kinetics and its temperature dependence allow identification of the conformers by IR absorption spectroscopy, which is supported by ab initio calculations of their vibrational spectra. For the CH_3CH_2COOD isotopologue, excitation of molecules isolated in different matrix sites results in site-dependent photoisomerization rates for the C_α-C and C-O internal rotations, which also confirms identification of the photoproducts.

Introduction

In a recent series of papers, we have studied the IR-induced rotational isomerization of formic and acetic acids isolated in low-temperature inert matrices.[1-7] These studies have been mainly motivated by our interest in the conformational dynamics of the carboxylic group as a way to understand the process of intramolecular vibrational energy relaxation, which plays an important role in molecular reactivity. Interestingly, the photolysis of formic acid was shown to be conformationally dependent, being acknowledge as one of the first clear cases of optical control of chemical reactivity.[4,8] The study of the conformational properties of simple carboxylic acids can improve our knowledge on more complex molecular systems with biological interest, where the conformation of this functional group plays an important role in determining their biological activity.[9-11] Furthermore, the understanding of the conformational properties of small molecules and their response to photochemical stimuli are essential to the evaluation of the potential use of more complex molecules with biconformational structure as molecular switches controlled by light.[12,13]

* To whom correspondence should be addressed. E-mail: emacoas@qui.uc.pt.

† University of Helsinki.

‡ University of Coimbra.

§ Present address: Department of Chemistry (CQC), University of Coimbra, P-3004-535 Coimbra, Portugal.

‖ Present address: Department of Chemistry, NanoScience Center, University of Jyväskylä, P. O. Box 35, FIN-40014, Finland

Compared to acetic acid, propionic acid (propanoic acid, CH_3CH_2COOH) has one additional internal rotational degree of freedom. Besides the methyl and hydroxyl rotations occurring in acetic acid, the internal rotation around the C_α-C bond should be taken into account in the case of propionic acid. Experimentally, only one conformer of monomeric propionic acid has been unequivocally characterized.[14-16] Both gas-phase electron diffraction and microwave spectroscopy studies have shown that this conformer exhibits a planar heavy-atom backbone, with a staggered arrangement around the C_β-C_α bond and *trans* arrangements around the C_α-C and C-O bonds (C-C-C-O and C-C-O-H dihedral angles of 180º).[14-16] Moreover, the electron diffraction results suggested that, in addition to the identified conformer, structures bearing a non-planar C-C-C-O skeleton should also contribute to the gas-phase equilibrium conformational distribution with an estimated population of ca. 40% (T= 488 K).[14]

The earlier computational studies on the conformational isomerism in propionic acid, undertaken at the ab initio Hartree-Fock (HF) level of theory with the relatively modest 6-31G* basis set,[17] and using the molecular mechanics (MM) approach[18] predicted two stable arrangements with respect to the C_α-C bond, the *trans* and *gauche* (C-C-C-O dihedral angle of ca. ±60º) arrangements. The doubly degenerate *gauche* arrangement has been estimated by MM to be 490 cm^{-1} higher in energy than the *trans* arrangement,[18] whereas the HF/6-31G* calculations predicted a slightly smaller *gauche*-*trans* energy difference (~340 cm^{-1}).[17] The *trans*-*gauche* barrier estimated by the HF/6-31G* calculations was ~ 420 cm^{-1},[17] which was in a good agreement with a more recent value of 490 cm^{-1} obtained using the density functional theory (DFT) method with the B3LYP functional and the 6-311++G(2d,2p) basis set.[19] The relative stability of these two C_α-C arrangements can be compared with other carbonyl compounds structurally related to propionic acid, such as propionyl fluoride and propionyl chloride (CH_3CH_2COX, with X= F, and Cl), which have been studied previously.[20,21] These molecules were shown to be stable in the *trans* and *gauche* conformations with respect to the C_α-C bond (C-C-C-X dihedrals of 180º and ca. ±60º, respectively).[20, 21] In solutions of liquid rare gases, the energy difference between the *trans* and the *gauche* conformers and the *trans* → *gauche* isomerization barrier were found to be 329 and 680 cm^{-1} in propionyl fluoride, and 505 and 820 cm^{-1} in propionyl chloride, respectively.[20,21] For chloroacetic acid ($CH_2ClCOOH$), the *gauche* arrangement around the C_α-C bond was estimated to be 120-400 cm^{-1} higher in energy than the *trans* form, with a *trans* → *gauche* isomerization barrier of ca. 500 cm^{-1} for the monomer isolated in rare-gas matrices.[22-24]

Computationally, in addition to the two stable arrangements around the C_α-C bond, propionic acid has two stable conformations differing in the arrangement around the C-O bond, corresponding to the planar *trans* and *cis* configurations characterized by C-C-O-H dihedrals of 180º and 0º, respectively.[18,19] Similarly to formic and acetic acids,[1,5] in propionic acid the *trans* arrangement of the carboxylic group is the lowest-energy configuration. According to the MM and DFT/B3LYP calculations, the energy difference between the two configurations is ca. 1700-2100 cm^{-1}.[18, 19] The *trans* to *cis* barrier associated with internal rotation around the C-O bond estimated by the same methods is 4300-4600 cm^{-1}.[19] These results are in good agreement with the data for formic and acetic acids (energy difference of ~ 1400-1800 cm^{-1} and *trans* to *cis* barrier of ~ 3900-4400 cm^{-1}).[25-28] For the matrix-isolated monomers of formic and acetic acids, the *cis* conformer is short-lived, even at 8 K, because of its conversion to the *trans* conformer by tunneling with a rate of ~10^{-2}-10^{-3} s^{-1},[3,7] which complicates the experimental characterization of the *cis* conformer of these molecules. A similar phenomenon can also be expected also for propionic acid.

In the present study, the rotational isomerization of monomeric propionic acid isolated in solid argon was investigated. The ground-state potential energy surface (PES) and the vibrational spectra of its different conformers were calculated at the MP2/6-311G++(2d,2p) level of theory. The computational results support analysis of the experimental data obtained using the low-temperature matrix-isolation technique combined with narrow-band pumping of individual vibrational transitions.

Experimental and Computational Details

The gaseous samples were prepared by mixing propionic acid (>99%), degassed by several freeze-pump-thaw cycles, with high-purity argon (99.9999%), in the 1:1000 or 1:500 ratio. The CH_3CH_2COOD species was obtained from the fully hydrogenated isotopologue by H/D exchange on both the inner surface of the sample container and the deposition line saturated with D_2O. The OH and OD isotopologues of propionic acid are referred to as PA-OH and PA-OD. The gaseous mixtures, initially kept at room temperature, were deposited onto a CsI substrate at 15 K in a closed-cycle helium cryostat (APD, DE 202A) and subsequently cooled down to 8 K. The IR absorption spectra (7900–400 cm^{-1}) were measured with a Nicolet SX-60 FTIR spectrometer. A liquid-nitrogen-cooled MCT detector and a Ge/KBr beam splitter were used to record the mid-IR absorption spectra, with spectral resolutions of 0.25 to 1.0 cm^{-1}. A liquid-nitrogen-cooled InSb detector and a quartz beamsplitter were used to record the near-IR (NIR) absorption spectra, with a spectral resolution of 0.5 cm^{-1}. Typically 100 to 500 interferograms were co-added.

Tunable pulsed IR radiation provided by an optical parametric oscillator (Continuum, OPO Sunlite with IR extension) was used to excite the first overtone of the hydroxyl stretching mode (2νOH or 2νOD) of various conformers of propionic acid. The pulse duration was ca. 5 ns, the spectral linewidth ~0.1 cm^{-1} and the repetition rate 10 Hz. The

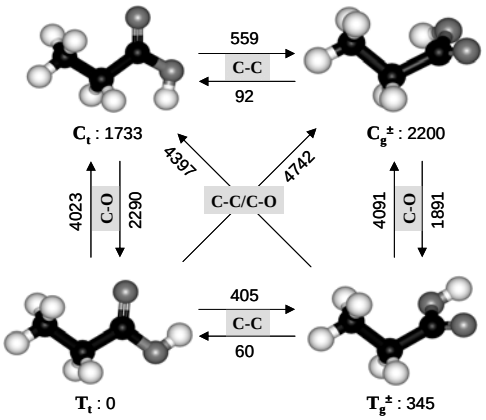

Figure 1. Conformers of propionic acid. Shown are the ab initio [MP2/6-311++G(2d,2p)] relative conformational energies and energy barriers for the internal rotation around the C_α-C and C-O bonds (in cm^{-1}).

pulse energy of the OPO in the 7000-5000 cm^{-1} spectral region is ~0.5 mJ. The Burleigh WA-4500 wavemeter measured the OPO radiation frequency providing an absolute accuracy better than 1 cm^{-1} for the pumping radiation. Whenever necessary, the IR absorption spectra were collected during pumping to compensate the *cis* to *trans* tunneling decay. In the latter case, the pumping beam was quasi-collinear with the spectrometer beam, and an interference filter transmitting in the 3300-1100 cm^{-1} region was attached to the detector to prevent its exposure to the pumping radiation.

The ab initio calculations were performed using the Gaussian 98 package of programs.[29] The structural, energetic and vibrational properties of the propionic acid conformers were studied at the MP2/6-311++G(2d,2p) level of approximation,[30] which is a higher level than the one used in previous studies.[17-19] The 1D and 2D potential energy curves connecting the conformers of propionic acid were calculated at the same level of theory. The calculated frequencies have been rescaled with the correction factors 0.94, and 0.97,

for bands observed above and below 2000 cm^{-1}, respectively. The scaling factors are used following Radom and Scott.[31] Transformation of the ab initio Cartesian harmonic force constants to the molecule-fixed internal coordinates system allowed the ordinary normal coordinate analysis as described by Schachtschneider.[32] This procedure evaluates the potential energy distribution (PED) associated with each normal vibrational mode under the harmonic assumption. The symmetry coordinates used to perform the normal coordinate analysis are defined in Table S1 provided as Supporting Information (SI).

Results

1. Computational Results. In agreement with previous theoretical predictions,[17-19] the present ab initio calculations give four nonequivalent minima on the PES of propionic acid. The geometries of the four conformers, their relative energies, and the barriers to internal rotation around the C-O and C_α-C bonds are shown in Figure 1. The potential energy profiles for conformational interconversion are shown in Figure 2. Only one possible arrangement around the C_α-C_β bond is stable, which minimizes steric repulsion between the methyl and methylene hydrogen atoms. In the present article, the stable arrangements with respect to the C-O bond (*trans* and *cis*) are denoted by the capital letters T and C, respectively, and the small letters refer to the arrangements around the C_α-C bond (*t* for the *trans*, and $g^\pm$ for the two degenerate *gauche* arrangements).

As generally found for simple carboxylic acids,[1,5,28] the *cis* arrangement around the C-O bond is higher in energy than the *trans* configuration by ca. 1800 cm^{-1} ($\Delta E_{C_t-T_t}$ ~ 1730 cm^{-1} and $\Delta E_{C_g^\pm-T_g^\pm}$ ~ 1860 cm^{-1}, see Figure 1), and the isomerization barrier for conversion of the *trans* into the *cis* arrangement is ca. 4000 cm^{-1} ($E_{T_t\rightarrow C_t}$ ~ 4020 cm^{-1}, and $E_{T_g^\pm\rightarrow C_g^\pm}$ ~ 4090 cm^{-1}, see Figures 1 and 2). The calculated energy differences between the conformers agree with the earlier computational studies whereas our T→C barrier is somewhat lower than the results at a lower level of approximation.[18,19]

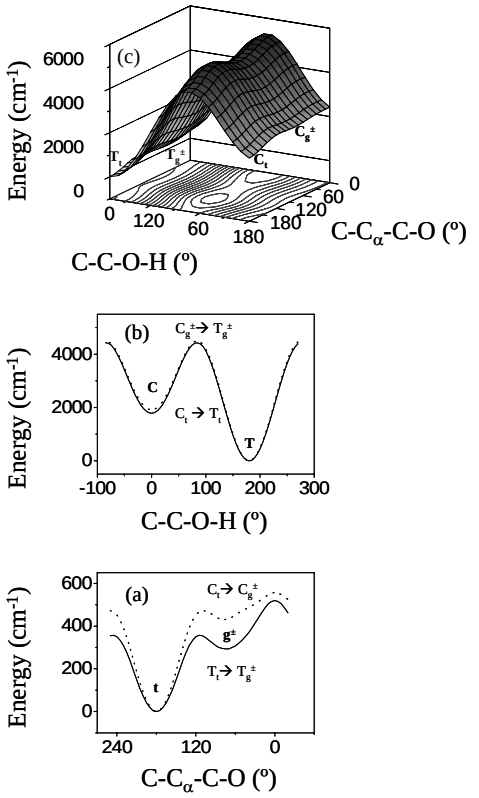

Figure 2. One- and two-dimensional potential energy surfaces (PES) of propionic acid as a function of the C_α-C, and C-O torsional coordinates. (a) Rotation along the C_α-C axis, which corresponds to the $T_t \leftrightarrow T_g^\pm$ (solid line) and $C_t \leftrightarrow C_g^\pm$ (dotted line) isomerization reactions. (b) Rotation along the C-O axis, which corresponds to the $T_t \leftrightarrow C_t$ (solid line), and $T_g^\pm \leftrightarrow C_g^\pm$ (dotted line) isomerization reactions. (c) Simultaneous rotation along the C_α-C and C-O axis. The lowest energy minimum is set to zero.

In agreement with known experimental and computational results,[14-19] the most stable arrangement around the C_α-C bond corresponds to the *trans* configuration, whereas the degenerate *gauche* configurations (C-C-C-O dihedral angle of approximately ±75º) are somewhat higher in energy than the corresponding *trans* forms ($\Delta E_{T_g^\pm-T_t}$~340 cm^{-1} and $\Delta E_{C_g^\pm-C_t}$ ~ 470 cm^{-1}).

The barrier for internal rotation around the C_α-C bond was found to be ca. 500 cm^{-1} ($E_{T_t \rightarrow T_g^{\pm}}$ ~ 400 cm^{-1} and $E_{C_t \rightarrow C_g^{\pm}}$ ~ 560 cm^{-1}).

The calculated energy difference between the *gauche* and *trans* C_α-C arrangements in propionic acid is similar to the corresponding values in lipids, saturated hydrocarbons (150-400 cm^{-1}),[33-36] and other α-substituted carbonyl compounds, such as propionyl fluoride, propionyl chloride and chloroacetic acid.[20-23] The energy barrier predicted for the *trans*→*gauche* C_α-C internal rotation in propionic acid is closer to those found in propionyl fluoride and propionyl chloride (680-820 cm^{-1})[20,21] rather than to the average values reported for saturated hydrocarbons (1000-1400 cm^{-1}).[33-36]

Direct interconversion between the two degenerate *gauche* configurations of the C-C-C-O moiety (i.e., the $T_g^+ \rightarrow T_g^-$ or $C_g^+ \rightarrow C_g^-$ processes) can also take place (Figure 2). The transition state for these processes corresponds to the *syn* configuration around the C_α-C bond. The calculated *syn* barriers for the $T_g^+ \rightarrow T_g^-$ and $C_g^+ \rightarrow C_g^-$ processes are ~ 180 cm^{-1} and 100 cm^{-1}, respectively. These values are somewhat smaller than those obtained previously at a lower level of theory (240 cm^{-1}).[17] The *syn* barriers found for propionic acid are also lower than the corresponding barriers in propionyl fluoride (258 cm^{-1})[21] and propionyl chloride (1230 cm^{-1} or 558 cm^{-1}, depending on the method used).[20]

The direct conversion between the conformers differing by internal rotation about *both* C-O and C_α-C bonds (the $C_g^{\pm}/T_t$ and $C_t/T_g^{\pm}$ pairs of conformers, see Figure 1) can be also estimated. The second-order transition state associated with the simultaneous rotation along the two torsional coordinates (C_α-C/C-O) was found in the 2D potential energy curve at ~ 4740 cm^{-1} above the conformational ground state. Interestingly, in this second-order transition state, the C-C-C-O and C-C-O-H dihedral angles agree with the first- order transition states found along each of the torsional coordinates (116º and 83º, respectively).

2. Experimental Results. The T_t conformer is the only form present in the as-deposited matrix. For both PA-OH and PA-OD, the spectrum of T_t shows the splitting of bands due to the interaction of the isolated molecule with inhomogeneous local surroundings (matrix site effect). For PA-OH, the absorption bands of the fundamental and first overtone of the hydroxyl stretching mode (νOH and 2νOH, respectively) are shown in Figure 3. Conformational isomerization was induced site selectively by using tunable narrow-band radiation as found for HONO[37] and formic acid.[2,38] The site selectivity upon excitation of the 2νOH mode of PA-OH is demonstrated in Figure 3, which shows holes burned in the νOH absorption envelope of T_t upon pumping at four different frequencies.

When the deposited PA-OH(D)/Ar matrix is irradiated at ~ 6960 cm^{-1} (2νOH) or ~ 5170 cm^{-1} (2νOD), the bands of the T_t conformer decrease and new bands emerge. The light-induced spectral changes are due to conformational isomerization induced by vibrational excitation of the T_t conformer. The emerging bands can be divided into two sets assigned to the $T_g^{\pm}$ and C_t forms (see later). The two sets of bands are distinguished by their behaviour upon IR pumping and dark decay kinetics at 8-15 K.

In the case of PA-OH, the spectral changes induced by excitation of the T_t form are shown in trace (a) of Figure 4. Trace (b) illustrates the changes taking place after several minutes in the dark. One set of light-induced bands quickly decreases (k ~ 6 x 10^{-2} s^{-1}) after interrupting the pumping, whereas the other set is much more stable (k ~ 10^{-6} s^{-1}). The quickly decaying bands (marked with dots in Figure 4) originate from the C_t conformer and the more stable bands belong to the $T_g^{\pm}$ form. In both cases, the decay of the photoproduced conformers regenerates the T_t form. Remarkably, the $T_g^{\pm} \rightarrow T_t$ recovering process is strongly enhanced at higher temperatures as shown in Figure 5 (1 order of magnitude variation in the rate

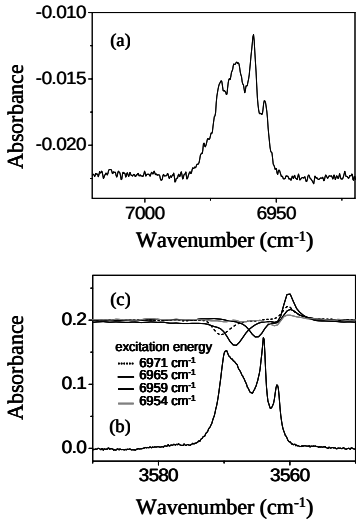

Figure 3. Absorption bands of the T_t and $T_g^{\pm}$ conformers of propionic acid in an Ar matrix at 8 K: (a) 2νOH (~6970 cm^{-1}) mode of T_t, (b) νOH (~3570 cm^{-1}) mode of T_t, and (c) difference spectra showing the photoinduced changes in the νOH absorption after irradiation of the 2νOH mode of T_t at different frequencies where the T_t bands decrease and the $T_g^{\pm}$ bands increase.

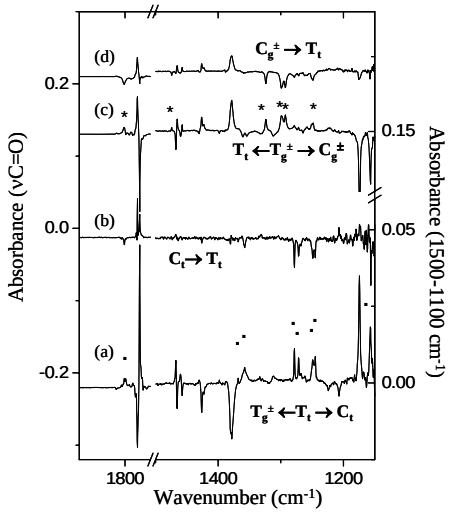

Figure 4. Spectral changes upon excitation of the 2νOH mode of T_t, and $T_g^{\pm}$ conformers [traces (a) and (c), respectively] and dark decay of the C_t (■) and $C_g^{\pm}$ (*) conformers [traces (b) and (d), respectively]. Difference spectra (a) and (c) are obtained by subtracting the spectra recorded before pumping from those recorded under pumping. Difference spectra (b) and (d) are obtained by subtracting the spectra recorded under pumping from those recorded after a few minutes in the dark.

constant upon changing between 8 K and 12 K).

Excitation of the 2νOH mode of the $T_g^{\pm}$ conformer (at ~ 6950 cm^{-1}) promotes its conversion back to the T_t form and its isomerization to a new species identified as the $C_g^{\pm}$ conformer [see trace (c) in Figure 4]. The photoinduced $T_g^{\pm} \rightarrow T_t$ conversion is a very efficient process, transferring *ca.* 70% of the molecules from the $T_g^{\pm}$ to the T_t state in a few minutes of irradiation. The bands of the $C_g^{\pm}$ conformer (marked with an asterisk in Figure 4) can be observed only *during* the pumping of $T_g^{\pm}$ because they quickly decay in the dark. The decrease of the $C_g^{\pm}$ bands is accompanied with a growth of the T_t bands, showing that this conformer decays to the most stable conformer. The fast dark decay of both C_t and $C_g^{\pm}$ conformers is due to a phonon-assisted tunneling process, which has been shown to be common for internal rotation around the C-O bond in simple carboxylic acids, like formic and acetic acids.[3,7]

For the deuterated isotopologue (PA-OD), the C_t and $T_g^{\pm}$ conformers produced by excitation of the T_t form are quite stable at 8 K. In fact, when compared to PA-OH, the C_t to T_t conversion by tunnelling slows down by *ca.* 4 orders of magnitude. Nevertheless, the spectral signatures of the two photoproduced conformers could also be reliably separated for this isotopologue. First, the emerging bands of the two photoproduced conformers grow at different rates when pumping at different frequencies within the 2νOD absorption of the T_t conformer [high-frequency pumping (*HF*) at ~5175 cm^{-1} and low-frequency pumping (*LF*) at 5170 cm^{-1}]. These results are shown in Figures 6 and 7 [traces (a) in both figures] as difference spectra, where the C_t and $T_g^{\pm}$

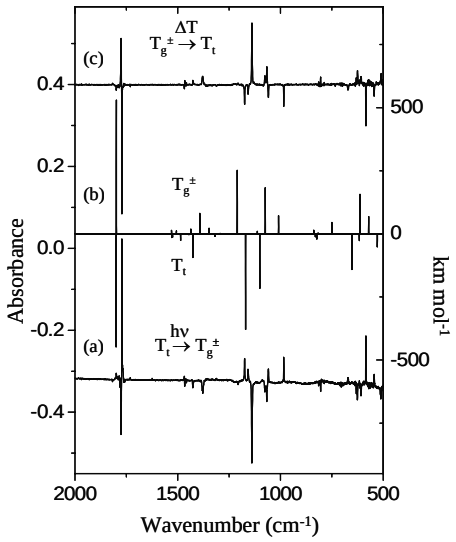

Figure 5. Difference IR absorption spectra for PA-OH showing (a) the effect of excitation of the 2νOH mode of the monomer isolated in an Ar matrix, (b) the MP2/6-311G(2d,2p) calculated spectra for the T_t (negative bands) and $T_g^{\pm}$ (positive bands) forms of propionic acid, and (c) the effect of annealing an Ar matrix containing the T_t and $T_g^{\pm}$ conformers at 12 K for ~20 min.

bands increase and the T_t bands decrease. Second, the two conformers decay at different rates in dark upon annealing. The $T_g^{\pm} \rightarrow T_t$ isomerization at 15 K is faster at least by two orders of magnitude than the $C_t \rightarrow T_t$ process [see trace (c) in Figure 7]. Finally, it is also possible to selectively excite the 2νOD mode of the $T_g^{\pm}$ conformer (which appears slightly redshifted from the 2νOD absorption of T_t). The excitation of $T_g^{\pm}$ decreases its bands, and a new set of bands emerges that can be assigned to the $C_g^{\pm}$ conformer, and the T_t form is partially recovered. Without the pumping of $T_g^{\pm}$, the $C_g^{\pm}$ conformer converts to the most stable T_t conformer. As for the $C_t \rightarrow T_t$ tunnelling, the $C_g^{\pm} \rightarrow T_t$ is much slower in PA-OD than in PA-OH (roughly by two orders of magnitude). Tables 1 and 2 present the observed frequencies for the four conformers of matrix-isolated PA-OH and PA-OD

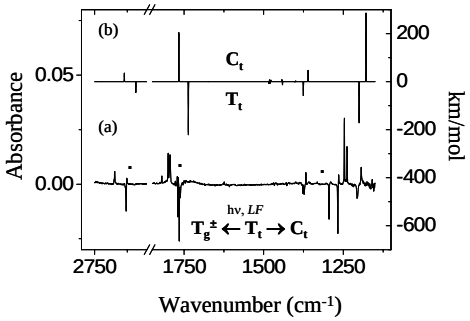

Figure 6. Difference IR absorption spectra for PA-OD showing (a) the result of vibrational excitation of the T_t conformer at 5170 cm^{-1} (LF) and (b) the MP2/6-311++(2d,2p) calculated spectra for the T_t (negative bands) and C_t (positive bands) forms. In plot (a) the bands of the C_t and $T_g^{\pm}$ (marked with dots) conformers increase, and the T_t bands decrease.

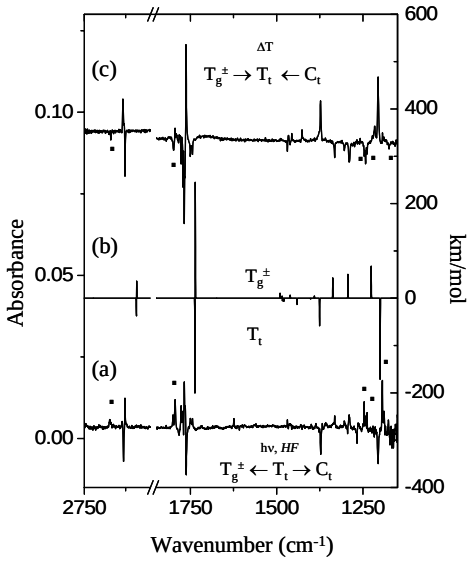

Figure 7. Difference IR absorption spectra for PA-OD showing (a) the result of vibrational excitation of the T_t conformer at 5175 cm^{-1} (HF); (b) the MP2/6-311++(2d,2p) calculated spectra for the T_t (negative bands) and $T_g^{\pm}$ (positive bands) conformers and (c) the effect of annealing an Ar matrix containing the T_t, $T_g^{\pm}$, and C_t forms at 15 K for ~15 min. In plot (a), the bands of the C_t (marked with dots) and $T_g^{\pm}$ conformers increase, and the T_t bands decrease. In plot (c), the opposite behavior is observed; the T_t bands increase, and the bands of $T_g^{\pm}$, and C_t (marked with dots) are bleached.

together with the corresponding calculated [MP2/6-311++G(2d,2p)] frequencies, intensities, and PEDs.

Discussion

1. Conformational cooling during sample deposition. Taking into consideration the calculated relative energies of the four conformers of propionic acid, the populations of the T_t and $T_g^{\pm}$ conformers are expected to be approximately 73% and 27 %, at room temperature (accounting for the degeneracy of the T_g forms), whereas those of C_t and $C_g^{\pm}$ should be below 1%. Note that at 488 K the estimated populations of the T_t and $T_g^{\pm}$ forms based on their computational relative energies are 58 and 42%, in good agreement with the experimentally estimated populations of propionic acid conformers with planar and nonplanar heavy-atom skeleton (ca. 50% and 40%, respectively).[14] Therefore, if the low-temperature matrix could efficiently freeze the equilibrium population of the deposited gaseous conformational mixture, it should have been possible to detect the presence of both T_t and $T_g^{\pm}$ forms in the deposited matrix. However, for both PA-OH and PA-OD, only one conformer was found to be present in the deposited matrixes, whose spectral signature closely matches that predicted for the most stable T_t conformer (see Figures 5 and 6 and Tables 1 and 2). The absence of the $T_g^{\pm}$ conformer can be attributed to its fast conversion to the lowest-energy conformer during deposition at 15 K. This conformational cooling is commonly associated with low isomerization barriers (< 400 cm^{-1}).[39,40] Indeed, the computational barrier for the $T_g^{\pm} \rightarrow T_t$ isomerization is ~60 cm^{-1}, which supports the fact that the $T_g^{\pm}$ form, presumably present in the gaseous mixture, can easily decay to the ground conformational state. In agreement with this interpretation, we observed the decay of the photoproduced $T_g^{\pm}$ conformer back to T_t by an over-barrier process with strong temperature dependence, which is consistent with the calculated $T_g^{\pm} \rightarrow T_t$ isomerization barrier.

2. Assignment of the spectra of PA-OH. The spectra of the T_t and $T_g^{\pm}$ conformers are compared in Figure 5. The difference spectrum shown by trace (a) was obtained by subtracting the spectrum of the deposited matrix from the spectrum recorded after several minutes of irradiation of T_t and 1 min in the dark. The dark period leads to a decay of the C_t conformer into the T_t form, hence this spectrum shows only the result of the $T_t \rightarrow T_g^{\pm}$ photoprocess. A comparison of trace (a) with the calculated spectra of T_t and $T_g^{\pm}$ shown in trace (b) demonstrates good general agreement between the experiment and theory. This agreement makes the assignment of the spectrum of both the T_t form present in the deposited matrix and the photoproduced $T_g^{\pm}$ form straightforward. However, two discrepancies between the calculated and experimental spectra of $T_g^{\pm}$ can be noticed. First, none of the four bands of $T_g^{\pm}$ predicted to appear in the 1400-1200 cm^{-1} region are clearly observed experimentally and the absence of the medium-intensity νC-O band predicted at 1350 cm^{-1} is especially remarkable. Second, the high-intensity band predicted at 1174 cm^{-1} (δCOH) appears as a doublet at 1174 and 1157 cm^{-1}. The first discrepancy is probably due to the computational overestimation of the band intensities and/or to the broadening of the experimental bands in this spectral region, which makes them difficult to discriminate from the background. Indeed, four broad weak bands are seen in the 1400-1200 cm^{-1} region that can correspond to the apparently missing $T_g^{\pm}$ vibrations (Table 1). However, it is highly probable that the observed doublet at 1174/1157 cm^{-1} is with due to a Fermi resonance between δCOH and the first overtone of the C-O torsion whose fundamental is observed at 584 cm^{-1}. Similar splitting of the νC-O or δCOH bands due to Fermi resonance was reported for formic and acetic acids.[6,38]

In the 3300-1100 cm^{-1} spectral window available for observation of the C_t

TABLE 1: Experimental[a] and Calculated [MP2/6-311++(2d,2p)][b] Frequencies for the Four Conformers of CH_3CH_2COOH Monomer.

assignment (PED)[c]	Tt			assignment (PED)[c]	Tg[c]			assignment (PED)[c]	Ct			assignment (PED)[c]	Cg[c]		
	ν_{exp}	ν_{calc}	I_{calc}		ν_{exp}	ν_{calc}	I_{calc}		ν_{exp}	ν_{calc}	I_{calc}		ν_{exp}	ν_{calc}	I_{calc}
νOH (98)	3568.7 3565.0	3564.6	23	νOH (98)	3560.2	3563.1	23	νOH (99)		3622.6	18	νOH (99)		3624.5	16
νHCH_2 a. (95)	3000.6	3003.0	4	νCH_2' (52) + νHCH_2' (38)	3007.4	3008.6	4	νHCH_2 a. (98)		3007.3	4	νCH_2' (50) + νHCH_2' (37)		3000.4	4
νHCH_2 s. (100)	2996.3	2999.4	4	νHCH_2 (84)	2989.8	2996.2	3	νHCH_2 s. (100)		3001.0	4	νHCH_2 (85)		2996.6	4
νCH_2 a. (94)	2957.1	2959.8	-	νHCH_2' (60) + νCH_2 (26)	2973.3	2988.2	2	νCH_2 a. (97)		2940.3	1	νHCH_2' (61) + νCH_2' (22)		2980.4	2
νCH_2 s. (100)	2952.4	2920.0	3	νCH_2 (94)		2937.0	2	νCH_3 (100)		2920.4	4	νCH_2 (83)		2915.5	4
νCH_3 (100)	2938.1	2918.8	4	νCH_3 (100)	2894.0 1798.6	2912.7	5	νCH_2 s. (100)	1807.3	2898.1	4	νCH_3 (99)		2909.4	4
	1817.0				1791.7				1804.1						
νC=O (81)	1776.0 1774.7	1745.3	74	νC=O (80)	1784.6 1771.3	1744.5	85	νC=O (83)	1801.4 1798.2	1773.4	61	νC=O (82)	1802.1	1769.6	72
δHCH_2 s. (87)	1466.2	1483.5	3	δHCH_2 (84)	1467.5	1490.3	3	δHCH_2 s. (88)		1481.6	2	δHCH_2 (55) + δHCH_2' (29)	1474.4	1488	4
δHCH_2 a. (90)	1457.9	1479.2	2	δHCH_2' (89)	1458.8	1484.1	2	δHCH_2 a. (89)		1477.4	2	δHCH_2' (59) + δHCH_2 (19)		1483.2	2
δCH_2 (97)	1426.6 1423.2	1441.2	4	δCH_2 (91)	1430	1460.9	2	δCH_2 (98)		1443.1	3	δCH_2 (80) δCH_3 (100)		1466.2 1396.5	1
δCH_3 (89)	1380.9	1445.3		δCH_3 (98)	1360.9	1391.6	2	δCH_3 (99)		1399.4	1	ωCH_2 (65)	1323.9	1328.0	21
ωCH_2 (46)	1377.8	1383.1	17	νC-O (14) + ωCH_2 (31)	1354.3	1350.5	13	ωCH_2 (68)	1368.1 1357.6	1361.3	20	$twCH_2$ (43)	1298.8 1292.7	1283.4	39
δCOH (44) + ωCH_2 (24)	1224.4	1278.9	2	ωCH_2 (51)	1332.6	1307.1	4	$twCH_2$ (74)		1274.0		δCOH (45) + $twCH_2$ (24)	1250.9 1248.7	1246.6	48
$twCH_2$ (74) + γCH_3 (19)	1207.5	1265.8		$twCH_2$ (48)	1310.7	1254.4		δCOH (71)	[FR]1278.4 1271.7	1254.4	100	γCH_3 (18) + δCOH (24) +		1174.7	
								γCH_2 + τC-O	[FR]1250.5 1246.0			νC-O (18) + γCH_2 (19)			
νC-O (25) + δCOH (24)	1138.6	1134.7	62	δCOH (48) 2τCO	[FR]1174.3 [FR]1157.1	1173.7	40	νC-O (34)	1156.2	1133.7	11	ωCH_3 (42)		1074.1	1
γCH_3 (37) + γCH_2 (31)	1075.8	1092.9		ωCH_3 (40)		1079.0	2	γCH_3 (37) + γCH_2 (30)		1087.9		γCH_3 (12) + νC-CH_3 (22) + $twCH_2$ (16) + νC-O (15)		1038.5	6
ωCH_3 (24) + νC-CH_3 (32)	1066.7 1066.6	1067.7	36	γCH_3 (13) + νC-C=O (22) + τωCH_2 (13) + νC-O (14)	1059.1	1041.7	33	ωCH_3 (23) + νC-CH_3 (32) + νC-O (23)		1069.0	6				
νC-CH_3 (44) + ωCH_3 (23)		999.6		νC-CH_3 (58)	984.0	978.9	12	νC-CH_3 (46) + ωCH_3 (25)		997.2	1	νC-CH_3 (57)		973.0	8
νC-C=O (46)	814.2 812.3	805.3	2	νC-C=O (37) + νC-O (21)	814.4 807.9	812.4	2	νC-C=O (41) + νC-O (21)		808.4	8	νC-C=O (34) + νC-O (22)		810.1	8
γCH_2 (33) + γCH_3 (33)	804.6	798.6	3	γCH_2 (42) + γCH_3 (33)	800.3	791.9		γCH_2 (35) + γCH_3 (34) + γC=O (20)		804.3	2	γCH_2 (44) + γCH_3 (33)		788.6	
τC-O (81)	625.6	632.3	25	γC=O (45)	671.5 668.6	727.2	7	δOCO (50)		608.3	1	γC=O (56)		715.5	
δOCO (49)	607.9	597.6	5	τC-O (75)	584.2	594.4	26								
γC=O (54)	510.7 502.8	512.6	8	δOCO (60)	544.2	553.7	11	γC=O (41) + γCH_2 (28) + τC-O (25) δCC=O (38)		561.9 459.1	2	δOCO (64) + νC-C=O (24)		570.8	2
												τC-O (90)		466.3	30
δCC=O (36) + δOCO (23)		456.9	6	δCC=O (75)		427.9	1	τC-O (74)		450.8	27	δCC=O (74)		438.6	3
δCCC (60)		246.8		δCCC (67)		238.3		δCCC (62) + δCC=O (35)		250.8	3	δCCC (70)		238.6	2
τC-CH_3 (96)		217.2		τC-CH_3 (89)		223.1		τC-CH_3 (96)		215.2		τC-CH_3 (93)		218.2	
τC-C (95)		56.7		τC-C (95)		33.1		τC-C (92)		62.9		τC-C (92)		37.3	2

[a] Only the bands affected by the NIR excitation experiments are here listed. The majority of the observed vibrational modes exhibit a site splitting of the absorption. [b] The ab initio harmonic frequencies are rescaled using the 0.94, and 0.97 correction factors for the regions above and below 2000 cm^{-1}, respectively. The calculated intensities were normalized by the intensity of the strongest band (C_t band at 1254.4 cm^{-1}).[c] In general, symmetry coordinates with contributions higher than 15% to a particular vibrational mode are shown. Symbols: ν - stretching; δ - bending; γ - rocking; ω - wagging; tw - twisting; τ - torsion; and FR - involved in Fermi resonance. (See details in the text).

conformer, the bands assigned to this form are observed at ~1800 cm^{-1} (νC=O), ~ 1360 cm^{-1} (ωCH_2), and ~1156 cm^{-1} (νC-O), in good agreement with the computational values of 1773 cm^{-1}, 1361 cm^{-1}, and 1134 cm^{-1}, respectively (Figure 4). In addition, two doublets are observed at ~1276 and ~1248 cm^{-1}, which are ascribed to δCOH, predicted at 1254 cm^{-1}. The fine structure observed for the νC=O and ωCH_2 vibrations of C_t, as well as for the bands ascribed to δCOH (Table 1), is presumably due to matrix site effects. However, the large splitting between the two δCOH doublets (~30 cm^{-1}) might have a different origin. A possible explanation for this observation is a Fermi interaction with the γCH_2 + τC-O combination mode, whose fundamentals were predicted to appear at ca. 804 and 451 cm^{-1} (Table 1).

Finally, the $C_g^{\pm}$ conformer gives rise to the bands observed at 1802 (νC=O), 1474 (δHCH_2), 1323 (ωCH_2), ~1290 ($twCH_2$, doublet), and ~1250 cm^{-1} (δCOH, doublet) [marked with asterisks in trace (d) of Figure 4]. These are the most intense bands predicted by the calculations in this spectral region, and their positions agree with the computational estimations (νC=O, 1770 cm^{-1}; δHCH_2, 1488 cm^{-1}; ωCH_2, 1328 cm^{-1}; $twCH_2$, 1283 cm^{-1}, and δCOH, 1247 cm^{-1}).

3. Assignment of the spectra of PA-OD. The assignment of the bands of the most stable conformer in the deuterated isotopologue is straightforward because of the generally good agreement between the experimental and calculated spectra for this form. The assignment of the $T_g^{\pm}$ and C_t conformers relies to a great extent on the results of the irradiation experiments where the pumping frequency was varied. As already mentioned, two pumping frequencies were used to excite the T_t conformer: high- frequency pumping (HF) at ~5175 cm^{-1} and low- frequency pumping (LF) at 5170 cm^{-1} (Figures 6 and 7).

The νOD and νC=O spectral regions are useful for the identification of both $T_g^{\pm}$ and C_t forms. These two modes are sensitive to the conformation of the carboxylic group. The νOD and νC=O modes of C_t appear blueshifted from the T_t bands by 46 cm^{-1} and 30 cm^{-1}, respectively (Table 2). The calculations predicted these shifts as 47 cm^{-1} and 30 cm^{-1}, in excellent agreement with the experimental results. The observed shifts are also in agreement with the available data for acetic acid where a change of conformation from the *trans* to the *cis* arrangement around the C-O bond leads to blue shifts in these modes of 44 and 30 cm^{-1}, respectively.[6,38] In the case of $T_g^{\pm}$, both νOD and νC=O modes were predicted to be shifted from those of T_t by less than 1 cm^{-1}. Accordingly, the bands assigned to this conformer are observed at 2627 (νOD) and 1780-1760 cm^{-1} (νC=O; quartet), which are close to the corresponding bands of T_t, observed at 2630/2631 and 1770-1762 cm^{-1}, respectively.

Most of the $T_g^{\pm}$ and C_t bands appear split due to matrix-site effects. For each conformer, the positions of the emerging bands remain unchanged for the two pumping experiments (HF and LF), as shown in Figures 6 and 7, but their relative intensity changes with the pumping frequency. This is due to the fact that the pumping efficiency of various matrix sites depends on the pumping frequency, as discussed elsewhere.[6,38] However, very interestingly, the HF excitation of the 2νOD mode of the T_t conformer promotes more efficiently the $T_t \rightarrow T_g^{\pm}$ conversion, whereas the LF excitation promotes the $T_t \rightarrow C_t$ conversion with a relatively higher efficiency. Although the bands of both photo-produced conformers ($T_g^{\pm}$ and C_t) appear as a result of both HF and LF excitation, their relative intensities are strongly affected by the excitation frequency. A detailed analysis of the spectral changes induced by the HF or LF excitations allows us to distinguish between the spectroscopic features origina-ting from molecules isolated in various sites. For example, there are three C_t absorptions in the 1500-1100 cm^{-1} region affected essen-tially by the LF excitation (Figure 6). These are the band at 1368 cm^{-1} (ωCH_2, predicted

TABLE 2: Experimental[a] and Calculated [MP2/6-311++(2d,2p)][b] Frequencies for the Four Conformers of CH_3CH_2COOD Monomer.

assignment (PED)[c]	Tt			assignment (PED)[c]	Tg±			assignment (PED)[c]	Ct			assignment (PED)[c]	Cg±		
	ν_{exp}	ν_{calc}	I_{calc}		ν_{exp}	ν_{calc}	I_{calc}		ν_{exp}	ν_{calc}	I_{calc}		ν_{exp}	ν_{calc}	I_{calc}
νHCH_2 a (95)	3005.6	3003.3	5	νCH_2' (52) + νHCH_2' (38)	3008.3	3008.6	5	νHCH_2 a (98)		3007.3	4	νCH_2' (50) + νHCH_2' (37)		3000.4	4
νHCH_2 s (100)	2996.2	2999.4	5	νHCH_2 (84)	2989.6	2996.2	4	νHCH_2 s (100)		3001.0	4	νHCH_2 (85)		2996.6	4
νCH_2 a (94)	2956.9	2960.1		νHCH_2' (60) + νCH_2' (26)	2972.2	2988.2	2	νCH_2 a (97)		2940.3	2	νHCH_2' (61) + νCH_2' (22)		2980.4	2
νCH_2 s (100)	2939.9	2920.5	3	νCH_2 (94)	2955.3	2937.0	2	νCH_3 (100)		2920.4	5	νCH_2 (83)		2915.6	4
νCH_3 (100)		2918.9	5	νCH_3 (100)		2912.7	5	νCH_2 s (100)		2898.1	5	νCH_3 (99)		2909.4	4
νOD (99)	2631.3 2630.4 2629.1	2592.3	16	νOD (99)	2627.1	2591.7	16	νOD (99)	2675.7 2672.9	2636.4	13	νOD (99)	2669.6	2638.6	11
νC=O (85)	1769.9 1765.9 1762.4	1736.9	78	νC=O (84)	1776.7 1771.3 1767.5 1762.4 1749.8 1744.0	1735.8	90	νC=O (86)	1820.0 1799.8 1794.1	1766.4	74	νC=O (85)	1798.1 1784.2	1762.6	86
												δHCH_2 (20) + δHCH_2' (28)		1488.5	4
δHCH_2 s (87)		1483.5	3	δHCH_2 (84)	1468.9	1490.2	4	δHCH_2 s (88)		1481.6	3	δHCH_2' (60)		1483.2	2
δ HCH_2 a (90)		1479.1	2	δHCH_2' (90)		1484.1	2	δHCH_2 a (89)		1431.7	2	δCH_2 (89)		1466.0	1
δCH_2 (98)	1466.7	1440.8	5	δCH_2 (91)		1460.8	2	δCH_3 (98)	1428.8	1398.2	3	δCH_3 (100)		1396.5	1
δCH_3 (93)		1401.6	1	δCH_3 (100)	1400.0	1390.8	2	δCH_3 (99)		1399.3	1	ωCH_2 (73)		1325.5	11
ωCH_2 (58)	1380.1 1376.7 1372.5	1375.6	21	ωCH_2 (60)	1331.5 1303.8	1337.4	16	ωCH_2 (70)	1367.8	1360.5	16	$twCH_2$ (58)		1278.8	20
$twCH_2$ (74)		1266.0		$twCH_2$ (47)	1289.6	1293.4	18	$twCH_2$ (74)	1264.4 1260.9	1274.0		νC-O (21) + γCH_3 (20)	1238.2 1216.1	1209.1	47
νC-O (41)	1294.6 1267.4 1206.7 1204.4	1200.2	61	νC-O (17) + γCH_3 (21) + $twCH_2$ (18)	1242.5	1226.1	25	νC-O (40)	1246.4 1238.1 1193.6	1178.5	100	γCH_3 (17) + γCH_2 (22) + $twCH_3$ (16)		1082.3	8
γCH_3 (37) + γCH_2 (31)		1092.7		ρCH_3 (24) + γCH_2 (21)		1087.8	1	ωCH_3 (37) + νC-CH_3 (34)		1089.3	7	ωCH_3 (38) + νC-CH_3 (21)		1062.6	17
ωCH_3 (38) + νC-CH_3 (34)		1090.7		ωCH_3 (43) + νC-CH_3 (22)		1067.4	4	γCH_3 (37) + γCH_2 (30)		1087.8					
νC-CH_3 (45)	1012.2 1000.8	1006.5	11	νC-CH_3 (67)		979.2	5	νC-CH_3 (51) + ωCH_3 (21)		998.7	1	νC-CH_3 (68)		979.3	10
δCOD (48)	963.8 956.5	964.0	25	δCOD (54) + νC-O (26)	984.0 978.9	962.8	38	δCOD (48) + νC-O (22)		9080	2	δCOD (55) + νC-O (24)		899.1	1
γCH_3 (34) + γCH_2 (33) + γC=O (22)		798.1	3	γCH_2 (40) + γCH_3 (31)		794.1	1	γCH_2 (35) + γCH_3 (34) + ρC=O (20)		803.7	2	νC-C=O (39)		802.6	10
νC-C=O (55)		763.8	2	νC-C=O (37)		778.1	1	νC-C=O (46)	802.5	793.3	11	δCH_2 (46) + γCH_3 (33)		786.4	
γC=O (38) + γCH_2 (28) + τC-O (28)		577.2	6	γC=O (47)		710.9	3	δOCO (48)		604.5	2	γC=O (57)		709.1	2
δOCO (39) + δCC=O (22)		570.0	5	δOCO (63)		526.7	12	$\gamma C=O$ (53) + γCH_2 (30)		549.0		δOCO (63) + νC-C=O (21)		558.0	2
δOCO (30) + δCC=O (29)		444.2	8	τC-O (87)		443.3	18	δCC=O (32) + δOCO (23)		438.8		δCC=O (72)		427.3	1
τC-O (72) + γC=O (21)		412.8	15	δCC=O (69)		421.8	2	τC-O (91)		342.7	16	τC-O (94)		347.4	15
δCCC (59) + δCC=O (38)		244.7	1	δCCC (60)		233.0		δCCC (60) + δCC=O (37)		248.5	3	δCCC (70)		237.0	2
τC-CH_3 (96)		215.7		τC-CH_3 (84)		222.2		τC-CH_3 (96)		215.2		τC-CH_3 (93)		217.9	
τC-C (95)		55.3		τC-C (96)		33.1		τC-C (92)		62.2		τC-C (92)		36.6	2

[a] Only the bands affected by the NIR excitation experiments are here listed. The majority of the observed vibrational modes exhibit a site splitting of the absorption bands. [b] The ab initio harmonic frequencies are rescaled using the 0.94, and 0.97 correction factors for the regions above, and below 2000 cm^{-1}, respectively. The calculated intensities were normalized by the intensity of the strongest band (C_t band at 1178.5 cm^{-1}). [c] Symmetry coordinates with contributions higher than 15% to a particular vibrational mode are shown. Symbols: ν - stretching; δ - bending; γ - rocking; ω - wagging; tw - twisting; and τ - torsion.

to be a medium-intensity band at 1360 cm^{-1}), the weak doublet at ~1263 cm^{-1} ($twCH_2$, predicted to be a very weak band at 1274 cm^{-1}), and the very strong doublet observed at ~1244 cm^{-1} (νC-O, predicted at 1178 cm^{-1} to be the most intense band of the spectrum of this conformer). In the same spectral window, the only band of C_t clearly

connected with the HF excitation is the relatively strong band observed at 1194 cm^{-1}, which is assigned to the νC-O mode of the site mostly influenced by the HF excitation (Figure 7). The T_t bands observed at 1380/1377 and 1295/1267 cm^{-1} are essentially associated with the sites affected by the LF excitation, which leads mainly to the $T_t \rightarrow C_t$ conversion (Figure 6). The two observed doublets for T_t agree reasonably well with the theoretical spectrum where two relatively intense bands are predicted at 1376 (ωCH_2) and 1200 cm^{-1} (νC-O) (Table 2). However, the T_t bands that are more affected by the HF excitation are observed at 1372 (ωCH_2) and 1207/1204 cm^{-1} (νC-O) (Figure 7), which can be correlated with the bands of $T_g^{\pm}$, observed at 1332 cm^{-1} (ωCH_2 mode, predicted at 1337 cm^{-1}), 1290 cm^{-1} ($tw CH_2$ mode, predicted at 1293 cm^{-1}), and 1242 cm^{-1} (νC-O, predicted at 1226 cm^{-1}).

Another interesting observation is the large splitting (40-90 cm^{-1}) between the two νC-O features responding differently to the HF and LF excitations, which is observed for both T_t and C_t conformers. The bands associated with the LF excitation exhibit a larger blue shift (60-100 cm^{-1}) relative to the ab initio calculated values, whereas those associated with the HF excitation almost match the calculated values. This observation points to a different mode coupling in the two sites, either between νC-O and other internal modes or between νC-O and matrix modes, which seem to be more important in the case of the LF-sensitive sites. Similar deviations (30-90 cm^{-1}) between the observed and calculated νC-O frequencies were previously observed for formic and acetic acids.[6,38]

The assignment of the $C_g^{\pm}$ bands is based on the spectral changes induced by excitation of $T_g^{\pm}$, although the relatively low concentration of the $C_g^{\pm}$ conformer limits the number of observed bands of this form. As expected from the calculations, the observed bands of $C_g^{\pm}$ appear slightly shifted but clearly distinguishable from those of the C_t form (Table 2), and they fit the most intense bands predicted by the calculations (νOD at 2670, νC=O doublet at 1798/1784, and νC-O doublet at 1238/1216 cm^{-1}).

4. Can the C-O and C_α-C rotations occur in a concerted way? Excitation of the 2νOH(D) mode introduces an energy in the molecule higher than the computed barriers for isomerization along each of the two internal rotation coordinates (C_α-C and C-O). All stepwise processes are energetically allowed, and for excitation of T_t and $T_g^{\pm}$, they were experimentally observed as described earlier. The energy barrier associated with the direct $T_t \rightarrow C_g^{\pm}$ and $T_g^{\pm} \rightarrow C_t$ processes, via concerted C-O/C_α-C internal rotation, is predicted to be 4300-4800 cm^{-1} (Figure 1), which is also smaller than the excitation energy. However, no experimental evidence that excitation of the 2νOH(D) modes of either T_t or $T_g^{\pm}$ conformers induces the concerted process is obtained. Indeed, for both PA-OH and PA-OD, neither the $C_g^{\pm}$ conformer is produced upon excitation of the T_t form nor the C_t conformer upon excitation of the $T_g^{\pm}$ form.

However, the $C_g^{\pm}$ to T_t decay occurs when the NIR irradiation is interrupted (at 8 K, with incident globar radiation below 3300 cm^{-1}). It is then, in principle, possible that the direct $C_g^{\pm} \rightarrow T_t$ conversion is taking place via the concerted mechanism. Because the calculated isomerization barrier for the $C_g^{\pm} \rightarrow T_t$ process is 2542 cm^{-1}, the globar radiation below 3300 cm^{-1} should not have a determinant role in the concerted process. In fact, the only modes with energy above the barrier that can be excited by the globar are the C-H stretching modes (predicted within the 3000-2900 cm^{-1} spectral range), but their cross sections are so small that they are not experimentally observed. Hence, though the concerted mechanism cannot be excluded, a stepwise process for conversion of $C_g^{\pm}$ into T_t seems to be more plausible. The $C_g^{\pm}$ form can first decay by tunneling to a vibrationally excited $T_g^{\pm}$ form, and then partial dissipation of the excess vibrational energy into the C_α-C rotational coordinate, above the $T_g^{\pm} \rightarrow T_t$ isomerization barrier, can lead to occurrence of this last process. The isotopic effect in the $C_g^{\pm} \rightarrow T_t$ decay rate

(slower rate by at least 2 orders of magnitude for PA-OD) supports a conversion mechanism involving tunneling. The proposed stepwise mechanism is consistent with the model for the dark C→T tunnelling decay in formic and acetic acids from the torsional ground state of the *cis* conformer into a vibrationally excited state of the *trans* form.[3,7]

Concluding Remarks

The conformers of propionic acid were studied by means of ab initio calculations, IR absorption spectroscopy and narrow-band NIR excitation in solid Ar. The calculations predicted the existence of four conformers, differing by internal rotation around the C_α-C and C-O bonds. For both PA-OH and PA-OD species, internal rotations were induced by excitation of the first overtone of the hydroxyl stretching modes of different conformers, and IR absorption spectroscopy was used to probe the photoinduced conformational changes.

The main results of this study can be summarized as follows:

(1) The IR absorption spectra of the four conformers of propionic acid isolated in solid argon are obtained and assigned based on the ab initio calculated spectra (Tables 1 and 2).

(2) Because of conformational cooling, the ground conformational state (T_t) is the only form initially present in the deposited argon matrix. The remaining three conformers ($T_g^{\pm}$, C_t and $C_g^{\pm}$) can be photoproduced by irradiation in the NIR region. Excitation of the 2νOH(D) mode is efficient in promoting the C_α-C and C-O internal rotations leading to the $T_t \rightarrow T_g^{\pm}$, $T_t \rightarrow C_t$, $T_g^{\pm} \rightarrow T_t$ and $T_g^{\pm} \rightarrow C_g^{\pm}$ isomerization processes. Although energetically allowed, no direct $T_t \rightarrow C_g^{\pm}$ or $T_g^{\pm} \rightarrow C_t$ photo-isomerization by concerted rotation around the C_α-C and C-O bonds was observed. The comparison of photochemical processes on propionic, acetic and formic acids can be found elsewhere. [41]

(3) For PA-OH, the C_t and $C_g^{\pm}$ conformers are short-lived species, due to fast $C_t \rightarrow T_t$ and $C_g^{\pm} \rightarrow T_t$ conversions in the absence of irradiation. The much slower decay of these two forms in the case of PA-OD (by ca. 2-4 orders of magnitude) proves the crucial role of tunneling in these isomerization processes.

(4) The 2νOH(D) absorption band is split by the matrix-site effect. For PA-OD, excitation of T_t was performed at two different frequencies within the 2νOD absorption band, leading to site dependent isomerization efficiencies that aid discrimination between the spectra of the photoproducts ($T_g^{\pm}$, and C_t).

(5) The $T_g^{\pm} \rightarrow T_t$ isomerization takes place in dark with an appreciable rate ($k \sim 10^{-6}$ s^{-1}), even at the lowest working temperature (8 K). The very low isomerization barrier associated with the $T_g^{\pm} \rightarrow T_t$ process (computationally estimated as 60 cm^{-1}) suggests that this isomerization could occur over the barrier. The strong temperature dependence of this process experimentally supports a low barrier for the $T_g^{\pm} \rightarrow T_t$ process.

Acknowledgements. We thank the Academy of Finland for financial support and the Finnish IT Center for Science (CSC) for providing the computational facilities. E. M. S. M. and R. F. acknowledge the Portuguese Foundation for Science and Technology (Ph.D. grants SFRH/BD/ 4863/2001 and POCTI/QUI/43366/ 2001) and the Calouste Gulbenkian Foundation.

Supporting Information Available: Definition of the internal symmetry coordinates used in the normal coordinate analysis of propionic acid. This material is available free of charge via the Internet at http://pubs.acs.org.

References and Notes

1. Pettersson, M.; Lundell, J.; Khriachtchev, L.; Räsänen, M. *J. Am. Chem. Soc.* **1997**, *119*, 11715.
2. Maçôas, E. M. S.; Khriachtchev, L.; Pettersson, M.; Juselius, J.; Fausto, R.; Räsänen, M. *J. Chem. Phys.* **2003**, *119*, 11765.
3. Pettersson, M.; Maçôas, E. M. S.; Khriachtchev, L.; Lundell, J.; Fausto, R.; Räsänen, M. *J. Chem. Phys.*

2002, *117*, 9095.
4. Khriachtchev, L.; Maçôas, E.; Pettersson, M.; Räsänen M., *J. Am. Chem. Soc.* **2002**, *124*, 10994.
5. Maçôas, E. M. S.; Khriachtchev, L.; Pettersson, M.; Fausto, R.; Räsänen, M. *J. Am. Chem. Soc.* **2003**, *125*, 16188.
6. Maçôas, E. M. S.; Khriachtchev, L.; Fausto, R.; Räsänen, M. *J. Phys. Chem. A* **2004**, *108*, 3380.
7. Maçôas, E. M. S.; Khriachtchev, L.; Pettersson, M.; Fausto, R.; Räsänen, M. *J. Chem. Phys.* **2004**, *121*, 1331.
8. Goez, M. *Angew. Chem., Int. Ed.* **2003**, *42*, 2336.
9. Cantor, C. R.; Schimmel, P. R. *Biophysical Chemistry*; W. H. Freeman, Co.: New York, 1980.
10. Huff, J. B.; Askew, B.; Duff, R. J.; Rebek J. *J. Am. Chem. Soc.* **1988**, *110*, 5908.
11. Tadayoni, B. M.; Parris, K.; Rebek J. *J. Am. Chem. Soc.* **1989**, 111, 4503.
12. Karle, M.; Bockelmann, D.; Schumann, D.; Griesinger, C.; Koert, U. *Angew. Chem., Int. Ed.* **2003**, *42*, 4546.
13. Berkovic, G.; Krongauz, V.; Weiss, V. *Chem. Rev.* **2000**, *100*, 1741.
14. Derissen, J. L. *J. Mol. Struct.* **1971**, *7*, 81.
15. Stiefvater, O. L. *J. Chem. Phys.* **1975**, *62*, 233.
16. Stiefvater, O. L. *J. Chem. Phys.* **1975**, *62*, 244.
17. Wiberg, K. B., *J. Am. Chem. Soc.* **1986**, *108*, 5817.
18. Teixeira-Dias J. J. C.; Fausto, R., *J. Mol. Struct.* **1986**, *144*, 199.
19. Lii, J. H. *J. Phys. Chem. A* **2002**, *106*, 8667.
20. Durig, J. R.; Li, Y.; Shen, S. Y.; Durig, D. T. *J. Mol. Struct.* **1998**, *449*, 131.
21. Durig, D. T.; Shen, S. Y.; Li, Y.; Durig, J. R. *Spectrochim. Acta A* **2004**, *60*, 1481.
22. Fausto, R.; Teixeira-Dias, J. J. C.; Gil, F. P. S. C. *J. Chem. Soc. Faraday. Trans.* **1993**, *89*, 3235.
23. Derissen, J. L.; Bijen, J. M. J. M. *J. Mol. Struct.* **1975**, *29*, 153.
24. Nieminen, J.; Pettersson, M.; Räsänen, M. *J. Phys. Chem.* **1993**, 97, 10925.
25. Goddard, J. D.; Yamaguchi, Y.; Schaefer, H. F. *J. Chem. Phys.* **1992**, 96, 1158.
26. Pettersson, M.; Maçôas, E. M. S.; Khriachtchev, L.; Fausto, R.; Räsänen, M. *J. Am. Chem. Soc.* **2003**, *125*, 4058.
27. Senent, M. L. *Mol. Phys.* **2001**, *99*, 1311.
28. Hocking, W. H. *Z. Naturforsch A* **1976**, 31, 1113.
29. Frisch, M. J. T., G. W; Schlegel, H. B.; Scuseria, G. E.; Robb, M. A.; Cheeseman, J. R.; Zakrzewski, V. G.; Montgomery, J. A.; Stratmann, R. E; Burant, J. C.; Dapprich, S.; Millam, J. M.; Daniels, A. D.; Kudin, K. N.; Strain, M. C.; Farkas, O.; Tomasi, J.; Barone, V.; Cossi, M.; Cammi, M.; Mennucci, B.; Pomelli, C.; Adamo, C.; Clifford, S.; Ochterski, J.; Petersson, G. A.; Ayala, P. Y.; Cui, Q.; Morokuma, K.; Malick, D. K.; Rabuck, A. D.; Raghavachari, K.; Foresman, J. B.; Cioslowski, J.; Ortiz, J. V.; Baboul, A. G.; Stefanov, B. B.; Liu, G.; Liashenko, A.; Piskorz, P.; Komaromi, I.; Gomperts, R.; Martin, R. L.; Fox, D. J.; Keith, T.; Al-Laham, M. A.; Peng, C. Y.; Nanayakkara, A.; Gonzalez, C.; Challacombe, M.; Gill, P. M. W.; Johnson, B. G.; Chen, W.; Wong, M. W.; Andres, J. L.; Head-Gordon, M.; Replogle, E. S.; Pople, J. A., GAUSSIAN 98. *GAUSSIAN 98, Gaussian, Inc., Pittsburgh, PA, 1998; Revision A. 9* 1998.
30. Jensen, F. *Introduction to Computational Chemistry*; John Wiley & Sons, Ltd.: Chichester, West Sussex, 1999.
31. Scott, A. P.; Radom, L. *J. Phys. Chem.* **1996**, *100*, 16502.
32. Schachtschneider, J. H. Technical Report; Shell Development Co.: Emeryville, CA, 1969.
33. Marsh, D. *Cell. Mol. Life Sci.* **2003**, *60*, 1575.
34. Kanesaka, I.; Snyder, R. G.; Strauss, H. L. *J. Chem. Phys.* **1986**, *84*, 395.
35. Herrebout, W. A.; Vanderveken, B. J.; Wang, A.; Durig, J. R. *J. Phys. Chem.* **1995**, *99*, 578.
36. Smith, G. D.; Jaffe, R. L. *J. Phys. Chem.* **1996**, *100*, 18718.
37. Khriachtchev, L.; Lundell, J.; Isoniemi, E.; Räsänen, M. *J. Chem. Phys.* **2000**, *113*, 4265.
38. Maçôas, E. M. S.; Lundell, J.; Pettersson, M.; Khriachtchev, L.; Fausto, R.; Räsänen, M. *J. Mol. Spectrosc.* **2003**, *219*, 70.
39. Reva, I. D.; Stepanian, S. G.; Adamowicz, L.; Fausto, R *Chem. Phys. Lett.* **2003**, *374*, 631.
40. Barnes, A. J. *J. Mol. Struct.* **1984**, *113*, 161.
41. Maçôas, E. M. S.; Khriachtchev, L.; Pettersson, M.; Fausto, R.; Räsänen, M *Phys. Chem. Chem. Phys.* **2005**, *7*, 743.

TABLE S1 – Definition of the internal symmetry coordinates used in the normal coordinate analysis of propionic acid.

coordinate	symmetry T_t/C_t	approximate description[a] T_t/C_t	$T_g^{\pm}/C_g^{\pm}$	definition[b]
S_1	A'	νC-C=O	νC-C=O	$\nu(C_1\text{-}C_2)$
S_2	A'	νC-CH_3	νC-CH_3	$\nu(C_1\text{-}C_3)$
S_3	A'	νC=O	νC=O	$\nu(C_2\text{=}O_9)$
S_4	A'	νC-O	νC-O	$\nu(C_2\text{-}O_{10})$
S_5	A'	νOH	νOH	$\nu(O_{10}\text{-}H_{11})$
S_6	A''	νCH_2 a	νCH_2'	$\nu(C_1\text{-}H_7) - \nu(C_1\text{-}H_8)$
S_7	A'	νCH_2 s	νCH_2	$\nu(C_1\text{-}H_7) + \nu(C_1\text{-}H_8)$
S_8	A''	νHCH_2 a	νHCH_2'	$\nu(C_3\text{-}H_5) - \nu(C_3\text{-}H_6)$
S_9	A'	νHCH_2 s	νHCH_2	$2\nu(C_3\text{-}H_4) - \nu(C_3\text{-}H_5) - \nu(C_3\text{-}H_6)$
S_{10}	A'	νCH_3	νCH_3	$\nu(C_3\text{-}H_4) + \nu(C_3\text{-}H_5) + \nu(C_3\text{-}H_6)$
S_{11}	A'	δCOH	δCOH	$\delta(C_2\text{-}O_{10}\text{-}H_{11})$
S_{12}	A'	δOCO	δOCO	$2\delta(O_9\text{=}C_2\text{-}O_{10}) - \delta(C_1\text{-}C_2\text{-}O_{10}) - \delta(C_1\text{-}C_2\text{=}O_9)$
S_{13}	A'	δC-C=O	δC-C=O	$\delta(C_1\text{-}C_2\text{-}O_{10}) - \delta(C_1\text{-}C_2\text{=}O_9)$
S_{14}	A'	δCH_2	δCH_2	$5\delta(H_7\text{-}C_1\text{-}H_8) - \delta(C_2\text{-}C_1\text{-}H_7) - \delta(C_2\text{-}C_1\text{-}H_8) - \delta(C_3\text{-}C_1\text{-}H_7) - \delta(C_3\text{-}C_1\text{-}H_8) - \delta(C_3\text{-}C_1\text{-}C_2)$
S_{15}	A'	δCCC	δCCC	$4\delta(C_3\text{-}C_1\text{-}C_2) - \delta(C_2\text{-}C_1\text{-}H_8) - \delta(C_2\text{-}C_1\text{-}H_7) - \delta(C_3\text{-}C_1\text{-}H_8) - \delta(C_3\text{-}C_1\text{-}H_7)$
S_{16}	A'	ωCH_2	ωCH_2	$\delta(C_2\text{-}C_1\text{-}H_8) + \delta(C_2\text{-}C_1\text{-}H_7) - \delta(C_3\text{-}C_1\text{-}H_8) - \delta(C_3\text{-}C_1\text{-}H_7)$
S_{17}	A''	twCH_2	twCH_2	$\delta(C_2\text{-}C_1\text{-}H_8) - \delta(C_2\text{-}C_1\text{-}H_7) - \delta(C_3\text{-}C_1\text{-}H_8) + \delta(C_3\text{-}C_1\text{-}H_7)$
S_{18}	A''	γCH_2	γCH_2	$\delta(C_2\text{-}C_1\text{-}H_8) - \delta(C_2\text{-}C_1\text{-}H_7) + \delta(C_3\text{-}C_1\text{-}H_8) - \delta(C_3\text{-}C_1\text{-}H_7)$
S_{19}	A'	δCH_3	δCH_3	$\delta(C_1\text{-}C_3\text{-}H_4) + \delta(C_1\text{-}C_3\text{-}H_5) + \delta(C_1\text{-}C_3\text{-}H_6) - \delta(H_5\text{-}C_3\text{-}H_6) - \delta(H_5\text{-}C_3\text{-}H_4) - \delta(H_6\text{-}C_3\text{-}H_4)$
S_{20}	A'	δHCH_2 s	δHCH_2	$2\delta(H_5\text{-}C_3\text{-}H_6) - \delta(H_4\text{-}C_3\text{-}H_6) - \delta(H_4\text{-}C_3\text{-}H_5)$
S_{21}	A''	δHCH_2 a	δHCH_2'	$\delta(H_4\text{-}C_3\text{-}H_6) - \delta(H_4\text{-}C_3\text{-}H_5)$
S_{22}	A'	ωCH_3	ωCH_3	$2\delta(C_1\text{-}C_3\text{-}H_4) - \delta(C_1\text{-}C_3\text{-}H_5) - \delta(C_1\text{-}C_3\text{-}H_6)$
S_{23}	A''	γCH_3	γCH_3	$\delta(C_1\text{-}C_3\text{-}H_5) - \delta(C_1\text{-}C_3\text{-}H_6)$
S_{24}	A''	τC-O	τC-O	$\tau(C_2\text{-}O_{10})$
S_{25}	A''	τC-C	τC-C	$\tau(C_2\text{-}C_1)$
S_{26}	A''	τC-CH_3	τC-CH_3	$\tau(H_4\text{-}C_3\text{-}C_1\text{-}C_2) + \tau(H_6\text{-}C_3\text{-}C_1\text{-}C_2) + \tau(H_5\text{-}C_3\text{-}C_1\text{-}C_2)$
S_{27}	A''	γC=O	γC=O	$\gamma(C_2\text{=}O_{10})$

[a] a, asymmetric; s, symmetric, ν, stretching, δ, bending, ω, wagging, tw, twisting, γ, rocking; τ, torsion. [b] See figure below for atom numbering.

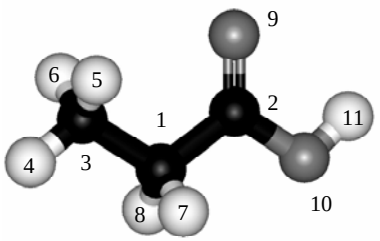

Appendix IX

Rotational isomerization of small carboxylic acids isolated in argon matrices: Tunneling and quantum yields for the photoinduced processes.

Ermelinda M. S. Maçôas, Leonid Khriachtchev, Mika Pettersson, Rui Fausto and Markku Räsänen

Phys. Chem. Chem. Phys. **2005**, *7*, 743-749

Rotational isomerization of small carboxylic acids isolated in argon matrices: Tunnelling and quantum yields for the photoinduced processes

Ermelinda M. S. Maçôas,[a,b] Leonid Khriachtchev,*[a] Mika Pettersson, [†a] Rui Fausto[b] and Markku Räsänen[a]

[a]*Laboratory of Physical Chemistry, University of Helsinki, PO Box 55, FIN-00014 Helsinki, Finland. E-mail: leonid.khriachtchev@helsinki.fi*
[b]*Department of Chemistry (CQC), University of Coimbra, P-3004-535 Coimbra, Portugal*

Received 1st November 2004, Accepted 17th December 2004
First published as an Advance Article on the web 12th January 2005

The quantum yields for internal rotation around the C-O bond induced by excitation of the first overtone of the hydroxyl stretching mode in formic, acetic, and propionic acids isolated in solid Ar are comparatively discussed. The tunnelling kinetics for isomerization from the higher energy arrangement of the carboxylic group (*cis*) to the lower energy arrangement (*trans*) in this series of compounds is also analysed. Finally, the quantum yield for the C_α-C isomerization in propionic acid was investigated and, in contrast with the C-O isomerization, shown to be probably sensitive to the local matrix morphology.

1. Introduction

For a number of molecules, rotational isomerization can be efficiently induced by vibrational excitation of the monomer isolated in low-temperature rare-gas matrices.[1-19] This process occurs when the energy deposited into the initially excited vibrational mode is transferred to the reaction coordinate. The mechanism of energy relaxation in the solid was described as a phonon-assisted intramolecular vibrational energy relaxation (IVR) where the lattice modes provide a thermal bath compensating the energy mismatch between the intramolecular vibrational states.[20,21] The relaxation rates are expected to depend on both the number of phonons involved and temperature of the phonon bath.

The experimental quantum yields for IR-induced rotamerization (rotational isomerization) in rare-gas matrices have been previously reported.[1,11-13] The quantum isomerization yield depends on the proportion of the energy relaxation channels that can deposit energy into the reaction coordinate as well as on the lifetimes of the molecular states involved so that the isomerization is in competition with possible non-reactive energy relaxation channels. The excitation energy, the host, and the nature of the excited mode may affect the IVR process and, consequently, they have been shown to affect the isomerization quantum yields.[11]

For formic (HCOOH, FA) and acetic (CH_3COOH, AA) acids, two stable geometrical arrangements are interconverted by rotation around the C-O axis, the *trans* and *cis* conformers shown in Fig. 1 (C-C-O-H dihedral angles of 180 and 0º, respectively).[5,22] The *trans* form is lower in energy by ≈ 1400-1800 cm^{-1} and the *trans* → *cis* isomerization barrier is ≈3900-4400 cm^{-1}.[23,26] These molecules were found mainly in the *trans* conformation in low-temperature matrices.[5,22] The resonant narrowband irradiation of individual vibrational transitions of the matrix isolated molecules in the

† Present address: Department of Chemistry, University of Jyväskylä, PO Box 35, FIN-40014, Finland.

2900-7000 cm^{-1} region induces the *trans* → *cis* conversion.[26,28] Infrared (IR) absorption spectroscopy provides reliable identification of the conformers because certain modes are very sensitive to conformation (see Table 1). For both FA and AA, the reverse isomerization from the higher energy conformer (*cis*) to the conformational ground state (*trans*) takes place by tunnelling.[28,29]

Intuitively, isomerization may take place when the energy transferred to the reaction coordinate (C-O torsion, τC-O) is higher than the isomerization barrier. However, for FA and AA, it was shown that this reaction occurs even when the excitation energy deposited into the reaction coordinate is below the isomerization barrier,[26-28] suggesting that tunnelling plays an important role in the photoinduced *trans* → *cis* isomerization process.

The effects of the medium and the nature of the excited state in the *trans* → *cis* isomerization have also been studied.[26,28] For FA, the quantum yield is practically independent of the local environment (matrix site), except when associated with excitation of hindered rotation of the molecule in the matrix.[26] Since AA shows no site structure, the matrix site effect on the quantum yield was not addressed. However, for AA, the isomerization quantum yield upon excitation of the 2νOH mode was shown to be relatively insensitive to the host (Ar, Kr, and Xe).[28] Additionally, excitation of different modes at energies higher than the barrier leads to similar isomerization quantum yields independently of the excited mode (≈20% for FA, and ≈2% for AA).[26,28] Therefore, the nature of the excited mode does not seem to be an important factor to the photoisomerization efficiency in these molecules.

The high efficiency of the isomerization process in FA was connected with the relatively large energy gaps in the vibrational manifold of this molecule, which delays the energy relaxation within the potential well of the initially excited conformer, hence favoring isomerization.[26] It was suggested

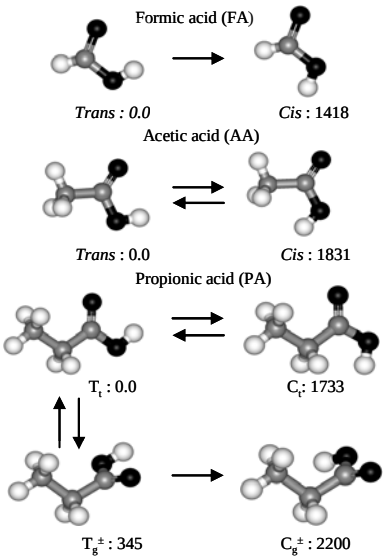

Fig. 1 Conformers of FA, AA and PA. The conformational energies calculated at the MP2/6-311++G(2d,2p) level of theory (in cm^{-1}) are shown. The arrows indicate the observed IR-induced isomerization processes. The IR-induced *cis* → *trans* process for FA has not been studied. The computational *trans* → *cis* barriers are 4096 and 4139 cm^{-1} for FA and AA, respectively. For PA, the $T_t \rightarrow C_t$, $T_g^{\pm} \rightarrow C_g^{\pm}$, $T_t \rightarrow T_g^{\pm}$ and $C_t \rightarrow C_g^{\pm}$ barriers are 4023, 4091, 405 and 559 cm^{-1}, respectively. The barriers are given taking into account the zero point energies.

that the one order of magnitude difference between the quantum yields for FA and AA is due to the methyl group in AA, which increases the number of energy relaxation channels competing with the photo-isomerization process.[28] The important role of the methyl group in the photo-isomerization process was supported by a large increase of the *trans* → *cis* isomerization quantum yield upon deuteration of the methyl group (by a factor of ≈5).[28] For AA, deuteration of the hydroxyl group was shown to reduce the isomerization quantum yield, in contrast to the effect observed for deuteration of the methyl group. In CH_3COOD (AA-OD), the *trans* → *cis* quantum yield is almost one order of magnitude

lower than in the fully hydrogenated species (AA-OH).[28] Additionally, for CH_3COOD and CD_3COOD, the *trans* → cis isomerization process has a lower quantum yield than the reverse IR-induced *cis* → *trans* process.[28] Similar observations have been reported for HONO isolated in solid Kr.[1]

Propionic acid (CH_3CH_2COOH, PA) has one additional internal rotational degree of freedom when compared with AA, the internal rotation around the C_α-C bond. With respect to the C-O rotation, PA is similar to FA and AA. Recently, the four PA conformers built up from combinations of the stable C-O (*trans* and *cis*) and C_α-C (*trans* and *gauche*, with C-C-C-O dihedral angles of 180º and ± ≈75º, respectively) arrangements have been identified using IR-induced isomerization in solid Ar.[30] The structure and energetics of the PA conformers predicted by *ab initio* calculations are shown in Fig. 1 and the characteristic vibrational frequencies for the T_t and C_t forms are given in Table 1. The IR-induced isomerization processes identified for PA isolated in solid Ar are also indicated in Fig. 1. The quantification of the isomerization quantum yields for the C-O and C_α-C rotations in propionic acid gives further insight into factors affecting the rotamerization process.

In the present work, we compare IR-induced rotational isomerization and tunnelling processes for formic, acetic and propionic acids in solid Ar. The data for FA and AA were previously reported,[26,28] and the results for PA are described here for the first time. By analysing comparatively the data obtained for all these species, it is possible to test previous interpretations and understand better how the vibrational density of states, deuteration of the hydroxyl group, and the matrix surrounding affect the isomerization process. It is not a purpose of this article to describe in detail spectroscopic identification and properties of the four PA conformers, and we present here only limited spectroscopic data (see Table 1).

2. Experimental details and methodology

The gaseous samples were prepared by mixing the carboxylic acids (> 99%), degassed by several freeze-pump-thaw cycles, with high purity argon (99.9999%), in the 1 : 500 to 1 : 2000 ratio. Hydroxyl-deuterated PA was obtained by H/D exchange on the inner surface of the sample container and the deposition line saturated with D_2O. The gaseous mixtures were deposited onto a CsI substrate kept at 15 K in a closed cycle helium cryostat (APD, DE 202A) and subsequently cooled down to 8 K. The IR absorption spectra (7900-400 cm^{-1}) were measured with a Nicolet SX-60 FTIR spectrometer. A liquid-nitrogen cooled MCT detector and a Ge/KBr beamsplitter were used to record the mid-IR absorption spectra with spectral resolution from 0.25 to 1.0 cm^{-1}. A liquid-nitrogen-cooled InSb detector and a quartz beamsplitter were used to record the near-IR (NIR) absorption spectra with spectral resolution of 0.5 cm^{-1}.

Table 1 Experimental characteristic frequencies for the conformers of FA, AA and PA exhibiting the *trans* or *cis* arrangements of the carboxylic group (C-C-O-H dihedral angle of 180º and 0º, respectively)[30,32,33]

	trans		cis		$[\Delta\nu OH(D)]_{cis\text{-}trans}$	$[\Delta\nu C{=}O]_{cis\text{-}trans}$
	νOH(D)	νC=O	νOH(D)	νC=O		
HCOOH	3550	1768	3617	1808	+ 67	+ 40
DCOOH	3550	1761	3616	1777	+ 66	+ 16
CH_3COOH	3564	1779	3623	1807	+ 59	+ 28
CD_3COOH	3564	1777	-	1798	-	+ 21
CH_3COOD	2629	1770	2674	1800	+ 45	+ 30
CD_3COOD	2630	1765	2673	1794	+ 43	+ 29
CH_3CH_2COOH	3567	1776	-	1802	-	+ 26
CH_3CH_2COOD	2630	1766	2674	1797	+ 44	+ 31

Typically 100 to 500 interferograms were co-added.

Tunable pulsed IR radiation provided by an optical parametric oscillator (Continuum, OPO Sunlite with IR extension) was used to excite vibrations of the studied molecules. The pulse duration was ≈5 ns, the spectral linewidth ≈0.1 cm^{-1} and the repetition rate 10 Hz. The pulse energy of the OPO in the 7000-5000 cm^{-1} spectral region was ≈ 0.5 mJ. The OPO radiation frequency was measured with a Burleigh WA-4500 wavemeter providing an absolute accuracy better than 1 cm^{-1} for the IR pumping radiation. The pumping beam was quasi-collinear with the spectrometer beam, and interference filters (transmitting in the 3650-3400 cm^{-1} or 3300-1100 cm^{-1} regions) were placed in front of the detector to prevent its exposure to the pumping radiation while recording spectra during irradiation.

The *ab initio* calculations were performed using the GAUSSIAN98 program at the MP2/6-311++G(2d,2p) level of approximation.[31]

The quantum yields of the rotamerization processes, $\phi(i)$, were extracted from the following equation:

$$\phi(i) = \frac{k_p(\nu)}{\sigma^i(\nu) I(\nu)} \qquad (1)$$

where $k_p(\nu)$ (in s^{-1}) is the averaged isomerization rate upon pumping at the frequency ν, $\sigma^i(\nu)$ (in cm^2) is the absorption cross-section of the mode *i* at the excitation frequency, and I (in s^{-1} cm^{-2}) is the averaged photon intensity of the pumping beam. The cross-section is obtained using the measured IR absorption at the excitation frequency, the estimated concentration of molecules in the excited matrix site, and the matrix thickness. For PA, the absorption cross-sections at the frequency used to excite the 2νOH and 2νOD modes of T_t are ≈ 3.6×10^{-20} cm^2, and (3.2-4.1) × 10^{-20} cm^2 (depending on the matrix site), respectively. For the 2νOH mode, the cross-sections for PA is smaller than the value obtained for the same mode of FA and A A by a factor of ≈ 5. In the case of the 2νOD mode, the σ values are ≈ 2-3 times smaller for PA than for AA (the value for FA has not been reported). These values correspond to the maximum of the absorption bands, and the smaller values for PA reflect essentially the fact that these bands are broader for PA than for FA and AA. The absorption cross-section of the 2νOD mode of the C_t conformer could not be measured directly due to its low concentration in the matrix. It was assumed that the absorption cross-section of the 2νOD mode of C_t is similar to the value for T_t by analogy with the data for *cis* and *trans* AA-OD.

Two methodologies have been applied to determine the pumping rate, k_p in eqn. (1). The most straightforward approach employs the IR-induced formation kinetics of the conformers. This approach was previously applied to the estimation of isomerization quantum yields for AA-OD.[28] In the present work, the PA concentration was followed by measuring the integrated absorption of the νOH or νOD modes upon IR pumping. To minimize errors on the determination of the pumping rates caused by reverse isomerization processes, only the points obtained during the first minutes of irradiation were considered. As an example, Fig. 2 shows the IR-induced formation kinetics for two conformers of AA-OD (*trans* and *cis)* and PA-OD (T_t and C_t).

The kinetics-based methodology could be used when the reverse isomerization was relatively slow. This is not the case for the $T_t \rightarrow C_t$ process in PA-OH where the back-reaction taking place by tunnelling is too fast to follow reliably the pumping kinetics. The C_t concentration saturates very quickly at a quite low level upon pumping the 2νOH mode of the T_t form. This stationary state is established as a result of the interplay between photoinduced generation of the C_t conformer and its depletion due to the $C_t \rightarrow T_t$ tunnelling. In this case, a way to obtain the pumping rate follows the procedure previously reported for the hydrogenated isotopologues of FA and AA.[26,28] At the equilibrium the pumping and tunnelling rates are equal, then:

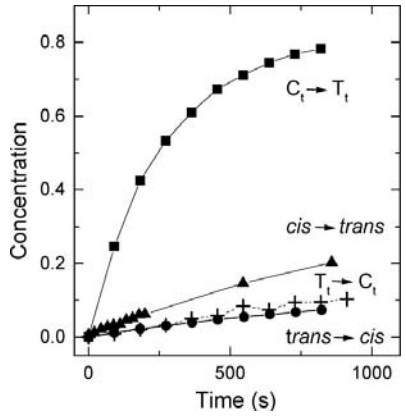

Fig. 2 Pumping kinetics measured for hydroxyl-deuterated AA and PA. The concentrations of the photoproducts are normalised by the initial concentrations of the pumped conformer. The pumping rates are extracted from a linear fit of the beginning of the kinetics curves. For AA, the pumping rates for the *trans* → *cis* (●) and *cis* → *trans* (▲) processes differ by a factor of ≈ 3, whereas for PA, the rates for the $T_t \rightarrow C_t$ *(+)* and $C_t \rightarrow T_t$ (■) processes differ by a factor of ≈ 25. The lines are merely guides. The T_t and C_t conformers in the LF site were pumped.

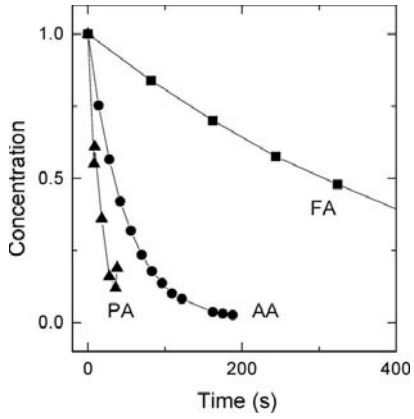

Fig. 3 Tunnelling kinetics for the conversion from the higher energy (*cis*) to the lower energy (*trans*) arrangement of the carboxylic group of fully hydrogenated FA (■, *cis* → *trans)*, AA (●, *cis* → *trans)* and PA (▲, $C_t \rightarrow T_t$*)* measured in solid Ar at 8 K. The lines are merely guides. The data are normalised by the initial concentrations.

$$k_p(\nu)[T_t]_{eq} = k_t(T)[C_t]_{eq} \quad (2)$$

where $k_t(T)$ is the tunnelling rate coefficient at the temperature *T*. Hence, the pumpingrate can be determined from the measured $C_t \rightarrow T_t$ tunnelling rate and the ratio of the T_t and C_t equilibrium concentrations. The tunnelling rate is extracted from the decay kinetics of the C_t conformer (see Fig. 3), which is obtained by recording IR absorption spectra every 10 s co-adding only 5 interferograms for each spectrum. The C_t/T_t concentration ratio at the equilibrium can be extracted from the changes in integrated absorptions upon pumping as described previously for FA.[26] The most important error of the isomerization quantum yield obtained from eqn. (1) can come from the estimated proportion of molecules isolated in various matrix sites, independently of the method used to obtain k_p. It was assumed here that the absorption intensity is independent of the matrix site.

As another approach, the quantum yield is a ratio of the number of molecules that undergo isomerization (N_{iso}) to the number of absorbed photons (N_{abs}):

$$\phi(i) = \frac{N_{iso}}{N_{abs}} \quad (3)$$

The value of N_{abs} per unit time is estimated from the absorbance at the excitation frequency, A_{exc}, the intensity of the incoming beam (in cm $^{-2}$ s $^{-1}$), I_0, and the irradiated area, *S*, as follows:

$$N_{abs} = \left(1 - 10^{-A_{exc}}\right) I_0 S \quad (4)$$

The number of isomerization events per unit time is calculated as follows:

$$N_{iso} = \frac{\left(\frac{\Delta A}{A_0}\right) n}{\Delta t} \quad (5)$$

where Δt is the irradiation time, n is the total number of molecules of the excited conformer, A_0 and ΔA are the initial integrated absorption and the change in integrated absorption for a given vibrational mode of the pumped conformer. ΔA is related to isomerization induced in a specific site, and it is measured directly from the difference IR absorption spectra. Note that ΔA for a given pumping time can be estimated only if the pumping kinetics is followed in real time, and N_{abs} can only be estimated if the NIR spectrum is measured before pumping.

3. Results and discussion

3.1. Identification of the conformers by IR absorption spectroscopy

For various isotopologues of FA and AA, excitation of the 2νOH(D) modes is efficient in promoting isomerization around the C-O bond (C-O isomerization).[26,28] The IR-induced changes in the νOH(D) and νC=O spectral region can be used to identify the conformers involved because they are very sensitive to the conformation of the carboxylic group (see Table 1). For FA and AA, the νOH(D) and νC=O modes appear blue-shifted by 40-60, and 20-40 cm^{-1}, respectively, in the *cis* as compared with the *trans* conformer.[32,33] For FA and AA, the traces (a) and (b) in Fig. 4 show the difference IR spectra where the increasing bands of the *cis* forms are clearly blue-shifted from the decreasing bands of the *trans* forms.

Similarly to FA and AA, PA is found after deposition in the ground conformational state, the T_t form (see Table 1 for the characteristic vibrational frequencies).[30] Excitation of the 2νOH(D) mode of T_t induces the C-O and C_α-C isomerizations, which lead to the production of the C_t and $T_g^{\pm}$ conformers, respectively. The bands of C_t are most clearly observed in the spectra recorded *under* pumping of T_t because its concentration quickly decreases when the excitation of T_t is interrupted, even at 8 K (see Fig. 3). The C_t form converts back to the most stable T_t form by tunnelling, in analogy with the *cis* → *trans* tunnelling observed for FA and AA.[28,29] For PA, trace (c) in Fig. 4 shows a difference spectrum obtained under excitation of the 2νOH mode of T_t. In this spectrum the emerging bands slightly red-shifted from those of T_t, in both the νOH and νC=O spectral regions are assigned to the $T_g^{\pm}$ form resulted from the C_α-C internal rotation. These small shifts agree with a predictable small effect of the backbone conformation on the vibrational modes localized in the carboxylic group. The weaker band rising at ≈1800 cm^{-1} is assigned to the νC=O mode of C_t, which is produced from T_t by internal rotation along the C-O bond. The νC=O band of C_t shows the expected large blue-shift from that of T_t. The νOH band is not observed for C_t most probably due to its low intensity and also

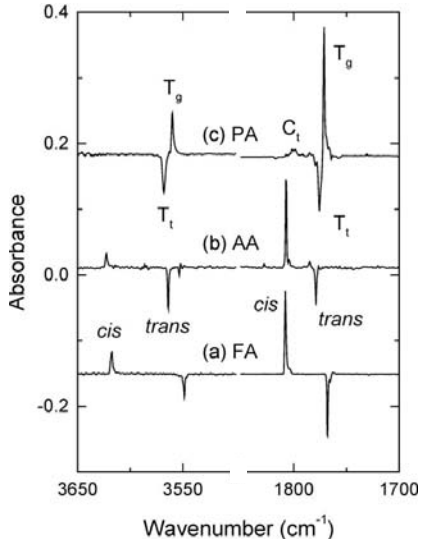

Fig. 4 Difference IR absorption spectra showing the spectral changes produced by excitation at the 2νOH frequencies of the ground state conformers of fully hydrogenated FA (a), AA (b) and PA (c). The difference spectra are obtained as spectra measured *after* pumping minus spectra measured *before* pumping for FA and AA, and a spectrum *during* pumping minus a spectrum *before* pumping for PA.

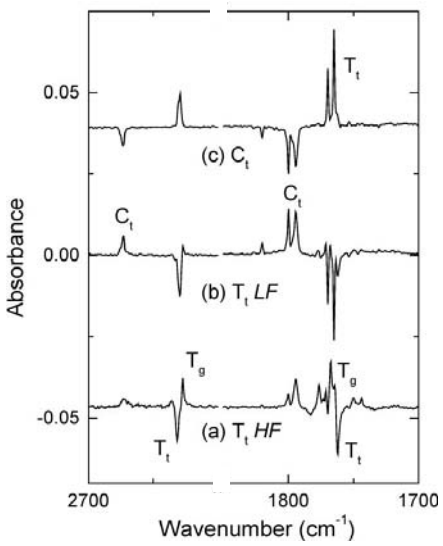

Fig. 5 Difference IR absorption spectra of PA-OD showing the conformational changes induced by excitation of the 2νOD modes of (a) T_t in the HF site (40 min), (b) T_t in the LF site (40 min), and (c) C_t in the LF matrix site (15 min). Traces (a) and (b) show the increasing of C_t and $T_g^{\pm}$ bands produced from T_t *via* the C-O and C_α-C isomerization and trace (c) shows the increasing of T_t bands produced from C_t due to the C-O isomerization. The pumped species are marked.

due to the fact that it is expected to appear at ≈ 3630 cm^{-1}, which is very close to the cut-off of the filter used to record the spectrum under irradiation.

As an important fingerprint of tunnelling, substitution of the tunnelling particle by a heavier isotope decreases the reaction rate significantly. Consequently, deuteration of the hydroxyl group of PA facilitates identification of the C_t conformer produced upon excitation of the ground-state T_t form. Spectra (a) and (b) in Fig. 5 show the results of conformational isomerization of PA-OD induced by excitation of the T_t form in two different matrix sites at 5175 and 5170 cm^{-1} (hereafter denoted as HF and LF, respectively). Similarly to PA-OH, the increasing bands in the two difference spectra, which appear considerably blue-shifted from the T_t bands, are assigned to the C_t conformer while the less shifted bands are due to the $T_g^{\pm}$ conformer. In agreement with our calculations, the $T_g^{\pm}$ bands are close to the T_t bands, and they appear slightly red-shifted or blue-shifted depending on the matrix site.

Additionally, the C_t form is much more stable for PA-OD than for PA-OH, which allowed us to perform pumping experiments with the C_t conformer of PA-OD. As seen in plot (c) of Fig. 5, excitation of the 2νOD of the C_t molecules previously produced in the LF site leads to the $C_t \rightarrow T_t$ isomerization.

3.2. Tunnelling rate for the C-O isomerization

For PA-OH, the $C_t \rightarrow T_t$ tunnelling is faster than the analogous *cis* → *trans* tunnelling for FA and AA (Fig. 4).[28,29] The tunnelling rate for the C-O isomerization observed for fully hydrogenated FA, AA and PA ($k_t \approx 2 \times 10^{-3}$, 2×10^{-2}, and 5×10^{-2} s^{-1}, respectively) correlates inversely with the barrier height for the isomerization, *i.e.*, the higher barriers reasonably correspond to slower tunnelling rates. The *cis* → *trans* barrier heights calculated in this study at the MP2/6-311++G(2d,2p) level of theory for FA, AA and PA, are 2676, 2308 and 2290 cm^{-1}, respectively. The tunnelling rate for FA is one order of magnitude slower than for AA, thus, reflecting the considerably higher barrier for the *cis* → *trans* conversion in FA as compared with AA (the computational difference between the barriers ≈ 370 cm^{-1}). For AA and PA, the calculated barrier heights differ only by ≈ 20 cm^{-1} and the tunnelling rates are closer to each other. The known solvation effect can change to some extent the relative energetics and the barriers, as it was discussed elsewhere,[29] however, this energy change should be similar for the species under study.

For FA, deuteration of the hydroxyl group decreases the *cis* → *trans* tunnelling rate by a factor of ≈ 3×10^3 (from 2×10^{-3} to 7×10^{-7} s^{-1}). For AA and PA, deuteration of the hydroxyl group decreases the tunnelling rate by even larger factors of 3×10^4 and 6×10^4

(from 2×10^{-2} to 7×10^{-7} s^{-1} for AA and from 5×10^{-2} to 8×10^{-7} s^{-1} for PA). It is remarkable that the effect of hydroxyl deuteration is higher for lower isomerization barriers. This effect is in contradiction with the expected trend for the penetration probability calculated according to the semi-classical WKB approximation.[34] It is probable that the tunnelling rate depends essentially on additional factors like the nature and distribution of the vibrational energy levels involved in the tunnelling process as pointed out in our previous studies on FA and AA.[28,29] Our present results support the previously suggested model. It should be also mentioned that the extraction of very small decay rates is complicated and produces a relatively large experimental error.

3.3. IR induced *trans*→*cis* C-O isomerization in the fully hydrogenated species

For the three molecules under study, the quantum yields obtained for the *trans* → *cis* C-O isomerization induced by excitation of the 2νOH mode of the ground state conformer are shown in Table 2. The strong decrease in the quantum yield from FA (10-20 %)[26] to AA (≈ 2 %)[28] was previously connected with the low-barrier methyl rotor in the latter molecule. The low-frequency modes of the methyl rotor are coupled with the initially excited mode or/and with intermediate vibrational modes participating in the energy relaxation, enhancing non-reactive relaxation channels.[35] Vibrations with large amplitudes such as τC-O and τC-CH_3 are usually very anharmonic and strong coupling between the two internal rotors in AA can be expected.

PA has one additional internal rotational degree of freedom when compared with AA, the C_α-C torsion (τC_α-C). This mode has a low vibrational frequency and it can contribute to the energy relaxation process in PA similarly to the τC-CH_3 mode. In fact, the computational frequency for the τC_α-C mode in T_t is 57 cm^{-1}, *i.e.* very close to the value of the Debye frequency for solid Ar

Table 2 Quantum yields for C-O isomerization induced by excitation of the 2νOH/2νOD modes of the fully hydrogenated and hydroxyl-deuterated FA,[26] AA,[28] and PA.

C-O isomerization quantum yields [a]	FA [b]	AA	PA
2νOH	1.7×10^{-1} (*s2*)	2.2×10^{-2}	1.4×10^{-2}
trans → *cis*	7×10^{-2} (*s1*)		
2νOD	----	3.6×10^{-3}	3.2×10^{-3} (*HF*)
trans → *cis*			5.0×10^{-3} (*LF*)
2νOD	----	1.2×10^{-2}	1.4×10^{-1}
cis → *trans*			

[a] The quantum yields have been estimated by eqn. (1), the estimated error is ±50%. For PA, the *trans* and *cis* form correspond to T_t and C_t, respectively. The two entries for FA and PA are associated with excitation of different sites (s1 and s2 in FA, and HF and LF in PA).[26,30] [b] No kinetic data available for excitation of 2νOD

(≈60 cm^{-1}),[36] which can favour energy transfer between lattice vibrations and molecular modes. Indeed, in addition to the C-O internal rotation, excitation of the 2νOH mode of PA induces the C_α-C internal rotation indicating that the excitation energy is channelled efficiently into the low-frequency C_α-C torsional mode. The quantum yield for the C_α-C isomerization ($T_t \rightarrow T_g^{\pm}$) is 1.4%. Despite of this additional reaction channel, competing with the C-O isomerization, the quantum yield for the C-O isomerization in PA (1.4%) is similar to the value for AA within our experimental error (see Table 2). A more quantitative analysis of the isomerization process should be based on the vibrational patterns in the overtone and combination spectral region derived from the precise anharmonic analysis. It is difficult to specify the involved relaxation channels for a relatively complicated system like PA with unknown anharmonic coupling between modes. In any case, the balance between the efficiency of the non-reactive and reactive channels is not changed significantly in PA as compared with AA. With respect to the C-O isomerization, the participation of the CH_3 group seems to be comparable to the effect of the CH_3CH_2 group. Thus, relatively large isomerization quantum yields may be expected for related

molecules with longer carbon chains, which is an interesting direction of research.

3.4. IR-induced *trans* → *cis* and *cis* → *trans* C-O isomerization in the OD-species

The $T_t \rightarrow C_t$ isomerization quantum yield for PA-OD (0.32-0.50 %) is similar to the value estimated for AA-OD (0.4 %). For both AA and PA, deuteration of the hydroxyl group decreases significantly the C-O isomerization quantum yield. This phenomenon should not be correlated with the lower excitation energy upon pumping the 2νOD mode (≈ 5100 cm^{-1}) when compared to the 2νOH mode (≈ 6900 cm^{-1}) or with the change of the zero point vibrational energy. Indeed, it was shown for FA and AA that the C-O isomerization quantum yields are nearly insensitive to the excitation energy as long as the energy is above the isomerization barrier.[26,28] Our explanation for the deuteration effect observed in AA was based on the participation of higher order couplings between the τC-O and the intermediate states involved in the IVR process for the OD species in comparison with the OH species. The higher order couplings for the OD species are due to a deuteration-induced decrease of the τC-O frequency, and therefore, at similar energies the τC-O mode is at a higher excited state in the OD species. This reduces the probability of energy transfer into the reaction coordinate for the deuterated species.[28] In this study, we also observed a decrease of the $T_t \rightarrow T_g^{\pm}$ quantum yield for PA-OD (<0.2%) compared with PA-OH (1.4%), indicating a significant effect even when the corresponding mode is not influenced much by deuteration. In order to justify this observation, we can speculate that the deuteration can decrease the coupling of the pumped mode [2νOH(D)] with the reaction coordinate.

In the case of PA-OD, the estimated quantum yield is much larger for the reverse $C_t \rightarrow T_t$ conversion (14 %) than for the $T_t \rightarrow C_t$ conversion (0.32-0.50%). This constitutes already the third reported observation pointing to the same direction, taking into account similar effects observed for the *cis* → *trans* isomerization in the AA-OD (Table 2)[28] and HONO.[1] For HONO, a quantum yield higher by a factor of 7 was found for the IR-induced conversion of the *cis* conformer (H-O-N=O dihedral angle of 0º) into the *trans* form (H-O-N=O dihedral angle of 180º) when compared with the *trans* → *cis* process.[1] Although the *cis* → *trans* energy barriers in AA and PA are lower than the *trans* → *cis* barriers, this fact is unable to fully justify the observed trend for two reasons: (1) the difference in the *cis* → *trans* and *trans* → *cis* barriers for HONO is very small (130 cm^{-1}) and (2) the quantum yields for FA and A A are quite independent of the excitation energy as long as the excited vibrational mode is above the isomerization barrier.[1,26,28] In the case of HONO, it was suggested that kinetic or potential couplings between the excited vibrations and nearly resonant vibrational states could be responsible for the more efficient energy transfer from the excited states to the reaction coordinate upon excitation of the *cis* isomer.[37,38] These factors may also be relevant for the carboxylic acids studied here.

3.5. Site-selective isomerization of PA-OD

Fig. 5 presents the result of irradiation for the hydroxyl-deuterated T_t conformer at two slightly different frequencies (5175 and 5170 cm^{-1}). The pumping at different frequencies excites molecules in different local matrix morphologies (matrix sites). It is seen that the ratio of the $T_t \rightarrow C_t$ and $T_t \rightarrow T_g^{\pm}$ reaction channels upon excitation of the 2νOD of T_t depends on the matrix site, in particular, excitation of the HF site is more efficient in promoting the C_α-C internal rotation than excitation of the LF site. The quantum yields obtained for the C_α-C isomerization process differ by a factor of ≈4 (0.16 and 0.042 % for HF and LF excitation, respectively) suggesting the site selectivity of this reaction channel (Table 3). On the other hand, the quantum yields for

the C-O isomerization upon pumping the HF and LF sites are similar within our experimental error (0.32 and 0.50 % for HF and LF excitation, respectively). The latter result is similar to the data on FA where no reliable site dependence of the C-O isomerization quantum yield has been observed.[26] For PA, we can compare the isomerization quantum yields for the two isomerization processes for molecules isolated in the same matrix site. The C-O isomerization is the preferred reaction channel for pumping of the LF site (5170 cm^{-1}), and the C-O isomerization quantum yield is higher than that associated with the C_α-C process by more than one order of magnitude. For pumping of the HF site (5175 cm^{-1}), the two photoprocesses are nearly as efficient. The quantum yields given in Table 3 were estimated by the two different methods described earlier [eqns. (1) and (3)], and the obtained values are rather independent of the method used.

The site dependence of the quantum yields is possibly contributed by restrictions to the C_α-C internal rotation imposed by the matrix cage. Indeed, the C_α-C isomerization involves rotation of heavy atoms, and hence it is associated with a relatively large reaction volume compared with the C-O isomerization, which deals essentially with motion of the light hydroxylic hydrogen atom. These arguments were used previously to explain the lack of NIR induced isomerization in fumaric acid.[39] However, in the case of PA, it was observed that the $T_g^{\pm} \rightarrow T_t$ dark process is thermally activated, and it is in minute timescale at 15 K. It follows that the corresponding barrier is quite low, which is consistent with the computational value of ≈ 60 cm^{-1}. This suggests that the $T_t \rightarrow T_g^{\pm}$ barrier should be relatively low as well (computationally ≈ 400 cm^{-1}), which does not support cage restrictions. As another explanation, some specific energy relaxation channels can contribute to the site selectivity of the process. In this image, the coupling of $\tau(C_\alpha\text{-}C)$ with the lattice vibrations may be important. It should be also noted that the estimation of the C_α-C quantum yields can be influenced by the overlap of the 2νOD bands of the $T_g^{\pm}$ and T_t conformers. Inspection of the band profiles associated with the two sites leads to the conclusion that this overlap may occur only for the LF site, which, in principle, can contribute to the site selectivity of the C_α-C process, decreasing the $T_g^{\pm}$ concentration for the LF pumping.

Table 3 - Quantum yields for C-O and C_α-C isomerization induced by excitation of the 2νOD modes of PA-OD isolated in two different matrix sites.

Quantum yields/10^{-3} [a]	HF site	LF site
$T_t \rightarrow C_t$ (C-O)	3.2 (3.5)	5.0 (5.5)
$T_t \rightarrow T_g^{\pm}$ (C_α-C)	1.6 (1.7)	0.42 (0.58)

[a] The values obtained from eqn. (1) are shown outside the parentheses and the results obtained from eqn. (3) are shown in parentheses. An error of ± 50% is estimated.

Another observation features unexpected energy redistribution in the molecule. The excitation of the 2νOD of C_t, which is mainly isolated in the LF site (C_α-C resistant site), induced exclusively rotation around the C-O axis leading to production of T_t, and no C_α-C isomerization ($C_g^{\pm}$) could be detected. In fact, only the bands of T_t increase under vibrational excitation of C_t [spectrum (c) in Fig. 5]. This observation is remarkable since the computational $C_t \rightarrow T_t$ barrier is larger than the $C_t \rightarrow C_g^{\pm}$ barrier by ≈ 1700 cm^{-1} so that the opposite trend could be expected. This observation may be relevant to the site selectivity of the isomerization process because the opposite $T_t \rightarrow C_t$ process in this site also dominated over the C_α-C isomerization.

4. Conclusions

The quantum yields for the C-O isomerization induced by excitation of the first overtone of the hydroxyl stretching vibration have been estimated for PA isolated in solid Ar, and compared with the

corresponding data on FA and AA.[26-28] The *cis* → *trans* tunnelling kinetics was also comparatively analysed. We observed the following trends:

(1) For the fully hydrogenated species, the C-O isomerization quantum yields for PA and AA are one order of magnitude smaller than the value for FA, which is probably caused by a smaller vibrational density of states in the latter molecule. On the other hand, the quantum yields for PA and AA are remarkably similar despite the higher vibrational density of states in PA, thus, indicating a 'saturation' effect.

(2) Similarly to AA, deuteration of the hydroxyl group of PA decreases significantly the C-O isomerization quantum yield. The explanation for the observed deuteration effect relies on the lower probability for energy transfer to the reaction coordinate in the deuterated species due to less efficient couplings between the initially excited vibrational mode and the τC-O reactive mode.

(3) In the case of PA-OD, the C-O and C_α-C isomerization quantum yields were estimated for excitation of molecules isolated in two matrix sites. A site-selective quantum yield was tentatively observed for the C_α-C isomerization whereas no significant site effect is found for the C-O isomerization. The latter fact corresponds to the data obtained for AA and FA.[26,28]

(4) For AA-OD and PA-OD, the C-O isomerization starting from the higher energy arrangement of the carboxylic group (*cis* → *trans* in AA; and $C_t \rightarrow T_t$ in PA) was shown to be more efficient than the reverse process. This corresponds to the previous observations in HONO,[1] and it is possibly explained by specific kinetic or potential couplings favouring the *cis* → *trans* conversion.[37,38]

(5) For the fully hydrogenated species, the measured tunnelling rates correlate inversely with the computational isomerization barrier. Surprisingly, the deuteration effect (decrease of tunnelling rate by several orders of magnitude) is stronger for the lower isomerization barriers (AA and PA). This fact features the influence on the tunnelling mechanism of factors like distribution and nature of the vibrational energy levels involved in the process as proposed earlier for FA.[29]

The results obtained for PA support the conclusions derived previously for FA and AA and increase their confidence. However, understanding of a number of processes is still lacking, which suggests further studies in this field.

Acknowledgements

The Academy of Finland is thanked for financial support. E. M. and R. F. acknowledge the Portuguese Foundation for Science and Technology (PhD grant SFRH/BD/4863/2001 and POCTI/QUI/43366/2001).

References

1 L. Khriachtchev, J. Lundell, E. Isoniemi and M. Räsänen, *J. Chem. Phys.*, 2000, **113,** 4265.
2 A. J. Barnes, *J. Mol. Struct.*, 1984, **113,** 161.
3 M. Räsänen, H. Kunttu and J. Murto, *Laser Chem.*, 1988, 9, 123.
4 S. Sander, H. Willner, L. Khriachtchev, M. Pettersson, M. Räsänen and E. L. Varetti, *J. Mol. Spectrosc.*, 2000, **203,** 145.
5 M. Pettersson, J. Lundell, L. Khriachtchev and M. Räsänen, *J. Am. Chem. Soc.*, 1997, **119,** 11715.
6 E. M. S. Maçôas, L. Khriachtchev, M. Pettersson, J. Lundell, R. Fausto and M. Räsänen, *Vib. Spectrosc.*, 2004, **34,** 73.
7 H. H. Gunthard, *J. Mol. Struct.*, 1984, **113,** 141.
8 R. N. Perutz, *Chem. Rev.*, 1985, **85,** 77.
9 T. Lotta, J. Murto, M. Räsänen and A. Aspiala, *J. Mol. Struct.*,1984, **114,** 333.
10 S. Kudoh, M. Takayanagi, M. Nakata, T. Ishibashi and M. Tasumi, *J. Mol. Struct.*, 1999, **479,** 41.
11 A. K. Knudsen and G. C. Pimentel, *J. Phys. Chem.*, 1991, **95,** 2823.
12 W. F. Hoffman and J. S. Shirk, *Chem. Phys.*, 1983, **78,** 331.
13 P. Roubin, S. Varin, P. Verlaque, S. Coussan, J. M. Berset, J. M. Ortega, A. Peremans and W. Q. Zheng, *J. Chem. Phys.*, 1997, **107,** 7800.
14 M. Poliakoff and J. J. Turner, in *Chemical and biochemical applications of lasers*, ed. C. B. Moore, Academic, New York, 1980.
15 H. Frei and G. C. Pimentel, *Annu. Rev. Phys. Chem.*, 1985, 36, 491.
16 H. Frei and G. C. Pimentel, in *Chemistry and Physics of Matrix-Isolated Species*, ed. L.

Andrews and M. Moskovits, Elsevier, Amsterdam, 1989.
17 M. Räsänen and V. E. Bondybey, *Chem. Phys. Lett.*, 1984, **111,** 515.
18 M. Räsänen and V. E. Bondybey, *J. Chem. Phys.*, 1985, **82,** 4718.
19 M. Räsänen, J. Murto and V. E. Bondybey, *J. Phys. Chem.*, 1985, **89,** 3967.
20 V. E. Bondybey, *Annu. Rev. Phys. Chem.*, 1984, **35,** 591.
21 F. Legay, in *Chemical and Biochemical Applications of Lasers*,ed. C. B. Moore, Academic, New York, 1977.
22 E. M. S. Maçôas, L. Khriachtchev, M. Pettersson, R. Fausto and M. Räsänen, *J. Am Chem. Soc.*, 2003, **125,** 16188.
23 J. D. Goddard, Y. Yamaguchi and H. F. Schaefer, *J. Chem. Phys.*,1992, 96, 1158.
24 W. H. Hocking, *Z. Naturforsch. A*, 1976, **31,** 1113.
25 M. L. Senent, *Mol. Phys.*, 2001, **99,** 1311.
26 E. M. S. Maçôas, L. Khriachtchev, M. Pettersson, J. Juselius, R. Fausto and M. Räsänen, *J. Chem. Phys.*, 2003, **119,** 11765.
27 M. Pettersson, E. M. S. Maçôas, L. Khriachtchev, R. Fausto and M. Räsänen, *J. Am. Chem. Soc.*, 2003, **125,** 4058.
28 E. M. S. Maçôas, L. Khriachtchev, M. Pettersson, R. Fausto and M. Räsänen, *J. Chem. Phys.*, 2004, **121,** 1331.
29 M. Pettersson, E. M. S. Maçôas, L. Khriachtchev, J. Lundell, R. Fausto and M. Räsänen, *J. Chem. Phys.*, 2002, **117,** 9095.
30 E. M. S. Maçôas, L. Khriachtchev, M. Pettersson, R. Fausto and M. Räsänen, *J. Phys. Chem.*, 2005, **109**, 3617.
31 M. J. T. Frisch, G. W. Schlegel, H. B. Scuseria, G. E. Robb, M. A. Cheeseman, J. R. Zakrzewski, V. G. Montgomery, J. A. Stratmann, R. E. Burant, J. C. Dapprich, S. Millam, J. M. Daniels, A. D. Kudin, K. N. Strain, M. C. Farkas, O. Tomasi, J. Barone,V. Cossi, M. Cammi, M. Mennucci, B. Pomelli, C. Adamo, C. Clifford, S. Ochterski, J. Petersson, G. A. Ayala, P. Y. Cui, Q. Morokuma, K. Malick, D. K. Rabuck, A. D. Raghavachari, K. Foresman, J. B. Cioslowski, J. Ortiz, J. V. Baboul, A. G. Stefanov, B. B. Liu, G. Liashenko, A. Piskorz, P. Komaromi, I. Gomperts, R. Martin, R. L. Fox, D. J. Keith, T. Al-Laham, M. A. Peng, C. Y. Nanayakkara, A. Gonzalez, C. Challacombe, M. Gill, P. M. W. Johnson, B. G. Chen, W. Wong, M. W. Andres, J. L. Head-Gordon, M. Replogle and E. S. Pople, *GAUSSIAN98 (Revision A. 9),* Gaussian, Inc., Pittsburgh, PA, 1998.
32 E. M. S. Maçôas, J. Lundell, M. Pettersson, L. Khriachtchev, R. Fausto and M. Räsänen, *J. Mol. Spectrosc.*, 2003, **219,** 70.
33 E. M. S. Maçôas, L. Khriachtchev, R. Fausto and M. Räsänen, *J. Phys. Chem. A*, 2004, **108,** 3380.
34 R. P. Bell, *The tunnel effect in chemistry*, Chapman and Hall, New York, 1980.
35 A. Mcllroy and D. J. Nesbitt, *J. Chem. Phys.*, 1994, **101,** 3421.
36 H. J. Jodl, in *Chemistry and Physics of Matrix-Isolated Species*, ed. L. Andrews and M. Moskovits, Elsevier, Amsterdam, 1989.
37 Y. Guan, G. C. Lynch and D. L. Thompson, *J. Chem. Phys.*, 1987, **87,** 6957.
38 F. Richter, M. Hochlaf, P. Rosmus, F. Gatti and H. D. Meyer, *J. Chem. Phys.*, 2004, **120,** 1306.
39 E. M. S. Maçôas, R. Fausto, J. Lundell, M. Pettersson, L. Khriachtchev and M. Räsänen, *J. Phys. Chem. A*, 2001,**105,** 3922.

ACADEMIC DISSERTATION